Proceedings of the Symposium on Mountain Meteorology

26 June, 1967
Fort Collins, Colorado

Edited by
E.R. Reiter and J.L. Rasmussen

Technical Paper No. 122
Department of Atmospheric Science
Colorado State University
Fort Collins, Colorado

Colorado State University

Department of Atmospheric Science

Paper No. 122

ROCEEDINGS

F THE SYMPOSIUM

N MOUNTAIN METEOROLOGY

JUNE, 1967
RT COLLINS,
LORADO

)ITED BY
R. REITER and
L. RASMUSSEN

Atmospheric Science
PAPER NO.
122

ARTMENT OF ATMOSPHERIC SCIENCE
)RADO STATE UNIVERSITY
T COLLINS, COLORADO

CONTENTS

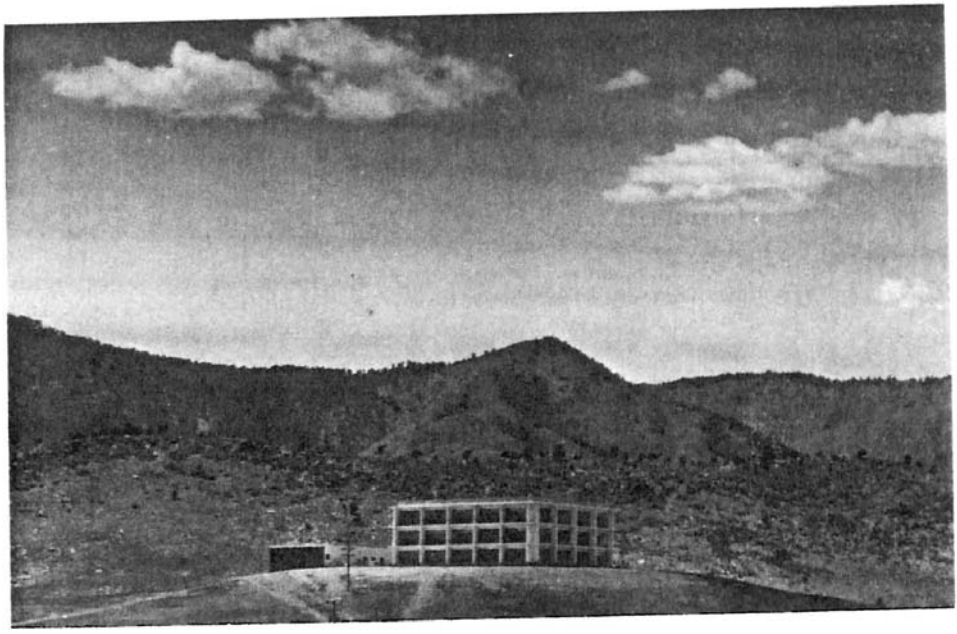

COLORADO STATE UNIVERSITY ATMOSPHERIC SCIENCE BUILDING

PREFACE

Even the largest orographic barriers in the northern and southern hemispheres are nothing more than small "wrinkles" in the face of the earth. Nevertheless, they exert a decisive influence on the atmosphere of our planet: The turbulent boundary layer behaves differently on an inclined surface, as compared with a level plane; local circulation systems are spawned by diurnal heating and cooling along mountain slopes; air flow over an orographic obstacle receives perturbation energy over a wide range of the spectrum of atmospheric motions, from short gravity waves to long planetary waves. Mountains, therefore, become a focal point of interest when one tries to grasp the physics of our atmospheric environment in numerical or geophysical model experiments. To the skier and mountaineer, of course, the serene beauty of snow-covered peaks will mean something altogether different from a small, yet perceptible, source of perturbations that may be expressed in terms of linearized differential equations.

To combine such abstractions with the splendor of reality, Fort Collins offers a congenial environment. The proper occasion for a "Symposium on Mountain Meteorology" arose with the completion of a new physical plant, housing the Department of Atmospheric Science, Colorado State University, with its complex and diversified research interests in which the nearby Rocky Mountains figure so prominently. This facility, built through collaboration of the National Science Foundation and the State of Colorado, owes its existence largely to the dynamic leadership and perseverance of Dr. Herbert Riehl, Head of the Department of Atmospheric Science.

Colorado State University has lent its generous financial support to the organization of this "Symposium on Mountain Meteorology". The Symposium was an official National Meeting of the American Meteorological Society who co-sponsored the symposium and greatly aided the Department in arrangements and publicity. The Link Foundation contributed materially by carrying the expenses of Dr. R. S. Scorer, Imperial College, London. The technical arrangements for this symposium lay in the capable hands of Mr. James L. Rasmussen.

Although a series of seven lectures, delivered by experts in the field, will not penetrate through each and every meteorological problem associated with mountains, it is hoped that this volume of "Proceedings" may at least serve as a guidepost to other researchers in the atmospheric sciences, who feel themselves attracted by the beauty of these rocky barriers.

Elmar R. Reiter
Professor of Atmospheric Science
Colorado State University

MEMORIAL

Man's efforts to conquer mountains, the atmosphere, and indeed life itself have often led to disaster. So also do man's efforts to delve in mountain meteorology inevitably involve risk.

Edward Everett Hale once wrote, "I am only one, but still am one; I cannot do everything but still I can do something." This favorite quote of Donald L. Livingston was always before him on his desk. It was this spirit of effort in studies of mountain meteorology that cost him his life prematurely at the age of 44 on a stormy 12 April 1967.

Don became involved in the atmospheric sciences by mistake. As a young boy just out of high school, entering the Navy just before World Was II, he selected "Aerographer" from among a list of available options. Too embarrassed to withdraw upon learning that this was not aerial photography, he began his studies that led to a career in atmospheric sciences.

His tour in the Navy lasted 11 years. During this time, covering World War II and the Korean War, he advanced to the rank of Chief Aerographer's mate.

His interests after leaving the Navy were consistently the exploration of ways in which meteorology might be used to benefit mankind. While working for a B.S. degree in Statistics and Research at Denver University, he worked as a weather engineer with Krick Associates. He subsequently served as Senior Analyst in conducting various research studies in the fields of economics and military weaponry with Martin Marietta Corporation during the early 1960's. His interests, however, remained more directly related to meteorology.

From 1964 to 1966 he acted as Field Director for the Colorado State University, Atmospheric Science Department, air pollution studies in the Denver area. Late in 1966 he formed, with associates, a service company for carrying out the field phases of research programs being conducted by various research groups. He served as chairman of the board of directors from the company's inception.

His dedication to another of his favorite quotes led to his fatal accident. "The difference between failure and success is doing a thing nearly right and doing it exactly right." While his primary responsibility with Western Scientific Services was not field servicing of equipment, it was essential that he know that it was operating properly under storm conditions for the Colorado State University mountain studies near Climax, Colorado. Storm conditions included 20 inches of snow in less than 12 hours and 30 to 40 mile per hour winds. Visibility was at nearly zero at the time of the fatal snow tractor accident.

His life is typified by his interest in principles of scouting. He was an Eagle Scout, served as Scoutmaster and Counselor for an Explorer Post of Boy Scouts. His talents were many. The lower picture shows one of his three-dimensional models of cloud systems moving over the Denver area. Several associates summed up his character: straightforward, honest, hard-working, dedicated, diplomatic, open-minded, no sense of quitting time, broad sense of humor. A memorial section for Donald L. Livingston is most fitting in this volume on mountain meteorology.

SMALL TO LARGE-SCALE FEATURES OF BOUNDARY LAYER STRUCTURE OVER MOUNTAIN SLOPES

Introducing a New Type of Mountain Circulation: The Thermo-Tidal Wind

Heinz H. Lettau
University of Wisconsin at Madison

1. Introductory Remarks

The effect of mountains on atmospheric processes will be best visualized if we compare our earth with an imaginary planet which has entirely flat continents. Otherwise, astronomical-geophysical conditions shall be the same; this implies identity of planetary orbit elements and radius, angular speed of rotation, axis inclination, mass and distribution of oceans, etc. The only difference shall be that there are neither mountains nor hills, nor terrain inclinations on the continents, with the only exception of a narrow strip of beach-slope along the coast lines. The question arises how the weather and the atmospheric circulation on the imaginary planet would compare with the familiar conditions on our earth. Some differences will be immediately obvious, but some are hidden, since we must also expect great similarities. Like on a level roof there will be no drainage of rain water, no surface-runoff, no rivers on these flat continents. Only the vertical fluxes due to evaporation and sublimation can dispose of precipitation falling on the lands. But will there really be no drainage at all? Seasonal accumulation of snow might be localized at least due to coastline effects; this may eventually result in the build-up of inland-ice domes at high latitudes, and consequently, glaciers may move towards the oceans representing gravitational drainage of a special kind.

In summertime there will be no cool uplands on our imaginary planet, and climatic regions could be neatly organized in zonal belts. But again, an existing continent-ocean contrast of albedo as well as thermal admittance must affect the surface heat-budget, and will certainly distort a strictly zonal pattern of daily mean temperatures and diurnal amplitudes. However, the original meaning of the word "climate" would be lost because in its Greek root form it refers to inclination of terrain slopes and subsequent differences in exposure to sunshine. Due to differential heating between tropical and polar zones, a general circulation of the atmosphere must exist on our imaginary planet. In spite of lack of topography it will exhibit certain features which we are used to consider being of orographic nature; for example, foehn winds will occur as so-called "free-foehn"; warm air will glide upwards, along a sloping surface of thermal discontinuity separating it from a cold air mass, to produce warmfront rains similar to orographic precipitation. Over convective updrafts, cap clouds will appear which resemble the banner clouds over mountain peaks. Rather than in the lee of mountain ranges the so-called lee-waves will develop when one air mass flows above another. In fact, there are certain meteorological consequences initially caused by local updrafts due to localized surface heating on truly flat ground which have been described in

the literature by the phrase "thermal mountain". An example is clouds over flat islands in the trade wind region which develop during the daytime phase of solar heating and resemble clouds over mountaineous islands in the absence of surface heating; see Malkus and Stern (1963). However, it shall be shown that an increase in heating intensity on mountain slopes may not under all circumstances lead to orographic-convective type updrafts, or clouds, and lastly rainfall. Thus, the phrase "thermal mountain effect" for example, as employed by Black and Tarmy (1963), may be quite often unapplicable in the sense of expressing a stimulation of rain; on the contrary, we will stress the point that deserts may be explained as a consequence of solar heating on mountain slopes. Indeed, the purpose of the following discussion is to investigate in detail some new and apparently paradoxical aspects of structure of the atmospheric boundary layer over terrain slope and mountain; in both respects, mechanical-kinematic, as well as thermodynamical or diabatic.

One may classify dynamical mountain effects into two major categories: (1) Modification of an existing current of the general circulation, and (2) generation of specific (local and regional) circulation systems. The borderline between the two categories is not always sharp or distinct. But obviously, it is quite important to specify exactly what is meant physically by "mountain effect". In some recent investigations in connection with numerical modeling of the atmosphere, the phrase has appeared that "mountains were put into the model". Unless more precisely defined, this statement can have different factual meanings because mountains are known to have kinematic, dynamic, and thermal-radiational effects. Even the simplest effort to consider nothing but the actual geometry of continent-wide mountain ranges leads to difficulties because there will be a limit for the lower end of the geometrical scale which can be taken into account numerically in a special problem. If one wants to deal with more than geometric-kinematic problems, difficulties are enhanced. For example, a host of physical features of the earth-air interface must be parameterized if one wants to specify the heating function or net-radiation realistically. Diurnal and seasonal variations of insolation are known to depend strongly on terrain slope and orientation. Variable snow cover on mountains does affect significantly the albedo as well as the thermal admittance and, thus, the local heat budget. The eddy transfer of momentum and mechanical energy depends certainly on aerodynamical surface roughness but these features are presently not very well understood for difficult terrain.

From the above listing, which is still rather incomplete, it may be concluded that there are many open questions concerning boundary layer structure over mountains. In my discussion I will begin with two special examples dealing with modification of existing air currents due to topography and will proceed with the investigation of certain significant effects of the diurnal heating and cooling cycles on mountain slopes. The result will be a new type of mountain circulation which apparently has not been discussed previously in the literature but which may prove to be highly significant for regional climatology, especially precipitation deficiency, along certain mountain ranges.

2. Examples for the Modification of Air Flow Patterns due to Mountains

2.1 Air Flow Near Isolated Peaks

Basically, the atmosphere is a very thin spherical shell concentric to the lithoshpere and hydrosphere so that the general circulation occurs predominantly in the form of horizontal air currents. Thus, mountains must represent significant obstacles to an existing circulation of the larger scales. Sometimes the question is asked how well an anemometric recording on a mountain peak compares with the wind at the same level in the surrounding free atmosphere. Even this relatively simple and elementary problem of mountain meteorology is not easily answered. This again was demonstrated as a result of recent research at the University of Wisconsin by Wahl (1966). Anemometer recordings from six mountain observatories in central Europe were

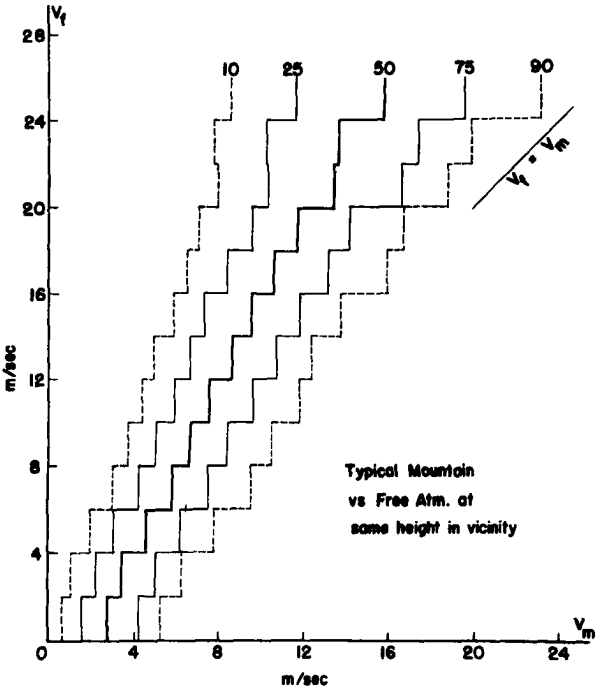

Fig. 1 Windspeed V_m (as measured at a mountain observatory) versus V_f (estimated for the same level in the free atmosphere, from Rawin-soundings in the vicinity of the peak). Climatic mean frequency distributions for V_f-classes (in 2 m/sec steps) are indicated by lines numbered 10 and 90 for lowest and highest decile, 25 and 75 for lower and higher quartile, and 50 for median value; after Wahl (1966).

compared with wind data from four Rawin stations at corresponding levels in the vicinity. Statistical analysis of several years of data showed, surprisingly, that the differences between summit and free flow were similar in spite of the fact that four of the observatories are located on medium-high and rather rounded mountain summits (like the Feldberg in the Black Forest) and one on a much higher and exceptionally ragged alpine peak (Zugspitze). A typical sample of the statistical results (including distribution) is illustrated in Fig. 1. Disregarding conditions at lower velocities one finds that the wind speed on the summit tends to average at about one half of that in the free atmosphere. This may indicate that the expected narrowing of streamlines over such topographical obstacles is overcompensated by frictional effects. In more detail the complexity of the problem is evident on Fig. 1 especially with regard to conditions at low wind speed at which the mountain range appears to create its own circulation system since recorded velocity tends to be in excess of that in free air. Obviously, a study of low-wind-speed cases would necessitate the evaluation of thermal gradients between mountain peak and free air. For more precise studies of air flow over summits, in terms of local boundary layer structure and "displacement thickness", consideration of wind direction will be a necessity.

2.2 Topography in Relation to Tornado Tracks

Various statistical approaches are possible if one wants to investigate how increased friction due to mountains modifies an existing atmospheric circulation. Let me mention only one special but very interesting case. It is known that the occurrence of tornadoes seems to be related to topography; a good example is the result of statistical studies in Arkansas by Asp (1956). Although the terrain does hardly affect the prevailing direction of tornado migration, Asp found statistically a pronounced channeling in three strips or "tornado alleys", separated by two shunted belts as represented roughly by the Ozark Mountains in the northwest of the state and the Ouachita Mountains west of Little Rock, Arkansas; see Fig. 2. Similar results have been reported from other parts of the central United States. However, the relationship between tornado alleys and terrain may be indirect and often camouflaged. This is true in Wisconsin, for example, according to a special investigation presently in progress in Madison based on a recent survey by Burley and Waite (1966).

The question arises of how to specify topography by a simple but conclusive, numerical parameter in order to be able to compare conditions in possible tornado alleys with those in shunted belts nearby. The method selected in our study at the University of Wisconsin employs spectral analysis of a terrain profile curve, h versus x, when h = topographical elevation above sea level and x = horizontal distance, stretching over at least 100 miles. Values of h can be read from topographical maps for fixed horizontal increments of Δx, either per mile or a fraction of it. The resulting x-series may be compared with the time-series representing turbulent or other fluctuations of any fluid dynamics variable. A spectral analysis of the h versus x series can be performed employing conventional statistical techniques.

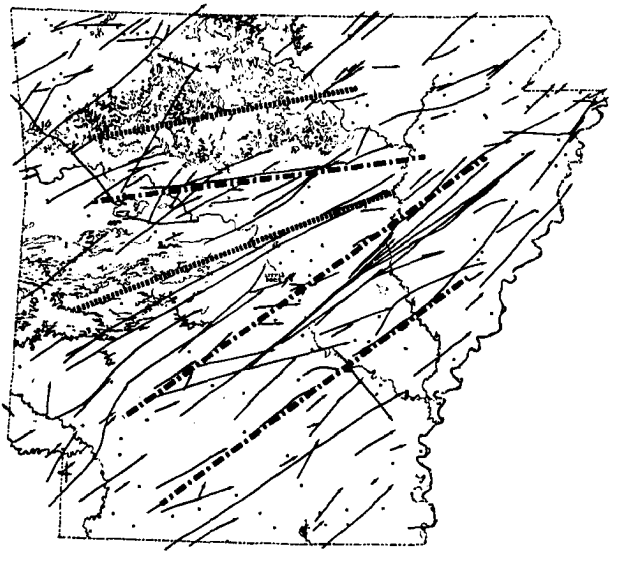

Fig. 2 Tornado paths, 1879 to 1955, in Arkansas, with indicated terrain contours of 1000 and 2000 feet above sea level; after Asp (1956). The superimposed straight lines (heavy dash-dots for supposed "tornado alleys", and heavy dots for "shunt regions") mark the positioning of detailed topographic profiles selected by R. Gallimore for calculation of the terrain-variance spectra shown in Fig. 3.

Superimposed on the reproduction of the original chart by Asp (1956) in Fig. 2 one finds five lines, two along the shunted region and three following tornado alleys. Along these lines R. Gallimore (a graduate student at Madison) has evaluated the h-versus-x series using detailed topographic maps. Fig. 3 shows tentative results of the subsequent spectral analysis normalized with the aid of total variances (indicated on the graph). The key in the upper right hand corner suggests that the topography spectrum for tornado alleys can be characterized by an overall decrease with an exponent of -3, while the shunted regions appear to follow the "minus-three" exponent only at lower wave numbers, changing to a "minus-one" exponent at a wave number of about one cycle per ten miles.

It appears worthwhile to show briefly what such exponent values (n) mean physically. Assume, for simplicity, that the normalized variance-spectral-density (p_i) represents the squared value (h_i^2) of average amplitude (h_i) pertaining to an elementary wave centered at a certain wave number[1] (k_i), or its reciprocal which is the wave length ($L_i = 1/k_i$); thus, with $p_i \sim h_i^2/k_i$, a given exponent value (n) in an

empirical power law ($p_i \sim k_i^{-n}$) corresponds to $h_i \sim k_i^{(1-n)/2}$, or $h_i \sim L_i^{(n-1)/2}$. Consequently, n = 3 suggests h_i being directly proportional to L_i; this is the special case of uniformity of slopes for all disturbances of any wave length (h_i/L_i = const). Correspondingly, n = 1 indicates that h_i is independent of L_i which is commonly referred to in spectral analysis as "white noise". For turbulence theory, another special case with n = 5/3 is highly significant since it applies to the so-called inertial subrange of the turbulent spectrum. This exponent

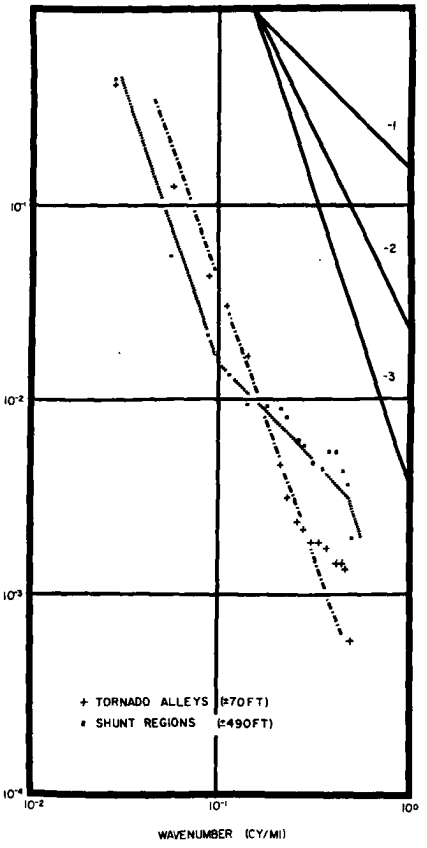

Fig. 3 Log-log diagram of normalized spectral density for terrain variability versus wave-number; separately for "tornado alleys" and "shunt regions" in Arkansas as depicted on Fig. 2. Straight lines in the upper right corner provide a code for estimating exponent values in power-law approximations of spectral density in certain wave-number ranges.

value implies a gradual increase of the ratio h_i/L_i with decreasing L_i, as schematically indicated in Fig. 4 together with the schematical interpretation of the exponent value n = 3, and a few others.

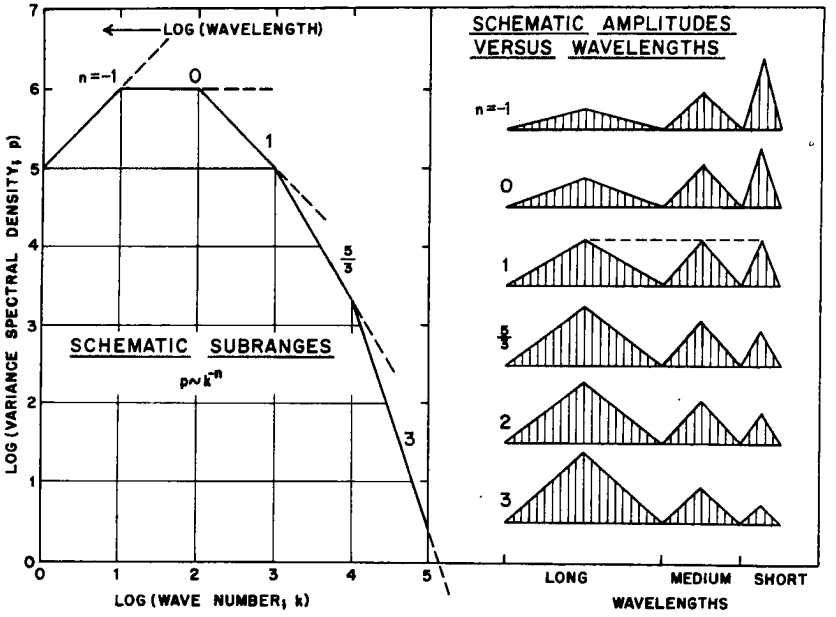

Fig. 4 Schematic interpretation of exponent values in power-law approximations for spectral density as a function of wave-number.

It may be added that such visual aids in illustrating the physical meaning of certain exponent values for subranges of spectral laws has proven to be quite helpful to the student, according to my personal experience, especially, when spectral laws are first introduced in connection with truly stationary statistical examples such as the above h versus x series, rather than turbulent time series with their fleeting and complicated structure.

With the above in mind the results shown in Fig. 3 appear to suggest that tornadoes tend to shy away (or even may not develop, unless conditions are especially favorable), when the terrain structure corresponds to white noise at wavelengths of ten miles and less. A "critical" scale of about ten miles appears to agree with horizontal over-all dimensions of the convective systems which generate tornadoes. This

tentative result invites further study; it will be acceptable only when supported by independent observational facts. However, in principle, it appears to conform with empirical findings which have led in aerodynamics to a distinction between boundary "waviness" and true "roughness". The latter concept will apply only when the interface structure corresponds to a random feature such as "white noise". Actual terrain waves may indeed lack aerodynamical significance. To a certain degree this statement was supported by the results of extended studies by Kung (1963). Kung estimated dissipation of mechanical energy in the atmospheric boundary layer utilizing the concept of "geostrophic drag coefficient" as developed by H. Lettau (1959, 1962). These estimates were compared with results obtained using a drag coefficient by Cressman (1960) which is based on the number of terrain ridges (of given amplitude) running, perpendicular to the wind, across a grid square of a numerical model of weather development. Interestingly, for the mountainous western parts of North America, Kung found that the Cressman coefficient produced overestimates of energy dissipation. The problem is far from being solved. Further work on aerodynamical effects of mountainous terrain are desirable and necessary before one can speak convincingly of "putting mountains into a numerical model", even with a restriction to kinematic aspects of the problem only.

3. Case Studies of Atmospheric Boundary Layer Structure Over Mountain Slopes -- Descriptive Features

3.1 The Air over the Peruvian Desert along the Pacific Slope of the Andes

3.1.1 General Description: Several decades of climatic records at a variety of stations, from Chile to Ecuador, have established that nowhere else on earth is there a desert of such extreme aridity than in the narrow strip (more than 3000 km long but hardly more than 30 to 100 km wide) parallel to the coastline, as well as crestline of the westernmost chain of the high Andes peaks. There can be a rather wide-spread maritime layer of overcast and occasional drizzle ("garúa") below approximately 800 m terrain elevation. Above this layer, however, the region has abundant sunshine, and desert conditions exist in spite of tropical latitude and the close vicinity of the unexhaustible moisture reservoir of the Pacific Ocean. The fact that snow-covered peaks are visible to the east enhances the impression that this desert is somehow strange, or out of place there. Pictures received from television cameras on artificial satellites illustrate the frequent lack of clouds in this narrow long region. An example is Fig. 5, taken by the Suomi-Parent camera aboard the Synchronous Satellite (ATS) which was launched in December of 1966. The ATS pictures included the western parts of South America only before the satellite had reached its final position above the central Pacific Ocean. Figure 6 is a reproduction of a chart constructed by Meigs (1956) showing the arid zones of the lands. It documents clearly the length and the narrowness of the desert region under discussion, as well as certain patterns of aridity over the continents which will be discussed in later sections. For further climatic details reference may be made to standard textbooks or monographs such as the one by Trewartha (1966).

Conventionally, the presence of relatively cool upwelled water along the coast is assumed to be the major factor which contributes to intensified aridity, by chilling and stabilizing the boundary layer of the atmosphere. Like other investigators, Trewartha (1966, pages 28 and 29) finds some puzzling features in connection with the conventional explanation of coastal deserts. For example, he notes that the cold upwelled water and the associated aridity in Peru and Ecuador continue remarkably farther equatorward than appears warranted by possible existing anti-cyclonic patterns of surface pressure. In my opinion, the weakest point in the textbook explanation of "cold-water deserts" is that cloud- or rain-producing circulation accelerations which lead normally to land and sea breezes (of either diurnal or seasonal cycles) should be stronger, the colder the water and the drier or warmer the land; this is to say that the circulation-generating physical forces

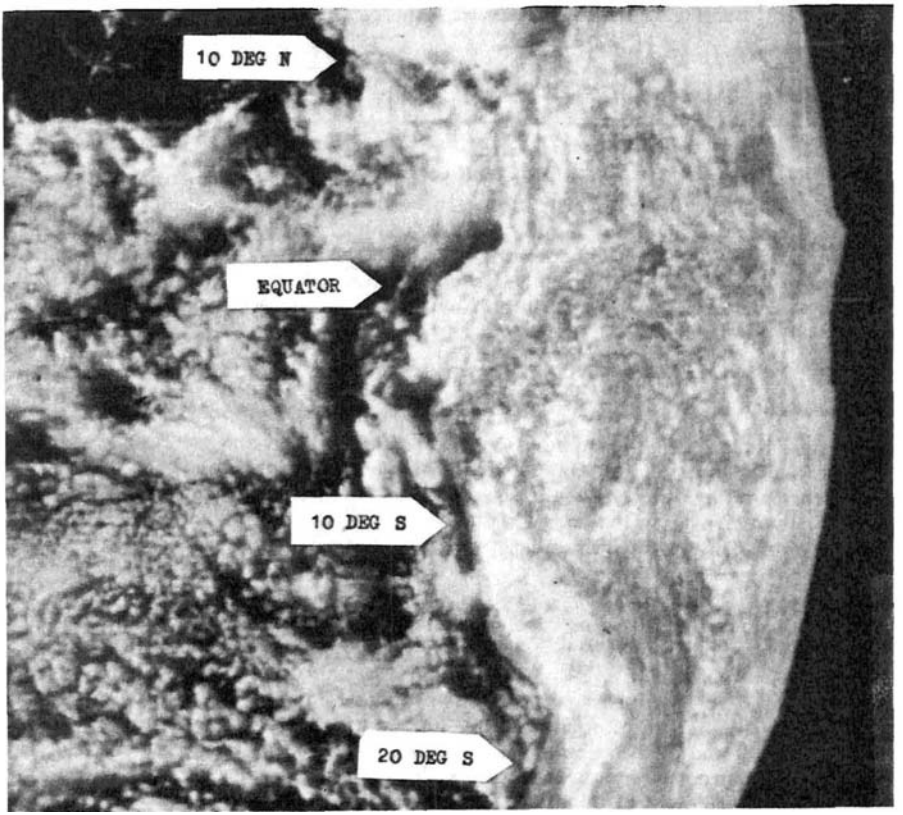

Fig. 5 Section of a photograph of the visible disk of the earth taken from an altitude of 22,300 miles by the Suomi-Parent Spin Scan Camera on the Application Technology Satellite (ATS), on December 10, 1966. The added "markers" indicate the Pacific coastline of the Americas at four latitudes. Note that the west slope of the Andes chain shows a narrow band of generally low cloudiness beginning at the equator.

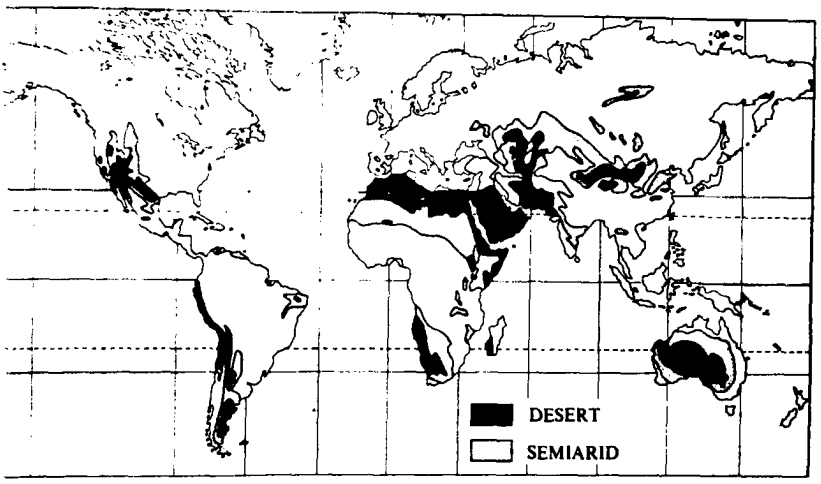

Fig. 6 Preponderance of dry regions of the Earth's continents (exclusive of the polar zones), after Meigs (1956). Note that the latitude circles shown include only equator, tropics (of Cancer and Capricorn), 30 deg and 60 deg (North and South). Certain tendencies towards an organization of dry regions with respect to equator and 30 deg latitude will be discussed in Section 6 as possible effects of mountain meteorology.

will be intensified if the thermal contrast between land and water is increased. The question arises whether or not both, the cold coastal current and the aridity, could be effects of the same common cause, rather than one being the cause of the other. A convincing answer will only come from detailed studies of the actual atmospheric circulations in the region.

As a consequence of my proposal for a field investigation of small-area meteorology and micro-meteorological wind action in connection with dune migration in the Peruvian desert, a University of Wisconsin expedition went to the Pampa de la Joya (about 17 deg S) during July of 1964. Here, an area of about 100 km^2 forms a gently sloping plateau between 1100 and 1300 m above sea level which is completely without vegetation but dotted by approximately 1100 individual sand dunes. The average crest height of the dunes is two to three meters and almost all show the perfect crescent-shape of the true barchan which is evidence that they are actively wind-driven.

According to Bailey (1906), climatic records taken in this dune field (at the railroad station of La Joya) from 1892 to 1895, did not show a single measureable rainfall; recorded were only occasional "traces" of less than 0.01 inch. The geographic environment is quite unique.

From our camp the towering massifs of Chanchani and El Misti (both exceeding 19,000 feet) were looming in the east at a distance of about 80 km. Towards the west, the stratus deck of the maritime layer (at about 800 m above sea level) was often visible since the coast was only 30 km away. It seems to be largely forgotten that repeated Harvard expeditions, before and around the turn of the century, had produced an excellent set of records for a systematic study of tropical mountain climatology. For several years a chain of climatic stations had been active, from Mollendo at the Pacific coast, via La Joya (1260 m), Arequipa (2400 m), and several other stations at ever higher altitudes, up to the summit of El Misti (5800 m). Hann (1909) has devoted several analytical studies to the climatology of this region. Details will be discussed in the next two sections.

From this wealth of existing climatic information only those elements will be singled out which are most relevant to the present discussion of boundary layer structure over mountain slopes. My thesis will be that the dominant factor which causes the extreme aridity of the Pacific slopes of the Andes, from Chile to Ecuador, is an atmospheric local-regional circulation of diurnal periodicity. The air motion is generated by the cycle of daytime solar heating and nighttime cooling on an extended mountain slope, together with resulting pressure gradient oscillations, and the effects of Coriolis accelerations. The ensuing "mountain slope breeze" is of a new type for which the name "thermotidal wind" is proposed. The main component of this air motion occurs in vertical planes parallel to the general direction of the contour lines of the terrain. As a secondary effect, subsidence of air down the slope can be stimulated during daytime which may be intense enough to overrule the "anabatic" or up-slope, daytime-phase of a direct circulation acceleration.

3.1.2 The Dunes of La Joya as Indicators of Mountain Breezes: Travelers who view the dunes of the Pampa de La Joya can hardly escape being impressed by the esthetically appealing, perfect, crescentic shape of the average barchan, in spite of its substantial bulk (of about 1000 tons of sand, on the average). For centuries these dunes have been known to migrate towards the north-northwest at an average rate of approximately one mile per one hundred years. Other striking features are the color contrast between the reddish-brown desert floor and the greyish-white barchan sand, or the intricate ripple patterns on the windward slopes. In Fig. 7 three medium-to-large barchans can be seen. Other photographs of the dune field may be found in textbooks of geomorphology, for example, see Leet and Judson (1958).

The dunes of La Joya have been the object of scientific studies for many decades. Direct information on monthly mean celerity for at least one individual barchan of average size is available for a period of several years; see Fig. 8, which was based on data supplied by Bailey (1906). Supplementary to the results summarized in Fig. 8, it is reported that the displacement of this dune occurred always in the same direction while the rate averaged 18.7 m/year in 1892 to 1894, 19.1 m/year in 1894 to 1896, and 17.5 m/year in 1896 to 1897. Thus, for a period of nine years (1892 to 1900) the mean celerity was 19.0 m/year, showing surprisingly little variability from year to year. More recently, interesting results were reported by Finkel (1959) who,

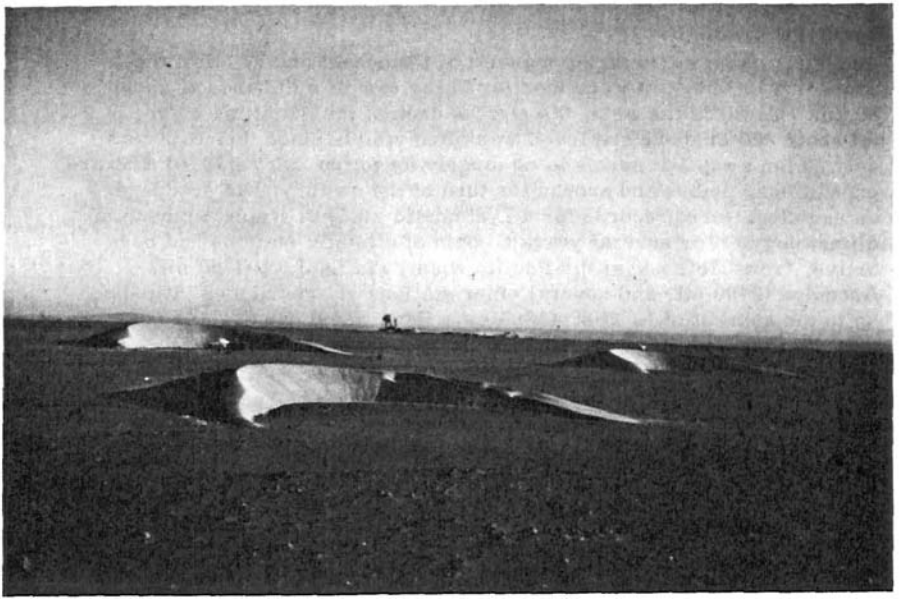

Fig. 7 The three barchans near the micrometeorological site of the University of Wisconsin Field Study Group in the Pampa de La Joya, July, 1964. The camera axis points roughly to SW. Note the S-shaped deformation on the east-horn (to the left) and the "notches" on the opposite west-horn, both caused by nighttime katabatic winds.

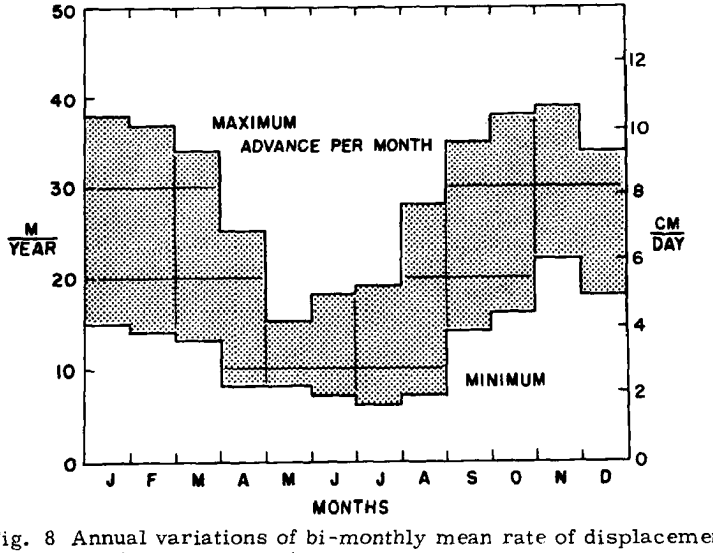

Fig. 8 Annual variations of bi-monthly mean rate of displacement (expressed in m/year, also cm/day) for one individual barchan in the vicinity of La Joya station. The width of the band depicts the range between the highest and lowest values during the years 1897 through 1900.

for the first time, evaluated two aerial photogrammetric surveys made in 1953 and repeated over the same region in 1956. A quantitative study of average dune celerity as a statistical function of height, shape, and size of individual barchans was thus begun. However, no micrometeorological data were at the time available for estimates of actual surface drag and a more detailed investigation of the dynamics and energetics of the air flow which moves the sand dunes. To fill this gap was the objective of the University of Wisconsin's field activities in July of 1964. As already attested by Bailey's observations, individual dunes tend to be remarkably persistent, in spite of their continuous migration. After our arrival at the field site we encountered no difficulty in identifying most of the individual barchans surveyed and photographed by Finkel seven years earlier. In addition to extending the period over which the dune migration can be studied area-wide, our work included measurements of momentum and heat exchange at the desert-air interface, and kinematics and aerodynamics of sand movement, naturally, and in the form of controlled experiments. Results will be published in a forthcoming report of the Center for Climatic Research at the University of Wisconsin. Here it may suffice to give the following summary: (i) Within the tolerance of only a few degrees the area average of multi-annual mean direction of dune migration is perpendicular to the general trend of fall-lines on the plateau; (ii) winds with proper direction and of sufficient strength (so that the friction velocity of the wind profile exceeds the threshold value necessary to start sand movements) occur daily but only for several hours around and after noon; (iii) functional relationships (considering surface drag, threshold velocity, dune geometry, sand density, etc.) can be established to explain bulk-sand transport; these relations are equivalent to a calibration curve so that the dunes can be usefully employed as climatic indicators of air flow; the measure obtained is of the nature of a directive dosage, that is, strength (above a critical threshold value) times duration of wind action in a certain azimuth.

On the basis of such calibration, Fig. 8 must mean that the speed of the dune-moving wind is positively correlated with local insolation intensity, since a pronounced annual variation of both elements shows the maximum value in the southern summer. Such behavior contrasts with that of winds which are dependent on the general circulation of the atmosphere; namely, their annual variation will exhibit maximum speed in winter (on any hemisphere), at the time when the meridonal gradient of insolation is greatest, rather than heating intensity at a given latitude. In addition to other points, this argument, too, supports a local-regional nature of the dune-moving winds on the Pampa de La Joya. However, it shall be demonstrated by the following that we are dealing here with neither a sea breeze nor a combined sea-mountain breeze. Both would also be classified as circulations due to local heating, with the wind blowing towards the shoreline and up the incline; conventionally, a mountain breeze would belong to the elementary type which is also known as "anabatic" flow; this has the opposite direction of a nocturnal phase, known as "katabatic" flow in a down-hill direction.

A close inspection of Fig. 7 reveals that each one of the three dunes visible is somewhat deformed. We refer here to the fact that the crestline appears slightly S-shaped on the east horn, while a few "notches" show on the west horn. By direct observation it was established

that these deformations (including a nocturnal "turning-up" of the crestline on the west horn) are caused by regularly occurring katabatic winds. Developing during the early evening hours, they continue to blow until one or two hours past sunrise. While their speed (measured at 3.2 m above the desert floor) is nearly as high as that of the daytime wind, ground drag and, subsequently, friction velocity are relatively low due to strong inversional stratification of air temperature. Thus, the katabatic wind is incapable to move the sand unless its intensity is locally reinforced, such as by the narrowing of streamlines in flow over obstacles. Only at the particular section where on Fig. 7 the notches and the S-shape can be seen, both conditions of sufficient obstacle height and steepness in the direction of flow are satisfied. We learned by observing that disturbances of the horn configuration created by night breezes tended to be straightened out a short time after onset of the dune-moving wind, which blew during our stay on the pampa with some regularity only between about one hour before and three hours after local noon. Since the katabatic flow follows the fall-line of the terrain and disturbs only the flanks of the dunes (while they march in the direction to which the horns are pointing) this disturbance can be taken as photographic evidence that the dunes migrate indeed nearly perpendicular to the fall-line of the slope. This, of course, is confirmed by direct surveys.

In summary, the dunes of the Pampa de La Joya must be considered as useful climatic indicators for existing air flow patterns. The information derived from them suggests that there are only two significant winds in the area, namely, the generally easterly nocturnal or katabatic flow, and a generally southerly daytime breeze which produces sand migration. Most remarkable is the fact that the two wind directions are about 90 deg apart rather than 180 deg as should be expected for a coherent and direct circulation system if caused by the diurnal cycle of insolation. On a mountain side or near a coastline this means that the anabatic phase of air circulation is missing on the pampa. Independent climatic data supporting the validity of this important conclusion shall be discussed in the next section.

In the literature one can find statements that dune migrations in the coastal desert of Peru are caused by a sea breeze. Certainly, there is daytime intensification of wind speed, all along the coast, but without a significant turning, or daytime appearance of significant onshore components. The rule seems to be that the wind remains nearly parallel to the general direction of the coastline. In another visit to Peru in 1966, I had the opportunity of viewing the coastal desert near Trujillo (about 8 degs) from overflights by light airplane. Barchans do exist, but fail to exhibit the perfect crescent shape of those on the Pampa de La Joya. The essential point to be made is, however, that horn orientation in the northern coastal desert, too, indicates a direction of dune migration more parallel than perpendicular to the coastline.

3.1.3 Evidence of Direct and Modified Diurnal Circulations: The extent of the overheated air layer developing over the Andean slope during daytime (even under southern winter conditions in July) is demonstrated in Fig. 9. This cross section between the Pacific coast and the summit region of El Misti incorporates terrain heights and air tem-

peratures. Free tropospheric temperatures were derived by averaging radiosoundings at Lima, Peru (12 deg S) and Antofagasta, Chile (24 deg S), since the mid-latitude for these two stations corresponds very closely to that of the Mollendo-Arequipa region. Entered on Fig. 9 are also climatic data for July (monthly mean temperatures, and mean spread between daily maximum and minimum) according to observations at Mollendo, La Joya, and Arequipa, based on the report by Bailey (1906), as summarized by Hann (1909). Additional measurements are included which were obtained on several days in July, 1964, by members of the University of Wisconsin group, while traveling on roads and highways up and down the slopes of the region. These temperatures were measured by a mercury-thermometer being held into the airstream on the shaded side of the cab of our trucks. They refer to times between mid-morning and late afternoon. Altogether the available temperature information demonstrates clearly the existence of a heated air layer at daytime, which follows the contours of the terrain. Naturally, the overheating at the actual desert ground was more intense; we measured on several days up to 46° C at the sand/air interface near the micro-meteorological site, and up to 65° C on the slipface of a barchan when the sun angle was right.

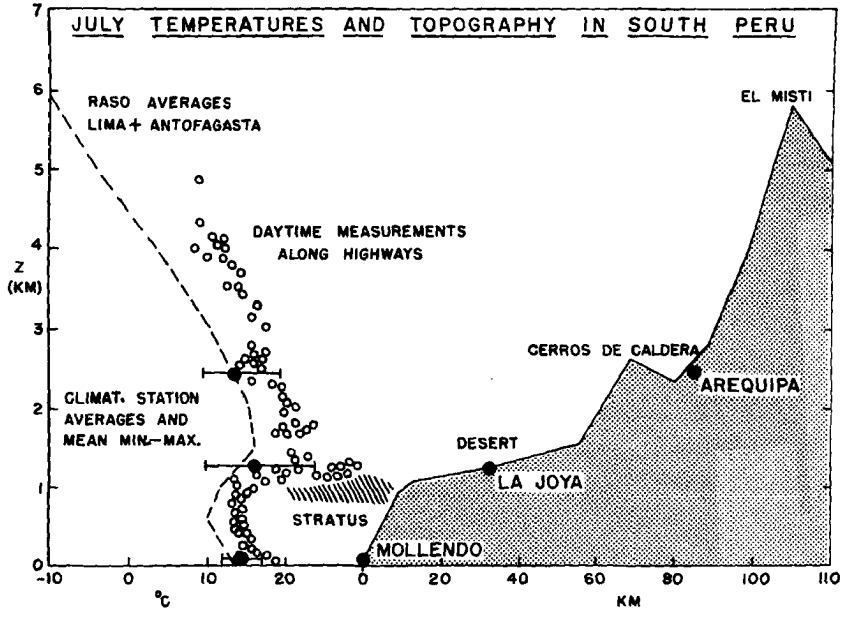

Fig. 9 Cross section (approximately in a west to east azimuth) at about 17 deg S latitude, from Mollendo on the Pacific Coast, towards the peak of El Misti, across the Pampa de La Joya, illustrating the intensity and extent of the overheated air layer along the Pacific slope of the Andes Mountains, during daytime even for southern winter conditions.

It is a well-known fact of mountain meteorology that heating of the air along a terrain slope affects systematically the pressure field. Fig. 10 shows July averages of hourly values of barometer readings at Mollendo and Arequipa, based on Bailey's data (1906). At this tropical latitude the semi-diurnal oscillation is the dominant feature. However, barometric differences between the stations show a 24-hourly variation, very similar to that of temperature. Note for later use, that the maximum value of the difference curve on Fig. 10 occurs 3 hrs. after noon. This suggests that the average or prevailing zonal pressure gradient (with the higher pressure over the Pacific Ocean) will tend to show a minimum value at daytime and a maximum at nighttime. According to elementary textbook discussions, a differential heating of air at any fixed level, as suggested in Fig. 9, or subsequent pressure gradients as illustrated in Fig. 10, should stimulate either

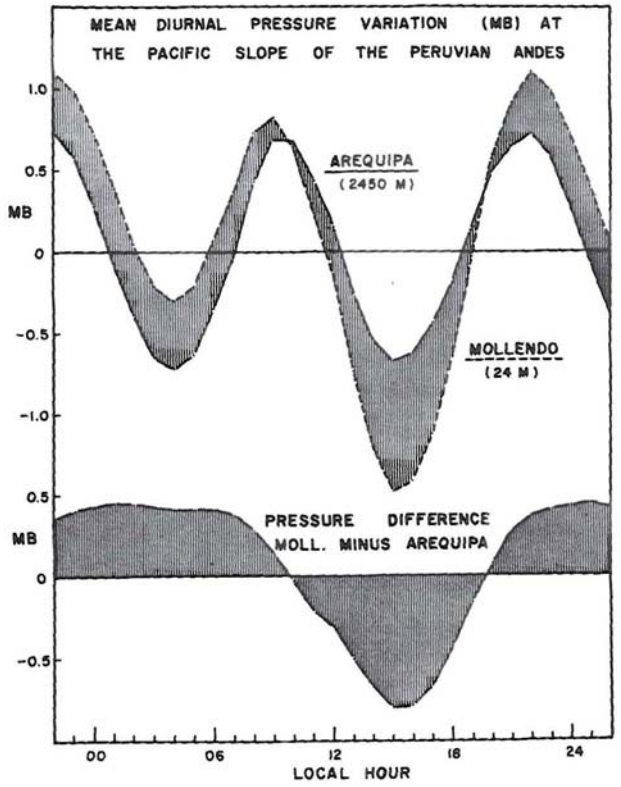

Fig. 10 Departure of hourly values of barometric pressure (in mb) from running-24-hour-means, for the two climatic stations Mollendo (at the Pacific coast) and Arequipa (about 100 km east of Mollendo); also shown is the diurnal variation of hourly pressure differences for the two stations. Trends were calculated from extensotables in Bailey (1906).

organized updrafts in the form of anabatic flow, or convective activity. In any case, clouds would be expected to form during daytime over the land, especially since the air in this particular region is not very dry. For example, according to Bailey (1906), the climatic averages at La Joya for the month of July, at 2 p. m., are 40% relative humidity and 72.4° F air temperature. Yet, surprisingly, the climatic observations as tabulated by Bailey show a diurnal variation of cloud cover with pronounced daytime minima as illustrated on Fig. 11. We also noticed at La Joya that the sky became bluer towards noon. During occasional visits at Mollendo, a slight thinning out of the stratus deck could be observed around midday; this, however, might have been a direct "burning-off" effect due to insolation absorption by the maritime layer. The only daytime or convective-type cloudiness noticeable at all in July of 1964 from our vantage point on the Pampa de La Joya was a string of small cumulus which occasionally developed around the cone of El Misti, with estimated cloud base at least 3000 m above sea level.

The facts, summarized above, suggest that during daytime, a subsidence prevails, or develops, in the region. The question arises why the existing pronounced overheating of the mountain slopes fails to generate updrafts and convective clouds. As shall be demonstrated later, the available Rawin soundings in Pacific South America do not indicate, at and below mean crest levels, a significant prevailing east

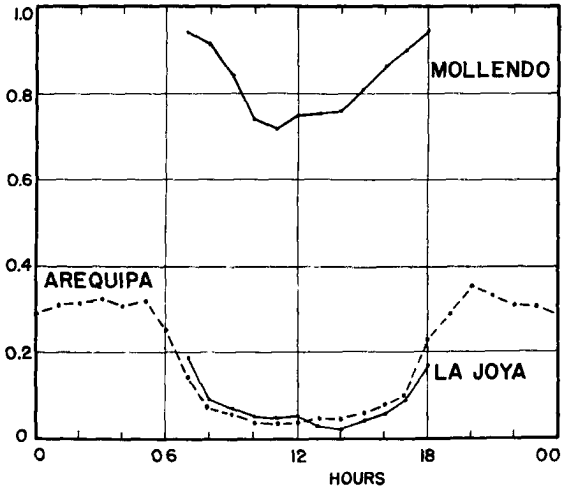

Fig 11 Climatic means showing diurnal trends of cloudiness at the Pacific slope of the Andes Mountains in Peru; see Fig. 9 for the relative location of the three stations. Hourly averages were calculated for three months (July through September), based on extenso tables of recordings during the years 1892 to 1895; a starlight recorder (and hence, hourly data for nighttime) was available only at Arequipa.

component of the general circulation; if this would exist at the proper levels, it might explain subsidence as a *foehn* effect of the Andes mountains. But even if foehn components would be present, the diurnal variation of subsidence-intensity, with a daytime maximum, needs explanation. In Fig. 12 the result of several types of hourly observations at our micro-meteorological station near La Joya are summarized including data on sand transport, friction velocity, etc. In relation to the present discussion, note the strong diurnal variation of wind speed at the 3.2 m level which reveals two maxima per day. Hourly values of wind direction indicated on Fig. 12 confirm that the nocturnal wind maximum represents the katabatic flow, while the daytime maximum is caused by the dune-moving winds. In Section 3.1.2, it was

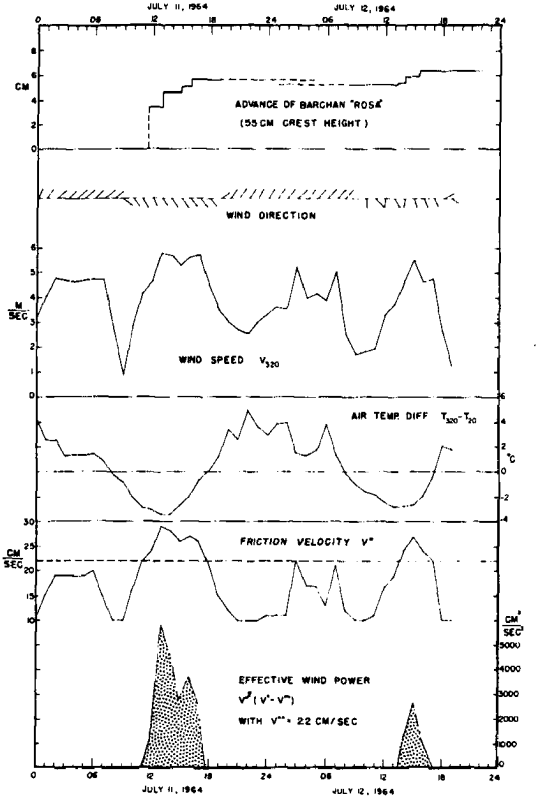

Fig. 12 Two-day summary of hourly meteorological data measured and evaluated by the University of Wisconsin Field-Study Group at La Joya. Included are measured advances of a small barchan; hourly values of wind direction and speed at 320 cm above the desert floor; vertical temperature difference between 320 and 20 cm; evaluated shear-velocity of wind action (with indication of the threshold-velocity -- dashed line-- for sand movement); and finally, calculated effective "wind power" with daily "dosage" being proportional to the hatched areas under the curve.

discussed that the angular spread between these two flow directions is essentially 90°. Relatively slight departures from the 90°-turning were occasionally observed. As illustrated on Fig. 13, the katabatic flow of July 12 (from 02 to 08 a. m.) came from northeast; in the morning, for about 40 minutes, beginning at 09 a. m., the wind tended to be anabatic but remained weak. Later, it became erratic until the onset of the dune-moving wind (from the south) at 11 a. m. which lasted for almost six hours. Sometimes the southwind appeared to set in with the passage of a miniature coldfront.

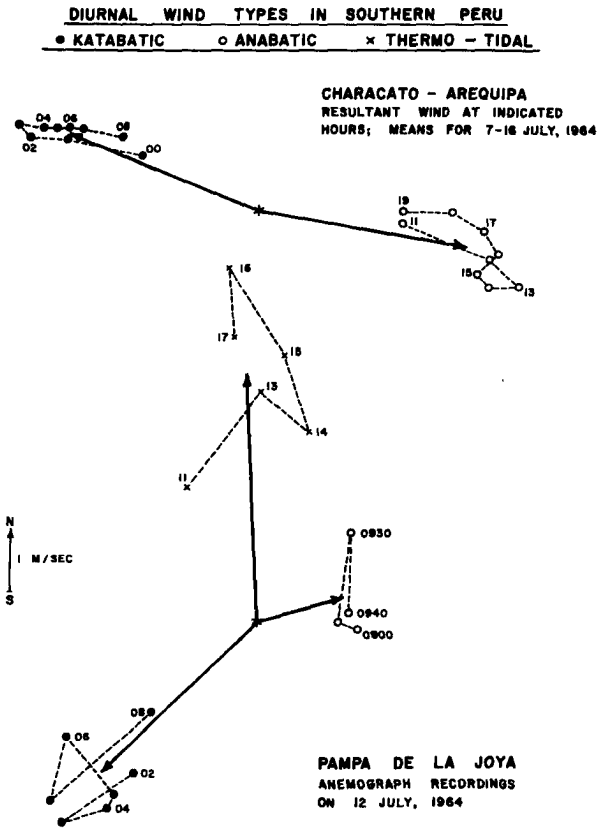

Fig. 13 Vector diagrams showing typical diurnal breezes at Arequipa (calculated from hourly anemograph recordings at the Geophysical Observatory Characato, averaged for the period 7 to 16, July, 1964) in comparison with winds in the Pampa de La Joya. Numbers at the end point of the wind arrows indicate the hour of observation (24-hr clock), full circles for local katabatic direction, open circles for local anabatic direction, while crosses denote the thermo-tidal breeze on the Pampa.

In the upper half of Fig. 13 resultant winds for every hour of a ten-day period are illustrated as derived from recordings at the Geophysical Observatory near Arequipa (see Fig. 9 for an illustration of relative geographic location). Obviously, at about 2500 m above sea level, only two wind directions prevail which are nearly 180 degrees apart. This contrasts remarkably with conditions in the lower desert region. Hann (1909) already noted that the diurnal change between nocturnal east and daytime west winds occurs with astonishing regularity at Arequipa, through all seasons. Our own experiences during repeated visits in July of 1964 confirm these findings, and we attempted to collect locally available meteorological information. In addition to the data used in Fig. 13, we obtained results of pilot balloon ascents, made twice daily by CORPAC personnel at the municipal airport. Averaged profiles of the west component for the ten-day period are presented in Fig. 14. Supplementing Fig. 13, the pilot balloon data at Arequipa reveal details of the vertical structure of the two opposing air currents. Apparently, at this altitude, the daily change of winds corresponds in a near-to-ideal manner to the katabatic-anabatic system of a direct circulation. This contrasts markedly with conditions in the desert regions at lower altitudes of the Andean slope. It can be concluded that there is sufficient evidence for a significant modification of the direct circulation, as far as the daytime phase is concerned, at and below altitudes of approximately 2000 m. The problem remains to prove that corresponding modifications occur on terrain slopes in other geographic regions, and also to justify such modifications theoretically.

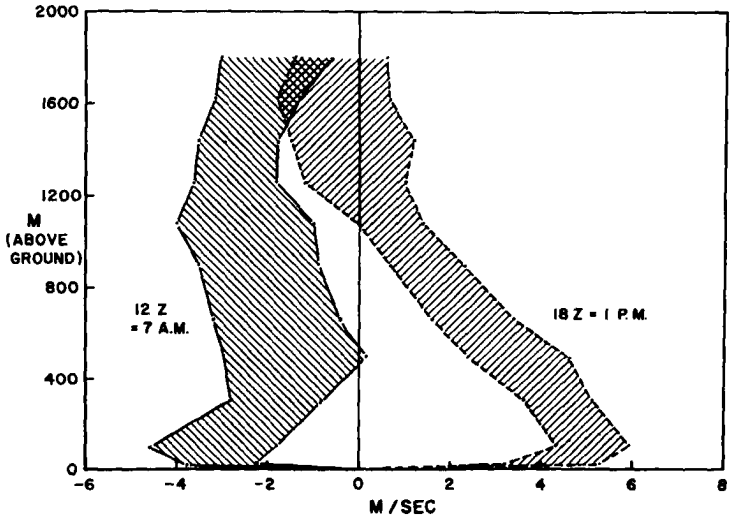

Fig. 14 Vertical profiles of west-component, calculated from two daily pilot-balloon soundings routinely made by CORPAC personnel at the Municipal airport of Arequipa, for the period 7 to 16 July, 1964. Local time is five hours behind indicated standard world (Z) times. The bands shown on this graph are one standard deviation wide and centered at the mean values computed separately for the local morning and afternoon soundings.

3.2 The Air over the Large-Scale Terrain Slope between the Mississippi River and the Rocky Mountains

3.2.1 The Low-Level Jet Stream: In the early 1950's, while being in charge of several research projects on atmospheric boundary layer structure, at the Geophysical Research Directorate of the United States Air Force, I conceived the idea of a coordinated major field experiment. It was proposed to carry out a comprehensive series of detailed meteorological measurements, at a carefully chosen site in uncomplicated terrain, from sub-surface levels to at least 2000 m above ground, using stands, masts, and towers, in combination with a variety of aerological techniques. These observations were to be concentrated on 24-hour periods during which initial and predicted synoptic conditions did promise isobaric gradients of sufficient strength, persistence, and uniformity so that the structure of the atmospheric boundary layer could be expected to respond, in an elementary fashion, to the natural cycle of daytime heating and nocturnal cooling at the earth-air interface.

This proposal led directly to the "Great Plains Turbulence Field Program" which was held in August and September of 1953, in the open and unobstructed grassy plains of north-central Nebraska, near the town of O'Neill (about 42.5 deg. N, and 98.5 deg. W). Details of the program and major results are summarized in the two volumes entitled "Exploring the Atmosphere's First Mile", edited by Lettau and Davidson (1957). Participating research teams from several universities and federal agencies concentrated their observations on seven around-the-clock "general observation periods", with bi-hourly data collection. Emphasis was put on detailed and representative measurements of directional wind shear throughout the entire boundary layer. New aerological techniques developed by the late G. Loeser -- compare Lettau and Davidson, Section 6.1 -- produced highly interesting and even spectacular results. Quite regularly at about sunset, the south wind began to increase in the layer of about 450 m above the ground, and to decrease at and above 1000 m. These developments led to a velocity peak, shortly after midnight, with a 22 to 24 m/sec south component at about 400 m; above this level of maximum speed there was a gradual approach to a slight north wind beyond 1500 m. An example of the extreme shear in the wind profile, positive below 400 m as well as negative above 400 m, is illustrated in Fig. 15. The term "low-level jet stream", first used in earlier work by Means (1954), appears fully justified, even though this air current is basically of geostrophic nature and has only superficial resemblance to a true jet (in which fluid spurts out of a nozzle, as a direct effect of inertia due to an initial pressure head).

During the last decade several reports have been published which deal with the descriptive analysis of the low-level jet stream. For example, there is the work by Hoecker (1963, 1965) who organized an observational program using a chain of special pilot balloon stations, roughly along the 35th parallel, between Little Rock, Arkansas, (81 m elevation) and Amarillo, Texas, (1098 m elevation and 10 degrees farther west); there is also the work by Bonner (1965) who analyzed statistically the geographic occurrence of the low-level jet stream over

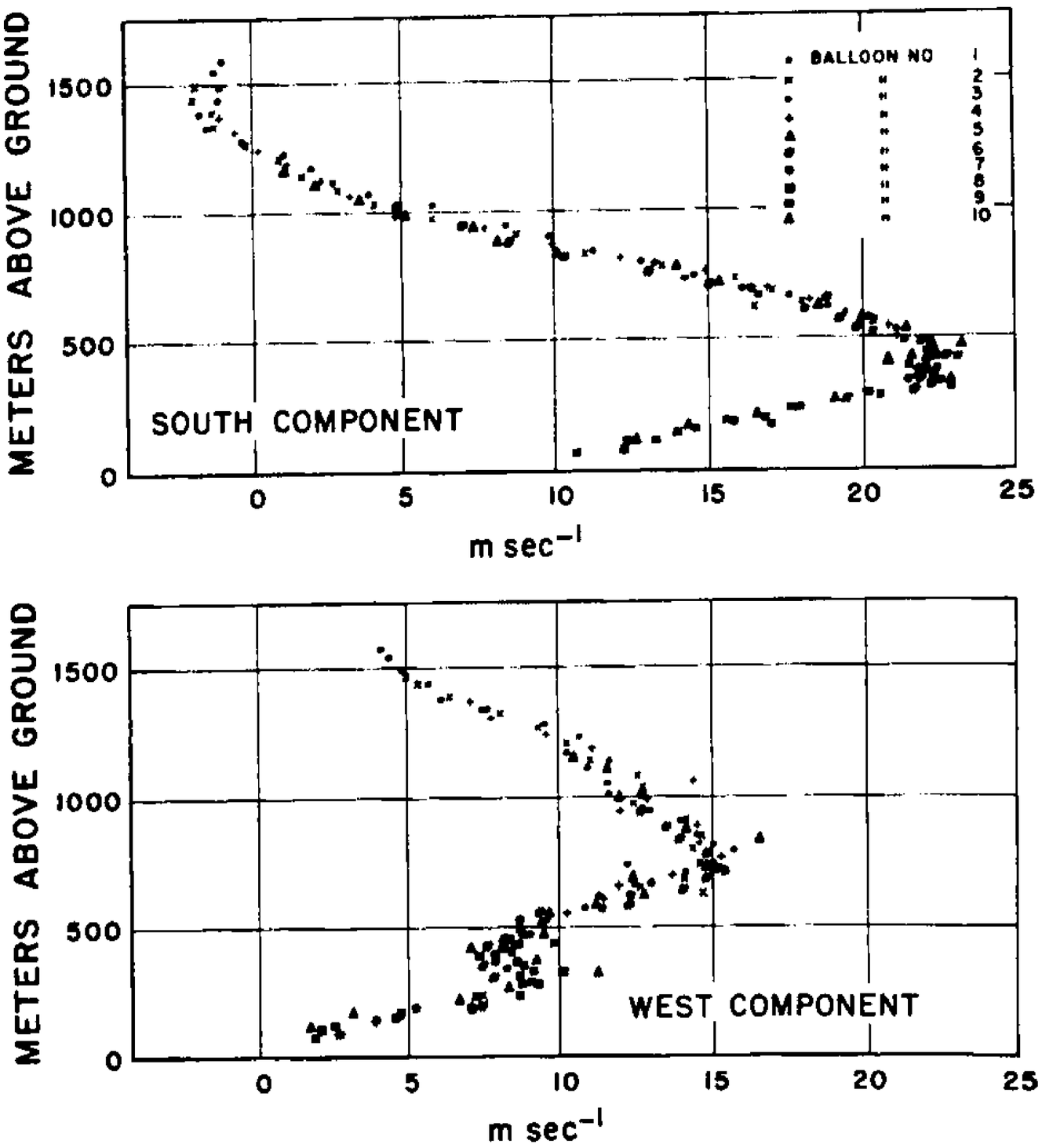

Fig. 15 Vertical profiles of the two horizontal components of air motion as observed during the Great Plains Turbulence Field Program near O'Neill, Nebraska. Exemplified is a peak-development phase of the low-level jet stream, at midnight 7 to 8 September, 1953. The profiles are based on more than 100 data points, all obtained within a total time of only four minutes, employing the Loeser-technique (phototheodolites, and a swarm of ten simultaneously rising, lamp-carrying balloons forming a vertical chain). For detail, consult Section 6.1 in Lettau and Davidson (1957).

the United States employing synoptic-network data from Weather Bureau pilot-balloon stations. Fig. 16 is reproduced from Bonner's report and illustrates several noteworthy features. For our discussion it is most significant that statistically the number of low-level jet observations shows a pronounced geographic maximum in central Oklahoma and Kansas. West of the Mississippi River, towards the Rocky Mountains, the phenomenon occurs five to six times more often than east of the Mississippi towards the Appalachian Mountains. For more details, reference must be made to the original report. It may suffice here to state that Bonner's charts, Hoecker's cross-sections, and other findings (including some to be discussed in Section 3.2.2) suggest that the low-level jet stream seems to prefer the mid-region of the east-facing terrain slope occupied by the midwestern United

States, and occurs at altitudes below the general crest-line elevation of the mountain ranges to the west. In north-central Nebraska, the region of the O'Neill experiment, where one appears to be far removed from real mountains, the terrain is also sloping at a rate of about 1:400, from west to east. The horizontal extent of this topographic incline is certainly comparable with that of meso-scale to synoptic-scale systems of meteorology, and the magnitude of the slope exceeds that of isobaric surfaces, or equals that of frontal discontinuities. It will be shown in later sections that the inclination of the terrain can indeed be highly important for generating circulations of diurnal periodicity, and that actually the low-level jet stream development of this region can be explained as a phenomenon of the boundary layer over large-scale mountain slopes, in a similar manner as the diurnal circulation in the desert region of Chile and Peru.

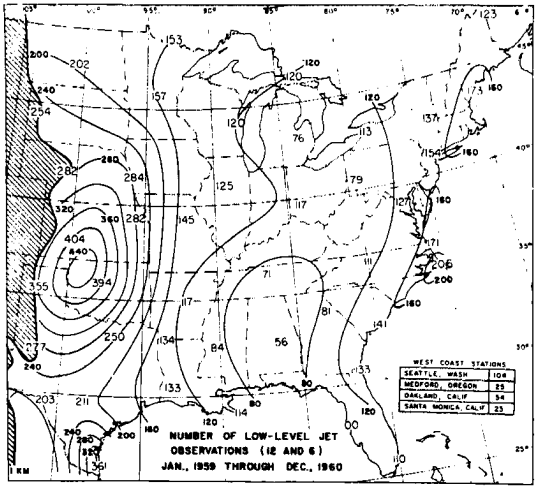

Fig. 16 Geographic distribution of a number of low-level jet occurrences for a total period of two years, according to evaluations by Bonner (1965) of United States Weather Bureau synoptic pilot-balloon network data.

3.2.2 Nocturnal Thunderstorms: Thunderstorms may develop whenever there is a sufficiently pronounced upwards motion of humid air, regardless of time, or geographic location. Over continents, thunderstorms occur most frequently during summer afternoons when, relatively speaking, solar heating is strong, the moisture level of the air is high, and the vertical gradient of temperature is steep. In the

region under discussion, a remarkable exception to this general rule is known to exist during the summer; namely, in parts of Kansas and Nebraska, up to 50% of all thunderstorms occur during the six hours between midnight and sunrise. Charts illustrating this peculiar regional-diurnal anomaly can be found in climatic source books; reference can also be made to Bleeker and André (1951). Specific charts which suggest very clearly that nocturnal thunderstorms over the Midwest are significantly correlated (in time and space) with the low-level jet stream have been prepared by Bonner (1966), or Pitchford and London (1962), in an extension of earlier work by Blackadar (1957) and others. We are dealing here definitely with non-frontal thunderstorms which are independent of disturbances of the general circulation. Among the factors which could explain a physical connection between low-level jet and strong convective actions are the following: (i) Destabilization aloft, due to injection of moist and warm air by the core of the low-level jet (that is, intensified horizontal advection which is strongly differentiated in the vertical). (ii) Convergence, or "piling-up" of air which forces it upwards, downstream of the region of maximum development of the jet.

The effect of convergence was investigated by Pitchford and London using an essentially synoptic-kinematic technique; computed patterns of vertical motion were found consistent with the observed convective activity. However, apparently not considered thus far has been a terrain effect or circulation acceleration up or down the general slope of the region. Possibly, this could represent an important contributing factor to the problem of daily cycles, with a diurnal alternating between stimulation and suppression of convective activity. It is suggested to link the diurnal period of thunderstorms with that of up-slope components which accompany the low-level jet stream, and to consider both in relation to the daily heating and cooling cycle of the lower atmosphere over terrain inclines of sufficient regional extent. Tentatively, let us outline the following points.

While air in the low-level jet moves essentially parallel to the contour lines of the slope, friction and Coriolis forces will set up secondary circulations in the direction of the fall-line. A natural tendency to updrafts during the day will exist in the region but may actually be suppressed, or overcompensated, by downslope components due to indirect causes. These modified circulations could be a consequence of the same basic processes which produce the low-level jet stream. At this point let us recall from section 3.1 the tendency towards daytime subsidence of air which appears to prevail over the Pacific slope of the Andes Mountains. A daytime downslope component over the midwestern terrain incline would indeed be a reasonable counterpart to the nighttime tendency to updrafts indicated by the nocturnal thunderstorms. The problem remains to explain certain differences in emphasis. Why is it that more spectacular appears to be the nighttime phase along the midwestern slope of the Rocky Mountains, and the daytime phase along the slope of the Andes Mountains? The major point of the argument, however, is the concept of secondary air circulation alternating diurnally between up- and downslope components, but just 180 deg out of phase, in comparison with an expected direct gravitational circulation, or a katabatic-anabatic wind system.

3.3 The Air Over Inland-Ice Slopes

As the third and last of the special case studies of boundary layer structure over mountainous terrain, the lower atmosphere over gigantic ice domes, such as found in Greenland and Antarctica, shall be briefly described. Here, net radiation at the snow-air interface is dominated by energy loss to space. Consequently, inversional thermal stratification prevails in the lower troposphere. On the flanks of the ice domes the denser air near the surface will show a tendency to downslope motion due to gravitational acceleration and katabatic winds of impressive strength can be frequently observed, but only in the coastal regions of Antarctica. According to Lettau and Schwerdtfeger (1967), in the interior of the continent with its uniform, gently sloped surface, and a shallow layer of extremely cold air in the lower atmosphere, the occurrence of a systematic downslope air-drainage, or even true katabatic winds, is the exception rather than the rule. Generally, the surface winds in Antarctica tend to blow at angles of at least 45° from the fall line of the terrain, so that lower elevations remain to the left of a man facing the wind. This is documented by many traverse reports and the climatic records of inland stations which have been so markedly improved in quantity as well as quality during the last decade. Furthermore, it is remarkable that frequently the surface wind is stronger, and shows significantly more persistence (measured by the vector-standard-deviation, the directional constancy, or any other suitable statistical parameter) than winds at and above the top of the inversion layer. Obviously, this noteworthy decrease of speed and constancy with height is contrary to the "normal" behavior of the wind in the boundary layer over most other parts of the earth's surface, wide land areas as well as oceans. This fact suggests that due to the peculiarities of topography and temperature stratification in the surface air over Antarctica, a mass distribution exists which causes a systematic alignment of the wind from the free atmosphere down to the surface level. In meteorological terms, this implies the effect of a terrain-induced thermal wind in the lower atmosphere.

In 1963, it was first demonstrated that such a special thermal wind can be generated by the pronounced horizontal gradient of air density which must exist in the lower atmosphere when cold air of approximately constant inversion depth lies over sloped terrain. Dalrymple, Lettau, and Wollaston (1966) used the South Pole observations from March to September, 1958, to show that the surface-wind regime at the Pole indeed can be explained by the "inclined surface-inversion" effect, together with internal friction and Coriolis force effects. In view of wider implications of the concept for the understanding of the surface-wind regime of a large part of the continent, it appeared desirable to test the theory with larger data samples for other Antarctic locations. In 1967, Schwerdtfeger completed such tests for Byrd Station, among other places, employing the observations of five winter periods, April to September, 1961, through 1965. Byrd is located at 80° S, 120° W, 1530 m above sea level, at a distance of about 700 km from the coast of the Amundsen Sea, 500 km from the nearest point on the Ross Ice Shelf; within a radius of about 100 km the surrounding terrain has an ascendent vector of about 2.5 m per km, towards the geographical azimuth of 57° when the South Pole is at 180°. The radiosonde-wind observations at Byrd Station were analyzed

by means of a new graphical method developed by Schwerdtfeger. Results for the layer between surface and pressure altitudes of 750 and 700 mb (corresponding to about 500 m and 1000 m above ground) are shown in Fig. 17.

For strong inversion cases, the thermal wind due to the terrain slope at Byrd has an average speed of 8 m/sec and a direction of 145^{o}, which compares well with the azimuth of 147^{o} for the terrain-contour lines of 1500 and 1550 m in the Byrd Station area. The importance of the thermal wind on the climatic regime of air motions in the Byrd area, and presumably over any gently sloped ice dome of sufficient extent, is made evident on Fig. 17 by separating the wind vector averages for days with strong inversion, from days which show a decrease of temperature with height of at least 0.1^{o} C per 100 m; the latter are labeled lapse-cases and are illustrated on the right-hand side of Fig. 17. Only for lapse cases is the wind aloft considerably stronger than near the surface which is the "normal" behavior; however, for the inversion cases, the wind speed decreases with height within the friction layer. This anomaly corresponds to findings by Dalrymple et al. (1963, 1966); based on their South Pole wind analysis they stated:

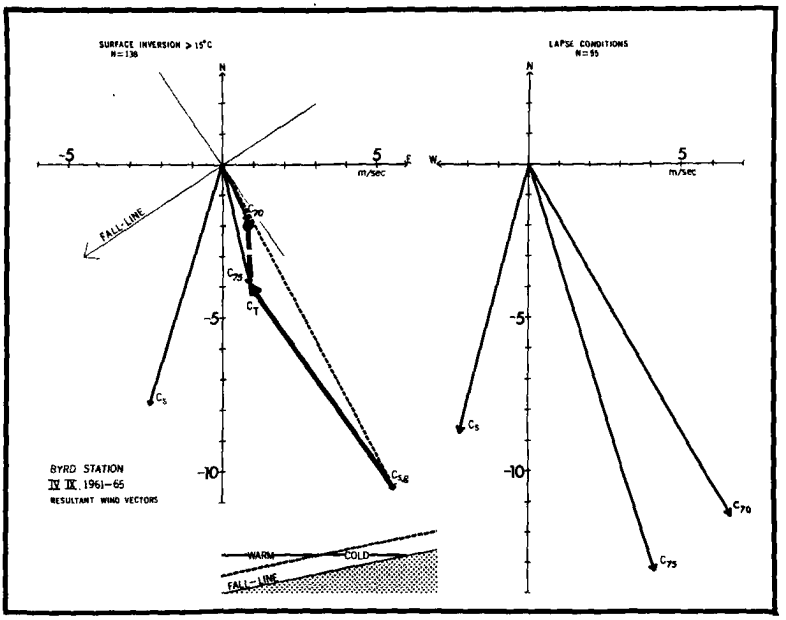

Fig. 17 Five-year vector averages of wind at Byrd station, April through September at station-level (s), 750 and 700 mb, on the left-hand side for strong inversion, on the right-hand side for lapse conditions.

"The results do indicate that the air motion in the lower atmosphere is controlled by surface friction and by the geostrophic motion in the free atmosphere above the inversion layer, modified (downwards) by the thermal wind due to horizontal temperature gradients which result from the general slope of the terrain".

It may be worthwhile to discuss briefly certain implications along the lines of thought as presented by Lettau and Schwerdtfeger (1967). Generally, it is expected that katabatic winds or, at least, the so-called air drainage, will occur where the terrain slope is sufficiently pronounced and the surface acts as a cold source. The basic theory of such direct gravitational circulations is reasonably well understood; for a list of references see Lettau (1966). However, there are at least two or three causes which impose limitations on the possible regional extent, and temporal occurrence of this type of flow over inland-ice slopes. Observations suggest that it is restricted to occasional outbursts when of sufficient intensity and to small horizontal extent, when it lasts for longer periods. Modifications of the circulation must also be expected due to the Coriolis force which, invariably, accompanies any fluid motion on earth, causing significant deflections of flow when the trajectory length approaches an order of about 100 km, or when the time required to traverse a region exceeds several hours. A second reason is that even moderate katabatic flow will rapidly exhaust an existing supply, or pool, of cold air, in a similar manner as a dam burst will drain a water reservoir. Any persisting katabatic flow will require either convergence from a vast drainage area, or a continuing, highly intense, cold source. If, however, an initially katabatic flow is modified by Coriolis acceleration, the air, partly, will begin to circle the cold source represented by an inland-ice dome; consequently, the modified circulation, with its components parallel to the contour lines will tend to preserve rather than exhaust the cold-air pool which overlays the higher terrain. A third reason may be an inherent instability of strictly katabatic flow, as originally suggested by A. Defant in 1933.

4. Theoretical Background for Elementary Dynamical Models in Mountain Meteorology

4.1 Basic Equilibrium Dynamics of the Horizontal Pressure Field

4.1.1 Introductory Remarks: Even though individual parts of the following derivations are of elementary nature, their combination will offer new insights into the physical nature of the atmospheric boundary layer over mountain slopes. Symbols and notations to be used follow conventional lines. For example, T = air temperature (in deg K); ρ = air density; $\alpha = 1/\rho$ = specific volume; p = air pressure; R = gas constant ($R = 287\ m^2/sec^2$ per deg K, for dry air); g = acceleration of gravity ($9.8\ m/sec^2$); f = Coriolis parameter = $2\omega \sin\phi$, where ω = angular speed of the earth's rotation, and ϕ = geographic latitude; t, x, y, and z are independent variables (time and spatial coordinates, with z = vertical coordinate); $h = h(x, y)$ = function of the horizontal coordinates which describes terrain elevation above sea level. Whenever possible, standard terminology is employed; for example, concepts of thermal wind and thermal vorticity, as defined in the "Glossary of Meteorology" published by the American Meteorological Society in 1959.

Non-standard concepts and relations will be explained upon introduction. The symbols $\vec{i}$, $\vec{j}$, and $\vec{k}$ shall denote unit-vectors in the three spatial directions. Derivatives, such as divergence and curl of vectors, and gradients of scalars are indicated by the three-dimensional del-operator; the horizontal gradients of pressure, temperature, terrain elevation, etc. will be written $\nabla_2 p$, $\nabla_2 T$, $\nabla_2 h$, etc., but for brevity, the subscript "2" is omitted in the two-dimensional Laplacian operator. Partial derivatives of scalar or vector functions with respect to the independent variables (also in certain cases derivatives with respect to specifically defined other variables) shall be denoted by subscripts; for example, $T_z \equiv \delta T/\delta z$, $P_x \equiv \delta p/\delta x$, etc.

Let the three-dimensional vector of air motion be $\vec{v} = \vec{i}\,u + \vec{j}\,v + \vec{k}\,w$; with $d\vec{v}/dt \equiv \vec{v}_t + \vec{v}.\,\nabla\vec{v}$.

The symbols $\vec{v}$, p, T, etc. shall indicate "representative" values of the dependent variables which implies that turbulent fluctuations ($\vec{v}'$, p', T', etc.), including the gustiness of the instantaneous wind vector, are eliminated with the aid of some numerical-statistical technique, such as calculation of "running means" for a certain time increment (say about ten minutes). The instantaneous values would be $\vec{v} + \vec{v}'$, $p + p'$, $T + T'$, etc. If density fluctuations are neglected, the equation of mean motion can be written as follows:

(1) $\quad d\vec{v}/dt + f\,\vec{k}\times\vec{v} + \alpha\nabla p + \vec{k}\,g = \nu\nabla^2\vec{v} - \overline{\vec{v}'\,.\,\nabla\vec{v}'}$

where ν = kinematic viscosity of the air, and the over-bar (which indicates the averaging process) appears exclusively in the eddy term representing the Reynolds stress per unit mass.

Any direct circulation on mountain slopes will be generated by gravity or the fluid interaction between gravity and vertical pressure gradient which is known as the buoyancy acceleration. Both, of necessity, must involve the w-component of air motion. An example is the katabatic-anabatic system which can be derived from equation (1) if the Coriolis acceleration is negligible; for further developments, and a list of references, see Lettau (1966). However, a major conclusion of the discussions in Section 3 was that Coriolis effects and subsequent modified circulations cannot be ignored in realistic models for the dynamics of mountain meteorology, if the horizontal extent of the terrain slope under consideration is at least of the meso-scale. Section 4.1 of this chapter deals exclusively with Coriolis effects; in 4.2, internal friction, and in 4.3, harmonic temporal variations are considered additionally. In the concluding Section 4.4, the basic theoretical model of thermo-tidal winds over mountainous terrain is introduced.

4.1.2 The Concept of Geostrophic and Thermal Wind; also of Geostrophic and Thermal Vorticity: Of prime importance for atmospheric dynamics in equation (1) is the acceleration due to horizontal pressure gradients ($\alpha\nabla_2 p$), and the change of this acceleration in the vertical,

(2) $\quad (\alpha\nabla_2 p)_z = \alpha_z\,\nabla_2 p + \alpha\nabla_2 p_z$.

For air motion in strictly horizontal planes, (1) reduces to the hydrostatic equation: after scalar multiplication by $\vec{k}$,

(3) $\quad p_z = -g\rho$; or, $\quad \nabla_2 p_z = -g\nabla_2\rho$,

which yields

(4) $\alpha \nabla_2 p_z = -g \nabla_2 \log \rho$.

Independently, there is the equation of state in direct, or differentiated, forms,

(5) $\alpha = RT/p = 1/\rho$; or, $\alpha_z / \alpha = T_z/T - p_z/p$; or,

$$\nabla_2 \log \rho = \nabla_2 \log p - \nabla_2 \log T,$$

which yield, together with (3),

(6a) $\alpha_z \nabla_2 p = g \nabla_2 \log p + (T_z/T) \cdot \alpha \nabla_2 p$, and also,

upon consideration of (4),

(6b) $\alpha \nabla_2 p_z = -g \nabla_2 \log p + g \nabla_2 \log T$.

Thus, after adding (6a) and (6b), the pressure terms on the right-hand cancel each other, and the height change of the pressure gradient acceleration (2) transforms into

(7a) $(\alpha \nabla_2 p)_z = (g/T) \nabla_2 T + (T_z/T) \alpha \nabla_2 p$.

Up to this point, the development deals with exact equations. In the following, we want to restrict the discussion to lower atmospheric layers of sufficiently small thickness ($\Delta_z = z_2 - z_1$) so that $T_z \Delta_z$ will not exceed $\pm$ 15 to 20 deg K. For T between 300 and 200 deg K this implies that the second term on the right-hand side of (7a) will remain within $\pm$ 10% of $\alpha \nabla_2 p$. Thus, whenever a significant horizontal gradient of temperature exists, the second term in (7a) can safely be neglected. Since the variability of $\nabla_2 T$ will exceed greatly that of the factor g/T, it is legitimate to substitute g/T_{oo} for the latter, with T_{oo} being a constant reference value. Thus, we can consider (7a) in a simplified version dependent only on the thermal structure of the atmosphere,

(7b) $(\alpha \nabla_2 p)_z = (g/T_{oo}) \nabla_2 T$.

The dynamic importance of the well-known equation (7a, or 7b) is most clearly demonstrated by the special balance of volume-forces per unit-mass, which leads to the concept of geostrophic motion. The geostrophic wind is defined as that specific horizontal velocity ($\vec{V}$) for which the Coriolis acceleration exactly equals the horizontal pressure acceleration; thus, for geostrophic motion, all but two of the factors in (1) vanish, leaving

(8) $f \vec{k} \times \vec{V} = -\alpha \nabla_2 p$; or, $\vec{V} \equiv \alpha f^{-1} \vec{k} \times \nabla_2 p$.

The defining identity (8) merely expresses the mathematical possibility of interpreting a given horizontal pressure field as the stream-function for the geostrophic wind. Certain derivatives of (8) provide additional information, such as the geostrophic vorticity (ζ), or the geostrophic shear ($\vec{V}_z$). The former is defined as the vertical component of the curl of the geostrophic wind. If the variability of the Coriolis parameter in (8) is neglected,

(9) $\zeta \equiv \vec{k} \cdot \nabla \times \vec{V} = f^{-1} \nabla \cdot (\alpha \nabla_2 p) = (\nabla_2 p \cdot \nabla_2 \alpha + \alpha \nabla^2 p) / f$,

where $\nabla^2 p \equiv p_{xx} + p_{yy}$, which is the horizontal Laplacian. With the aid of (8) and the developments (2) through (7b),

(10) $\vec{V}_z = (g/Tf) \vec{k} \times \nabla T + (T_z/T) \vec{V} \approx (g/T_{oo} f) \vec{k} \times \nabla T$.

The vector $\vec{V}_z$ defines the differential form of the thermal wind. Quite often the term is employed for the vertically integrated geostroph-

ic shear, over a height increment $z_2 - z_1$; then, the thermal wind is taken as the finite vector difference $\vec{V}_2 - \vec{V}_1$ between levels z_2 and z_1. However, equation (10) serves as the basis for defining another derivative, namely the thermal vorticity (ζ_z) which is the vertical component of the curl of the geostrophic shear. Conventionally, the variability of the factors f and 1/T are neglected, which yields

$$(11) \quad \zeta_z \equiv \vec{k} \cdot \nabla \times \vec{V}_z = (g/T_{oo}f) \nabla^2 T = g(T_{xx} + T_{yy})/T_{oo}f.$$

Given an isobaric map, geostrophic wind and vorticity can be calculated at any latitude excepting only the equator. But, even for $\phi = 0$, geostrophic equilibrium can be defined by taking into account the meridional variations of both, the Coriolis parameter and the pressure gradient, when crossing the equator. The real wind will be approximated by $\vec{V}$ only to the degree to which the special balance of forces in (8) approximates the complete balance as expressed by (1). In the atmospheric boundary layer, the force of internal friction must, by definition, be significant which causes typical and systematic departures of the actual from the geostrophic wind. Nevertheless, the geostrophic wind field retains its importance and can be considered as equivalent to a forcing function. Namely, when there are day-to-day changes in the pressure field, due to migrating cyclones and anticyclones, the temporal variation of the actual wind vector at a given location tends to be closely coupled with that of geostrophic velocity. Furthermore, when geostrophic vorticity is calculated from a given synoptic pressure chart at a fixed time of observations, it expresses the geographic distribution of intensity and direction of rotational tendencies in the geostrophic field (cyclonal versus anticyclonal), which are normally very closely confirmed by the actual wind field. These tendencies to rotational circulation of air are significant in the lower atmosphere because of their direct connection with large-scale patterns of vertical motion; normally, subsidence goes with anticyclonic, and upwelling of air with cyclonic rotation. Even though the actual wind vector may depart from the geostrophic velocity, basic tendencies to either cyclonic or anticyclonic curvature of streamlines are generally retained, as documented by the elementary fact that isobars are always drawn with due regard to all available simultaneous observations of wind direction and speed.

Correspondingly, if synoptic pressure charts at two or more atmospheric levels (or, equivalent charts of absolute topographies of constant pressure surfaces) are compared with the synoptic distribution of layer-mean temperature (or, equivalent charts of relative topographies between surfaces of given pressures) experience has shown that both, thermal wind and thermal vorticity express reliably any existing height changes of dynamic conditions which apply to actual winds nearly as well as to geostrophic winds. Based on such facts from synoptic meteorology it shall be shown in the following sections that the theoretical concepts of thermal vorticity and thermal wind offer new approaches to an understanding of the dynamics of meteorological effects of mountainous terrain.

4.1.3 Simplified Theoretical Model for Thermal Effects of Topography: It can be assumed that, primarily, the terrain structure will affect the energy budget at the earth-air interface. Short and long

wave radiation are influenced by a combination of physical factors such as surface pressure, precipitable water in the air, turbidity, also topographic slope and albedo, to name only a few of those which are directly or indirectly related to elevation above sea level. Rather than attempting to consider details of net radiation, let us take as the starting point a simple mathematical dependency of surface temperature on terrain elevation, and of air temperature on relative distance from the ground, z-h. Let, for $z \geq h$ only,

(12) $T = T_o + T_h h + T_z(z-h)$, where $T_o(x,y)$ describes the horizontal temperature distribution at a reference surface (for example at sea level), while T_z and T_h are vertical gradients, T_z in the air (positive for "inversion", and negative for "lapse"), and T_h along the terrain contours (positive when higher ground is relatively warm and negative when higher ground is relatively cool).

There are several special cases of the temperature distribution (12). Topography has no thermal effect when either h = constant = 0, or, when $T_z = T_h$, everywhere. In both cases (12) reduces to

(13a) $T = T_o + zT_z$; or, $\nabla_2 T = \nabla_2 T_o + z\,\nabla_2 T_z$.

Topographic influences are enhanced when either $T_z = 0$, or, $T_h = 0$. In the special case of $T_z = 0$, all isothermal surfaces are vertical,

(13b) $T = T_o + T_h h$; or, $\nabla_2 T = \nabla_2 T_o + T_h \nabla_2 h$, when, additionally, and for simplicity, $\nabla T_h = 0$. In the case of $T_h = 0$ the earth-air interface is isothermal and all lines of equal temperature are parallel to the contour lines of the terrain, such that

(13c) $T = T_o + T_z (z-h)$; or, $\nabla_2 T = \nabla_2 T_o - T_z \nabla_2 h$, when, again for simplicity, $\nabla_2 T_z = 0$. Actual conditions may be of intermediate form and correspond to none of either (13 a, b, or c). For the purpose of a more general discussion it can be assumed that $\nabla T_z = \nabla T_h = 0$, so that (12) describes some type of unspecified conditions by the following field of horizontal gradients and curvature,

(14a) $\nabla_2 T = \nabla_2 T_o + (T_h - T_z)\,\nabla_2 h$; or, $\nabla^2 T = \nabla^2 T_o + (T_h - T_z)\,\nabla^2 h$.

As suggested in the introductory Section 1, conditions on an entirely flat continent shall be compared with those on mountainous land. Flatness of terrain implies that $\nabla_2 h = \nabla^2 h = 0$, so that in place of (14a) we have

(14b) $\nabla^2 T = \nabla^2 T_o$. Terrain effects are emphasized by letting $\nabla_2 T_o = \nabla^2 T_o = 0$, so that

(14c) $\nabla^2 T = (T_h - T_z)\,\nabla^2 h$. Evidently, the last equations together with (11) permit us to investigate thermal vorticity in relation to terrain structure. Note, that in (14a to c) the horizontal Laplacian is to be considered.

4.1.4 Steady-State Terrain Effects in Terms of Thermal Vorticity: If continents were flat, the combination of (11) with (14b) alone would produce significant results. If the sea level field of pressure were featureless, there would be anticyclonic curvature aloft in a relatively warm region (where $\nabla^2 T_o < 0$), and correspondingly, cyclonic curvature aloft over a relatively cold region (where $\nabla^2 T_o > 0$). Let us remember, however, that this simple relationship holds true only

when $\nabla^2 T_z$ is indeed negligible. In any case, to be more realistic one must consider that there can be high and low pressure centers on the synoptic sea level chart. Even for $\nabla^2 T_z = 0$, the height variation of isobaric curvature will depend on the coupling between variations (in the horizontal directions) in surface pressure and temperature, disregarding the uninteresting case of zero-correlation between p_1 and T_o. If the correlation is positive an anticyclone has a relatively warm core (or $\nabla^2 p_1 \sim \nabla^2 T$) and a cyclone a relatively cold one. Schematically, the resulting height variations of pressure patterns due to fields of thermal vorticity are summarized in Table 1. Such changes are, of course, well familiar to the synoptic meteorologist. The specific benefit derived here is that this summary establishes a relatively simple basis of comparison for the appraisal of the more complex thermal vorticity effects in the boundary layer over mountainous terrain.

For $\nabla^2 h \neq 0$, it is realistic to consider possible couplings between topography and pressure patterns at the lower reference level. A positive correlation (where $\nabla^2 p_1 \sim \nabla^2 h$) is less interesting than a negative correlation (where $\nabla^2 p_1 \sim - \nabla^2 h$, or the region of a mountain massif coincides with a low-pressure area).

Such couplings shall be taken into account in Section 4.1.5. In the schematic summary on Table 2, however, a featureless isobaric chart at the lower reference level is assumed. With Table 1 as a basis of comparison, the results of combining equations (14c) and (11) are self-explanatory. To exemplify the scheme, consider the atmospheric boundary layer over the extended ice-dome of Antarctica. Experience has shown that higher ground is relatively cold, and that normally an inversion prevails in the air above the ice. Then, it follows from Table 2, that the thermal vorticity is positive; in a concrete example, this may apply to the layer between 850 and 750 mb, which surrounds or envelops a large-scale ice-dome. With a featureless isobar pattern at the lower level (say at 850 mb), there would be a cyclonal pattern aloft (say at the 750 mb surface). Only relative changes of geostrophic vorticity are predicted by thermal vorticity; thus, it is also legitimate to state that in absence of a pressure pattern aloft (say, at the 750 mb surface), an anticyclonic pattern will be produced at the lower level (say, at 850 mb) by positive thermal vorticity in between. The elementary baric wind law of synoptic meteorology then confirms the statement in Section 3.3 that a traveler on antarctic slopes will find, generally, lower elevation at his left-hand side if he faces the wind. Of course, he remembers that a cyclone's direction of rotation is counterclockwise on the Northern, but clockwise on the Southern hemisphere.

4.1.5 Steady-State Terrain Effects in Terms of Thermal Wind: To complete the discussion of consequences of geostrophic balance, we consider the standard reference level (z_1) and the possible coupling between the large-to-meso-scale patterns of pressure (p_1) and continental topography (h). It is practical to employ the concept of thermal wind rather than thermal vorticity as in the preceding section. Let us define an empirical coefficient γ, which has the physical dimension of acceleration (cm/sec^2) in the following statistical-descriptive relation between horizontal gradients of p_1 and h,

(15a) $$\alpha \nabla_2 p_1 \approx - \gamma \nabla_2 h \ .$$

Table 1. Schematic summary showing, qualitatively, vertical transition of an isobaric pattern at a given (lower) level, due to specified pattern of layer-mean temperature between the two levels:

Isobar Pattern (at level z_1) Geostr. Vortic. (sign of $\nabla^2 p_1$)	Anticyclonic -		Cyclonic +	
Relative Temperature Therm. Vortic. (sign of $\nabla^2 T$)	Warm Core -	Cold Core +	Warm Core -	Cold Core +
Isobar Pattern (aloft at z_2)	Enforced Anticycl.	Reduced Anticycl., Tending to Cyclonic	Reduced Cyclonic, Tending to Anticycl.	Enforced Cyclonic

Table 2. Schematic summary, showing that convex and concave terrain forms for featureless isobar field at lower level z_1, and for specified vertical gradients of temperature (T_h along the terrain contours, T_z in the air), result in thermal vorticity and, subsequently, tendency towards isobar patterns aloft; "erratic" indicates that information is insufficient to specify tendency:

Terrain Pattern (curvature) Sign of $\nabla^2 h$	Elevation, or, Dome (convex) -			
Temp. of Higher Ground Sign of T_h	Relatively Warm +		Relatively Cold -	
Vertical Grad. in Air	Inversion	Lapse	Inversion	Lapse
Sign of T_z	+	-	+	-
Sign of $T_h - T_z$	Erratic	+	-	Erratic
Therm. Vortic. (sign of $(T_h - T_z)\nabla^2 h$)	Erratic	-	+	Erratic
Isobar Pattern aloft	Undetermined	Anticyclonal	Cyclonal	Undetermined
Terrain Pattern (curvature Sign of $\nabla^2 h$	Depression (concave) +			
Therm. Vortic. (Sign of $T_h - T_z$) $\nabla^2 h$, for T_h and T_z as specified above)	Erratic	+	-	Erratic
Isobar Pattern aloft	Undetermined	Cyclonal	Anticyclonal	Undetermined

The coefficient γ can be approximately uniform in sign and magnitude only for meso-to-large-scale topographic features. In combination with the geostrophic wind formula (8), relation (15) predicts a geostrophic vector $\vec{V}_1$ which is parallel to the general trend of the contour lines of the terrain. Specifically, with reference to the case studies in Section 3.1 and 3.2, a geostrophic south wind will be expected over Oklahoma, Kansas, and Nebraska, as well as over the desert region of Peru and Chile, since average synoptic or climatic sea level isobars will show low-pressure areas in the Rocky Mountain States of Colorado and Utah, as well at the Altiplano of Peru and Bolivia, respectively.

For simplicity, let us assume that due to the diurnal cycle of insolation, the isotherms in the atmospheric boundary layer move up and down in such a manner that the isothermal surface remains parallel to the terrain. As discussed in connection with equation (14), this must mean that $T_h = 0$, so that the horizontal gradient of temperature is determined by lapse-rate and terrain contour, $\nabla_2 T = -T_z \nabla_2 h$. This topographic effect, when combined with the simplified version of the thermal wind equation (10), yields
(15b) $\vec{V}_z = -(g\, T_z / T_{oo} f)\, \vec{k} \times \nabla_2 h$. It follows from (15a) and (8) that the thermal wind (15b) is either parallel or antiparallel to the geostrophic wind. Upon writing $\vec{V}_z\, \Delta z = \vec{V}_2 - \vec{V}_1$, the geostrophic wind at the level z_2 is obtained as
(15c) $\vec{V}_2 = \vec{V}_1 (1 + g\, T_z\, \Delta z / \gamma\, T_{oo})$. An atmosphere where only speed but not direction of the geostrophic vector changes with height--as in (15c)-- is conventionally referred to as "equivalent-barotropic"; its significant property is that geostrophic motion will not result in advection of heat, in spite of existing baroclinicity (or non-barotropy) due to horizontal temperature gradients.

If γ is positive, the geostrophic speed in (15c) decreases with height for $T_z < 0$ (lapse condition); conversely, it increases with height for inversion cases ($T_z > 0$). For a quantitative illustration let us consider numerical data which are representative of North-Central Nebraska. Here, $f = 1.0\ 10^{-4}\ sec^{-1}$, so that a geostrophic speed of $V_1 =$ 10 m/sec corresponds in (8) to a pressure gradient acceleration of $0.1\ cm/sec^2$. For the average terrain inclination of 1:400, (15a) yields $\gamma = 40\ cm/sec^2$, or $g/\gamma = 25$, so that (15c) can be numerically reformulated as (15d) $\vec{V}_2 = \vec{V}_1 (1 + 25\, (T_2 - T_1) / T_{oo})$. Temperature soundings during the Great Plains Turbulence Field Program in North-Central Nebraska showed that the top of the nocturnal inversion is at about 400 m above ground, with $T_2 - T_1 = 6^oK$ (per 400 m) and $T_{oo} =$ 290^oK. Thus, equation (15d) would predict $V_2 = 15$ m/sec for $V_1^{oo} = 10$ m/sec. Beyond 400 m, T_z was negative during the night. Lapse conditions, of course, prevailed during the entire day, and significant diurnal variations were observed up to 1500 m above ground. During the O'Neill experiments, the observed low-level jet showed indeed maximum development near the top of the nocturnal inversion which would be in line of a direct response to a forcing function as represented by diurnal variations in thermal wind. As follows from the above developments, geostrophic speed in the lowest 400 m (or about the lower 25% of the total boundary layer thickness) is very strong at nighttime and very weak at daytime, while at and beyond 1500 m it remains relatively weak at all hours of the day. More detailed testings will be presented in Section 5.

If it is conceded that the above simple model of diurnal cycles of thermal winds represents actually the forcing function of the low-level jet stream development (as observed at O'Neill and elsewhere in Nebraska, Kansas and Oklahoma) it would appear to follow that diurnal wind variations in the Pampa de La Joya would be basically the same as in the mid-western United States. Namely, equation (15c) contains only T_z as a factor, while the coupling between p_1 and h and, of course, the diurnal variation between lapse and inversion conditions are indeed similar at the two regions. This would contradict the statement in Section 3.1 that a low-level jet in the Pampa de La Joya appears to reach peak intensity around noon, rather than midnight. In order to eliminate such apparent discrepancies, it will be necessary to expand the theoretical model so that it includes effects of internal friction as well as the quasi-tidal nature of the forcing function. This shall be done in the following Sections, 4.2 to 4.4.

However, this discussion of consequences of geostrophic balance should not be concluded without demonstrating that the extremely simple relation (15c) already offers a basic explanation for the remarkable geographical distribution of low-level jet occurrence on Bonner's chart, Fig. 16. Namely, climatological data show that there is a relatively uniform pressure gradient at sea level between the Bermuda high and the Rocky Mountain low. Consequently, for uniform $\nabla_2 p_1$ the coefficient γ in (15a) must change sign across the Mississippi River valley, and will be positive for the east-facing slope towards the Rocky Mountains, and negative for the west-facing slope towards the Appalachian. This implies reversal of sign in relation (15c) so that the geostrophic speed V_2 at the top of the nocturnal inversion over Tennessee and Alabama would be reduced rather than increased in comparison with V_1. In other words, the low-level jet stream on the Appalachian slope would be a daytime development; but then, it can be expected to be distorted by convective disturbances. This may in part explain the scarcity of low-level wind maxima over Tennessee and Alabama; see Fig. 16. Finally, it will be domonstrated that not only the sign but also the magnitude of the empirical coefficient γ is important. The following numerical summary is valid for $V_1 = 10$ m/sec at temperate latitudes (where $f \approx 10^{-4}$ sec $^{-1}$) and an inversion intensity corresponding to $(T_2 - T_1) / T_{oo} = 0.02$ (or, 6^oK with $T_{oo} = 300^oK$). Without difficulty, a similar tabulation could be constructed for a variety of wind and temperature-gradient conditions, and other geographic regions. The essential feature is the assumed variation of terrain slope in Table 3.

Table 3. Schematic illustration of geostrophic wind ratio as a function of terrain slope, assuming $V_1 = 10$ m/sec, constant temperature inversion, and negative coupling between p_1 and topography:

Terrain Slope:	1:4000	1:1000	1:400	1:100	1:10
g/γ in (15c) :	2.5	10	25	100	1000
V_2/V_1 in (15c):	1.05	1.2	1.5	3.0	21.0

The numbers in the summary can be interpreted as indicating that weak slopes will not produce any significant amplitudes of the thermal-wind-forcing-function; on the other hand, steep slopes would produce effects of such intensity that a complete breakdown of this mechanism

is likely. Only moderate terrain slopes of the order of 1:400 appear to cause effects of realistic magnitude. Obviously, this reasoning needs further fortification before it can be considered conclusive. Of course, the summary in Table 3 refers only to temperate latitudes and conditions which correspond to the low-level jet stream over the midwestern United States.

4.2 Basic Steady-State Dynamics of the Atmospheric Boundary Layer

4.2.1 The Ekman Spiral and Universal Spirals for Fully Developed Mechanical Turbulence: In an atmospheric region where the horizontal pressure gradient is approximately constant, the air motion in response to this forcing function will be steady and horizontally uniform. To describe the atmospheric boundary layer the horizontal components of equation (1) can then be reduced to a form which expresses a balance between three forces, namely, that of pressure gradient, Coriolis, and internal friction. For convenience, the pressure gradient acceleration will be replaced by the geostrophic term with the aid of the identity (8); let us denote horizontal components of the geostrophic wind vector by $U \equiv \vec{i} \cdot \vec{V}$ and $V \equiv \vec{j} \cdot \vec{V}$. Then, equation (1) yields (16a)

$$-(v\text{-}V)\ f = \nu u_{zz} - \overline{\vec{v}' \cdot \nabla u'}\ ; \text{ and, } (u\text{-}U)\ f = \nu v_{zz} - \overline{\vec{v}' \cdot \nabla v'}\ .$$

The turbulent contribution to friction would vanish in strictly laminar flow. Furthermore, if in the laminar case, U and V were height-independent, the system (16a) has an exact solution which is known as the classical Ekman-spiral flow. However, it follows from this solution, and the numerical value of molecular viscosity ν in air, that for ordinary geostrophic wind speeds the Reynolds number of Ekman-spiral flow would be at least 10^5 which exceeds by a factor of 100 or so the critical value for existence of laminar flow states. Thus, turbulence will be generated and eddy stresses must become significant. To account for this, Ekman's solution is derived with an apparent or eddy viscosity $K_{Ek} > \nu$. This value is defined by the following two simultaneous relations,

$$\text{(16b)}\quad \nu u_{zz} - \overline{\vec{v}' \cdot \nabla u'} \equiv K_{Ek} u_{zz}\ ; \text{ and, } \nu v_{zz} - \overline{\vec{v}' \cdot \nabla v'} \equiv K_{Ek} v_{zz}\ , \text{ with}$$

the additional requirement that K_{Ek} is independent of height.

In classical Ekman-spiral flow the geostrophic wind is also independent of height. Hence, the reference frame of Cartesian coordinates can be turned so that U vanishes and V expresses total geostrophic speed. Then, the Ekman solution which satisfies the boundary conditions $u_o = v_o = 0$ at $z = 0$, and $v_\infty = V$ with $u_\infty = 0$ at $z = \infty$, is (for the northern hemisphere),

$$\text{(16c)}\quad u = -V e^{-\eta} \sin\eta\ ; \text{ and, } v = V(1 - e^{-\eta}\cos\eta). \text{ where (16d)}$$

$\eta \equiv z (f/2K_{Ek})^{1/2}$. It follows that for small height, or η very small in comparison with unity, $u \approx \eta V$ as well as $v \approx \eta V$. Thus, wind direction near the surface must deviate by 45 deg from the direction of the geostrophic wind or the orientation of the surface isobars. Throughout the boundary layer, with increasing distance from the ground, the wind vector according to (16c) veers gradually, and spirals (with slight overshoots) ultimately into the geostrophic vector.

In the real atmosphere, the deviation angle between wind near the ground and the isobars is known to depend on the aerodynamic surface-roughness (z_o) and experience has shown that it varies between about 10 to 25 deg for smooth ground, and about 25 to 40 deg for rough ground. Spiral solutions which are significantly more realistic than Ekman's can be found in the literature. For the purpose of the present discussion it may suffice to make reference only to a recent study of the boundary layer in a barotropic atmosphere which resulted in a relatively comprehensive "universal spiral solution"; see Lettau (1962). This model is based on the assumption that viscous effects in (16a) can be neglected and that instead of (16b) we have

$$(17a) \qquad \begin{cases} \nu\, u_{zz} - \overrightarrow{v'} \cdot \nabla u' = -\overline{(w'u')}_z = (v^* \ell\, u_z)_z , \\ \nu\, v_{zz} - \overrightarrow{v'} \cdot \nabla v' = -\overline{(w'v')}_z = (v^* \ell\, v_z)_z , \end{cases}$$

where

$$(17b) \qquad v^{*4} = \overline{(u'w')}^2 + \overline{(v'w')}^2 ,$$

v^* = friction velocity as a function of height, and ℓ = the lateral length scale of turbulence for which a non-monotonic height dependency is assumed. This model approaches the well-known logarithmic wind profile in the form of an asymptotic case of the universal spiral solution in the vicinity of the ground (that is in the surface layer, which includes roughly the lowest 5% of the atmospheric boundary layer thickness).

With the aid of a suitable computer program, the non-linear system (16a, 17a, and 17b) was solved under due consideration of the proper boundary conditions. The resulting universal spiral solution as tabulated in Lettau (1962), includes wind and stress spirals, relationships between surface stress and forcing function (utilizing the geostrophic drag coefficient), deviation of surface layer wind direction from the isobars, scale heights, etc. Such relations have been completely parameterized with the aid of the scaling factor $V/z_o f$, known as the surface Rossby number. This number is given, or predictable, once the external conditions of the boundary layer flow are specified.

Of direct importance for the present discussion are only two special results from the universal spiral solution. Firstly, eddy diffusivity in the atmospheric boundary layer is shown to exhibit a height variation which is essentially non-monotonic; it will increase almost linearly from the ground value to a maximum at a level of about ten percent of the full boundary layer thickness; aloft in the upper 90%, it will decrease gradually to relatively small values at the top of the boundary layer. Thus, for estimates of overall responses to unsteady forcing function modified by terrain influences, its substitution by a height-independent K_{Ek} may not distort the findings as would be the case if the truly effective eddy diffusivity would monotonically increase with height. Secondly, it is quite evident that the basic 45 deg deviation between surface stress and geostrophic wind makes the Ekman spiral too bulky (or, overly well-rounded) in comparison with more realistic spiral solutions. However, of prime interest here is mountainous terrain which possesses a relatively large surface roughness (z_o), and will thus be characterized by relatively small surface Rossby numbers. Thus, another point supports the conclusion that, when anywhere, the Ekman model may be a tolerable approximation for rough ground or mountainous terrain.

Finally, it should be mentioned that in a supplement of Jeffreys' original attempts of wind classification, Johnson (1966) suggested the term "geotriptic" wind to indicate the type of air motion which results from a balance between the three elementary accelerations singled out in equation (16), namely, those due to pressure force, Coriolis force, and internal friction force. Of practical value for the following discussion of wind-spiral analysis will be a succinct terminology to indicate the orientation of the Cartesian axis frame of horizontal coordinates. Fig. 18 illustrates three possibilities of interest, which are referred to as geographic, geotriptic, and geostrophic. These systems are defined by the orientation of the y-axis (or ordinate axis), which can be either parallel to the local meridian (that is the true north azimuth), or the surface stress (that is wind direction in the atmospheric surface layer), or the geostrophic wind (that is the orientation of the surface isobars), respectively. Each system has special advantages. In numerical models of the general circulation, the geographic system will be suited best; for theoretical investigations of the boundary layer structure,the geostrophic system is preferred as evidenced by the

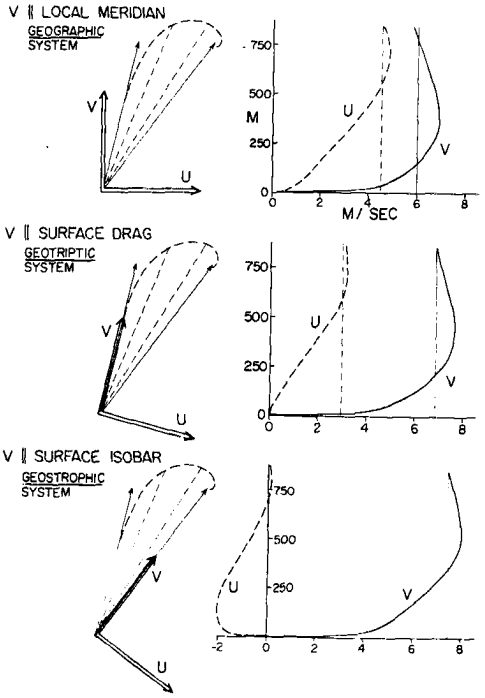

Fig. 18 The three basic systems of axis-orientation for the study of wind spirals in the atmospheric boundary layer; exemplified for a theoretical wind spiral with surface Rossby number of $10^{6.5}$. The vertical lines on the right-hand side represent the components of the same geostrophic wind in the three systems.

expression of the Ekman spiral (16c); however, if observed wind data are desired to be analyzed, the geographic system is inconclusive, and the geostrophic system cannot be used since only rarely the azimuth of the geostrophic vector can be determined with the same accuracy as the actual surface wind; this fact alone would make the geotriptic system best suited for wind profile analysis in the atmospheric boundary layer. However, the most important advantage of this system lies in the fact that upon height integration between ground and top of the boundary layer, the geostrophic departure component v-V in the geotriptic system must vanish, while the component U-u produces the total ground drag. The first statement can be confirmed by inspection of Fig. 18. The wind spiral used to illustrate the three systems is a verification of Lettau's universal solution for an arbitrarily assumed special value of the surface Rossby number of 3,200,000; that is, in a concrete example of verification, V = 16 m/sec, and z_o = 5 cm, with $f = 10^{-4}$ sec^{-1}.

4.2.2 Ekman Spiral with Thermal Wind: The discussion in Section 4.2.1 was restricted to mechanical turbulence or, to a thermally neutral or barotropic atmosphere. Real boundary layers will depart from this elementary or adiabatic state, due to the important process of surface heating and cooling. For horizontally undifferentiated boundary conditions, a diabatic state of surface and boundary layers results which is and has been investigated at many locations. Also relatively attractive have been the problems resulting from systematic horizontal differences in energy-budget structure, normally referred to as internal boundary layer development, or air mass modification along wind fetches, or simply as boundary layer structure with horizontal advection, of heat or other properties of the atmosphere. Relatively little attention thus far has been devoted to possible effects of thermal winds in boundary layer studies, even though the extension of steady-state Ekman-spiral flow to include the case of a linear height variation of geostrophic wind has been presented more than five decades ago by Hesselberg and Sverdrup (1915). For brevity, their solution will be quoted only for the equivalent barotropic atmosphere, that is, for a height variation of speed but not direction of geostrophic wind. Then, the use of the geostrophic system of coordinates is still convenient; see Fig. 19. Specifically, with U = 0, $V = V_o + zV_z$, and V_z = const, the distorted spiral is given by,

(18) $u = -V_o e^{-\eta} \sin \eta$; and, $v = z V_z + V_o (1 - e^{-\eta} \cos \eta)$. The same boundary conditions are satisfied as specified for (16c). A comparison of (18) with (16c) immediately shows the type of distortion mentioned above.

Hesselberg and Sverdrup (1915) explained very clearly the limitations of their solution and emphasized that the elementary distortion of the Ekman spiral is valid exclusively for constant thermal wind. For thermal wind varying with height, they proposed a solution based on series expansions. However, the really important point could possibly be that the assumption of constant eddy diffusivity is much more aggravating than restrictions concerning the structure of the thermal wind. It appears necessary to clarify this problem before progressing to the discussion of slope-induced thermal winds in boundary layers over mountainous terrain. This will be at least partly achieved by a discussion of actual boundary layer wind profile data with thermal

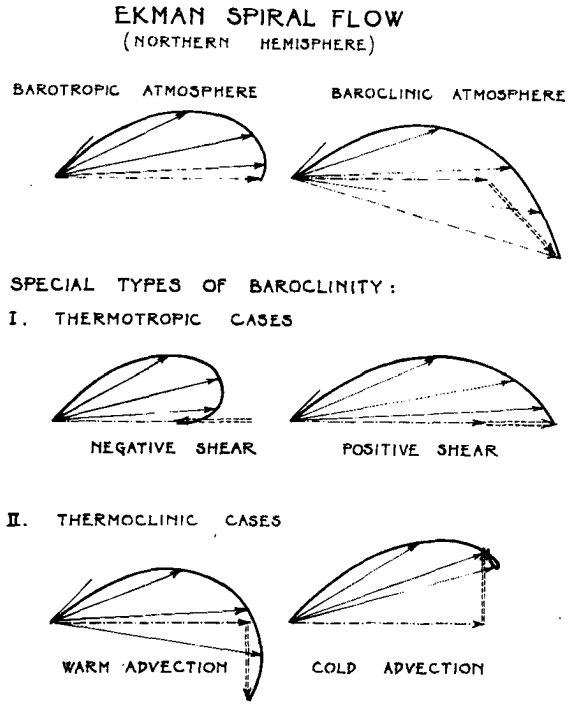

Fig. 19 Ekman spiral distortions by height-independent thermal wind. In order to distinguish four special types of baroclinity, the word "thermotropic" is used as an alternate for equivalent-barotropic, while "thermoclinic" is used here for the very special baroclinity condition where the thermal wind is perpendicular to the geostrophic wind at the interface.

wind over featureless terrain in the following section. Examples of distorted Ekman spirals are illustrated in Fig. 19, using the Hesselberg-Sverdrup solution for constant thermal wind.

4.2.3 Boundary Layers with Thermal Wind over Featureless Terrain: In atmospheric boundary layer research, the last decades have brought gradual refinement in observational as well as analytical techniques for wind profile studies. Field experiments, like the O'Neill program, have demonstrated that under suitable weather conditions over well-defined boundaries, a series of soundings in the lower 1000

to 2000 m of the troposphere can produce empirical data on wind (and wind shear) of a representativeness and accuracy which exceeds significantly that of possible calculation of the geostrophic vector from independently observed barometric fields. As evidenced by equation (16a) the evaluation of friction forces, and subsequently, the Reynolds stresses, requires accurate knowledge of geostrophic departure components, (v-V), as well as (u-U), as functions of height. Of course, the probable error of such differences is at least as large as that of individual U and V values. In view of the horizontal scale involved, and relatively weak horizontal, in combination with relatively strong vertical, barometric differences in the presence of barometric noise, a significant improvement in the accuracy of horizontal pressure gradient determination is unlikely. Consequently, the possibility became more and more interesting that the geostrophic vector can be derived with satisfactory accuracy from sufficiently detailed wind observations. This particular feature of atmospheric boundary layer physics is due to Coriolis effects and subsequent veerings (or turnings) of wind direction with distance from the ground. Namely, there must exist at least two clearly identifiable levels within the atmospheric boundary layer where shear components pass through zero but where curvature is finite, so that a true component maximum occurs; this implies that at least at one level $u_z = 0$ while $v \neq 0$ and $u_{zz} \neq 0$, and at another level $v_z = 0$ while $u \neq 0$ and $v_{zz} \neq 0$. Lettau (1950) demonstrated the practical use of such level values in the analysis first for the barotropic state of atmospheric boundary layers; an extension to include baroclinity was presented several years later; see Lettau (1957). This supplement made it possible to re-analyze an experimental set of very accurate wind soundings in the maritime boundary layer near the Scilly Islands, made by Sheppard, Charnock, and Francis (1952); this re-analysis was especially interesting because Sheppard et al. had concluded that a frictional wind spiral did not exist over the North Atlantic Ocean. Lettau (1957) -- also later Lettau and Hoeber (1964) in their analysis of Hoeber's detailed soundings in the maritime boundary layer near the island of Helgoland -- demonstrated the influence of baroclinity by determining and separating out the geostrophic wind shear in the boundary layer. After elimination of the thermal wind, a clearly defined frictional wind spiral became evident in all maritime boundary layers under investigation.

The discussions in Section 4.1 suggest that a superimposition of internal friction and thermal wind is highly important for the structure of boundary layers over large-to-meso-scale mountain slopes. Conditions over featureless terrain thus can serve as a model for this study. The discussion of illustrative examples also shows the advantages of employing the geotriptic system of coordinates. In Lettau and Hoeber (1964) the term "anti-triptic" has been used but it can now be said that the word "geotriptic", as proposed by Johnson (1966) and explained in Fig. 18, is preferable and shall be used later on.

A wind hodograph in the geotriptic system is most readily obtained when results of pilot balloon soundings, as routinely conducted daily at a given station over a period of years, are grouped according to a specified sector of surface wind direction, and averaged separately. From soundings, statistically grouped in this manner by Gregg (1922), an example for eight surface wind sectors (of 45 deg each) is given on

the left-hand side of Fig. 20. The hodographs with surface wind from north, and also from the northwest, would indeed appear to support a statement to the effect that "a frictional wind spiral does not exist". However, one cannot fail to note a general trend in all eight hodographs. Obviously, its cause is the climatological feature of winter seasons in this continental region (East Nebraska), namely, the persistent and extremely strong horizontal temperature gradient, with coldest air over Canada to the north and northeast of Nebraska. By a rather simple procedure, it can be shown that we are dealing with the effect of thermal wind which must accompany this meridional gradient of temperatures. Let us construct, level for level, the resulting mean wind vectors for pairs of hodographs having surface wind directions exactly 180 deg apart. With such procedure any systematic effect which is fixed with respect to geographic azimuth (like the thermal wind) will be preserved, while any systematic effect which is fixed with respect to surface wind direction (such as the veering due to internal friction) enters once with a plus and once with a minus sign and thus will tend to cancel out. This vector averaging was applied to the four hodograph pairs of opposite surface wind directions shown in Fig. 20, whereupon the resulting means after prorating with respect to height, or thermal winds, were subtracted from the observed winds. For all eight sectors, the reduced hodographs shown on the right-hand side of Fig. 20, demonstrate clearly the frictional veering in the form of wind spirals which now resemble to a satisfactory degree the theoretical solutions

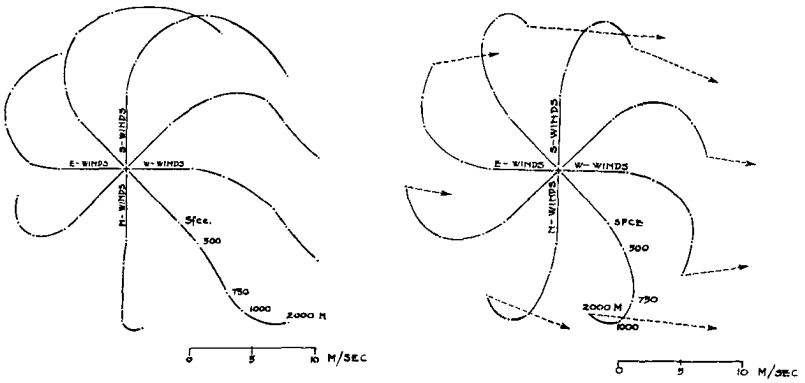

Fig. 20 Mean observed and reduced hodographs for eight sectors of surface wind direction at Drexel, Nebraska (41.3 deg N., 90.2 deg W., 396 m elevation), for about 500 soundings during winters of 1915 to 1920, based on data published by Gregg (1922). Using five levels (mast anemometer to 2000m), the hodographs on the left show observed, on the right reduced data, illustrating systematic thermal wind effects in the atmospheric boundary layer due to meridional temperature gradients over featureless terrain.

as illustrated in the example shown in Fig. 18. In an extension of the author's earlier work (unpublished, but used in lectures and teaching, as illustrated by Fig. 20), Johnson (1962) applied to Gregg's data systematically the more general technique of separating out thermal winds similar to the procedure described by Lettau and Hoeber (1964). Results obtained by Johnson are shown in Fig. 21. Note the interesting detail that under certain conditions the thermal wind may cause "loops" in the observed wind spiral, as for northwinds in Ellendale.

The important point here is the empirical support by Fig. 20 and 21 of the conclusion that in natural boundary layers the effects of thermal winds (even rather strong ones) can be linearly superimposed on effects of turbulent friction forces. In a first direct application to boundary layers with strong thermal wind over terrain slopes, the author adapted the above described method of analysis to wind soundings over the Antarctic incline which surrounds the South Pole; reference is made to Dalrymple, Lettau, and Wollaston (1966). For more recent developments in this field, see the discussion in Section 3. 3.

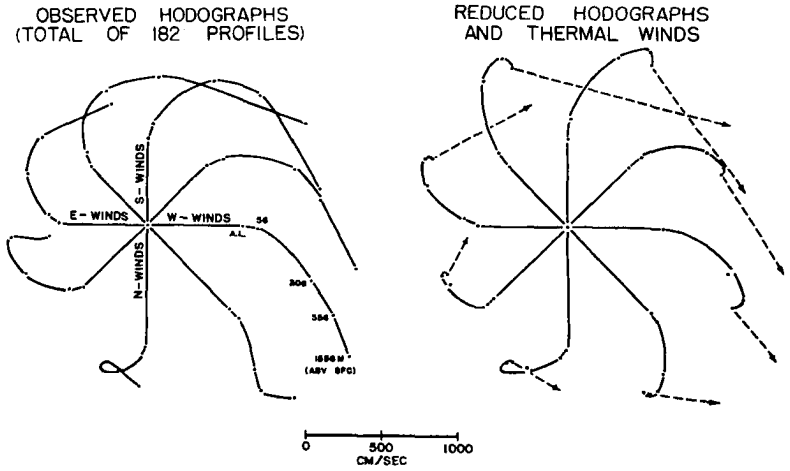

Fig. 21 Mean and reduced hodographs for eight sectors of surface wind directions at Ellendale, N. Dakota, (46.0 deg N, 98. 6 deg W. 444 m elevation) for 182 soundings during the winters of 1918 to 1920; analyzed by Johnson (1962) based on data by Gregg (1922). In comparison with Fig. 20, the thermal winds superimposed on frictional spirals are of different intensity for pairs of hodographs with opposite surface winds.

4.3 Boundary Layer Response to Harmonic Forcing Functions

4.3.1 Remarks on Atmospheric Tidal Oscillations: According to Chapman (1951) atmospheric oscillations on a worldwide scale are conveniently called "tides" even when their origin is thermal and not gravitational. In fact, experience shows that the actual semi-diurnal lunar oscillations of barometric pressure are relatively small in comparison with semi-diurnal solar oscillations, although the moon exerts a gravitational forcing function of larger amplitude than the sun. This somewhat paradoxical situation used to be attributed to extraordinary resonance, that is to extremely fine "tuning" of the free oscillation of the atmosphere to the period of the solar gravitational forces. However, in recent literature on atmospheric tides, more and more arguments are provided against extraordinary resonance magnification; instead, thermal causes (as for example, absorption of solar radiation combined with emission of longwave radiation in the air and at the lower boundary, with subsequent cycles of heating and cooling) are emphasized; reference can be made to summary reviews as that presented by Siebert (1961). On the other hand, the study of surface layer temperature and heat transfer oscillations has been, traditionally, a concern of micrometeorology with emphasis on the small-scale processes of turbulent heat conduction in the boundary layer, as well as convection in the lower troposphere. Theoretical work on heat diffusion in the two-layer-system (air-submedium) in response to cycles of insolation, appears to be well researched at numerous national and international organizations, presumably in direct relation to the ever-growing number of publications in the international literature dealing with results of observational programs in micrometeorology. Presently, at the University of Wisconsin, research activities in this field are devoted to a theoretical approach initially outlined by Lettau (1951), and now being extended to include more realistic models of eddy structure and convection, in surface and boundary layers.

From the above, it appears that a gap may exist in the coverage of atmospheric oscillations, with one group of researchers being interested mainly in the very large-scale, the other in the very small-scale type. However, Chapman (1951) already mentioned that in a realistic specification of tidal forcing functions, possible effects of the ocean-continent distribution should be included. It may be added that consideration of continental topography would be a reasonable next step towards smaller scales. Actually, certain aspects of fine "tuning", in the resonance theory of the atmospheric oscillator, used to be explained by a dynamic influence of the large mountain chain from Alaska to Fireland. On the other hand, studies of atmospheric processes at the small-scale end of the spectrum, including the consideration of boundary layer structure over terrain slopes lead toward ever larger scales; moreover, there is a unifying feature in the fact that solar energy is supplied in cycles (either diurnal or annual, with subsequent higher harmonics).

With this factual background, it is proposed now to reduce the above-mentioned gap. This will justify the use of the word "tidal" for wind oscillations of the meso-to-large scale as long as they originate from solar cycles. The physical nature of this solar forcing function, of primary interest here, is insolation absorbed at sloping ter-

rain; eddy diffusion of heat sets up secondary gradients of temperature in the horizontal direction which corresponds to a dynamically significant thermal wind when the extent of the slope is sufficiently large. Certain formal analogues to tides in the wind field of an atmospheric boundary layer with oscillating geostrophic shear, will be made evident in the following sections.

4.3.2 General Notes on Forcing versus Response Functions[1]:
In a physical system, let F (t) denote a harmonic forcing function while the response of the system to F (t) is another harmonic function of time described by r (t). Specific examples can readily be found in a variety of systems with controlled variations of either pressure, or voltage, or heating intensity, etc., so that r (t) expresses variations in either velocity, or electric current, or temperature, respectively. Let $i \equiv \sqrt{-1}$, ω = frequency, ψ = phase angle, and A and B = amplitude values of variables in proper physical dimensions so that

(19a) $F(t) = A\, e^{i\omega t}$; and, $r(t) = B\, e^{i(\omega t - \psi)}$. The ratio F/r has a real and imaginary part. The absolute value of this complex ratio defines the impedance (Z) of the system, while the quotient between imaginary and real parts defines the phase-lag,

(19b) $F/r = (A/B)\, e^{i\psi} \equiv Z\, e^{i\psi}$; $Z \equiv A/B$. Most commonly the concept of impedance is used in electric circuitry for alternating currents. In this case, Z is the amplitude ratio of a controlled voltage (V) and the resulting current (j), when the harmonically varying potential is applied across a circuit containing resistance (R), inductance (L), and capacitance (C). The equation of the problem is

(20a) $V_t = C^{-1} j + R\, j_t + L\, j_{tt}$, with

(20b) $V = A\, e^{i\omega t}$; or, $V_t = i\omega V$, so that in view of (19a) and (19b),

(20c) $j = Be^{i(\omega t - \psi)} = (V/Z).\ (\cos\psi - i \sin\psi)$, whereupon (20d)

$Z^2 = R^2 + (\omega L - 1/\omega C)^2$; and, $\tan\psi = (\omega L - 1/\omega C)/R$.

The homogeneous form of (20a) is known as the "telegrapher's equation". The solution consists of the sum of a transient plus a harmonic current. The former dies out exponentially with time, like the charging current of a capacitor. The discussion, therefore, may be restricted to the harmonic or quasi-static part of the solution which has the same frequency as the forcing voltage but differs in phase by the angle ψ. It may suffice here to recall from standard textbook discussions that depending on the relative magnitude of circuit elements (ideally, reduceable in three ways, to either pure resistance, or pure inductance, or pure capacitance) the current will be, respectively, either exactly in phase with the voltage, or lag by 90 deg (one quarter period), or lead the voltage by 90. These relations can also be expressed with the aid of the "natural" or "resonant" frequency $\omega^* = (LC)^{-1/2}$. Three elementary types of response can be described as follows: (i): At resonance frequency (that is, $\omega = \omega^*$), the impedance equals the resistance and the current is exactly in phase with the voltage, $\psi = 0$.

---

[1] In order to conform simultaneously with standard notation in other fields, it is unavoidable to employ in Section 4.3.2 certain symbols (as j, u, x, V, R, etc.) in a different physical meaning than in all preceding or following sections. Also the subscript t will indicate total differentiation with respect to time, since we are dealing in Section 4.3.2 with ordinary differential equations.

(ii): At relatively high frequency ($\omega \gg \omega^*$) inductance is the predominant factor of impedance; the current lags the voltage, $0 < \psi \leq 90$ deg.
(iii): At relatively low frequency ($\omega \ll \omega^*$) capacitance predominates, the current leads the voltage, $-90 \text{ deg} \leq \psi < 0$.

Another well-known geophysical example is the mechanical response of a seismograph towards the forcing function given by earth tremors. In this case, F acts on a mass (m) subject to a restoring force and a dissipative or frictional force. When x(t) denotes a geometric displacement, let the restoring force be k x, and the dissipative force Rx_t whereupon the equation of the problem is (21a) $F = k\,x + Rx_t + m\,x_{tt}$.

A comparison of (21a) with (20a) shows the analogies between restoring factor (k^{-1}) and capacitance, friction factor and resistance, also mass and inductance. The equation for mechanical impedance contains an additional factor ω, due to the appearance of F in (21a) in comparison with F_t or V_t on the left-hand side of (20a). Differentiation of (21a) with respect to time, and consideration of speed of displacement, $u = x_t$, rather than displacement, makes for perfect analogy with (20a) since
(21b) $F_t = k\,u + Ru_t + mu_{tt}$. Seismologists consider sometimes the resonance factor $1/Z$ instead of the impedance. Also the characteristic dependency of phase (either lagging or leading) in relation to differences between exciting frequency of the earth tremor and the resonance frequency of the sensor is conventionally expressed by the statement that a seismograph tends to register displacement amplitudes if the earth tremor is of relatively low frequency ($\omega \ll \omega^*$) and acceleration amplitudes if it has relatively high frequency ($\omega > \omega^*$).

The following discussions of atmospheric boundary layer response to forcing functions with solar day period offer an opportunity for a practical application of the concepts of impedance, and lagging or leading, in relation to a "natural" frequency in the response of the system.

4.3.3 Boundary Layer Response to Oscillating Geostrophic Wind: In analogy to tidal theory, dynamical response in the atmospheric boundary layer to a harmonic forcing function of controlled variations in geostrophic wind and shear will be treated as a quasi-static, or quasi-steady, problem. The small difference (little more than 200 seconds) between the sidereal and solar day will be neglected so that the basic forcing frequency ω is the same as in the Coriolis parameter. Three more assumptions will be made in the treatment of equation (1). First, internal friction will be expressed by the Ekman formulation (16b); second, horizontal uniformity of the wind field is assumed, whereupon the total time derivative $d\vec{v}/dt$ can be reduced to the partial derivative $\vec{v}_t$; third, the temporal variations in the pressure field are assumed to correspond to an equivalent barotropic state of the lower atmosphere which implies that, during a full cycle of V, a fixed geostrophic system of coordinates can be used because $U = 0$ at all times. These assumptions will restrict the validity of conclusions. Nevertheless, the gist of the discussions in Sections 4.1 and 4.2 was that a restrictive model of this type may still simulate to a tolerable degree the actual wind oscillations over large-scale mountain slopes.

For these assumptions, (1) yields the following two equations of the two horizontal components of what can be referred to as "tidal Ekman

Flow",

(22a) $u_t - (v-V)f = K_{Ek} u_{zz}$; and, $v_t + u f = K_{Ek} v_{zz}$, where the geostrophic wind speed $V = V(t)$ represents the forcing function. A formal analogy to (20a) or (21b) can be established by a simple process of elimination of dependent variables. This is achieved in the first form of (22a) with the aid of u_t and u_{zz} derived from the second form; a corresponding procedure serves to eliminate v in the second form.

$$(22b)\quad \begin{cases} V = v + K_{Ek} f^{-2}(-2v_{zzt} + K_{Ek} v_{zzzz}) + f^{-2} v_{tt} \, . \\ -V_t = uf + K_{Ek} f^{-1}(-2u_{zzt} + K_{Ek} u_{zzzz}) + f^{-1} u_{tt} \, . \end{cases}$$

In comparison with simple electric and mechanical systems, the major difference in (22b) is the more complicated structure of the resistance term due to the fact that we are dealing with second order partial rather than ordinary differential equations. Boundary conditions for (22b) are exactly the same as specified for the Ekman spiral (16c). Note that on the left-hand side of the second equation in (22b), an additive term with V_{zz} will appear if not, as assumed here, geostrophic shear V_z is independent of height.

Because only periodical processes are considered, the forcing function

$$(23a)\quad V(t,z) = \bar{V} + \bar{V}_I \cos \omega t$$

and the formally defined response functions

$$(23b)\quad \begin{cases} u(t,z) = \bar{u} + \bar{u}_I \cos \omega t + \bar{u}_{II} \sin \omega t, \\ v(t,z) = \bar{v} + \bar{v}_I \cos \omega t + \bar{v}_{II} \sin \omega t, \end{cases}$$

represent a system with separation of independent variables because barred values are functions of z only. It can also be said that the overbar denotes 24-hourly averages at a certain level. The amplitudes of the response functions are $(\bar{u}_I^2 + \bar{u}_I^2)^{1/2}$ and $(\bar{v}_I^2 + \bar{v}_{II}^2)^{1/2}$, and the phase angles, $\tan^{-1}(\bar{u}_{II}/\bar{u}_I)$ and $\tan^{-1}(\bar{v}_{II}/\bar{v}_I)$. The problem is to express impedance and phase angle in terms of the three parameters K_{Ek}, f, and ω. This is achieved by inserting (23a and b) into (22a) and considering the four simultaneous differential equations in z which are given by the sum of factors of $\sin \omega t$, and of $\cos \omega t$, respectively. Lettau (1964) presented a solution for the v-component; this solution has later been completed by MacKay (unpublished term paper at the University of Wisconsin) for proper boundary conditions of u.

For oscillating thermal wind, the amplitude of the forcing function V will be a linear function of height; let

(24a) $\bar{V}_I = \bar{V}_{I,o} - z\bar{V}_{I,z}$, and consider, in addition to η as defined in (16d), the following convenient abbreviations,

(24b) $a \equiv f/2(f-\omega)$; $b \equiv f/2(f+\omega)$;

$$\alpha \equiv \eta / \sqrt{2a} \; ; \; \beta \equiv \eta / \sqrt{2b} \, .$$

With the aid of the above identities, the Lettau-MacKay solution is

(24c) $\bar{v}_I = (a + b)\ \bar{V}_I - \bar{V}_{I,o}(a\, e^{-\alpha} \cos\alpha + b\, e^{-\beta} \cos\beta)$

$\bar{v}_{II} = \bar{V}_{I,o}(a\, e^{-\alpha} \sin\alpha - b\, e^{-\beta} \sin\beta)$

$\bar{u}_I = -\bar{v}_{II}\, \omega/f - \bar{V}_{I,o}(1/2\, e^{-\alpha} \sin\alpha + 1/2^{-\beta} \sin\beta)$

$\bar{u}_{II} = \bar{v}_I\, \omega/f - \bar{V}_{I,o}(1/2\, e^{-\alpha} \cos\alpha - 1/2\, e^{-\beta} \cos\beta),$

while $\bar{u}$ and $\bar{v}$ are given by the Hesselberg-Sverdrup solution (18). Note that in subsequent expressions for the impedance a term like $a + b$ appears which is the same as $f/(f^2 - \omega^2)$. Siebert (1961) remarks that the theory of atmospheric tides always results in amplitudes which are proportional to $1/(f^2 - n^2)$ where n equals the frequency of the tidal force. Thus, for a given n there will be a " critical" latitude for which the denominator in the amplitude vanishes. However, Siebert (page 136) provides clues that in reality this does not lead to singularities at the "critical" latitude.

In boundary layer response described by equations (24c) the "critical" latitude is where $f = \pm\ \omega$ or, $1 = \pm\ 2 \sin\phi$, that is 30 deg N or 30 deg S. With a gradual approach to such "critical" latitude, any possible increase in wind component amplitudes will of certainty make the inertia terms of $d\vec{v}/dt$ large, so that consideration of $\vec{v}_t$ alone will be unsatisfactory and equations (22a) must be modified to correct for this condition.

The above discussion suggests also that tidal Ekman flow, when studied as a function of latitude relative to the "critical" value of 30 deg N or 30 deg S, will exhibit similar trends as known from electric or mechanical systems for methodical variation of exciting frequency relative to the natural frequency of the system. Concerning phase relationships, it can be concluded that for a given solar forcing function along one and the same meridian, the response of a boundary layer wind component may "lag" at latitudes poleward of 30 deg, while it "leads" equatorward of 30 deg. At the "critical" latitude it will be in phase but resistance will dominate the response, probably resulting in relatively small impedance.

It will be an interesting problem to investigate how such excitations, generated in the boundary layer, are communicated into the free atmosphere aloft. Siebert (1961) emphasizes that contrary to simpler vibration problems the resonance of a global tidal wave cannot be determined by its period alone, since the appropriate resonance parameter is the so-called equivalent depth of the atmosphere, which depends also on vertical structure of tropo-, strato-, and mesosphere.

4.4 The Thermo-Tidal Wind of Mountain Meteorology

The remaining problem is to combine the elementary considerations of the preceding sections. From 4.1 we recall that meso-to-large-scale mountain massifs can produce a thermal wind parallel to the general trend of the contour lines which, in turn, may run parallel with the isobars at some lower reference level. Due to diurnal cycles of solar heating on such slopes, seesaw variations of thermal wind or geostrophic shear will produce a harmonic forcing function in the

atmospheric boundary layer. From Section 4.2 we consider the result that geostrophic shear is known to be additive to frictional shear, within a tolerable degree of approximation From Section 4.3 we recall that for a harmonic forcing function as given by diurnal variations of geostrophic wind and shear, the boundary layer flow responds dynamically with an impedance such that 30 deg is a significant latitude for phase relationships. This is interesting for applications to continent-wide terrain slopes which extend from polewards of 30 deg latitude across the equator; see Table 4.

Table 4. Schematic summary showing sign combinations of the two impedance parameters [$f = 2\omega \sin \phi$ = Coriolis parameter, and $f^2 - \omega^2 = \omega^2 (4 \sin^2 \phi - 1)$] as functions of latitude from pole to pole.

Latitude Range:	90 N to 30 N	30 N to Eq.	Eq. to 30 S	30 S to 90 S
Sign of f :	+	+	-	-
Sign of $f^2 - \omega^2$:	+	-	-	+

In the following, a few illustrations of boundary layer structure over mountain slopes will be given. The summary in Table 4 shows a remarkable asymmetry of sign combinations between the northern and southern hemisphere. This fact explains why in illustrations of thermo-tidal winds we will have to specify both the latitudinal range (either polewards or equatorwards of 30 deg) and the hemisphere. Further specifications concerning daytime or nocturnal phases are necessary while the specification of azimuth into which the slope is facing, is mostly for geographical reference.

To exemplify characteristics of tidal Ekman flow and, specifically, the significant differences in phase angles polewards and equatorwards of 30 deg latitude, Fig. 22 shows two sequences of v-profiles, at arbitrarily selected latitudes of 45 deg and 23.5 deg, for the same forcing function, that is a seesaw oscillation of V pivoting about a fixed value at the level near the top of the Ekman layer where $\eta = \pi$ in (16c). The

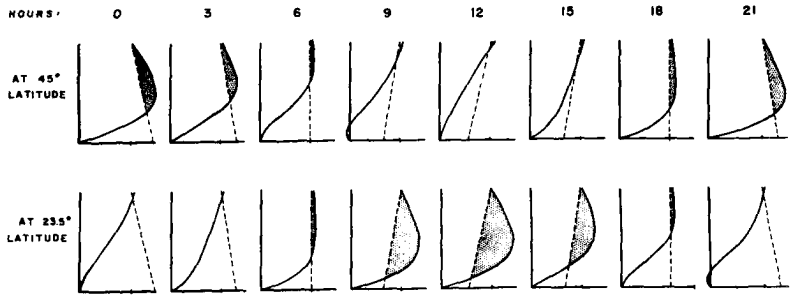

Fig. 22 Example of tidal Ekman flow, showing time-varying v-profile structure for every third hour during a 24-hourly cycle of forcing geostrophic wind and shear (V, dashed lines), contrasting the results of response computations for two latitudes (one poleward and one equatorward of 30 deg). Note differences in phase angle and intensity of super-geostrophic values (that is, low-level jet occurrence).

maximum phase of V at the ground level was assumed to occur at zero hours, and profiles were computed for every three hours throughout the 24-hr cycle, using the solution given by Lettau (1964). It was found that for the two latitudes chosen the phase angles differed by nearly twelve hours or, 180 deg. Specifically, v leads V (by about two hours) at 45 deg latitude, while v lags V (by about ten hours) at 23.5 deg latitude, in terms of the discussion in Section 4.3.2.

Fig. 23 depicts, schematically, possible steady-state distributions of temperature and wind components in the boundary layer when geostrophic wind and shear are restricted to the direction of the contour-lines of the terrain. This illustration supports discussions in Sections 4.1 and 4.2, and demonstrates the special but not unusual thermodynamic conditions for which a frictionally induced cross-isobar component of air motion may counterbalance a direct circulation system (that is, one derived from the equation of motion without regard to Coriolis forces). For this purpose, and with reference to the discussions of "modified" diurnal circulations in Section 3, profiles of kata-

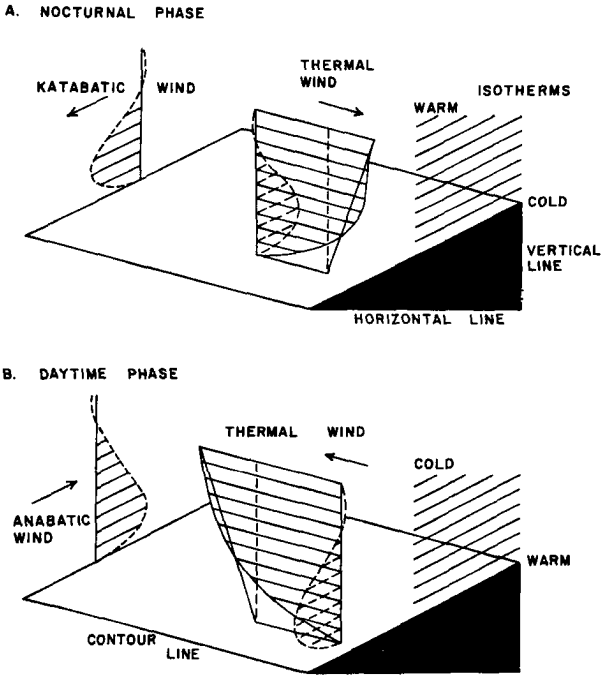

Fig. 23 Scheme of steady-state boundary layer wind profile over sloping terrain on the northern hemisphere, contrasting nocturnal and daytime phases of temperature stratification, and resulting geostrophic shear. The two cases refer to overall geostrophic wind parallel to the contour lines, so that frictionally induced cross-isobar flow counteracts direct katabatic and anabatic circulations which follow the fall-line.

batic and anabatic flow are also included in the scheme on Fig. 23. In terms of developments in Section 4.1, the assumption is that $T_h = 0$, whereupon, due to (13c), the thermal wind in (10) becomes proportional to $-T_z \vec{k} \times \nabla h$. Also, concerning the pressure field at the horizontal reference level below the slope, a barometric low under elevated terrain is assumed in the upper half of Fig. 23 (that is, $p_1 \sim -h$), whereupon for inversion ($T_z > 0$) or, the nocturnal phase, the direct circulation may indeed be overruled by the frictionally induced component of the spiral flow. A corresponding counteraction to anabatic flow for the daytime phase ($T_z < 0$) will require a barometric high under elevated terrain (that is, $p_1 \sim +h$), as depicted in the lower part of Fig. 23. In a logical extension of the argument, the corresponding cases with support of direct circulations could be constructed. More interesting is the remaining step, namely, the consideration of impedance and phase angles in the response to harmonic variations of geostrophic wind and shear over mountain slopes.

Obviously, the descriptive parameters of meteorological terrain effects can be arranged in a great variety of possible combinations. As an example related to one of the case studies of Section 3, Fig. 24 illustrates the nocturnal phase of thermo-tidal winds for two slope

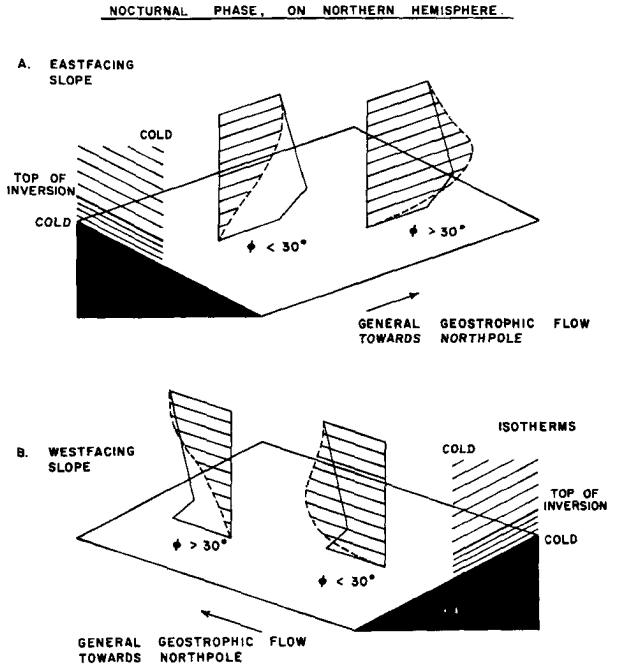

Fig. 24 Scheme of northern-hemispheric thermo-tidal wind on mountain slopes in the nocturnal phase; showing geostrophic shear due to indicated thermal stratification, and v-profiles according to theory, for latitudes poleward and equatorward of 30 deg. The indicated general direction of geostrophic wind corresponds to a case of $p_1 \sim -h$ in the upper part, and $p_1 \sim +h$ in the lower part of the illustration.

inclinations of opposite sign on the northern hemisphere, both polewards and equatorwards of 30 deg latitude. The indicated prevailing geostrophic southwind could correspond to climatological barometric gradients between the Bermuda High and the relatively warm Rocky Mountain Low, so that the wind profiles shown may simulate conditions on the large-scale inclines of the Mississippi River basin. The illustration suggests that low-level jet stream maxima north of 30 deg latitude can be nocturnal only on the east-facing slope. This may include, first of all, the regions of Oklahoma, Kansas and Nebraska, but possibly, also the Appalachian slope on the Atlantic side, where indeed Bonner's chart shows a noticeable increase of frequency of low-level wind maxima occurrence; see Fig. 16.

At the end of Section 4.1.5, results, as implied on Fig. 24, had been discussed and it was pointed out that wind conditions on the desert slope of Peru would need an additional explanation of the feature that thermo-tidal wind maxima occur as a daytime and not as a nocturnal phenomenon. It may suffice here to refer to Fig. 22 which illustrates that the solution (24) predicts significant phase changes in the response to the forcing function of geostrophic winds poleward and equatorwards of 30 deg latitude. It can very well be that at 17 deg S the wind response lags by nearly one-half period the forcing geostrophic wind which will have a minimum value in the early afternoon, as evidenced by the plot of barometric differences on Fig. 10. Concerning observations of wind profile structure on the Pacific slope of the Andes chain, more detail will be discussed in Section 5.

5. Observational Testings of Predictions Based on the Theory of Thermo-Tidal Winds

5.1 Diurnal Variations of Wind Velocity in the Boundary Layer over the Midwestern United States

5.1.1 Introductory Remarks: In Section 4.3 it was concluded that the term "tidal" can be used in connection with harmonic oscillations of meteorological elements when they are caused by cycles of insolation. Obviously, this definition would include annual cycles which, at the geographic poles, are exclusively the only solar cycles of significance. While a case study of the boundary layer over antarctic or arctic ice domes has helped to clarify the dynamic effects of an inclined inversion layer, the annual cycle of insolation has here only secondary importance, and quasi-steady "inversion" winds should be excluded from the class of thermo-tidal motion. Instead, the term geotriptic winds, as suggested by Johnson (1966) and discussed in Section 4.2, should be applied. In fact, the "inversion" wind will, in steady cases, follow from a balance between the three forces of pressure gradient, Coriolis, and internal friction; it appears legitimate to disregard a possible distinction between barometric gradients superimposed on the boundary layer by migrating disturbances or general circulation, and those caused by negative net-radiation at the ground surface and the resulting thermal stratification over meso-to-large-scale terrain slopes. Consequently, the use of the name thermo-tidal winds will be restricted to oscillating air motions caused by insolation cycles of diurnal frequency in the boundary layer over mountain slopes,

provided that these are of sufficient extent to bring Coriolis forces into play.

Thus, for the preliminary testings of the concept, only the two cases described in Sections 3.1 and 3.2 will be considered and we shall begin with the air over the large-scale terrain slope between the Rocky Mountains and the Mississippi River.

5.1.2 Thermo-Tidal Theory and the O'Neill Data: Detailed testings of predictions derived from thermo-tidal theory of boundary layer dynamics will amount to a substantial program of data analysis, which just has entered an initial phase. It is self-suggestive to give, for first comparison, preference to the most detailed and systematic observations available. In this respect, the Great Plains Turbulence Field Program is still unique; the sixth of the seven "General Observation Periods" which began in the early morning of 31 August, 1953, and was continued through the late morning of 1 September, was the relative best experiment; see Lettau and Davidson (1957; Volume II). Since 24-hourly cycles are of primary interest, an available computer program for harmonic analysis was applied to representative wind-component data in the geographic system, as published in Table 7.1, page 533, Volume II of Lettau and Davidson. Another computer program permitted to transform the component data for each level into a geotriptic system (for this particular day, with the y-axis pointing into the azimuth N 7.3 deg E) as well as a geostrophic system (with the y-axis pointing into N 30.0 deg E). In other words, the average departure angle between surface layer wind and the orientation of the surface isobars on this day was 22.7 deg, a value of a magnitude to be expected for open prairie country. Vertical profiles of 24-hourly averages, also amplitude and hour of maximum phase for wind components in all three systems, are plotted in Fig. 25.

Inspection of Fig. 25 reveals the important fact that means and amplitudes tend to approach zero at a level of about 2.2 km, which happens to be slightly above the highest level of data evaluation (2000 m). This suggests that on this day the lower atmosphere was indeed satisfactorily close to an equivalent-barotropic state; moreover, 24-hr means and amplitudes show a generally linear height change, or, a nearly height independent, but harmonically varying thermal wind. This implies that a geostrophic system of coordinates is indeed uniquely defined, since only a seesawing V-component, and no U-component, of geostrophic velocity occurs during the entire 24-hourly period. Note also, that vertical profiles of phase angles indicate, somewhat surprisingly, that the upper layers lead the lower layers; namely, the closer the wind level to the ground surface, the later the hour of maximem phase. This finding, of course, is valid only for levels at and above 100 m, which are included in Fig. 25. With the aid of detailed wind profile observations between 0.25 m and 16 m, obtained during the O'Neill experiments, it is easily shown that in the surface layer the maximum phase of wind speed occurs, first of all, during daytime, and secondly shows retardation with height. This reflects, in part, the opposite diurnal variation of wind speed, well-known, for example, from anemometer recordings on radio towers above and below a "neutral" level which may be found at about 50 to 150 m. Quite clearly, the lowest surface layer must be excluded from our consideration because here the Ekman assumption is most unsatisfactory.

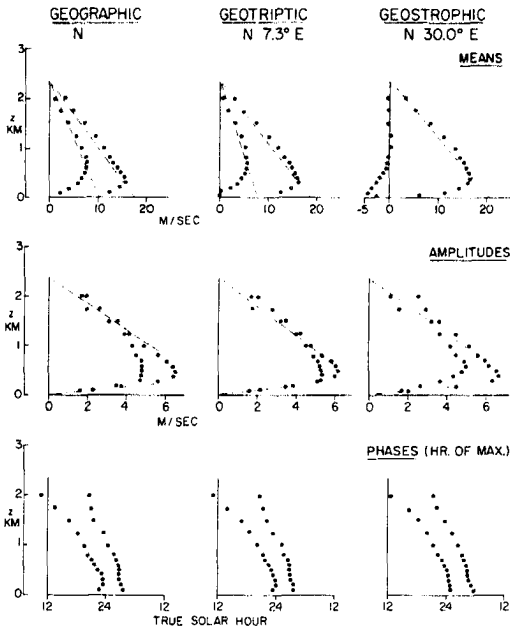

Fig. 25 Results of Fourier Analysis (24-hr mean, also amplitude and phase angle of the first harmonic) of representative wind components in the lower 2000 m above the prairie country in North-Central Nebraska, on 31 August, to 1 September, 1953. Full dots are u-components, open circles v-components of horizontal air motion employing three different coordinate systems (as defined on Fig. 18) with the indicated y-axis orientation.

We recall from Section 4 that the tentative mathematical model of thermo-tidal winds requires for verification essentially only one empirical parameter which is K_{Ek}, because f is fixed for a given latitude; for O'Neill, at ϕ = 42.5 deg N, f = 0.985 10^{-4} sec^{-1}. Using the 24-hourly averages of wind components in the geostrophic system, the comparison with the Hesselberg-Sverdrup solution (18) suggested, for this particular day, $\bar{V}_o$ = 21.0 m/sec, $\bar{V}_z$ = -0.010 sec^{-1}, and K_{Ek} = 2.2 m^2/sec. This effective viscosity may appear relatively low; it fixes the height-scale of the solutions (18) and (24c); specifically, (16d) for this K_{Ek} yields $\eta = \pi$ at 670 m above the ground; this level is marked in Fig. 26.

The empirically derived geostrophic shear of 0.01 sec^{-1} corresponds to a constant thermal wind which--according to equation (10)--requires an over-all horizontal gradient of air temperature of -3° C per 100 km (colder towards the ESE). The southerly geostrophic wind

at ground (or lower reference level) calls for a barometric low towards the WNW and higher pressure towards the ESE from O'Neill. When z is in meters, the forcing function (in m/sec) is fairly closely approximated by (24a) in the form, $V(t,z) = 21.0 - 0.01\,z + 5.5\cos\omega t$, and is valid for the height range between ground and 2000 m, disregarding tentatively amplitude variation with height. Thus, at all times during this particular day, the lower troposphere remains in an equivalent-barotropic state.

For the geostrophic system of coordinates, vertical profiles of amplitudes and phase angles of the response functions as defined by (23b) and numerically specified by (24b and c) were calculated with the aid of a computer program. In Fig. 26 results are plotted in a form which permits direct comparison with observational data (on a slightly enlarged scale, but otherwise the same as in Fig. 25). Considering the restrictive nature of the tentative model, the general agreement between theory and observation may be judged as fair.

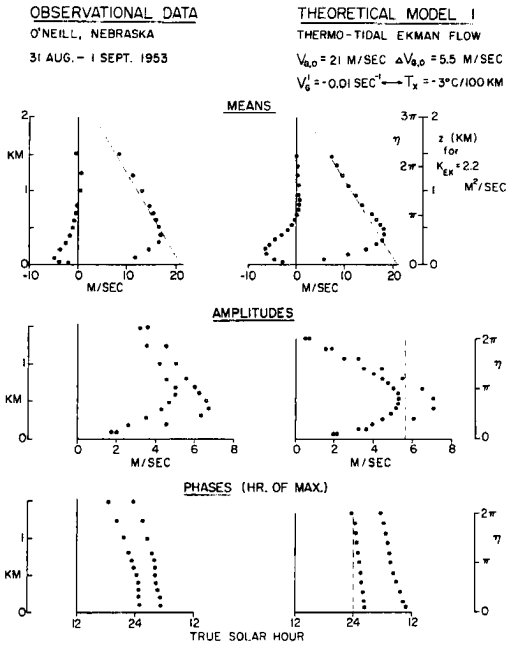

Fig. 26 Comparison of 24-hr means, amplitudes and phase angles in diurnal variations of wind components (geostrophic system; u denoted by dots, v by open circles), between observation and theory of thermo-tidal winds. Note that geostrophic wind, geostrophic shear, and effective eddy viscosity are exclusively derived from the 24-hourly means.

Note especially the relative magnitude of u and v components at and below $\eta = \pi$ (that is, at and below $z \approx 700$ m), and also that, indeed, the theoretical phase angles confirm the leading of higher and lagging of lower wind levels. Discrepancies can be described by saying that the theoretical profiles tend to be too well-rounded; obviously, this is a consequence of the Ekman assumption. The same tendencies are also noticeable when theoretical 24-hr means, amplitudes, and phase angles for the two wind components are used to calculate wind vectors for a variety of levels at a given time of the day, and series of hodographs are constructed. Results, in comparison with observations, are shown on Fig. 27, for every three hours of the full diurnal cycle. Note that the wind profile measurements were obtained for all even hours; the values for the odd hours (3, 9, 15, and 21 on Fig. 27) are averaged from the two bracketing even hours. Fig. 27 shows strikingly the overall daily development in the atmospheric boundary layer over Central Nebraska; it is characterized by weak vectorial wind shear during daytime, and extremely strong vectorial shear with pronounced velocity peaks in a narrow layer around 400 m at nighttime. This trend is generally well-simulated by the thermo-tidal theory, even though the computed hodographs appear somewhat rounded. It may be concluded that theory can predict an essential feature of boundary layer wind oscillations, namely, the low-level jet stream as the nocturnal phase of a forced oscillation due to seesawing geostrophic shear caused by insolation on a meso-to-large-scale terrain slope.

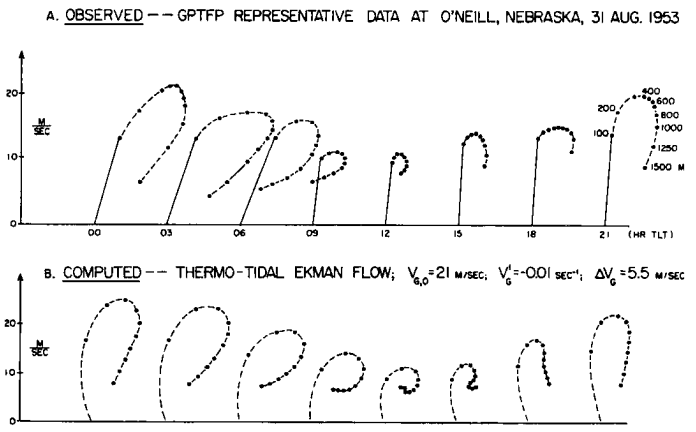

Fig. 27 Diurnal trends in boundary layer structure depicted by a series of hodographs (between 100 and 1500 m above ground) for every third hour of the day. Above, directly observed during the Great Plains Turbulence Field Program over the large-scale terrain slope of Northern Nebraska; below, calculated thermo-tidal winds for latitude $\phi = 42.5$ deg, and indicated parameters which describe the forcing function of geostrophic wind and shear, and its diurnal amplitude.

It may be added that harmonic analysis was also applied to other periods of the O'Neill program and likewise to the hourly wind soundings at Oklahoma City of the special program reported by Hoecker (1961). The results confirmed the findings as summarized in Fig. 27 for O'Neill; however, it became quite evident that the wind soundings in Hoecker's program did not equal the representativeness and accuracy of that at O'Neill.

The dynamics of thermo-tidal cross-isobar flow over the Midwestern United States, specifically, the tendency towards upslope motion during the maximum phase of diurnal wind development, under external conditions which may be applicable to the cases of nocturnal thunderstorms--see Section 3.2--is work for the future. It appears, from tentative analyses, that this phenomenon requires a truly baroclinic development of the lower troposphere, and not just the equivalent-barotropic case treated above. It may be added that the observational periods during the O'Neill program were selected (with the aid of synoptic weather analysis and forecasts supplied by the United States Weather Bureau in Kansas City) so that they did not coincide with local thunderstorms or other disturbances. Thus, the O'Neill samples may be representative only for fair-weather. Jet-stream developments at Californian slopes are evidenced in data presented by Frenzel (1962).

5.1.3 Brief Review of Previous Theories of the Low-Level Jet: Assuming horizontal pressure gradients constant in time and space, Blackadar (1957) proposed that the mechanism which generates the low-level jet is the diurnal cycle of insolation and, subsequently, that of convective turbulence and eddy viscosity associated with the variations in vertical lapse rate of temperature in the boundary layer. Normally, in the course of the day, convection dies out in the late afternoon, whereupon the frictional forces decrease significantly and rather abruptly. Then the upper strata of the boundary layer are no longer sapped by significant contributions to the downward transfer of momentum, to cover the frictional ground drag. Relieved of such restraints, the wind aloft speeds up, and once started, the development tends to build up and overshoot which may imply the formation of the low-level jet. As in any oscillation, the overshoot then corrects itself and the wind dies down again. In such manner Blackadar explains the phenomenon as a free oscillation which starts at that hour of the day when the restraint by a relatively strong friction force in the boundary layer is released. The period of inertia oscillation equals one-half pendulum day, or the sidereal day divided by $2 \sin\phi$. This statement can be immediately confirmed with the aid of the discussions in Section 4.3 and the value of "natural" frequency of the system (22) in the homogeneous case, that is, for zero intensity of the forcing function. The period of inertia oscillations thus decreases with latitude and it could very well be that at latitudes of the Central Unites States a pulse exerted in the form of sudden restraint-release in the late afternoon will lead to an overshoot which culminates around midnight, as observed in O'Neill.

Essentially, the low-level jet was explained by Blackadar by a mechanism which would produce a regular diurnal variation of wind velocity in the boundary layer over any (featureless or mountainous)

continent surface, and pronounced effects should be expected close to 30 deg latitude where the solar day equals approximately the half-pendulum day. As early as 1841, Espy had suggested that diurnal courses of convection intensity could be the cause of certain opposite trends evidenced by diurnal variations of wind speed in the lower versus the upper portion of the frictional layer; this climatological fact was known from wind observations on top of relatively isolated hills, and later confirmed by anemometry on tall radio towers in otherwise featureless country; Koeppen, in 1883, added more detail, while Wagner (1936) in further extension of the Espy-Koeppen concept, showed that the occurrence of daytime maxima of wind speed in the lowest 10 to 20 percent of the boundary layer coincides with the vertical regime where 24-hourly mean eddy viscosity typically increases with height, while in the upper 80 to 90 percent nighttime maxima occur and the eddy viscosity decreases with height. It may be noted that a corresponding non-monotonic profile of eddy viscosity applies to the theoretical model of barotropic boundary layer structure developed by Lettau (1962) and discussed in Section 4.3.2. Because the daily speed maximum in the upper part coincides with the occurrence of the minimum in the lower part of the boundary layer, there is obviously a tendency to a jet-like development in the Espy-Koeppen-Wagner model. However, Blackadar and Buajitti (1957) found, with the aid of calculations based on a great variety of theoretical solutions for diurnally varying eddy viscosity, that it was not possible to produce a satisfactory agreement with such extremely strong nocturnal peak values of wind velocity as, for example, depicted on Fig. 15. Moreover, Blackadar's theory fails to explain the geographic distribution of low-level wind maxima as shown so strikingly on Bonner's chart, Fig. 16. Even more, this chart provides only negative support if one would expect an enhancement of the phenomenon near 30 deg latitude. In a specific test of the free inertia oscillation hypothesis, Bonner (1965) established for the significant range of geographic latitude between South Texas and North Minnesota that there is a constant rate of diurnal turning of the vectors of geostrophic departure (and about equal to 15 deg per hour) when according to the theory of free inertia oscillations these rates should have systematically differed by about 50 percent.

Another theory was propagated by Wexler (1961) who emphasizes certain apparent analogies between the midwestern low-level jet (looking at it as a relatively shallow current emerging from the subtropical anticyclone over the Gulf of Mexico and being deflected by the east-facing slopes of the Rocky Mountains, also showing anticyclonal horizontal curvature due to the meridional variation of the Coriolis parameter) and the Gulf stream of the Atlantic (roughly paralleling the above air current but located along the shelves of the eastern continental United States). Wexler attributes this analogy to a suggestion by C. Newton and elaborated it after finding that Wagner's previous attempts to explain the nocturnal acceleration of the current, by drainage of cold air from radiationally cooled higher ground toward the west, was unsatisfactory. Hoecker (1963) attempted to decide empirically whether Blackadar's or Wexler's concept was valid but, using his special network, was unable to arrive at a clear decision, because he found that data "at times" seem to refute both theories; as one solid result he states that there seems to be no trade-wind source of the

low-level jet as had been suggested by Wexler. Bonner (1965) also weighs the two theories in the light of his statistical analysis of synoptic wind data and concludes that the two theories are not mutually exclusive. Bonner suggests that the nocturnal southerly jets arise from the superposition of a diurnal oscillation of boundary layer winds upon broad-scale synoptic patterns over the continental United States.

There are, of course, also studies which refer to the presence of the large-scale terrain slope. Sangster (1967) attempted to specify numerically a diurnal oscillation of geostrophic speed but arrived at a pressure gradient variation which would produce the wind maximum at midday; thus, he referred to the fact that, actually, the maximum speed of the low-level jet occurs at around midnight, as paradoxical. Most recently, the theoretical problem of diurnal boundary layer wind oscillations above sloping terrain was investigated by Holton (1967). The changes of density stratification as induced by insolation cycles in the thermal boundary layer on a topographical slope are considered as a source of potential energy which drives a diurnal wind oscillation. Holton finds, however, that the use of the Ekman assumption in his boundary layer model does not permit him to duplicate the extreme positive and negative shears and also the correct time of the maximum phase of the observed low-level jet over the midwestern United States.

The contrast between the new theory presented in this paper and the Blackadar and Wexler theories may be summarized by the following. The model of thermo-tidal winds requires the presence of a large-to-meso-scale terrain slope with the additional feature of a definite statistical or thermodynamic coupling between large-scale barometric fields and terrain contours; see Section 4.1 for the discussion of the resulting patterns of thermal wind and vorticity. To a degree this incorporates certain broad aspects of the special Newton-Wexler analogy. However, general mountain meteorology enters decisively with the specification of forcing functions of diurnal frequency due to seesawing geostrophic shear produced by insolation cycles in the boundary layer over large-scale topographical inclines. While Wexler tried to explain the low-level jet exclusively as a phenomenon of the east-facing Rocky Mountain slopes, Blackadar's basic concept would apply anywhere on continental surfaces (featureless or mountainous). In this respect, the mountain-meteorological model as proposed here is less discriminating than Wexler's but more so than Blackadar's. It applies to terrain slopes on any continent provided they are of sufficient horizontal extent and under a favorable synoptic-climatological regime with respect to both, the intensity of insolation cycles and the regional pattern of the overall general circulation systems of the atmosphere.

It should be added that seesawing geostrophic shear may be generated far from pronounced terrain slopes. The best climatological example will be a coastline which separates different regimes of thermal boundary layer development due to a discontinuity in thermal admittance between land and ocean surfaces. Low-level jet streams of some persistence, that is, without daily periodicity, may exist even over apparently uniform level surfaces, for example, over the ocean when there is a line of discontinuity of thermal admittance due to water depth, or horizontal current boundaries. Furthermore, they

may be met in connection with certain semi-persistent synoptic patterns in a local region, as described by Kuettner (1959) in New England, when strong negative geostrophic shear occurs due to the temporary presence of a cold anticyclone to the west over Eastern Canada.

5.2 Diurnal Trends in Wind Structure over the Andean Incline

A climatological analysis of aerological wind observations at the western coast of South America is certainly beyond the scope of this presentation. For this, we refer to recent literature, for example, a summary in the form of vertical cross sections for the seasons, with listings of previous work, and data sources, by Schwerdtfeger and Martin (1964). We merely want to supplement the discussion in Section 3.2 which dealt with diurnal wind structure along the Pacific incline at about 17 deg S. This supplement is interesting in the light of thermo-tidal theory because the Andean Mountain chain crosses the equator as well as 30 deg S which are two latitudes of significance in the dynamic boundary layer response to solar cycles. Let us remember the results illustrated in Fig. 22 in the form of time series for v-component profiles using a geostrophic system of coordinates where V (t) is the forcing function. A more complete verification of the solution (24) in Section 4.3 must also take into account the u-component and it follows that the lagging versus leading of the v-component is accompanied by characteristic differences between veering and turning of the wind vector.

In order to test this particular prediction of the simple theoretical model (24), standard synoptic wind observations which are available twice daily were employed, from the two Chilean radiosonde stations Antofagasta (23.4 deg S) and Quintero (32.7 deg S). Wind data were analyzed for the two southern-hemispheric summer seasons of Dec., 1961, through February, 1962, and Dec., 1962, through February, 1963. Representative terrain profiles are shown in Fig. 28. They demonstrate again that we are dealing here in every respect with a more than meso-scale terrain feature of monumental bulk; namely, an angle of inclination of about 1:50 prevails for lateral profile lengths of 150 to 200 km, stretching longitudinally over thousands of kilometers, since the total distance between La Joya and Quintero of about 1800 km is approximately the same as the distance from La Joya to the equator.

An apparent difference of the terrain profile for 17 deg S as depicted on Fig. 28 in comparison with Fig. 9 is explained by the fact that on Fig. 9 only levels of temperature measurements (excepting the peak of El Misti) were considered, while the terrain profiles on Fig. 28 were averaged from altitude readings (every 5 km) along five parallel lines drawn on topographical maps, perpendicular to the coast and 10 km apart, bracketing the geographic location of the indicated wind station. This evaluation, also the wind analysis in Fig. 29, was carried out by Mr. K. Rao, at the time,a graduate student at the University of Wisconsin.

Radiosonde wind data were available from published records for the hours of 00 and 12 standard world (Z) time (about 7 p.m. and 7 a.m. local time) which, at this season, corresponds to shortly before

sunset and shortly after sunrise, respectively, or the end and the beginning of the solar heating cycle. From published speed and direction values, wind components in the geographic system were calculated at all standard pressure levels and then averaged for the season, separately for the two winters. On this basis, hodographs of vector-mean winds were constructed as illustrated on Fig. 29. Approximately, the pressure level of 850 mb corresponds to 1.6 km, 700 mb to 3.2 km, and 500 mb to 6 km. It may briefly be noted that the 00 Z averages at Antofagasta seem to be quite similar to mean winds at Lima, at about 12 deg S. Rudloff (1959) has summarized wind observations at Limatambo Airport for the years 1953 to 1956 and reports strong south winds (showing remarkable persistence) below 1000 m, northwesterly directions between 1000 m and 3000 m (with speed and constancy decreasing with height), and easterly winds above 3000 or 4000 m. Incidentally, this confirms the statement in Section 3.1 that there is hardly any indication of average Foehn components along the Peruvian incline due to lack of east components below the crestline level of the Andes.

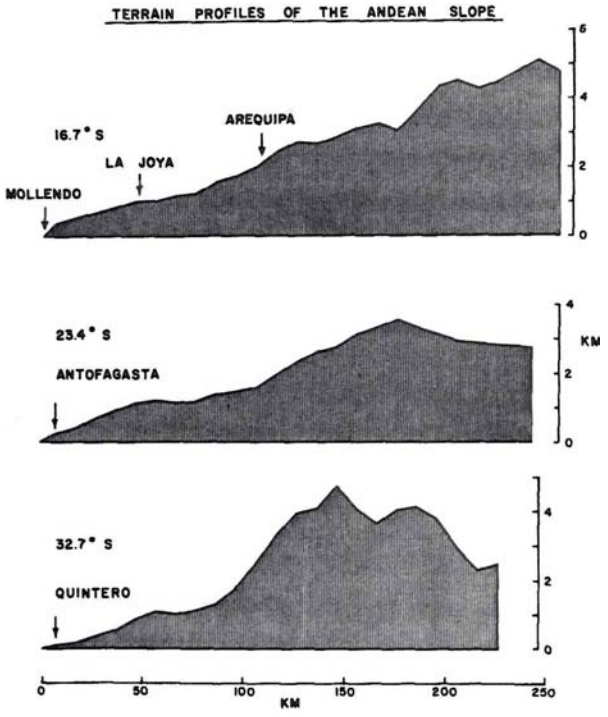

Fig. 28 Terrain profiles for the Andean incline (averages for strips of about 50 km width bracketing marked localities, and running inland perpendicular to the general direction of the coastline), centered at the three indicated geographic latitudes.

The essential feature shown in Fig. 29 is the highly intriguing manner in which veerings of the wind vector with height alternate with turnings, from station to station, as well as end of day to beginning of day. For brevity, reference is made to the description in the caption of Fig. 29. Note that these peculiar wind conditions occur mainly below about 700 mb, or approximately 2.5 km, which is somewhat below the elevation of the average crestline of the mountain chain to the east of the stations, see Fig. 28. The results from the first summer season studied seem to be fairly well confirmed by those from the second summer. However, merely two samples per day taken 12 hours apart cannot be satisfactory for a conclusive testing of predictions based on thermo-tidal theory. It will be necessary to obtain more detailed wind profiles from the Andean incline based on round-

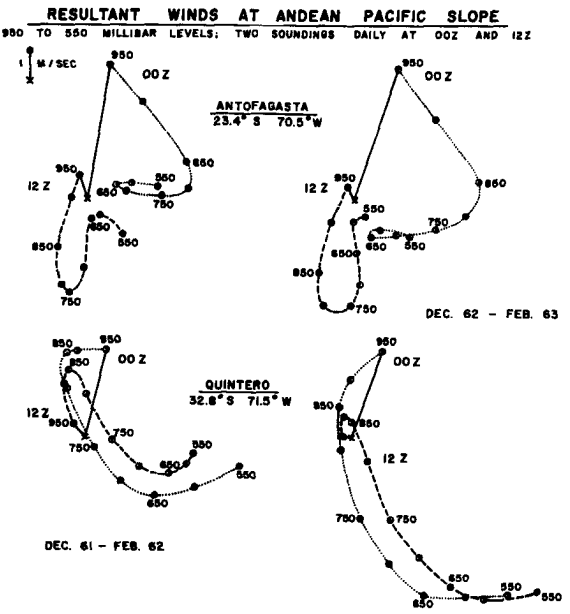

Fig. 29 Resulting winds at standard levels between 950 and 550 mb, for two synoptic aerological stations at the Andean incline. Upper half: Antofagasta (equatorwards of 30 deg S); lower half: Quintero (polewards of 30 deg S). Left half: Summer season averages for 1961, 1962; right half: Summer season averages for 1962, 1963. Dotted hodographs: Data for 00 Z or, locally, at about the ending of the daily insolation cycle; dashed hodographs: Data for 12 Z or, locally, at about the beginning of the daily insolation cycle. Note that at 00Z both stations in both years show tendency to low-level wind maxima, but in combination with clockwise turning (veering) at Antofagasta and counterclockwise turning at Quintero; while at 12 Z, winds show turning at Antofagasta and veering at Quintero.

the-clock pilot balloon soundings and supported by meteorological measurements using instrumented aircraft and other methods. Plans for an aerological program within the framework of renewed University of Wisconsin field work in this area are under way.

6. Concluding Remarks; Speculations on General Importance of Winds in the Boundary Layer over Large-Scale Mountain Slopes

6.1 Brief Appraisal of Geotriptic Mountain Currents as Environmental Factors

In addition to atmospheric dynamics there seems to be a complex of fields, climatological, geographical and biological, as well as technological, which are affected to various degrees by the specific environmental conditions generated by geotriptic air currents in the boundary layer over large-scale mountain slopes. In Section 3.2 the relationship between the low-level jet stream of the midwestern United States and occurrence of nocturnal thunderstorms was mentioned. It may be added that Schweigger (1959), speaking from personal experience of wind and weather observations in the region over many years, mentions that nighttime lightning displays over the Andean Mountains are a familiar spectacle to the sailor in coastal waters of Peru.

In one of the earliest studies of southerly wind maxima at low levels, Means (1954) connected the phenomenon with weather conditions which lead to river floods in Kansas. Wexler (1961) states that airplane pilots are grateful for 30 or more knots tailwinds when flying north before dawn. But there are also special hazards as summarized by Barad (1961). The strong winds can make landing maneuvers of light airplanes difficult, and sometimes be the cause of forest fire "blow-ups".

There are also direct wind effects on plant and animal life. The traveler in the Oklahoma "panhandle", or eastern Kansas, will note that trees growing along the roads and around the farms show "wind-training", or "flagging" towards the north. These terms describe an effect of relatively strong and persistent winds which causes bending of the growing branches until they point permanently into the leeward direction. This phenomenon may reflect more the steady-state condition of a broad southerly current partly due to the Rocky Mountain barometric low rather than the nocturnal low-level jet stream of the region.

The persistent south winds in the boundary layer together with the nighttime intensification will not only aid airplanes traveling north, but also serve to transport floating particles, like dust, or spores, over long distances. Especially interesting is a migration of spores observed every summer. The spores which cause stem rust of wheat in the Canadian provinces of Manitoba and Saskatchewan can only originate in southern regions, like New Mexico; for details on similar problems of aphid migration, reference can be made to Medler (1967). Birds are known to utilize special vertical-lateral mountain slope circulations of diurnal periodicity. Professor A. Hasler of the Zoology Department at Madison, once mentioned that one of his teachers had lectured on the remarkable feeding habits of South American con-

dors. While these birds nest in the high ranges, they were reported to feed regularly on dead fish washed ashore along the Pacific beaches, thus crossing the desert strip twice daily and covering substantial vertical as well as horizontal distances. Possibly, these condor flights could provide indicators for preferred times of updrafts or downdrafts prevailing along the fall-line of the Andean incline and thus clarify the thermo-tidal nature of these winds and their regional occurrence. Unfortunately, efforts to locate literature references on the condor's feeding schedule were not successful, and cooperation by any reader who could supply information would be appreciated.

From the Andes region near Cali, Colombia (about 5 deg N), Lopez and Howell (1967) report that watching the flight patterns of buzzards has helped to estimate the vertical extent of rather intriguing daytime "katabatic" downslope air currents on the east flanks of the western Cordillera, where also occasional grass fires are spreading normally downhill in further support of such unusual daytime flow patterns. These observations are mentioned to illustrate the kind of meteorologically significant information which may be derived from indirect breeze indicators. Another example was the utilization of barchan orientation and migration in Section 3.2. In the case of sand dunes, however, it should be added that the information value will be highest if the observed facts are reported as objectively as possible. For instance, some unwarranted bias may have been introduced into the literature by Bowman's (1916) choice of the term "sea breeze" in connection with the dune movement in the Pampa de La Joya, even though the included climatic results from the Harvard project in the form of wind roses for La Joya showing overwhelming predominance of either south or east winds rather than breezes from the sea. Bowman also expresses some surprise that the coastal region seems to be relatively cloudfree at times when dune migration is most intense. In spite of the fact that these dunes move nearly parallel to both, the general direction of the coastline and the contour lines of the terrain, Troll (1952) likewise refers to barchan movements in the Pampa de La Joya as due to a "sea breeze" which is not terminated at the slope of the coastal range. However, Troll emphasizes the different nature of the diurnal circulation at higher elevations of the Andes mountains which he classifies as "Ausgleichs'Winde" according to Wagner's scheme since they indeed blow mainly perpendicular to the contour lines. Oscillations of this type are shown in Fig. 13 for Arequipa.

On a visit at the high-altitude observatory "Hochkanzel" (located at 3970 m, 7.5 deg S and 70.3 deg W) in March of 1966, I learned that at this latitude and elevation there is hardly ever a wind direction other than due west observed during most of the daylight period, and due east during the remainder of the diurnal cycle. Howell (1965) has described the "diurnal tide" of this region. However, at the foothills of the lofty ranges and green valleys surrounding the Hochkanzel, there lies the coastal desert where barchans again suggest shore-parallel rather than on-shore winds to be prevailing. The regional circulation pattern is indeed complicated and clearly calls for more detailed and better distributed wind profile measurements.

6.2 Speculations on Dry-Humid Contrasts in Climate and Weather as Possible Effects of Thermo-Tidal Slope Winds

Existing intercontinental similarities in large-scale climatic patterns have long been recognized. Koeppen (1931) constructed a representative scheme by combining observational climatic data from all five continents. This well-known "ideal continent" shows maximum aridity just equatorwards of 30 deg latitude at the west coasts of both hemispheres; the axes of these dry areas extend eastwards and slightly polewards but not to the east coasts. Discounting slight effects on the outlines of arid zones due to differences in zonal width of the "ideal continent", Koeppen appears to emphasize symmetry with respect to the equator, just as the characteristic pattern of mean isobars (including the location of the permanent cyclones and anticyclones) of the general circulation over lands and oceans tends towards symmetry between the hemispheres. While this seems to be confirmed by observations of the mean pressure distribution, the dry regions of the continents actually fail to be symmetrically arranged. For instance, Meigs' chart (Fig. 6) evidences rather strikingly an asymmetry of desert regions along three out of four coastlines of Africa and America, the only continents stretching through both hemispheres. Fig. 6 shows that the west coast of South America is dry south of the equator and humid to the north. A similar pattern exists on Africa's west coast while the east coast, most strikingly, is dry north of the equator and humid to the south. Meigs' chart also suggests that the latitude of 30 deg (north as well as south) coincides rather closely with zonal boundaries of deserts; examples are the Namib in South Africa, the Atacama in South America, also the Gobi in Asia.

In its restricted form, the tentative theory of thermo-tidal winds was already able to predict marked asymmetries in wind structure, either for different slope orientation at the same geographic latitude, or at the same slope for the two hemispheres with intriguing reversals between veering and turning at 30 deg. Such predictions based on Table 4 are exemplified in Fig. 22, or schematically illustrated in Fig. 24. They can be compared with observed facts such as shown on Fig. 16 concerning slope orientation, or Fig. 29 concerning significance of the 30th parallel. However, thus far no predictions are possible for the dry-humid contrast of a mountain slope. To achieve this, the tentative theoretical model must be supplemented by consideration of eddy diffusivity variations in height and time. Without going into detail, the physical consequences of time variations in resistance can be demonstrated with the aid of the analogy to electric circuitry; see Section 4.3.2. Namely, when resistance varies harmonically in direct coupling with the forcing function, the first harmonic of the responding current will be superimposed by a second harmonic as well as a continuous charging component. Correspondingly, the forcing function of thermo-tidal winds on mountain slopes, with feedback due to eddy diffusivity being large during heating and small during cooling, will cause an imbalance between geotriptic upslope versus downslope trajectories of air in the boundary layer. Whether up or down dominates will be decided by the combination of all parameters discussed in Section 4. One can expect reversals of mean lateral flow where the mountain range crosses the significant latitudes listed in Table 4. General downdrafts will reduce clouds, updrafts will stimulate them

and induce, possibly, precipitation. These may be subtle tendencies, but repeated day after day, they may explain aridity patterns if the mountain region under discussion is not too frequently disturbed by migrating cyclones.

Along a two-dimensional range which is under the influence of a uniform barometric gradient, one slope may be wet equatorwards but dry polewards of the 30th parallel, while the other slope will show the opposite relations. It will be necessary to put large-scale terrain slopes on Koeppen's "ideal continent" to explain the asymmetry of aridity evidenced on real continents.

The developments in Section 4.1 proved the need for consideration of the coupling between temperature, terrain contours, and large-scale barometric patterns. An assumption, made for simplicity only, was that surfaces of equal temperature move diurnally towards and away from the interface, so that the temperature gradient along the terrain slope (T_n) vanishes. This assumption may be legitimate only for the lower or middle part of the terrain slope. Normally, higher elevations will be cooler than midslope and lower regions, especially in the presence of snow pack. If the high ground remains relatively cold, thermal vorticity (see Table 2) produces cyclonic curvature aloft. This may stimulate clouds which reduce insolation and even may add new snow in a self-perpetuating process. The study of correlations between seasonal anomalies of temperature in higher mountain areas and convective activity in the foothill region may be promising.

In this connection, a unique feature of the coastal desert should be mentioned, the El Niño phenomenon of northern Peru. During a century there may be 8 to 12 isolated years in irregular sequence during which rather heavy summer rains occur. The El Niño event has been described by a number of writers; for references see Trewartha (1966). These rains seem to be due to several causes combined in a manner which is not yet satisfactorily understood. It appears possible that a consideration of the thermo-tidal wind scheme may help to explain why these rains once started tend to persist for weeks and months. Once a mounatin slope is wetted, insolation during the following day will partly be expended in the evaporation process, thus reducing the heating of air in the boundary layer and, consequently, the intensity of the forcing function. This weakens the thermo-tidal winds and hence also the normally prevailing tendency to counteraction of direct buoyancy effects. Clouds may form, reducing insolation furthermore, and new showers may occur. The following day will find even more favorable conditions for the same processes. It is known also that during El Niño periods, the upwelling of cool water along the coast stops and the air on the beaches gets hot and humid. Thus, the process is internally self-supporting due to the involvement of several local-regional factors. Only the initial stimulation of the process has to come from external causes, or a disturbance of the general circulation patterns.

The heating of continental inclines could be reduced not only by psychrometric cooling or cloud shadows, but also by surface albedo increase. This fact is interesting with regard to recent proposals to possibly stimulate convective activity and hence rain showers by artificial albedo-decreases in the form of blackening many square miles of tropical coastal deserts with asphalt coatings; see Black and Tarmy

(1963). However, in view of the reactions of thermo-tidal winds and subsequent overruling of direct circulations by geotriptic downslope or off-coast components, any increase in surface heating on a sufficiently large horizontal scale may enlarge an existing aridity. This means an interesting reversal of the so-called thermal mountain effect mentioned in Section 1.

6.3 Speculations on Glaciation Cycles

The self-supporting effect of geotriptic circulations over relatively cool uplands can be applied to the inversion layer over ice caps of continent-wide extent. We follow here thoughts outlined by Lettau and Schwerdtfeger (1967). Emphasis on the importance of a direct and purely gravity-driven circulation in the boundary layer over large-scale ice domes had lead several decades ago to the concept of the "glacial anticyclone". As presented by Hobbs more than 50 years ago, a semi-permanent glacial high-pressure center was expected to overlie the ice caps of Greenland and Antarctica. Hobbs suggested that such anticyclones played an important part in world-wide atmospheric circulation, but modern theory backed by observations made in Greenland as well as in Antarctica, leads to doubts about the validity of the concept of a "glacial high". In fact, with regard to attempts to explain temporary features such as Pleistocene glaciation, it can be argued that Hobbs' concept, quite paradoxically, links together several processes of which each one would tend to reduce snow accumulation Namely, anticyclonic weather will not produce fresh snowfall; if katabatic flow is strong enough to cause central subsidence, it will remove loose snow by wind-drift across the bounding coastline; and in summer, lack of cloud cover permits plenty of insolation with resulting sublimation of snow.

In significant contrast to Hobbs' thoughts, the concept of geotriptic winds due to a substantial inversion layer which envelops a snow dome, inevitably leads to positive thermal vorticity aloft and the more realistic picture of a cold-core barometric low; see Table 2 in Section 4.1. Thus, winds aloft will tend to circulate cyclonically about the snow dome. Subsequent surface friction at middle and upper levels leads to radial inflow of air, and the resulting upwelling to cloud formation and precipitation. In short, it is argued that a reversal of the concepts, from Hobbs' glacial high at lower levels to a cold-core low aloft represents the important feature. Under certain circumstances the build-up of a glacial ice dome resulting from the processes related to a cold-core low is self-enforcing until the accumulation of snow has reached a point when either the air is too cold to carry water vapor, or the load forces the continental crust to yield. This will reduce the inclination angle of the flanks of the snow dome and weaken the forcing function of geotriptic inversion winds. Together with the divergent mass discharge by glacier movements these secondary processes thus reduce the causes which originally lead to the formation of the cold-core low. Snow accumulation may stop, and the ice dome, after leveling out, could shrink and possibly disappear, on a time scale which may be of the order of 10^4 to 10^5 years as suggested by Pleistocene glaciation of various continental regions on earth. It can be expected that a new theory of ice ages could possibly be built on these concepts. Only the initial stimulus for a snow pack

to grow and its preservation over several summers would have to come from external causes, or a disturbance of the general circulation patterns. Once started, there will be feedback and self-enforcement of snow accumulation until the above mentioned processes generate self-destruction.

7. Acknowledgments

Expressions of sincere gratitude are due to those persons and organizations who in many ways have contributed to develop the concepts of the thermo-tidal wind, in the course of more than a decade devoted to research in atmospheric boundary layer dynamics. Certain ideas can be traced back to impressions gained during the O'Neill program of 1953 which was supported by the United States Air Force Cambridge Research Center. Incidentally, now I am inclined to say that the original title, "Great Plains Turbulence Field Program", may have been a misnomer; "Great Slope Turbulence Field Program" would have been a more appropriate name. Further research support and stimulations came from the United States Army organizations in Fort Huachuca, Arizona, and Natick, Massachusetts. Decisive has been the field work in the Peruvian desert which was made possible by the Center for Climatic Research (organized and directed by R. Bryson) at the University of Wisconsin under grant from the National Science Foundation. Another milestone was a field trip to South America supported by W. Howell's organization.

The gradual development of the theoretical aspects has been immeasurably helped and stimulated by personal contact with distinguished colleagues in many parts of the world. I appreciated very much the opportunities to present various stages of the development in the form of technical papers or seminar talks during the last three years at places including Bonn, Germany; Dallas, Texas; Fort Huachuca, Arizona; Lima, Peru; Madison, Wisconsin; Melbourne, Australia; Milwaukee, Wisconsin; Natick, Massachusetts; New Haven, Connecticut; Washington, D. C.; and last not least, Fort Collins, Colorado.

It is impossible to name the many persons who have contributed discussion remarks. Again and again, I have been urged to prepare a written version of my presentations. Finally, this has been achieved thanks to the kind invitation to the present symposium, organized by Dr. Reiter. The completion of the manuscript was also greatly helped by my temporary assignment (during July of 1967) to the National Center for Atmospheric Research at Boulder, Colorado, and by the cooperation of Dr. K. Lettau. In all likelihood, part of the ideas put forward will be controversial, but there is a real challenge which, it is hoped, will lead to a desirable re-orientation of present research towards a dynamic climatology with due consideration of the role of mountains for the regional-local energy budget, and boundary layer conditions in realistic models of the earth's continents.

REFERENCES

Asp, M. O., 1956: Geographical distribution of tornadoes in Arkansas, Monthly Weather Rev., 84, 143-145.

Bailey, S. I., 1906: Peruvian meteorology 1892-1895, Annals Astr. Obs. Harvard College, 39, part 2, Cambridge, Mass.

Barad, M. L., 1961: Low altitude jet stream, Scient. Amer., 205, 120-131.

Black, J. F., and B. L. Tarmy, 1963: The use of asphalt coatings to increase rainfall, J. Appl. Meteor., 2, 557-564.

Blackadar, A. K., 1957: Boundary layer wind maxima and their significance for the growth of nocturnal inversions, Bull. Amer. Meteor., 38, 283-290.

Blackadar, A. K., and K. Buajitti, 1957: Theoretical studies of diurnal wind variations in the planetary boundary layer, Quart. J. Royal Meteor. Soc., 83, 486-500.

Bleeker, W., and M. J. André, 1951: On the diurnal variation of precipitation intensity particularly over central United States, and its relation to large-scale orographic circulation systems, Quart. J. Royal Meteorol. Soc., 77, 260-271.

Bonner, W. D., 1966: Case study of thunderstorm activity in relation to the low-level jet, Monthly Weather Rev., 94, 167-178.

Bonner, W. D., 1965: Statistical and kinematical properties of the low-level jet stream, Res. Paper 38, Satellite and Mesomet. Res. Prog., Univ. of Chicago.

Bowman, I., 1916: The Andes of Southern Peru, Holt Comp., New York.

Burley, M. W., and P. J. Waite, 1966: Wisconsin tornadoes, Wisconsin Acad. of Science, Arts, and Letters, 54, 1-35.

Chapman, S., 1951: Atmospheric tides and oscillations, Compendium of Meteorology, Amer. Meteor. Soc., 510-530.

Cressman, A. P., 1960: Improved terrain effects in baroclinic forecasts, Monthly Weather Rev., 88, 327-342.

Dalrymple, P. C., H. H. Lettau, and S. H. Wollaston, 1966: South Pole micrometeorology program: Data analysis, Antarctic Research Series, Amer. Geophys. Union, 9, 13-58.

Finkel, H. J., 1959: The barchans of southern Peru, J. of Geology, 67, 614-647.

Frenzel, C. W., 1962: Diurnal wind variations in central California, J. Appl. Meteor., 1, 405-412.

Gregg, W. R., 1922: An aerological survey of the United States, Monthly Weather Rev., 20, 78 pp.

Hann, J., 1909: Zur meteorologie von Peru, Sitzungsber. Akademie d. Wiss., Wien, Math. -Naturwiss. Klasse, 118, Part II, 1283-1372.

Hesselberg, T., and H. U. Sverdrup, 1915: Die reibung in der atmosphere, Veroeff. Geophys. Inst., Univ. Leipzig, 2nd Series, 1.

Hoecker, W. H., 1965: Comparative physical behaviour of southerly boundary layer wind jets, Monthly Weather Rev., 93, 133-144.

Hoecker, W. H., 1963: Three southerly low-level jet systems delineated by the weather bureau special pibal network of 1961, Monthly Weather Rev., 91, 573-582.

Holton, J. R., 1967: The diurnal boundary layer wind oscillation above sloping terrain, Tellus, 19, 199-205.

Howell, W., 1965: Twelve years of cloud seeding in the Andes of northern Peru, J. Appl. Meteor., 4, 693-700.

Johnson, Jr., W. B., 1966: The geotriptic wind, Bull. Amer. Meteor. Soc., 47, 982.

Johnson, Jr., W. B., 1962: Climatology of atmospheric boundary layer parameters and energy dissipation derived from Gregg's aerological survey of the U. S., Section 7 of Final Report of Studies of the Three-Dimensional Structure of the Planetary Boundary Layer, Univ. Wisconsin.

Koeppen, W., 1931: Grundriss der Klimakunde, De Gruyter, Berlin und Leipzig, 388 pp.

Kuettner, J., 1959: The band structure of the atmosphere, Tellus, 11, 267-293.

Kung, E. C. T., 1963: Climatology of aerodynamic roughness parameter and energy dissipation in the planetary boundary layer over the Northern Hemisphere, Ann. Report, 1963, ed. by H. Lettau, Univ. Wisc. Sect. 2, Madison, 37-96.

Leet, D., and S. Judson, 1958: Physical Geology, 2nd ed., Prentice Hall, Englewood, N. J.

Lettau, H. H., 1950: A re-examination of the Leipzig wind profile, Tellus, 2, 125.

Lettau, H. H., 1951: Theory of surface temperature and heat transfer oscillations near a level-ground surface, Transactions, Amer. Geophys. Union, 32, 189-200.

Lettau, H. H., 1957: Windprofil, innere reibung und energie umsatz in den unteren 500 m ueber dem meer, Beitr. Phys. Atmosph., 30, 78-96.

Lettau, H. H., and B. Davidson, 1957: Exploring the Atmosphere's First Mile, Two Vol., Pergamon Press, New York and London.

Lettau, H. H., 1959: Wind profile, surface stress, and geostrophic drag coefficients in the atmospheric surface layer, Advances in Geophys., 6, Academic Press, New York, 241-256.

Lettau, H. H., 1962: Theoretical wind spirals in the boundary layer of a barotropic atmosphere, Beitr. Phys. Atmosph., 35, 195-212.

Lettau, H. H., 1964: Preliminary note on the effect of terrain slope on low-level jets and thermal winds in the planetary boundary layer, Ann. Report of Studies of the Effects of Variations in Boundary Conditions on the Atmospheric Boundary Layer, Sect. 4, Univ. Wisconsin.

Lettau, H. H., and H. Hoeber, 1964: Ueber die bestimmung der hoehenverteilung von schubspannung und austauschkoeffizient in der atmosphaerischen reibungsschicht, Beitr. Phys. Atmosph., 37, 105-118.

Lettau, H. H., 1966: A case study of katabatic flow on the South Polar plateau, Antarctic Research Series, Amer. Geophys. Union, 9, 1-11.

Lettau, H. H., and W. Schwerdtfeger, 1967: On the dynamics of the surface wind regime over the interior of Antarctica, Antarct. J. of the U. S., 2, 200-203.

Lopez, M. E., and W. E. Howell, 1967: Katabatic winds in the Equatorial Andes, J. Atmosph. Sciences, 24, 29-35.

Malkus, J. S., and M. E. Stern, 1963: Tropical rain induced by a small natural heat source, J. Appl. Meteor., 2, 547-556.

Means, L. L., 1954: A study of the mean southerly wind maximum in low levels, Bull. Amer. Soc., 35, 166-170.

Medler, J. T., 1967: Migration of aphids, Unpublished manuscript - Part of a Technical Report (NC 67), in preparation at the Entomology Dept., Univ. of Wisc., at Madison.

Meigs, P., 1956: Future of Arid Lands, Amer. Assoc. Advancement of Science, Publ. 43, Washington, D. C.

Pitchford, K., and J. London, 1962: The low-level jet as related to nocturnal thunderstorms over Midwest United States, J. Appl. Meteor., 1, 43-47.

Rudloff, W. H. B., 1959: Meteorology in Peru, United Nations (WMO) Report TAA/PER/8, New York, 46 pp.

Sangster, W. E., 1967: Diurnal surface geostrophic wind variations over the Great Plains, ESSA, Central Region, Techn. Memo., 13, Kansas City, Missouri, 11 pp.

Schweigger, E., 1959: Die Westkueste Suedamerikas im Bereich des Peru-Stroms, Keyser Verlag, Heidelberg, 513 pp.

Schwerdtfeger, W., and D. W. Martin, 1964: The zonal flow of the free atmosphere between 10 N and 80 S in the South American sector, J. Appl. Meteor., 3, 726-733.

Sheppard, P. A., C. H. Charnock, and J. R. D. Francis, 1952: Observations of the Westerlies over the sea, Quart. J. Royal Meteor. Soc., 78, 563.

Siebert, M., 1961: Atmospheric Tides, Advanc. Geophys. (H. Landsberg and J. VanMieghem, eds.) 7, Academ. Press, New York, 105-187.

Trewartha, J. T., 1966, The Earth's Problem Climates, Univ. Wisc. Press, Madison, Wisc. 334 pp.

Troll, C., 1952: Die lokalwinde der tropengebirge und ihr einfluss auf niederschlag und vegetation, Bonner Geogr. Abhandl., 9, 124-182.

Wagner, A., 1936: Zur theorie des taeglichen ganges der windverhaeltnisse, Gerlands Beitr. Geophys., 47, 172.

Wahl, E., 1966: Windspeed on Mountains, Final Report AF 19 (628)-3873, Univ. Wisc.

Wexler, H., 1961, A boundary layer interpretation of the low-level jet, Tellus, 13, 368-378.

DISCUSSION

Question: William Gray, CSU, Ft. Collins, Colorado

Are there soundings to the right and left of the low-level jet in the U. S. which, in fact, verify a thermal, hydrostatic, explanation of this jet?

Reply: Dr. Lettau:

To my knowledge only the Weather Bureau Special Pibal Network of 1961, between Little Rock, Arkansas, and Amarillo, Texas, as reported by Hoecker (1963) was of sufficiently large scale to produce detailed windsoundings to the right and left of the low-level jet over the U. S. Special measurements to obtain the spatial distribution of density stratification in the atmospheric boundary layer over the great slope of the midwestern U. S. were not available to me but would certainly be highly desirable, especially when obtained by instrumented aircraft in cross-stream flights at various levels, and around the clock. However, I want to emphasize that the explanation outlined in my presentation is not just of thermal-hydrostatic nature. On the contrary, it involves in a highly significant manner also the effects of internal friction as well as a forced "tidal" oscillation of flow structure in response to solar-day harmonic seesawing of thermal winds, with a dynamical impedance of the boundary layer that is dependent on the Coriolis parameter so that equator, and 30 deg North and South latitude are significant for "lagging" versus "leading" between forcing and response functions.

Question: Glenn E. Stout, Ill. State Water Survey

Reference is made to Fig. 2 which showed the tornado distribution in Arkansas. The differences between the Ozarks Mts. and the flatlands were probably due to poor population distribution in the hill region. Therefore, was the relationship of wind difference in the free air vs. mountain air related to these observations?

Reply: Dr. Lettau:

Mr. Asp of the U.S. Weather Bureau, who constructed the chart referred to by Dr. Stout, has obviously been aware of the possibility of statistical bias due to variations in population density in Arkansas. However, his conclusions in his 1956 article appear to suggest that the data on tornado frequency in various parts of the state are more systematic than explainable in a trivial manner.

CAUSES AND CONSEQUENCES OF STANDING WAVES

R. S. Scorer
Imperial College, London

1. Mountain Disturbances and Lee Waves

The problem as first posed and solved by Lyra and Queney gave rise to an integral which represented the steady flow of an air current over a mountain ridge, the current being undisturbed far upstream and downstream. Classical methods for the study of small amplitude waves were used and it appeared simplest to consider a stream which had uniform wind and static stability up to infinite height. Even in the simplest case it is quite difficult to evaluate the integral, and the amplitude of the disturbance appears to increase indefinitely at great heights; so a disproportionate effort has been given to the mathematical aspects, particularly the precise formulation of the initial and boundary conditions. At one time a proposal was put up within the Meteorological Office to make observations of the airflow over the mountains of Wales to see what boundary conditions it actually corresponded to, but it was abandoned mainly because it would not have been possible to discriminate between the alternatives!

Obsession with the problem of obtaining a unique solution has led some writers to expend great effort to settle a matter of small practical consequence with considerable elegance, but at the same time to ignore aspects of mountain waves which are of great importance to aviation and which are easily observable. It is with these matters that I shall be concerned. I agree with Queney's view that it is not legitimate to suppose that a given airstream may be presented to a given mountain and that a unique steady flow with no disturbance far upstream can necessarily be obtained. Certainly the problem cannot be properly treated by the classical small amplitude theory, and it is therefore not merely a question of getting the correct formulation of the problem. There may not even be a unique or a steady solution.

There are two quite distinct aspects of the flow over an obstacle which emerge from any theory, and emerge very nicely from the small amplitude theory. They are that close to an obstacle in a stream there must be a disturbance of some sort from smooth horizontal flow which will die away at a great distance downstream, and that there may be a train of waves set up which can extend indefinitely downstream over level ground. These we shall call the mountain disturbance and the lee waves.

The lee waves are important not simply because quite large ones can be set up by the flow of air over an ordinary mountain range, larger in some cases than the mountain itself, and spectacular ones by such ridges as the Californian Sierra Nevada or the Southern Alps of New Zealand, but rather because some quite remarkable effects arise when the wave train produced by one mountain is augmented by that of another situated in the right phase relationship (Fig. 1). A small change of wind strength or direction might change the relative phase of two superposed lee wave trains so that they become additive with perhaps sudden and occasionally costly consequences. For example, to the west of Sheffield there is a complicated pattern of hills known by glider pilots often to produce lee waves. They sometimes give neighboring regions of gale and calm within the city under the troughs

and crests of the waves. In a recent episode many roofs were blown off including that of a professor of geography at the University who was forced to take cognizance of yet another aspect of the local climate! Because of the additive effect, the waves in such cases are larger at the lee end of the hilly area than any over the hills themselves.

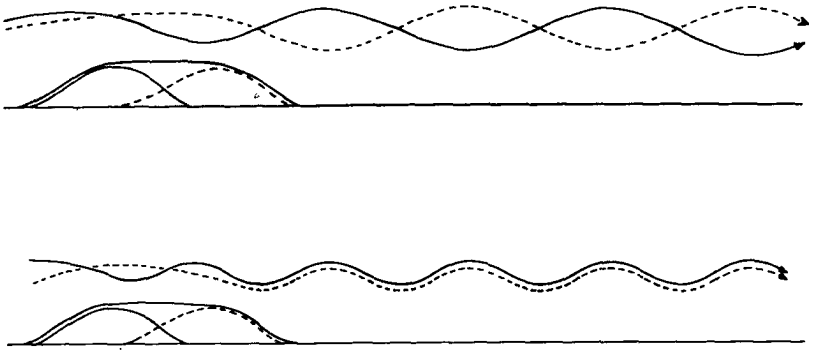

Fig. 1. Superposition of lee wave trains: The mountain ridge indicated by the dashed line produces a wave pattern shown by the dashed streamline. A similar mountain further upstream produces the wave shown by the continuous line. Added together they form a mountain indicated by a continuous line and in the upper diagram the wavelength is such that the wave trains cancel out, while in the lower diagram the amplitude is doubled. Since the wavelength is determined by the component of the wind across the ridge only, the same airstream could produce large amplitude lee waves or no lee waves at all, according to its direction.

Lyra described the flow of a uniform stream over a brick-shaped obstacle as consisting of lee waves (Fig. 2), and gave some of the features of his solution as the explanation of some lee wave phenomena that had already been observed. But as soon as the sharp corners are taken off his obstacle, much of the waviness disappears (Fig. 3), and we now know that real lee waves are not contained in his solution of the problem for a uniform airstream.

Unlike the wavy disturbance near the obstacle, lee waves have a definite level of maximum amplitude, usually in the lower troposphere, which means that the curvature of the profile of wave amplitude expressed as a function of height must change sign somewhere in the troposphere. To express this mathematically we note that the equation for the displacement, ζ, in standing waves in 2D in the xz-plane contains the following terms:

$$(1) \qquad \frac{\delta^2 \zeta}{\delta z^2} = (k^2 - \ell^2)\,\zeta$$

These terms are always important, and are in many cases the only important ones in the equation. Here

$$(2) \qquad \ell^2 = \frac{g\beta_o}{u_o^2} \text{ , where}$$

$$(3) \qquad g\beta_o = \frac{g}{\theta}\frac{\delta\theta}{\delta z_o}$$

is the static stability, u_o being the wind far upstream and θ the potential temperature on the streamline. On the assumption that periodic disturbances are possible, a wavelength $2\pi/k$ has been assumed.

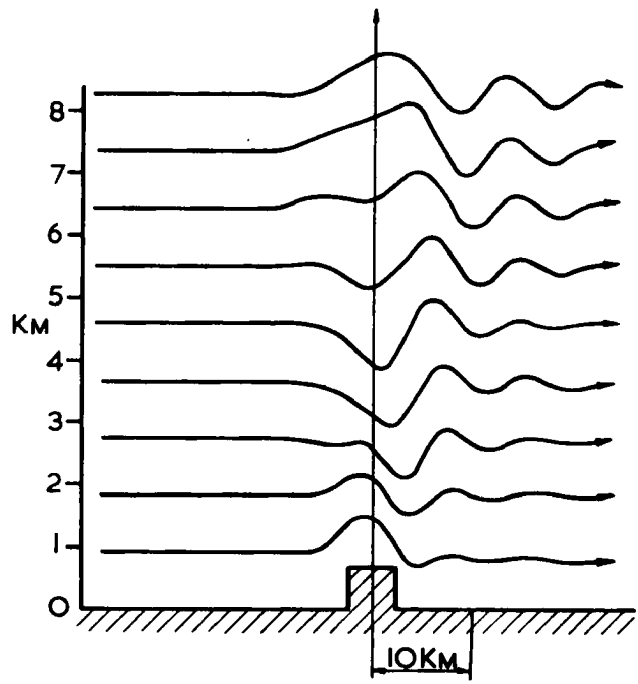

Fig. 2. Apparent lee waves over a sharp cornered obstacle: The streamlines show several successive wave crests whose amplitude decreases exponentially downstream but increases upwards, according to Lyra's original theory for a uniform airstream over a ridge.

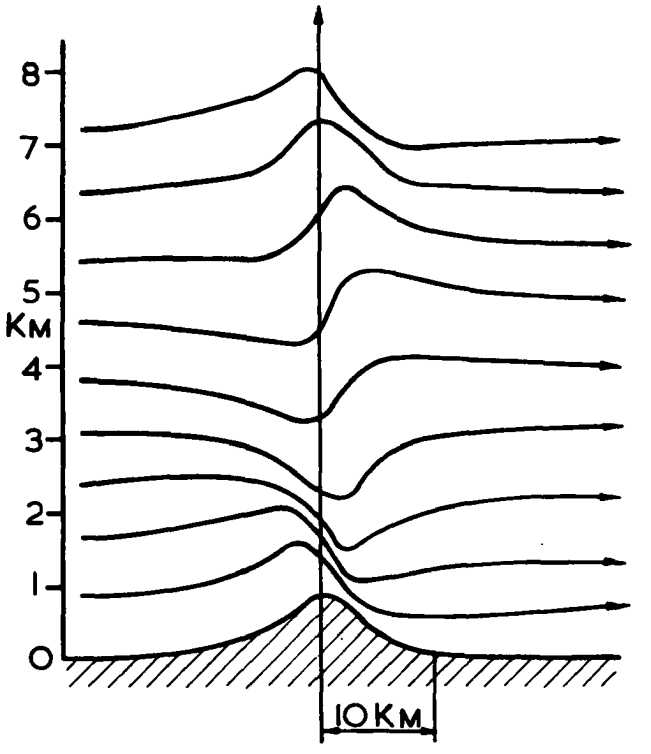

Fig. 3. Absence of "lee waves" in a uniform stream over a smooth obstacle: In this case there is only one important wave crest or trough on each streamline.

This equation is such that unless it is zero everywhere ζ cannot be zero except at isolated heights, and so if the energy of the waves is to be finite, ζ must approach zero asymptotically at great height (Fig. 4). The ζ-profile must have a positive curvature there, and above some height, where $l = l_s$ (the suffix s denoting a superior layer),

(4) $$k^2 > l_s^2$$

But in order that ζ shall have opposite curvature somewhere, for otherwise it could not be zero at the ground, there must be an inferior layer (denoted by suffix i) in which

(5) $$l_i^2 > k^2.$$

k, therefore, takes a value which is intermediate between l_i and l_s .

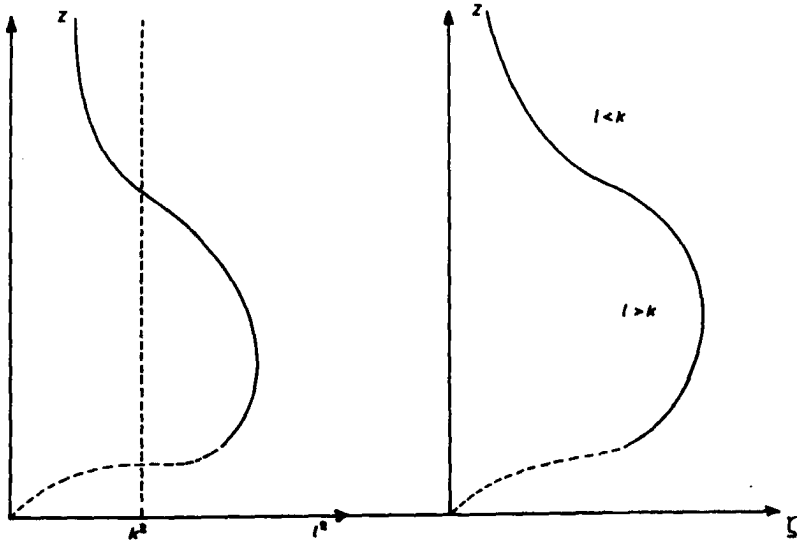

Fig. 4. Profile of lee wave amplitude: According to equation (1) the curvature of the profile of ζ must correspond to an exponential decrease upwards at the top, but must be reversed somewhere lower down in order that ζ shall be zero at the ground. We have indicated in this case that the stability may go to zero near the ground so that the curvature is again reversed; thus, provided that there is sufficient stability (large l^2) in some middle layer, l may be less than k near the ground in lee waves.

The restoring force on a parcel displaced vertically a distance ζ is $g\beta\zeta$, which means that $(g\beta)^{1/2}$ is the natural frequency with which it would oscillate if it were frictionless, had no virtual mass in its motion through the fluid, and did not become deformed. It is also the frequency with which adjacent columns would oscillate up and down if β were uniform throughout the atmosphere. Since u_0 is the horizontal speed, one would expect the horizontal wavelength to be closely associated with the quantity l. That simple idea is not enough because we can see that l must vary with height if lee waves are to exist. To the surprise of those writers who argue that a very stable upper layer, such as the stratosphere, would tend to suppress vertical motions and behave like a rigid lid and therefore trap waves in the troposphere, the opposite is evidently the case; for waves to be trapped, the stability in the upper layers must be less, and because this is often achieved within the troposphere, lee waves are common.

In a given airstream the waves of very short length always die out rapidly with height, and the important ones are those for which k^2 is comparable with l^2. This means that the vertical wavelength, which is twice the distance between horizontal nodal surfaces at which

the wave amplitude is zero, which is represented by $2\pi/(l^2-k^2)^{1/2}$, is the same order of magnitude as the horizontal wavelength of lee waves. In the atmosphere this is found typically within the range 1 to 20 miles, and so nodal surfaces can be expected often within the troposphere. Russian writers appear to have been unduly concerned with this aspect of lee waves.

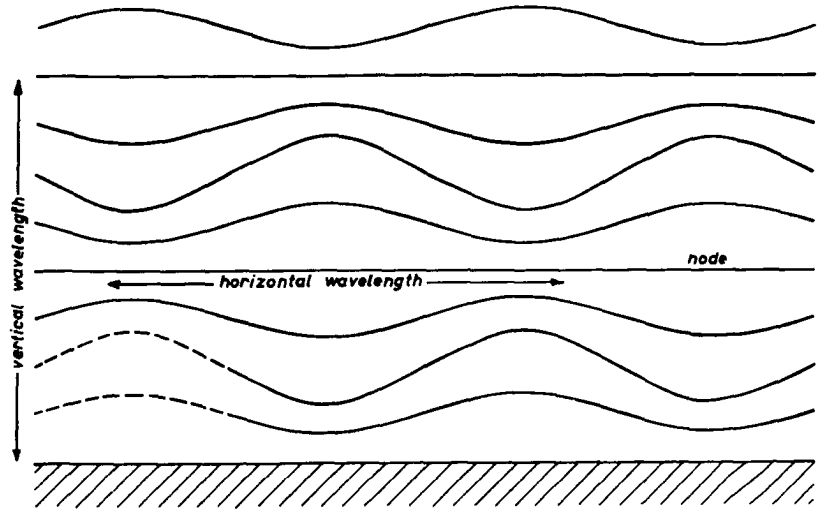

Fig. 5. Waves at a nodal surface: Waves may have a sufficiently short vertical wavelength (or sufficiently deep lower layer) for there to be a nodal surface within the lower layers. Generally, the horizontal and vertical wavelengths are of comparable magnitude with l^{-1}, and perturbations of vertical and horizontal velocity are comparable with one another.

Because the longer wavelengths in a Fourier representation of a mountain die away upwards less rapidly, they contain the dominant features of the mountain disturbance, which is therefore largely characterized by the properties of the disturbance corresponding to k=0 . It is readily shown that since the pressure and the vertical displacement are continuous, functions of height, ζ and $\frac{\delta\zeta}{\delta z}$ must certainly be continuous if l^2 is continuous, and in most cases of discontinuities of l also. Ignoring the exceptions, which can be treated separately and do not introduce any essentially different result, we see that ζ must therefore have a smooth profile. If l^2 decreases upwards the curvature of the ζ-profile also decreases upwards (because for k= 0 , $\zeta'' = -l^2\zeta$) and ζ achieves a greater amplitude than if l^2 had remained constant. Therefore, when lee waves are trapped, the mountain disturbance will generally have a greater amplitude at levels above the height of the lee wave maximum. This is no longer strictly true if l^2

becomes very small high up so that it is comparable with or less than the values of k^2 making the major contribution to the mountain shape; but we can say that generally the most spectacular lee waves and mountain disturbances will both occur in the same kind of airstream, namely one in which l_s^2 is considerably less than l_i^2 .

Conversely we may say that if l^2 takes a very small value near the ground, and in particular if there is a deep neutral (adiabatic) layer at the bottom, mountain disturbances are likely to be much smaller and lee waves will probably disappear. The rest of this paper will be concerned with the properties of waves and phenomena produced by them, and without losing anything we can concentrate on the lee waves alone. But before discussing these matters we ought to justify the use of the very simple equation (1) which was first derived on the very restrictive assumption that the amplitude was small.

2. Justification of the Use of the Simplest Form of the Equation

The full equation, to obtain which we assume only that the motion is two dimensional, steady, inviscid, and adiabatic, is

$$\frac{\delta^2\zeta}{\delta x^2} + \frac{\delta^2\zeta}{\delta z^2} - (\alpha_o - 1/2\,\beta_o)\left\{(\nabla\zeta)^2 - 2\,\frac{\delta\zeta}{\delta z}\right\}$$

$$(6) \qquad -\left(\frac{\delta z_o}{\delta z}\frac{\delta}{\delta z} + \frac{\delta z_o}{\delta x}\frac{\delta}{\delta x}\right)\log\frac{\rho_o}{\rho} + \frac{g\beta_o}{u_o^2}\left(\frac{\rho}{\rho_o}\right)^2\zeta = 0$$

in which the density ρ varies along a streamline. The shear and thermal stratification are represented by

$$(7) \qquad \alpha_o = \frac{1}{u_o}\frac{du_o}{dz_o}, \quad \beta_o = \frac{1}{\theta}\frac{d\theta}{dz_o}$$

All quantities with suffix o are constant along a streamline, and therefore vary with x and z in a wavy flow field; the equation is therefore "horribly non-linear"! Nevertheless many terms are always relatively small and some when the particle displacement is restricted to less than one kilometer or so. The only term which can commonly become as large as the terms retained in equation (1) is

$\alpha_o\left\{2\,\frac{\delta\zeta}{\delta z} - (\nabla\zeta)^2\right\}$, and there are plenty of interesting situations in which this is small simply because the shear is small. It is therefore worth while to study the consequences of ignoring it. Actually, even this term has only a modifying effect on most of the arguments to be presented and does not destroy their general validity. Since α_o cannot be large over a great depth simply because u_o itself is limited, the situations in which α_o cannot be neglected can usually be handled by assuming it to be constant in shallow layers. In that case the chief worry arises from the terms $(\nabla\zeta)^2$ and $\zeta\rho^2$ which are always non-linear, and from the fact that the boundary conditions at interfaces, between layers in which the equation is linear, are non-linear.

The remarkable discovery made by Long and independently by Yih is that to get as far as equation (6) no restrictive assumption about amplitude of the wave disturbance is necessary. This means that although some restriction has to be put upon ζ to progress to a tractable form of (3), it is

still possible for the streamlines to be vertical and have closed circulations. In the classical perturbation theory the slope of the streamlines is restricted to small values because the horizontal and vertical velocity components may only be slightly perturbed.

We may therefore regard (1) as correct for large amplitudes in the knowledge that, although not correct for all, the conclusions drawn will be correct for many situations. From our point of view the chief difficulties are:

(1) an equation like (6) which is valid for arbitrarily large amplitude cannot be obtained for non-2D motion, so that the less 2D the mountains are, the less valid are the conclusions.
(2) when the equation is non-linear, steady periodic wave solutions may no longer be possible, and it is a matter of some speculation what the flow is like when the amplitude is large--whether it is mainly unsteady, whether the waves break when they are large, whether disturbances travel upstream to modify the profile so that steady waves are possible, or whether the stream undergoes a transformation rather like a hydraulic jump on the downstream side of the mountain. Or something else!

3. The Amplitude Profile

We are concerned in this section with the way in which the amplitude varies with height. The profile of the airstream in which lee waves are occurring is infinitely variable. Some sort of comparison can be made if we consider airstreams all of which have the same lee wave length and which are all the same above a certain height but differ in their lowest layers. The seven cases chosen for calculation all have $l_s^2 = 0.75$ km^{-2} above 2 km, and their lee wave length is 2π km, which is quite typical. We imagine the waves in each case to be set off by the same obstacle so that we get some sort of comparison between the amplitudes occurring in different streams as well as how the amplitude varies with height. As we progress from case 1 to case 4 we gradually replace the stability in bottom layer by a sharp inversion at its top. The value of l_i^2 accordingly decreases. We then replace the sharp inversion by a gradually thickening stable layer of decreasing stability, until we return to the first case again.

In Table I the details of the airstreams are given. l_i^2 is the value of

Table I.

Case no.	l_i^2 km^{-2}	ϵ %	Approx. Inversion at 2 km °C	Depth of middle layer km	l_j^2 km^{-2}
1	2.04	0	0	--	--
2	1.79	1	2.7	--	--
3	1	2	5.4	--	--
4	0	3	8	--	--
5	0	0	0	0.25	5
6	0	0	0	0.37	5
7	0	0	0	0.65	3.25
1	---	0	0	2.0	2.04

l^2 in the bottom layer, and l_j^2 is the value in the middle layer in cases 5, 6, 7. ϵ is the change in density at the sharp inversion at 2 km, and the approximate temperature discontinuity which would produce it is given in the next column.

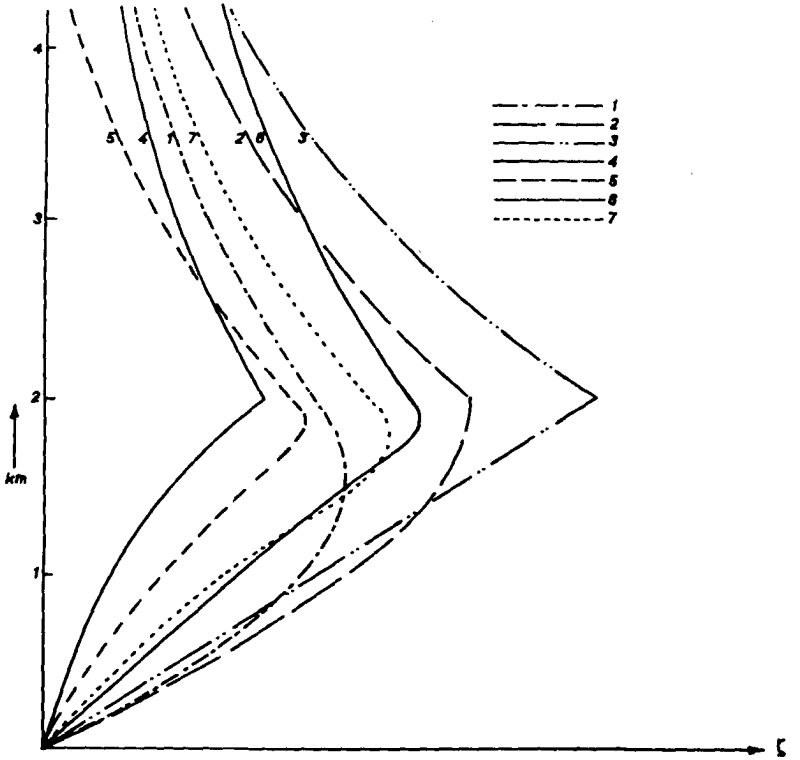

Fig. 6. Lee wave amplitude profiles in different airstreams with the same lee wave length: The lee wave amplitude is shown as a function of height for seven airstreams flowing over the same 2D ridge. All airstreams are the same above 2 km with $l_s^2 = 0.75\ km^{-2}$, and all are such that the lee wave length is 2π km. At 2 km the wind is assumed to be continuous and in case 1 the density is also continuous there and l^2 is constant below. In case 2 there is density discontinuity and the air is therefore less stable below 2 km. In case 3 the discontinuity is greater and the stability below decreased accordingly. Case 4 has the greatest discontinuity and an adiabatic layer below. In 5, 6, and 7 we have a very stable layer replacing the discontinuity with gradually increasing thickness so that eventually we return to case 1 in which it occupies the whole depth down to the ground. Most outstanding is the sharp maximum of the amplitude where the air is most stable and this occurs most characteristically at the top of a cloud layer. Table I gives the details of the values of l^2 in the seven cases.

In these cases we have no nodal surfaces, and all the properties illustrated here are those which would be found above the uppermost nodal surface if there were one. Equation (1) shows that the curvature of the profile is proportional to $l^2 - k^2$, and this is infinite at a discontinuity of density. Since there are no nodal surfaces in these simple models to satisfy the two conditions:

(1) the amplitude decreases exponentially in the top layer
(2) the amplitude is zero at the ground

sufficient curvature to turn the curve round as we descend it must be achieved at some level. Where the inversion is more intense, less stability is needed in the layer below.

One of the most notable features, which has long been observed by glider pilots in Britain, is that when there is an inversion it is likely to be the height of the amplitude maximum. This also happens to be the most likely place to find the top of a cloud layer, and conversely cloud layers tend to produce sharp inversions at their tops. Therefore if there are wave clouds present they are likely to have their tops at the surface where the wave amplitude is a maximum.

A second feature is that adiabatic layers near to the ground will tend to decrease the overall amplitude of the disturbance and the lee waves.

4. Waves in the Lee of an Isolated Hill

The wave pattern behind a ship may be regarded as the result of superposing the systems of parallel lee waves that would be formed by 2D ships all arranged so as to pass through the position of the actual ship. Likewise an isolated hill can be regarded as the superposition of many 2D ridges through the position of the hill and so it is to be expected that a similar pattern of waves would be formed. Small amplitude theory shows that this is in fact so. The semi-angle within which the wave pattern is confined, which is about 19 $1/2^{\circ}$ in the case of a ship, may vary from as little as 5° to as much as 35° in typical cases. Theoretically the angle could be much larger than this if there were a very stable, very shallow layer of air flowing under one of moderate stability.

In practice the mountain disturbance of an isolated hill decreases in amplitude rather rapidly with height (like $z^{-1/2}$) and the lee waves decrease in amplitude downstream (like x^{-1}) by comparison with the values for a 2D ridge of the same cross section.

In the wave pattern illustrated by an example in Fig. 7, there are two systems of waves, and in the atmosphere it is to be expected that the transverse waves would be most easily observed, although when the hill is elongated along the wind the waves inclined to the stream direction might be seen.

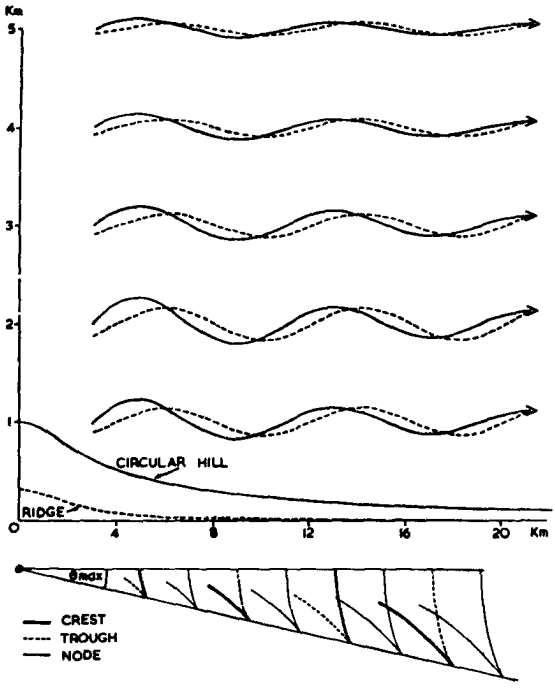

Fig. 7. The wave pattern of an isolated hill: The lee waves of an isolated circular hill in the central vertical plane are shown compared with the waves produced in the same airstream by a symmetrical 2D ridge which has the same amplitude as the second wave due to the hill. The lower diagram shows half of the wave pattern in plan. It is confined within a wedge-shaped region.

The amplitude of the waves is proportional to the mountain height and they are both arbitrary. The height scale therefore only applies to the streamlines; the airstream has $\ell_s^2 = 0.5\ \text{km}^{-2}$ above 2 km, and $\ell_i^2 = 1.5\ \text{km}^{-2}$ below 2 km, and is such that $\theta_{max} = 12.3^{\circ}$.

5. Effects of Smooth Stable Waves

Sounding balloons passing through a wave system show a periodically varying rate of rise. Fig. 8 illustrates what the tracks of balloons would be through a wave system together with the temperature profiles which would be recorded by them. The main feature is that the very stable layers which appear as a result of the waves, although wind anomalies would also be recorded. Although the temperature and wind measurements may be correct the values of their vertical gradients would be quite erroneous and a local Richardson number should not be calculated from them.

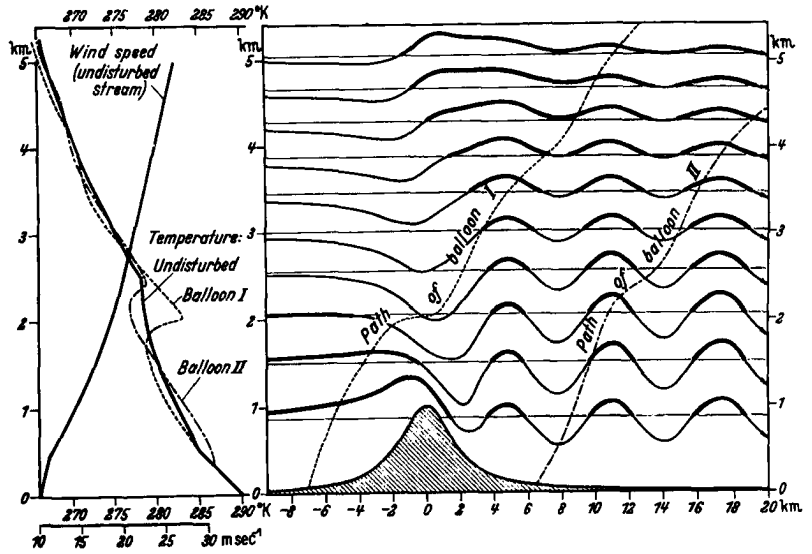

Fig. 8. Balloon soundings in lee waves: Airflow over a ridge under conditions favorable for lee waves. The undisturbed wind and temperature profiles are shown on the left together with the temperature vs. height profiles recorded by two balloons ascending at 5 m sec^{-1} through the waves. The lowest half kilometer is adiabatic, $\ell_s^2 = 0.75\ km^{-2}$ above 2.5 km, and ℓ_i^2 is variable in between such that $\ell_i > k$ for a wavelength of 2π km.

The most common characteristic of wave clouds is their smooth top, which, as has already been mentioned, often has a very stable layer just above it. This smoothness can be disrupted in three main ways.

(1) when the air becomes statically unstable as a result of cloud formation
(2) by billows, which appear as transverse rolls
(3) by centrifugal instability, which produces longitudinal corrugations.

The last two of these are discussed in later sections. The first most probably produces castellanus. In fact the lines, which are almost characteristic of castellanus, in many cases originate in wave crests, these being the points on the streamlines at which condensation first occurs. Billows are not generally due to any condensation effect, for billow clouds usually display no static instability.

One of the more interesting forms of wave clouds is orographic cirrus. This is a trail of ice crystals which extends far downwind from the source wave cloud, the wave cloud itself being mainly a water droplet cloud. The

condensation does not occur until water saturation is reached and if freezing occurs in a supercooled wave cloud the ice cloud does not evaporate until the air reaches a lower level. The difference in altitude between the water condensation level and the ice evaporation level is roughly one hundred meters for every degree of supercooling at the condensation level.

Wave clouds can, of course, be recognized by their almost stationary position in a moving airstream, but the smooth upwind edge is another characteristic by which they can be instantaneously recognized.

6. Billows

Billows do not occur only in waves, for they are common in frontal clouds. They occur very readily in an existing layer of cloud if shear is present and then they take the form of parallel rolls across the direction of shear. But in waves the billow motion can occur in clear stably stratified air, and then the cloud serves only to make the motion pattern partly visible.

The likelihood of the occurrence of billows is indicated by the Richardson number, which is the ratio of the static stability forces to the destabilizing inertia forces caused by shear. Thus

$$\text{(8)} \qquad \mathrm{Ri} = \frac{g\beta}{u'^2}$$

and for a very shallow layer with a large gradient of potential temperature and velocity the equivalent number is

$$\text{(9)} \qquad \mathrm{Ri} = \frac{g\Delta T\,\Delta h}{T\,(\Delta u)^2}$$

Clearly when Δh, the thickness of the layer, is very small so also is the Richardson number, and when Δh is zero, we have to consider Helmholtz instability at a discontinuity. In waves, two effects can alter the Richardson number:

(1) the squeezing of a layer, which alters the gradients of potential temperature and velocity
(2) the tilting of a layer, which generates vorticity in a stable layer, with the upper part of the layer flowing uphill and the lower part downhill.

To study these effects we use Bernoulli's equation for steady motion in the form

$$\text{(10)} \qquad gz + 1/2\ q^2 + \theta\,\varpi = H$$

= Constant along a vortex line or streamline.

where $\varpi = \gamma\ RT\ /(\gamma - 1)\ \theta$, and q is the air speed. Since the vorticity generated in waves about a vertical axis is negligible we can say that H is a constant over the surface composed of all the streamlines through a horizontal line far upstream. This is strictly true if the motion is 2D and is a good enough approximation if the slope of the streamlines is not large enough to produce horizontal gradients of potential temperature normal to the horizontal acceleration vector.

Let Δ denote the magnitude of the difference in a quantity between two streamlines and, δ the change along a section of a streamline, the quantity $\Delta\varpi$ is virtually unchanged because it is related to the pressure by

$$\text{(11)} \qquad \varpi = \frac{\gamma R}{\gamma - 1}\left(\frac{p}{p_1}\right)^{\frac{\gamma - 1}{\gamma}}$$

and the change in height of the fluid is supposed small and the change δp is assumed to be the same all through the layer. Thus Bernoulli's equation gives that $\delta (1/2\ q^2)$ is the same on the two streamlines and so $\Delta(1/2\ q^2)$ is constant along the layer. Therefore

(12) $$q\ \Delta q = \text{constant}$$

along the streamlines, and so a discontinuity of velocity would be increased by a decrease in q. The magnitude of the shear in a layer of finite thickness Δh is unchanged because the flux in the layer represented by $q\Delta h$ is constant. Therefore

(13) $$\frac{\Delta q}{\Delta h} = \text{constant along a horizontal streamline.}$$

However, the static stability is increased by a decrease in Δh, for

(14) $$\beta = \frac{1}{\theta}\ \frac{\Delta\theta}{\Delta h}$$

and θ and $\Delta\theta$ remain constant along any streamline. Thus the Richardson number is decreased where the flow is decelerated.

The effect of tilting the streamlines can be determined by considering two adjacent streamlines undergoing an equal change in pressure due to a change in altitude. In that case, since $\delta\theta = 0$ we have

$$\delta (\Delta\ 1/2\ q^2) = \delta (\Delta(\theta\varpi))$$

$$= \Delta\theta\ \ \delta\varpi \qquad \text{or}$$

(15) $$\delta (\Delta q) = \Delta\theta\ \frac{\delta\varpi}{q}$$

The rate of generation of vorticity is equal to the stability multiplied by the tilt, and this gives the same result as equation (15) because

$\delta\varpi = \frac{\gamma R}{\gamma - 1}\ \frac{\delta T}{\theta}$, $\frac{dT}{dZ} = \frac{(\gamma - 1)\ g}{\gamma R}$, the rate of generation of vorticity is $q\ \frac{d}{ds}\ \frac{\Delta q}{\Delta h}$, and the tilt is $\frac{dz}{ds}$. The consequence of this result is that

(16) $$\delta\ u' = \frac{\beta\theta}{q}\ \ \delta\varpi$$

Let us suppose, now, that we have a given wave form, so that at a particular level, θ and q are given together with $\delta\varpi$, which represents the amplitude of the wave. The amount of shear generated, $\delta u'$, is then proportional to β. If the Richardson number given in the form (8) were originally infinite because of no shear, the value attained in the wave would be proportional to β^{-1}. Therefore, rather unexpectedly perhaps, the most stable layers develop the smallest Richardson numbers in waves, and so billows are most likely to develop there.

If in a wave there is some deceleration, any existing shear will be unchanged but the value of β, and therefore Ri, is reduced. The most favorable circumstances for the decrease of Ri are therefore forward shear decelerating uphill or backward shear decelerating downhill. In using this result it must be remembered that the uphill side of a wave might have been preceded by a downhill side. The maximum forward shear generated in a wave occurs at the wave crest, and so if the wave amplitude increases with height (to give a deceleration) the wave crest is the most favored

position for instability, and one can imagine a great variety of circumstances, combining cloud layers with shear layers and stable layers to give billows in waves.

The orientation of the billows is very difficult to predict because two factors may interfere with it. The first is any existing shear in an airstream which may be in a different direction from that generated in waves. This will alter the final direction of the shear. In 2D motion, shear out of the plane of the disturbance does not alter the pattern of motion, and the velocity of a particle normal to this plane remains constant along a streamline. There may, therefore, be a component of shear, of unknown amount, varying with height, which will alter the direction of the total shear. Even in the absence of shear normal to the plane of the disturbance, the second factor enters; this is the yawing motion due to the alteration of the component in the plane.

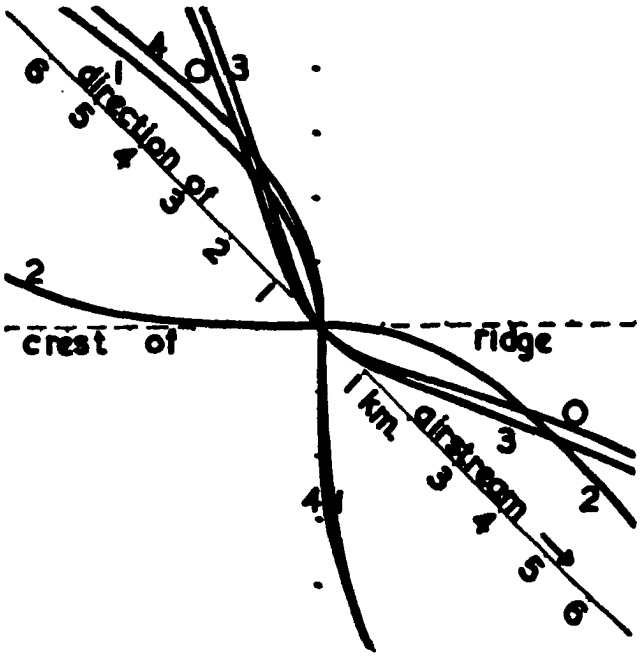

Fig. 9. Yawing motion produced by oblique flow over a ridge: Tracks of air particles at heights of 1, 2, 3, and 4 km in the passage of a uniform airstream over a 2D ridge when the undisturbed flow is inclined at 45° to the ridge. Over the ridge crest, shear in many different directions is possible. Similar variations in shear direction can occur in lee waves.

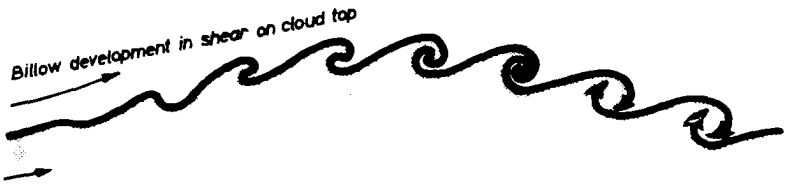

Fig. 10. The probable nature of billow motion induced by sloping stream surfaces: The growth of billows by the rolling up of the vortex "sheet" formed in the inclined flow at layers of great static stability. The billow spacing is determined by the thickness of the layer.

7. Centrifugal Instability

This type of instability occurs when a stream possessing vorticity is set in curved motion round a bend in the opposite direction. Thus if a stream with forward shear is curved upwards or one with backward shear is curved downwards, centrifugal instability occurs if there is no static stability of greater magnitude to prevent it.

In a cloud the static stability may be very small so that this may be a common occurrence when lee waves with large curvature in a vertical plane take place. But that is really not enough to produce important instability because the duration is only during passage through a wave crest, and the motion is stabilized in a trough. We know that clouds can produce castellanus in waves, and so there is time for instability of the order of magnitude of, say, half the difference between the wet and the dry adiabatic lapse rates to produce overturning, and so we know that centrifugal instability would be important if it could overcome typical values of the static stability by a factor of 1.5 or 2.

A calculation which Wilson and I carried out showed that instability might appear if a wind shear of the order of 4×10^{-2} sec^{-1} existed in a stream with waves of length 2π km and maximum amplitude of $\pm$ 1.2 km. Such large values of shear are only likely to occur in shallow layers (the value given represents a shear of 40 m sec^{-1} per km), and in any case if such a shear existed in a very deep layer such a large wave amplitude would be unlikely. The shallow shear layer, on the other hand, has only a negligible effect on the wave form; and so the curvature of the streamlines can be calculated assuming it to be absent.

Actual large shear layers usually occur in the form of a jagged velocity profile; that is to say, several thin layers of alternately forward and backward shear occur. These shear layers are often observed and they are thought to be caused by a centrifugal instability on a much larger scale. Thus, at a jet exit (or entrance perhaps) or where the air mounts an extensive plateau or mountainous region, the flow is not in geostrophic balance and centrifugal instability might occur in the sense that the curvature of the airflow in space is in the opposite direction to the vertical component

of vorticity. Wilson later calculated a stability criterion, including the static stability and a form of (eddy) viscous stress, for geostrophic flow for which

$$\frac{du}{dy} > f \tag{17}$$

which is similar to what would be obtained if the flow were not in geostrophic balance and satisfied (17) even if it would not have satisfied it if the velocity had been in balance with the existing pressure field. He showed that very flat cells in the form of thin interleaved layers of air penetrating sideways across the flow would be the form taken by the instability and this would explain the jagged velocity profiles often observed in jet streams and over large mountain masses.

The criterion for centrifugal instability in the trough or crest of a wave is approximately

$$k q^2 \frac{\delta}{\delta z} \log \frac{q^2}{2\theta} > g\beta \tag{18}$$

where k is the curvature of a streamline and q the speed. If the curvature is upwards, it is regarded as positive, and so in a wave trough, the quantity $q^2/2\theta$, which corresponds, in a compressible fluid, to the dynamic pressure $\rho q^2/2$ in an incompressible one, must increase upwards for instability. In computing whether this criterion is satisfied, it is necessary to take into account the vorticity generated by the static stability because this is stabilizing, and so the complete wave form has to be known, as well as the curvature of the streamlines where it is a maximum.

The question also arose whether the kind of instability supposed in the analysis, in the form of longitudinal corrugations of the stream surfaces, would be that which occurred; and it has recently been proved that this is the most unstable kind of instability.

8. Rotors

It remains now to describe the main features of the other major form of disturbance which can occur in otherwise smoothly flowing waves, namely, rotors. Their existence was known before any theories for a stratified atmosphere had been formulated. Lyra gave an explanation in terms of boundary layer separation in what he termed the lee waves, but which we now know could not possibly produce such large amplitude disturbances. It appeared that the ordinary linearizing techniques could not possibly treat a motion in which the streamlines became vertical, and for this reason, the analogy with a hydraulic jump has been a popular form of explanation of rotors. But there are essential objections to this analogy. In 1953, Long discovered how the equation could become linear even if the streamline slope were not nearly horizontal, and the outcome of that analysis is described above in section 2. It means that we can write down the very simple criterion for a rotor to occur, namely that somewhere

$$\frac{\delta \zeta}{\delta z} > 1 \text{ or } < -1. \tag{19}$$

This really says that the streamlines slope backwards somewhere and the fluid has therefore been turned over and become statically unstable.

According to this criterion, rotors will first appear as the amplitude of a wave is built up where the slope of the ζ-profile is largest. This is usually at the ground in lee waves, although other possibilities are envisaged in Fig. 11.

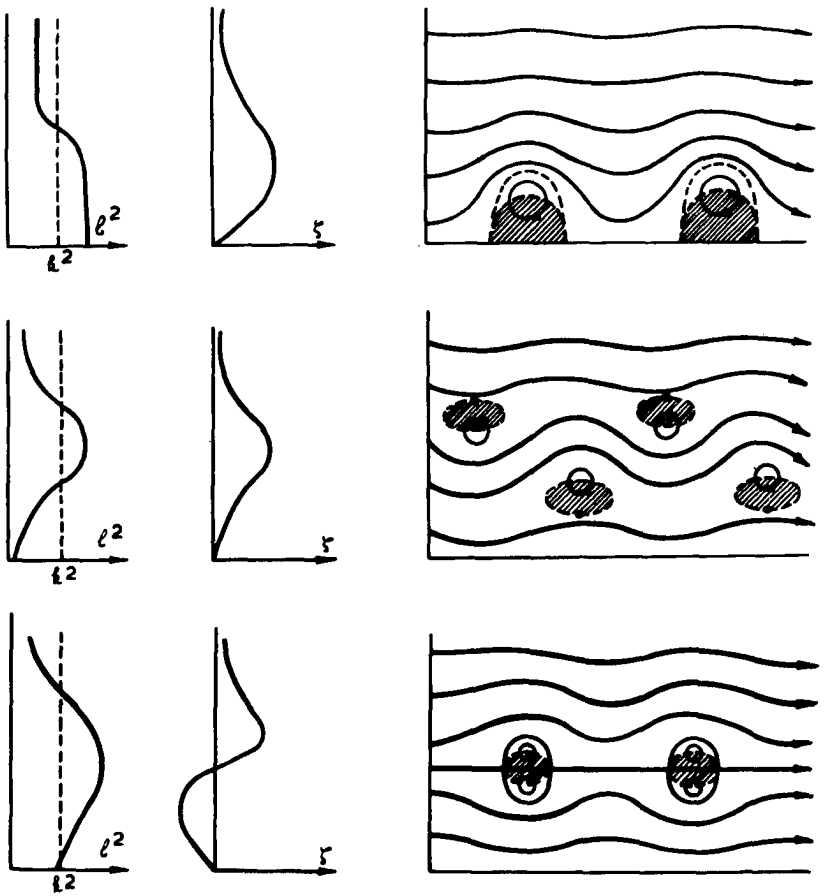

Fig. 11. The positions of rotors in relation to the profile of l^2: Different types of rotors: (a) Typical profile of l^2 and in lee waves with the pattern of streamlines when the amplitude is large enough for rotors to occur at the ground. (b) Profiles for a situation in which rotors can occur away from the ground.

(c) Profile for an airstream in which the lee waves have a rotor at a nodal surface away from the ground.

The air in the shaded region is statically unstable. In cases (a) and (c), the unstable air is entirely within the closed circulation, but in case (b) this is not so, and considerable unsteadiness is, therefore, likely.

From this it is seen that rotors may occur in wave troughs (or crests), but that if they do this away from a nodal surface, they will be of the open type; that is to say the region of static stability lies partly outside the closed circulation of the rotor so that air stirred by static instability can pass on downstream. This may lead to unsteadiness of the flow or a much smaller rotor amplitude in the next wave; but there is no real mathematical justification for that statement.

Now that rotors are at least theoretically possible in a linear theory in some airstreams, it is clear that something very similar will occur in airstreams for which the equations are not strictly linear.

9. The "Critical Layer"

It has become fashionable to refer to a layer of air at which the wind vanishes relative to the wave form, i.e., relative to the ground in ordinary lee waves, as a critical layer. The steady motion linear equations become nonsensical there because at least one coefficient, namely l^2, becomes infinite, and since these are not necessarily rendered incorrect by the largeness of the wave amplitude, it is probable that the escape to reality must be made through unsteadiness rather than through non-linearity. "Turbulence" is often described as occurring there when waves occur, and the steady theory, in so far as it suggests anything, suggests that layers of small rotors should be found. In any case, it is clearly a level to be watched, because if the static stability disappears in it, there will be a tendency for a "cats' eye" flow pattern to develop, that is to say, a billow type of motion; and Queney long ago offered this as one possible solution to the problem. Observations of Gerbier are summarized in Figs. 12 and 13.

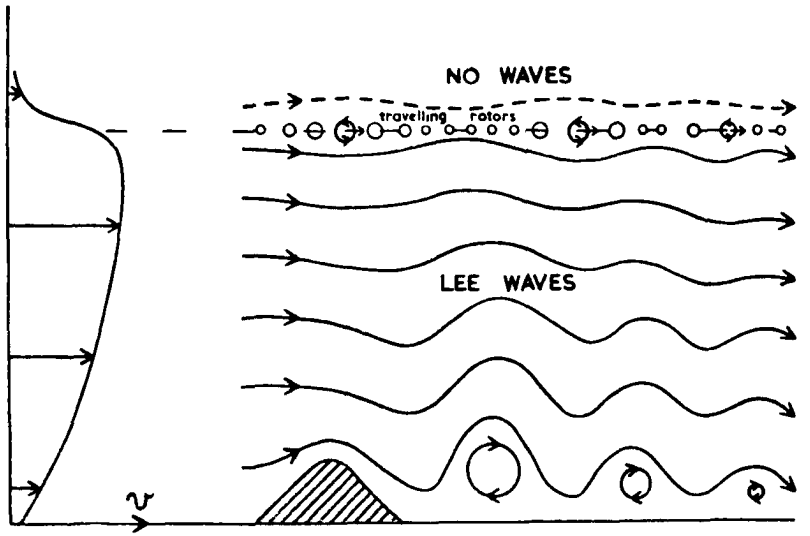

Fig. 12. Disturbance at level of no wind: At the level where the wind falls rapidly to zero, unsteady small rotors are thought to account for the observed air motion.

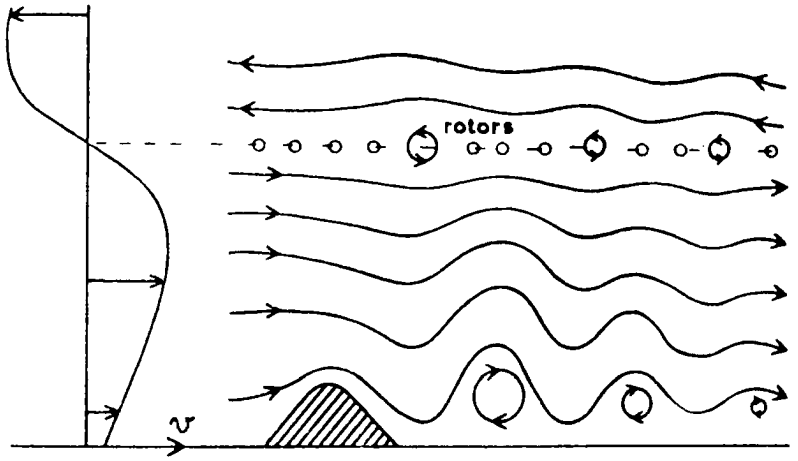

Fig. 13. Rotors at level of wind reversal: At the level of a wind reversal, steady rotors are sometimes observed with their amplitude large in-between rotors on the ground.

10. Outstanding Problems

There are many unsolved problems and any assessment of their importance can only be subjective; therefore, what I offer need not be regarded as a firm or even a lasting opinion, but the view of the moment. The critical layer appears to have plenty of scope for theoretical advance in spite of the brainpower that has already been applied, for that served mainly to determine that new techniques would be needed to solve it. I see no likelihood of profitable advance by analogy with hydraulic jumps because as soon as stable stratification is introduced, jumps, if they exist, become infinitely indeterminate because we do not know how to determine which layers become stirred up, whereas in a uniform fluid this does not matter because no permanent damage is done to the density profile. However, knowing that all the classical methods have failed, it is clearly necessary to exploit new physical concepts. Of these, further use of the idea of rotors can certainly be made, but the most profitable way in which steady flow theory can be improved is by finding out how those streams for which the equation is linear and, therefore possibly periodic and steady, can be produced in nature.

REFERENCES

Gerbier, N., and M. Berenger, 1961: Experimental studies of lee waves in the French Alps, Quart. J. Roy. Met. Soc., 87, 13.

Long, R. R., 1953: Some aspects of the flow of stratified fluids: I-A theoretical investigation, Report No. 2, 7, Johns Hopkins University, Dept. of Civil Engineering.

Lyra, G., 1943: Theorie der stationaren leewellenströmung in frier atmosphäre, Z. angew, Math. u. Mech., 23(1) 12.

Queney, P., 1947: Theory of perturbations in stratified currents with applications to air flow over mountain barriers, Miscell. Report No. 23, 31, U. of Chicago, Dept. of Met.

Scorer, R. S., 1953: Theory of airflow over mountains: II-The flow over a ridge, Ibid., 79, 70.

Scorer, R. S., 1954: Theory of airflow over mountains: III-Airstream characteristics, Ibid., 80, 417.

Scorer, R. S., 1961: Atmospheric turbulence in relation to aircraft, Symposium Proceedings, Paper No. 7, Ministry of Aviation, H. M. S. O.

Scorer, R. S., and M. Wilkinson, 1956: Waves in the lee of an isolated hill, Quart. J. Roy. Met. Soc., 82, 419.

Scorer, R. S., and S. D. R. Wilson, 1962: Secondary instability in steady gravity waves, Ibid., 89, 532.

Wilson, S. D. R., 1964: Instability in a geostrophic wind with a transverse wind-speed gradient, Ibid., 91, 132.

Yih, S., 1965: Dynamics of Nonhomogeneous Fluids, Macmillan, 109 pp.

DISCUSSION

Question: Mr. Paul A. Sauer, USAF-FE Warren

In the case of wind blowing obliquely toward a mountain range, can a general cut-off angle be designated beyond which the probability of moderate or severe turbulence associated with the mountain wave is small? (Say, below 15%, for example). Note: Moderate and severe turbulence defined with reference to effects on large passenger-carrying aircraft.

Reply: Dr. Scorer:

There is no cut-off in the ordinary sense because with a suitably chosen airstream, instability can be generated over any hill. In practice there will be less CAT if the wind is nearly along a ridge than when it blows across, but we must not forget that sometimes the largest lee waves produced by a system of ridges occur when the airstream is inclined simply because that is the case in which wave trains of different ridges happen to be additive.

If any "cut-off" is claimed to be observed, we can say that it is the kind of thing to be expected, but no theory says that it will be absolute.

Question: Mr. David D. Houghton, NCAR

How far do you think linear theory can be extended to explain the various secondary (smaller scale) features associated with standing mountain waves? For example, in the discussion on centrifugal instability, no mention was made about the effect of the forces causing the curved flow on the stability of the smaller perturbations. How valid then is the argument of dynamic instability in this case?

Reply: Dr. Scorer:

All the mechanisms that I have suggested for producing disturbances in smooth waves are in the category of local instability. They are like gravitational static instability and do not depend on boundary conditions. Still less do they depend on dissipating mechanisms such as viscosity because at the molecular level these are negligible, and at the eddy level they do not come into play until after the instability has occurred.

In the case of centrifugal instability no special or different conditions arise. The forces causing the curved flow are those which produce the instability. The theory of the instability is in every case a linear one which asks whether a small perturbation on the smooth wave flow will grow spontaneously or not, and is of the standard classical kind.

Question: Mr. Ignaz Vergeiner, NCAR

Would you care to comment on the turbulent boundary layer near a mountain since you yourself have put forward an explanation of rotor eddies shedding off a mountain periodically as being caused by separation of the turbulent boundary layer? (I have that from Queney's WMO publication of 1960, ed. Alaka, explaining an observation by Forchtgott). Do

you know of any observations of the boundary layer, conditions for separation or the way in which stability of the airstream inhibits separation of the boundary layer?

Reply: Dr. Scorer:

Clearly, somewhere down the line, my comments on the phenomenon of the periodic shedding of eddies from the lee side of a mountain have been misinterpreted. I did not use any concepts of the turbulent boundary layer, but only the concept of separation, which is a quite independent idea.

Separation is affected by many things, and I think there are three worthy of special note. The first is that a steady solution of the problem without separation may not be possible which means that the upper layers are not capable of a steady motion which would produce the pressure field below required to keep the surface air moving along the boundary, and in this case periodic separation is possible, but there is no complete theory for this--it is a guess! Secondly, anabatic winds up a warm hillside undoubtedly cause separation and this is a major cause of the disappearance of waves during a sunny day. Thirdly, katabatic winds undoubtedly cause adhesion of the flow to a lee hillside and, thereby, induce wave flow above. Very often the strong wind under the first lee wave trough is called a katabatic wind because it begins at the time the katabatic wind occurs which stops the flow from separating.

Other mechanisms were discussed in my paper, "Theory of Airflow over Mountains IV--Separation from the Surface" in Quarterly Journal of the Royal Meteorological Society in about 1955.

Question: Dr. P. Koteswaram, NCAR

Does "centrifugal instability" have any effect upwind of the mountain barrier?

Reply: Dr. Scorer:

Only a quite neglibible effect because the curvature there is always much smaller than downwind.

Question: Mr. Freeman M. Smith, SWCRD U.S.D.A.

What is the smallest scale to which the principles of initiation and propagation of standing waves can be applied? I.e., do the principles hold for flow in plant canopies?

Reply: Dr. Scorer:

On the whole, I would not expect the mechanism of gravity wave propagation to have any application to the motion in plant canopies. The motion there is too much influenced by the drag of the plants.

Question: Mr. Stephen J. Leadabrand, CSU--NSF Research

What are the longest observed wavelengths of these waves and what is the primary factor in determining the wavelength of the wave?

Reply: Dr. Scorer:

The longest wavelengths are in the neighborhood of 20 miles. There is no useful answer to the question, what is the primary factor, because it is a combination of several factors, and only this combination, that makes the waves possible at all. The greater the stability and the smaller the wind velocity, the shorter is the wavelength, but without certain types of profile of wind and static stability, there would be no waves at all, so that often a mechanism sets in, for example in the morning, to lengthen the wavelength; but after it has acted to lengthen it a certain amount, the waves disappear. At the same time the amplitude could be altered drastically, while the wavelength is changing and the direction in which it is altered drastically could be one way for one mountain and another way for another mountain. Perhaps this kind of answer explains why wave clouds have not got into climatology very much yet!

Question: Mr. Glenn E. Stout, Illinois State Water Survey

(1) There is evidence of considerable difference in area variation of hail damage to crops in Kansas and Nebraska. What happens when intense thunderstorms build in the region of standing waves?
(2) The isle of Hawaii in the Pacific creates an upwind effect that triggers bands of precipitation in the trade winds. Would you discuss the upwind as well as the downwind effects?

Reply: Dr. Scorer:

(1) I do not agree with the implication that standing waves influence the location of hailstorms. Generally intense thunderstorms do not build up in standing waves and vice versa. I think the prima facie case for a connection between the two is very poor.
(2) Although any upwind effect depends partly on the mechanism whereby gravity waves are propagated, it is much more complicated than that when diurnal and rain effects are involved in the neighborhood of large islands. Interesting though the problem is, it is not the one to which I addressed myself in this paper, and I am not qualified to pontificate epigramatically on the subject.

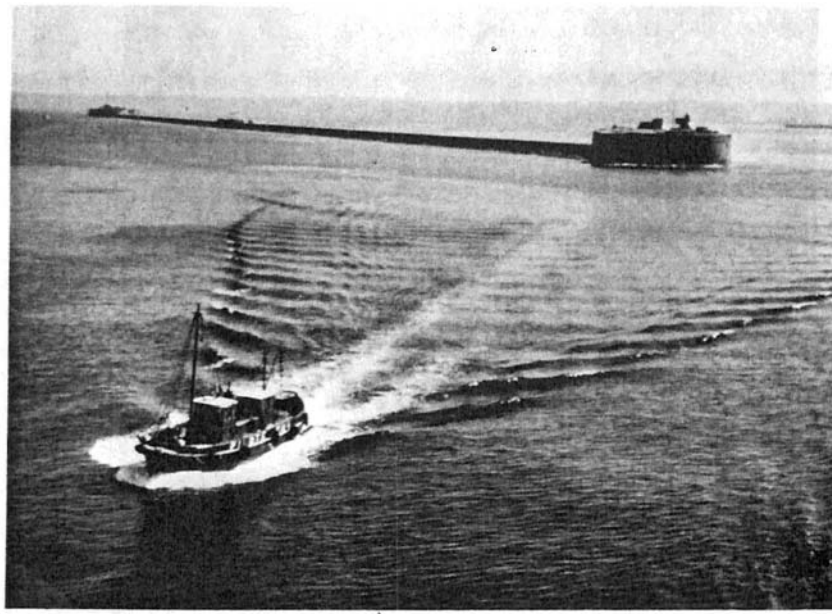

Plate I. The wave pattern of a ship (compare with Fig. 7, bottom).

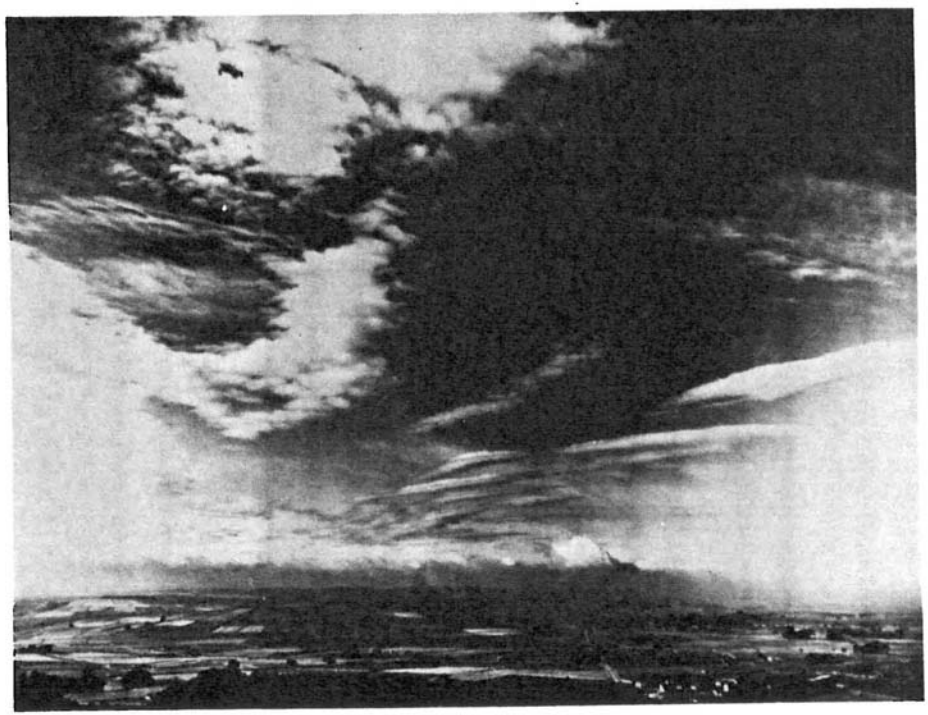

Plate II. An early morning sky in hilly country showing evidence of the 'radial' waves as well as transverse waves in the pattern of an isolated hill.

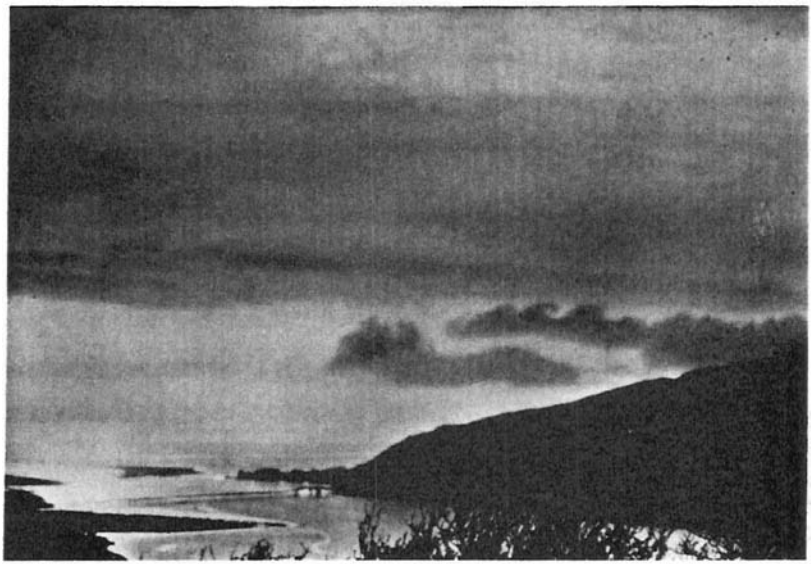

Plate III. Helmholz instability made visible on the top of a cloud whose surface--a very stable layer--was tilted as the air ascended a hillside (see Fig. 10).

VALLEY WIND, SEA BREEZE, AND MASS FIRE: THREE CASES OF QUASI-STATIONARY AIRFLOW

Konrad J. K. Buettner
Department of Atmospheric Sciences
University of Washington, Seattle, Washington

ABSTRACT*

The sea, valley, and into-fire winds are similarly caused by a localized heat source. Theories, computations, models, and field observations are of varied caliber. There is no ideal valley in nature. Thyer's theory of the anti-valley wind system is checked against field tests. A valley wind and an anti-valley wind on top of it, upslope wind and a broad ascending air stream above a ridge, could be ascertained. These three components start and end at the same time. At night,nearly equal but opposite winds blow. For a given temperature pattern, the pressure and wind pattern can be calculated.

Reasonable values for the into-fire wind result from a simple theory based on pressure and winds around a hot volume of air.

---

* Contribution No. 154, Department of Atmospheric Sciences, University of Washington.

VALLEY WIND, SEA BREEZE, AND MASS FIRE: THREE CASES OF QUASI-STATIONARY AIRFLOW

Konrad J. K. Buettner
Department of Atmospheric Sciences
University of Washington, Seattle, Washington

1. Introduction: Comparison of the Three Systems

Mesoscale phenomena show three kinds of cellular motions: (1) those of dynamic character such as the closed and open cells seen by their cloud systems in satellite pictures, (2) those of local dynamic origin as exemplified by foehn and mountain waves, and (3) those caused by a local heat or cold source. Only the latter will be discussed here. At first glance, the story of the driving force in all three items mentioned, sea breeze, valley wind, fire wind, is obvious. Land is warmer than sea on a sunny day and vice versa. The same holds for mountain slopes versus air in the adjacent plains. There is no obvious counterpart for the heat generated by a fire; however, we could compare into-fire wind and glacier wind. Anti-fire or into-fire wind, following meteorological use, blows into the fire; this is called a "fire storm" by the public. A glacier wind, of course, is small in magnitude compared to an into-fire wind.

All three wind systems prefer fair weather; the sea breeze and valley wind because solar radiation is their primary cause; the forest fire because it needs dry fuel. Clear nights promote surface cooling causing very weak land breezes and strong mountain winds, whereas most forest fires become dormant at night because of low winds and high relative humidity. Wind speeds of all three systems reach their maximum at about thermal noon, i. e., around 1500 local time (Fig. 1, 2).

All three systems are caused by a similar sequence: a heat source variable in time and space creates corresponding temperature and density gradients which cause pressure gradients and subsequent winds. Our knowledge about the wind system is, as a rule, better than that of the other data just mentioned. The airflow of the sea breeze and valley wind system is mostly a closed one; air returns at a higher level as anti-sea breeze, anti-land breeze, anti-valley wind and anti-mountain wind. No such anti-system is known for mass fires. The return flow may be anywhere, as indicated by the spread of the plume.

In all three occurrences, the largest horizontal pressure gradients are at the surface. In the sea breeze and mountain wind system, the highest temperatures are at the ground. A fire might be considered as a volume of uniform low density creating a horizontal pressure gradient, increasing from top to bottom of the flame. These pressure gradients cause a maximum of wind speed as close to the ground as the friction permits.

The amount of observational and theoretical investigation is quite different for our three types of systems. The sea breeze covers large parts of the globe which are easily accessible on the ground. The ideal

case, namely a long straight coastline dividing a large water body from a large and uniform flatland, is frequently realized.

As Estoque (1961) states, however, only very few observations cover a sea breeze system sufficiently in time and space. He compares observations along the coast in Massachusetts with results from his computer model. This model, as compared to Thyer's in the next section, makes the differences between the sea system and the valley system clear. Whereas valley wind and mountain wind differ little in speed, the land wind is minute compared to the sea breeze. Estoque models this fact by having the nearground eddy diffusivity, K, depend on Richardson's number. The return flow is fed in the sea system everywhere by vertical wind components

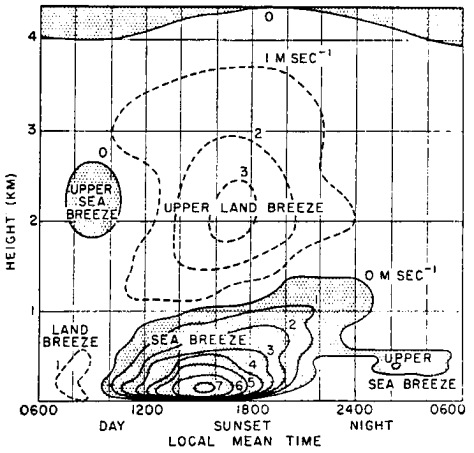

Fig. 1. Average velocity isopleths for the land and sea breeze in Batavia (Sumatra, lat. 5°S)

(up over land, down over sea); in the valley this vertical feeder seems to be restricted to the ridges where vertical motion is very strong.

Solar or infrared heat supply, surface temperature deviations, and overall wind pattern in the sea and valley cases are comparable (Table 1). Heat supply and temperatures are, of course, larger by powers of ten in a mass fire. Here we also meet violent eddies or fire devils for which the quasi-laminar flow in the sea and valley system has no equivalent.

The sea system responds to Coriolis forces and it develops a cold front-type character on arrival at stations inland. The valley system has no fronts; the fire, of course, has one.

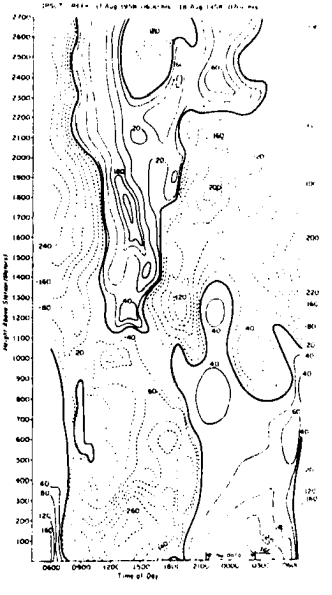

Fig. 2. Valley parallel velocity isopleths of Ipsut Creek on 17-18 August, 1958. Speeds in m/min. Dotted: up-valley, Straight: down-valley.

TABLE 1 - Comparison of magnitudes and data of the sea, valley, and fire wind systems

			sea	valley	fire
Heat supply cal $cm^{-2}min^{-1}$			1/2	0.2	10^4
ΔT	^oK		10	10	600
Δp	mb		1	1	1
$\|u\|$ observed	m/sec	day	3	3	10-100
$\|u\|$ observed	m/sec	night	0.3	2	----
$\|v\|$ observed	m/sec	day	3	< 1	1
$\|v\|$ observed	m/sec	night	0.3	< 1	----
$\|w\|$ observed	m/sec	day	--	3	10-100
calculated	m/sec	day	0.1	---	----
height of lower system, km,		day	1	1(ridge)	0.1-2
depth of anti-system, km		day	1	1	
begins at (summer)		day	10	8	----
ends at		day	20	24	----
Corolis involved			yes	no	no
frontal progresses at km/hr			10	---	----
cumuli caused			inland near front	on ridges	above fire

This list contains order of magnitude comparisons of certain variables in the three systems.

Comments:

ΔT and Δp are differences between system and environment.
u, v, w are wind components where u is perpendicular to coast, parallel valley and into fire.

2. The Valley Wind System

There is no semantic problem in the words 'sea' or 'land breeze' and in the word 'fire'. It is not that simple for the term 'valley wind system'. After Webster, 'valley' comes from Latin 'vallis'. It is "an elongate depression, usually with an outlet between bluffs or between ranges of hills or mountains". If we omit "usually", this fits our purpose well. A round depression in the ground, for example, is no valley, but a hole. An elongated depression, closed or open on both ends, or generally symmetrical on both ends, is a trough or saddle, not a valley. If, from a plain, a large embankment rises under a certain angle, we see a slope, not a valley. Observing or calculating what happens to these features does not, per se, constitute a solution of the valley and mountain wind problem.

Most valleys in nature were formed by a river or ice erosion. Usually the ridge line and the bottom line descend if we progress from mountain to the open plains. But, it can be otherwise as the Maloja effect shows, namely, a wind may seemingly be blowing into the "wrong" valley or a valley wind may be blowing "down"-valley. We therefore call the mountain end "proximal" (frequently the "upper" valley), the valley end, "distal". The terms 'valley' and 'mountain winds' refer to winds blowing up and down the valley, respectively; the return flow above is called the anti-system.

The "ideal" valley has not yet been found. It should be large, straight, steep, but not canyon-like, dry, open to the adjacent plain and closed at the upper end. Of the six valleys tested, the best (Carbon River) is crooked, i. e., heads first N, later W; two show Maloja effects, i. e., winds blowing over from another valley (Figs. 3, 4, 5); one is so wide that gradient winds easily destroy the local system; one has only 300 m ridge height and shows Maloja effects at night and has no recognizable anti-system of its own; one shows glacier wind only.

The study of these winds was nursed first with the pibals of the old airport at Innsbruck, Tyrol, which long had the best series of data. Unfortunately Innsbruck lies at the center of a 'T', the horizontal bar symbolizing the mighty East-West Inn Valley and the vertical bar, the equally large confluence of Stubai and Wipp from the South.

3. Mount Rainier Valley Wind Observations

During the summers of 1958-60, tests were made in many valleys of the Mount Rainier system (Buettner, 1959, Buettner and Thyer, 1961, 1966, Thyer, 1962, 1966). The most important valley for the understanding of the wind system and, therefore, the most investigated valley, was that of the Carbon River. We shall see below how close this comes to being "ideal". Other valleys tested showed these anomalies: the Lower White River (Fig. 3, 4) (46° 46.5'N, 121° 35'W, 935 m) shows Maloja-type reversal from 1200 to 1330 (at this time a high mountain slope down valley from the station is insolated). The Upper White River (Fig. 5) (46° 54'N, 121° 38'W, 1235 m) shows "correct" mountain winds from 2000 to 0800 and "correct" valley wind only from 0800 to 1100. From 1100 to 2000, we have Maloja-type reversal caused obviously by the Fryingpan valley, which is larger and not glaciated.

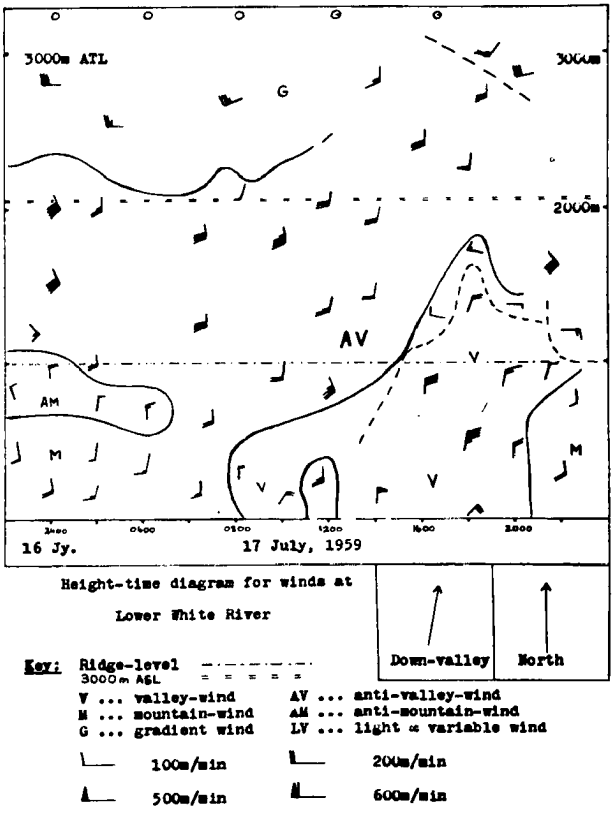

Fig. 3. Height-time diagram for winds at Lower White River. See Maloja effect at 1200.

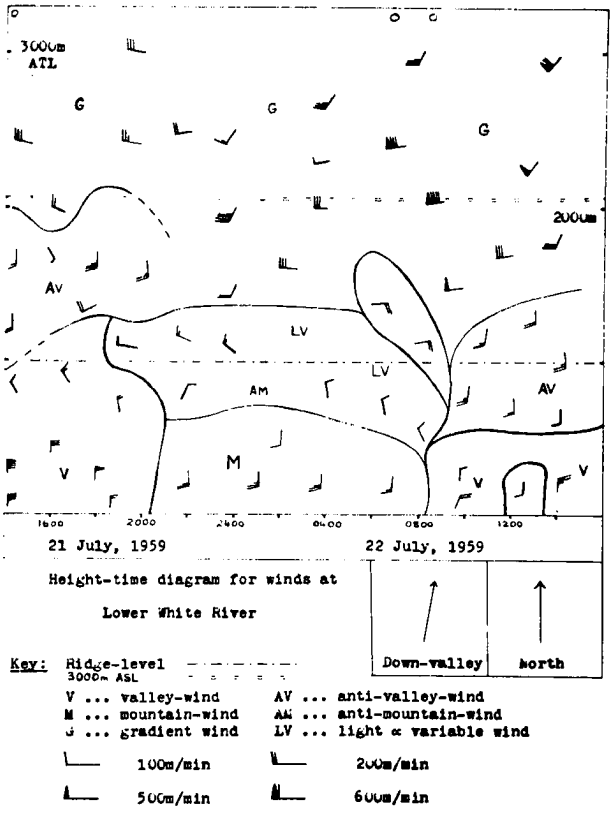

Fig. 4. Height-time diagram for winds at Lower White River. See Maloja effect at 1200.

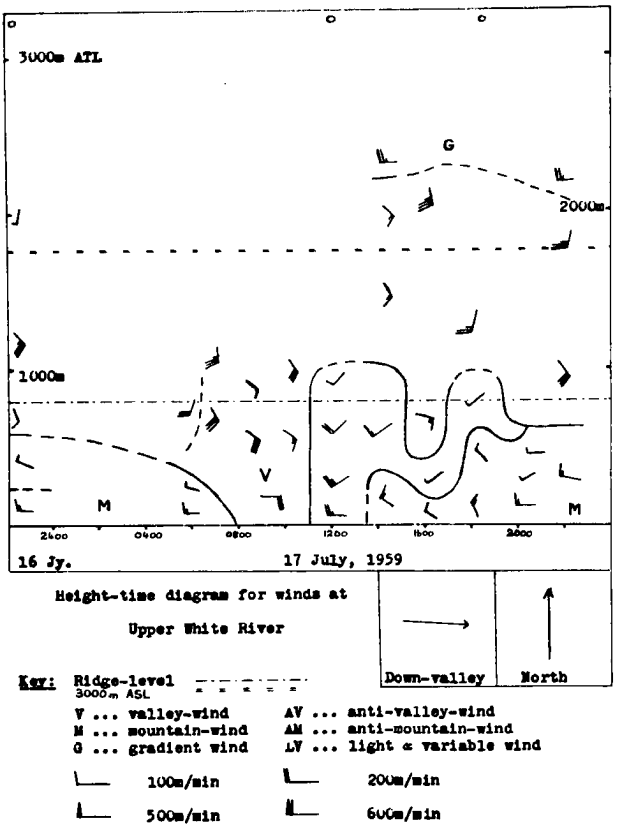

Fig. 5. Height-time diagram for winds at Upper White River. Maloja effect from 1100 to 2000.

By far, the largest of our valleys is the well-built Cowlitz valley, tested at Randle (Fig. 6) and Packwood. Here we see on 5, 6, July, 1960, the best developed and strongest (up to 500 m/min., day and night) valley and mountain wind as well as clear-cut anti-winds. This was a day of weak gradient winds. On June 28, 29, 1960, however, with a moderate gradient wind parallel to the valley, the valley wind system could not be distinguished from the gradient winds. The valley has a broad floor, thus allowing the general wind flow to dominate and obscure the valley wind system.

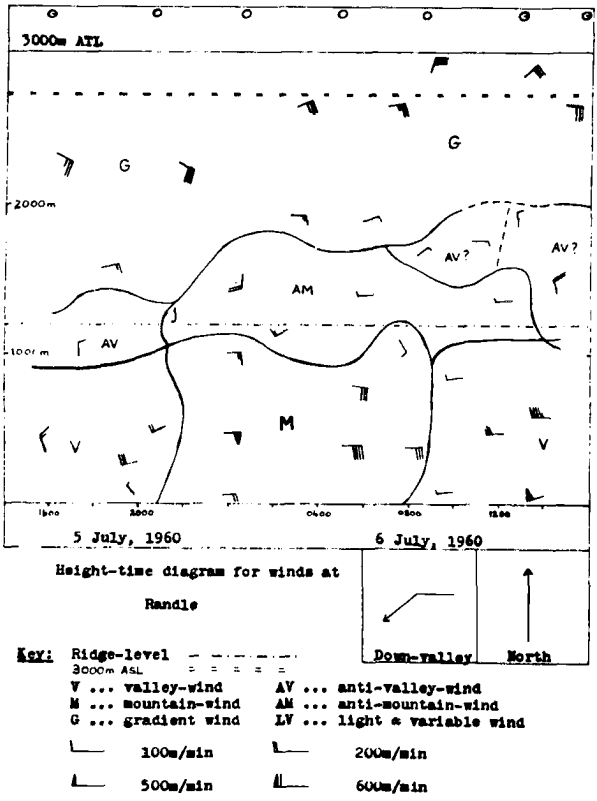

Fig. 6. Same for Randle in Cowlitz River Valley, a very broad valley.

A station below the terminus of the mighty Nisqually glacier (46° 48'N, 121° 44.5'W, 1800 m) showed only glacier wind.

Some of these anomalies were expected from a map survey; some came as a surprise.

All our valleys radiate from a common center, the 4350 m glaciated Mt. Rainier. This causes a systematic difference of the anti-wind system as compared with that of the Alps. Any anti-system will either be over the specific valley or will tend to be integrated in the direction of adjacent valleys, most of which are radial to Mt. Rainier. This is in contrast to the Alps which have a huge overall anti-system between a main E-W ridge and the plains to the N and S.

The Carbon River valley was tested from Thompson's Ranch (46° 59'N, 121° 57'W, 475 m) to Mystic Knoll (46° 54.39'N, 121° 46.04'W, 2030 m). The proximal end is a wide, sloping plateau above 2000 m, adjacent to a very steep incline, the Willis Wall (2700 to 3900 m). The valley then stretches for about 20 km, directed first N, later W. The distance, ridge to ridge, is mostly around 3 km, the bottom width between 0.5 and 1 km. The ridges are about 1000 m above valley bottom. Most slopes are about 45° steep. The valley bottom is practically flat at the distal end and rises by 21° near glacier terminus.

The area of the valley bottom is small compared to the areas of the slopes--quite contrary to the Cowlitz valley (Fig. 6). The slopes are uniformly covered with mature conifer virgin forest. Only a few roads and rock slides gave us open spaces to investigate slope wind with pibals. It took some good mountaineering skill to man these stations. Only days with weak gradient winds and without lower and middle clouds are included in this discussion.

It is doubtful, however, whether long summertime averages of all days for a valley help us much to explain the undisturbed day winds. We saw, e.g., that a strong cross-valley gradient wind depresses the valley wind and anti-valley wind below ridge level; averaging them would combine antiwinds of some days with valley winds for other days.

4. Valley Wind Model

N. Thyer describes in detail (1962, 1966) the past theories of valley winds. He had to reject, as not pertinent, the many slope-wind theories. The slope heating causes the up-slope wind; but this is not the valley wind.

After deliberations about two dimensional solutions, it became clear that they would not solve our problem. Nothing was left other than to try a three dimensional model.

N. Thyer's theory is based on this simplified set of equations:

$$(1)\quad \frac{Dv}{Dt} = -\frac{1}{\rho}\nabla p + K\nabla^2 v - \vec{g}$$

$$(2)\quad \frac{D\theta}{Dt} = K\nabla^2\theta$$

(3) $\nabla \cdot v = 0$

(4) gas law, Poisson's law

where v is velocity, ρ is density, p is pressure, g is gravity, and K is assumed to be the (constant) eddy viscosity and eddy heat conductivity. The boundaries are a horizontal valley open at distal and closed by a vertical wall at the proximal end. Initially $v = 0$ and the temperature lapse rate is $6.5^{\circ}Ckm^{-1}$ throughout. Then as a step function, the valley walls release a constant heat of 0.13 cal cm^{-2} min^{-1}.

We shall, in the following, sometimes use night and day conditions alternatingly. In Thyer's data, both cases are just opposite; and, therefore, all wind types are the same except for a 180° shift.

The main calculation could be done on the IBM 790 for a time equivalent to 120 sec. real time. The results in Figures 7, 9, 10, and 12 show essentially six wind components to prevail two minutes after this ideal

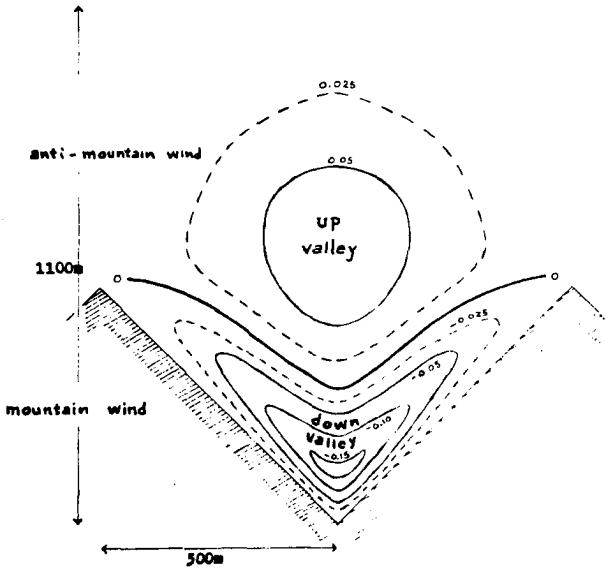

Calculated parallel mountain wind speed, 120 sec. after negative heat input started. Units: m/sec (Thyer)

Fig. 7. Calculated parallel mountain wind speed, 120 sec. after negative heat input started. Units: m/sec (Thyer).

"sunrise". All six components are of similar magnitude, about 0.2 m/sec. or 0.4 knots, at their maximum. We see:

(a) A longitudinal, up-valley component of the valley wind (Fig. 7): This corresponds to the observed valley wind in the Carbon Valley (Figs. 8, 9).
(b) A longitudinal down-valley wind aloft: This is the anti-valley wind (Fig. 7). For verification, see Figs. 8, 9, and 11.
(c) A cross-valley wind, (Fig. 10) in the valley directed from the axis to the wall in a shallow layer near the slopes: For verification, see Figs. 8 and 11.
(d) A broad wind system opposite the cross-valley wind above ridge level and normal to the valley axis (Fig. 10). The veering of the antiwind above the North Rim in Fig. 11 is a possible confirmation.

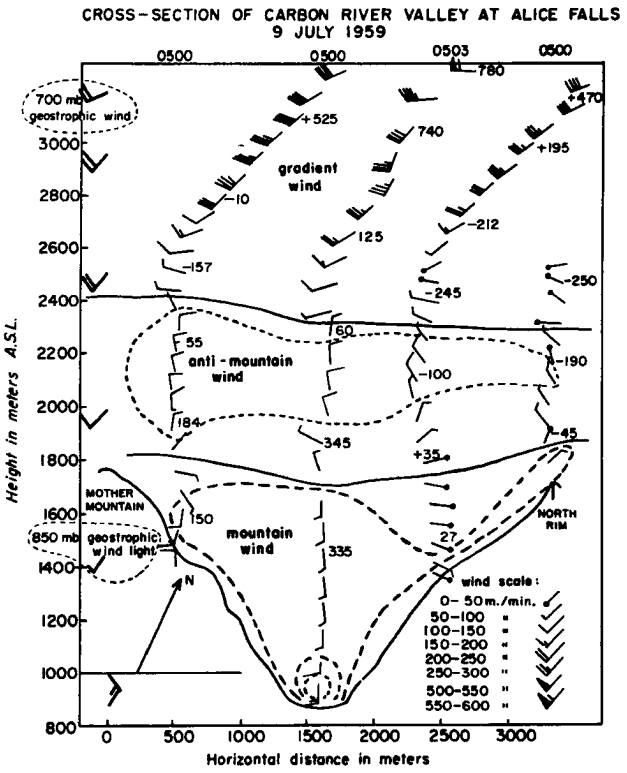

Fig. 8. Cross-section of wind vectors and valley-parallel speed isotachs. Geostrophic winds extrapolated from synoptic maps. All arrows fly related to geographical coordinates (the mountain wind in the valley is a valley parallel S-wind). Horizontal distance is measured down valley from release point.

(e) An upward vertical component along the slopes (see c) extending above the ridges (Fig 12): This feature is termed the 'slope wind' and verification can be found in the trajectories of constant lift balloon flights in Fig. 13.

(f) A descending vertical component in midvalley below the ridge level (Fig. 12): This downflow has--without mathematical proof--also been claimed by Defant (1948, 1951), but as far as is known, has never been observed.

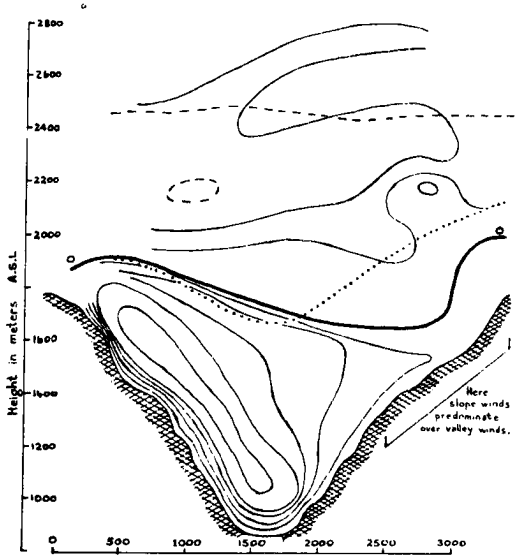

Fig. 9. Isopleths of valley-parallel component of wind measured in a cross-section of the Carbon River valley at Alice Falls, 1300, 9 July, 1959. Winds are up-valley below the zero line, and down-valley above it.

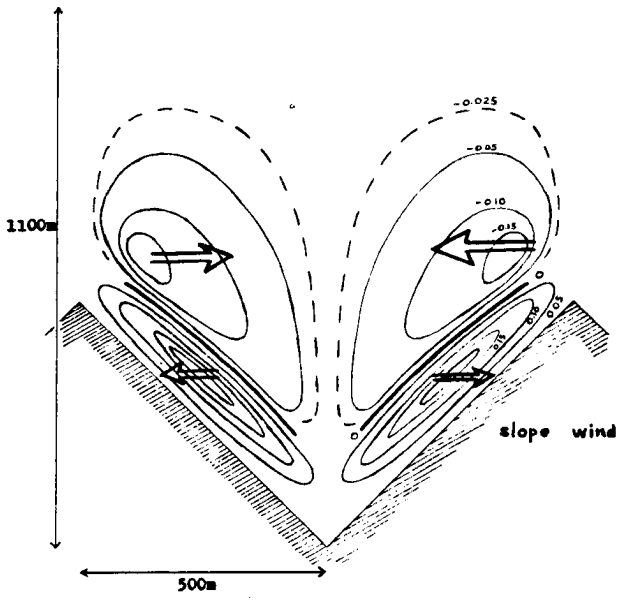

Calculated cross valley wind speed,
120 sec. after heat input started.
Units: m/sec (Thyer)

Fig. 10. Calculated cross-valley wind speed, 120 sec. after heat input started. Units: m/sec (Thyer).

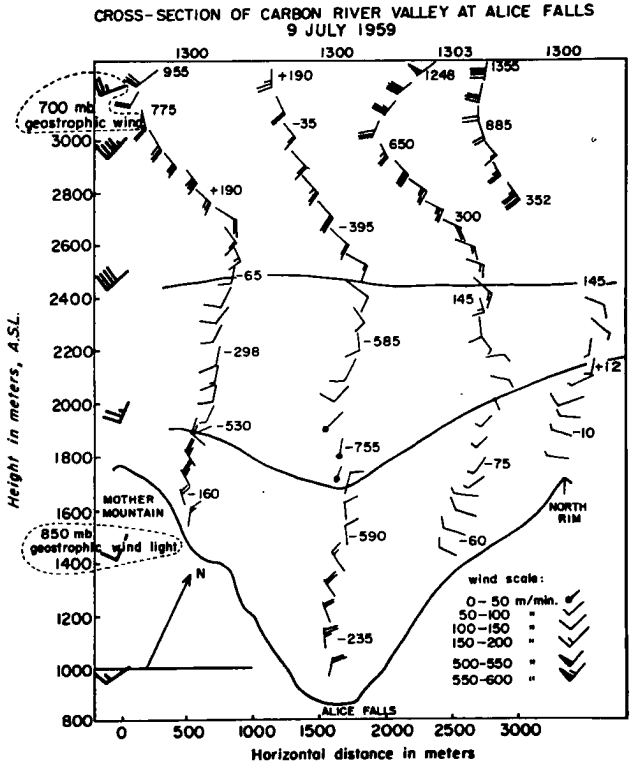

Fig. 11. Similar to Fig. 8. The valley is filled with valley wind; in the layer above ridge level, anti-valley and geostrophic winds blend. Horizontal distance is measured down valley from release point.

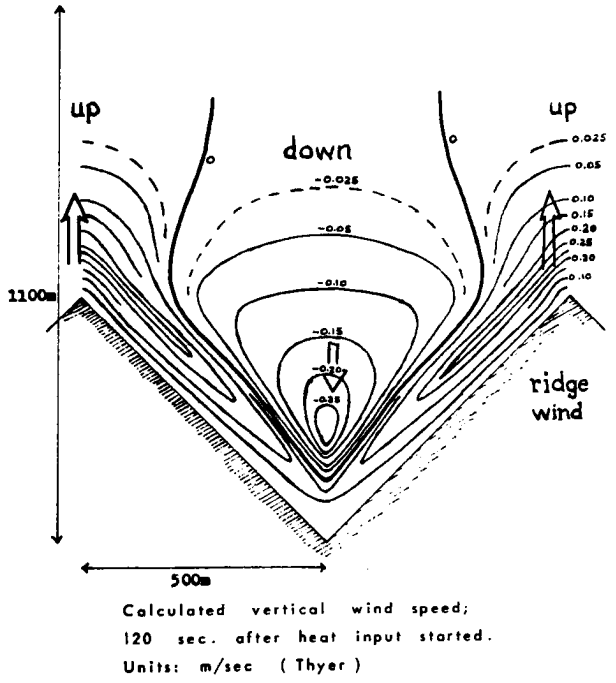

Fig. 12. Calculated vertical wind speed; 110 sec. after heat input started. Units: m/sec (Thyer).

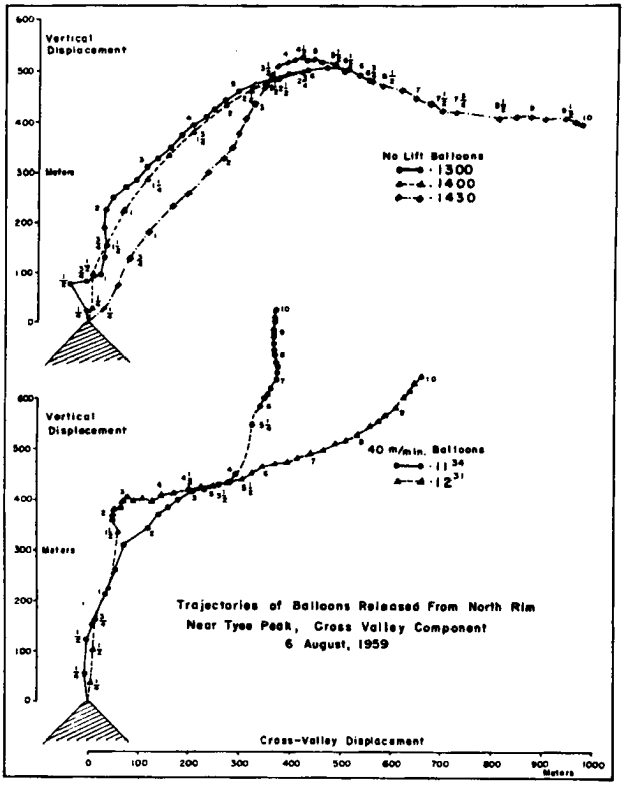

Fig. 13. Trajectories of balloons released from North rim near Tyee Peak, cross-valley component, 6 August, 1959.

Whereas components (a)-(e) increase from some 0.2 m/sec, as requested by theory, to an observed value around 4 m/sec (Fig. 20) after an hour or two, an equivalent vertical down wind of the magnitude requested in (f), is out of the question. Even a tenth of this value would have been observed in double theodolite tests, or by our no-lift balloons (Fig. 13), which went to the valley axis and about 400 above ridge showing less than 0.2 m/sec or 0.4 knots, downwind. Actually one balloon (Fig. 13) shows up-wind, one down-wind, and a third, neither. This might also be caused by other effects such as a lee wave of a weak gradient wind, balloon decay, etc. The downwind, if it exists, is certainly small.

There is no a priori reason for all six components to grow at the same rate. In fact, there is a good one for component (f) to cease growing soon. This component, as Fig. 14 shows, carries heat from the slopes and ridges into the middle of the valley, changing the overall pressure pattern.

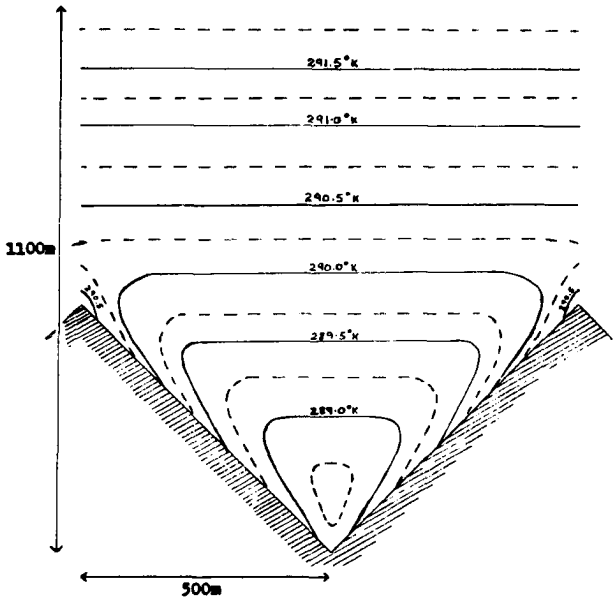

Calculated isopleths for potential temperature; 120 sec. after heat input started (Thyer)

Fig. 14. Calculated isopleths for potential temperature; 120 sec. after heat input started (Thyer).

Thyer's computations show that all six components mentioned above start concurrently. There is no time of slope-winds-only as requested by Wagner and Defant (1948, 1951). In balloon tests, one sees all kinds of minor deviations from the simple theory. Generally even the "best" valley is far from ideal. So these minor deviations do not mean much. Sometimes they are easy to explain, e.g., late evening sun on a NW facing slope at a time of beginning nighttime regime.

Fig. 15 shows Thyer's computation of valley parallel winds in mid-valley. The picture is similar to Fig. 7, but speeds of valley and of anti-valley winds are less. We do not have good proof of this decrease of lower and upper wind system as one goes from distal mouth to proximal origin of the valley in our valley-parallel series (Figs. 16, 17, 18).

Figs. 16, 17, 18 contain results of a concurrent series of tests of 5 stations along the Carbon River axis. The valley and mountain wind layer

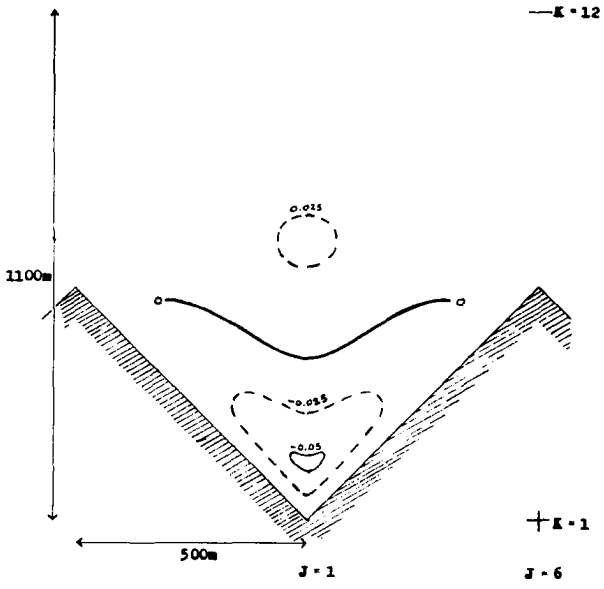

Isopleths of u for I = 4 at 120 seconds.
Cross-section at mid-valley.

3 - dimensional valley of length 500m, half-width 500m, height 1200m, with isothermal plain of length 500m.
Grid: a = 100m b = 100m c = 100m

Heat input to air 0.13 cal cm^{-2} min^{-1} Lapse Rate 6.5 deg/Km
Eddy viscosity 10.0 m^2 /sec Speed accuracy 0.01m/sec
Iteration interval 30 sec. Speeds in meters/sec.

Fig. 15. Isopleths of u for I=4 at 120 seconds. Cross-section at mid-valley.

depths decline; so do their speeds. Since, however, the ridge height also declines at higher levels, results are ambiguous.

From Fig. 19, it becomes evident that, with the reversal of winds with height, ascending pilot balloons (rate of ascent 300 m/min) may return over the launching site approximately 5 minutes after release.

The daily variation of lower and upper wind is seen in Fig. 20. In August, the switch from night to day regime occurs around 0900 PST and the reverse around 2000.

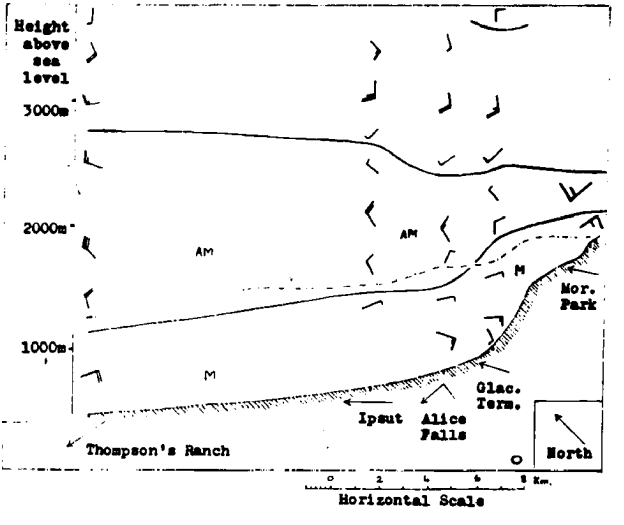

Longitudinal Section of Carbon River Valley

showing winds for 0200, 18 August, 1958 (Mor. Park, 2400 & Aug., 1960)

Key: Ridge-level
Local down-valley direction

V ... valley-wind
M ... mountain-wind
G ... gradient wind
AV ... anti-valley-wind
AM ... anti-mountain-wind
LV ... light & variable wind

100m/min
200m/min
500m/min
600m/min

Fig. 16. Night conditions along Carbon River Valley. Data of Moraine Park taken from another similar series.

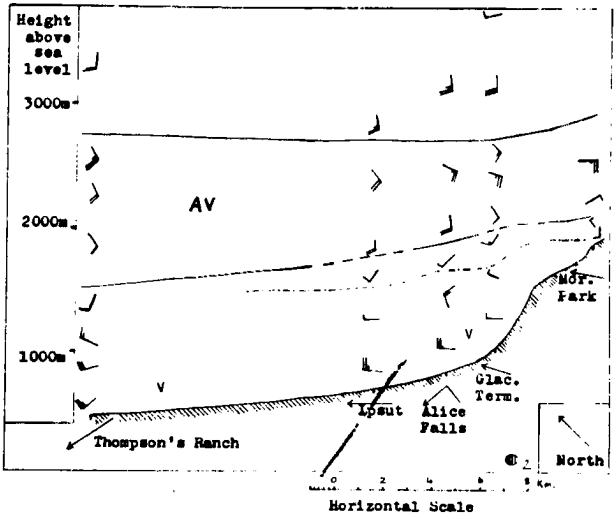

Longitudinal Section of Carbon River Valley

showing winds for 1400, 17 August, 1958

Key: Ridge-level
Local down-valley direction

V ... valley-wind
M ... mountain-wind
G ... gradient wind
AV ... anti-valley-wind
AM ... anti-mountain-wind
LV ... light & variable wind

100m/min
200m/min
500m/min
600m/min

Fig. 17. Day conditions along Carbon River Valley. Data of Moraine Park taken from another similar series.

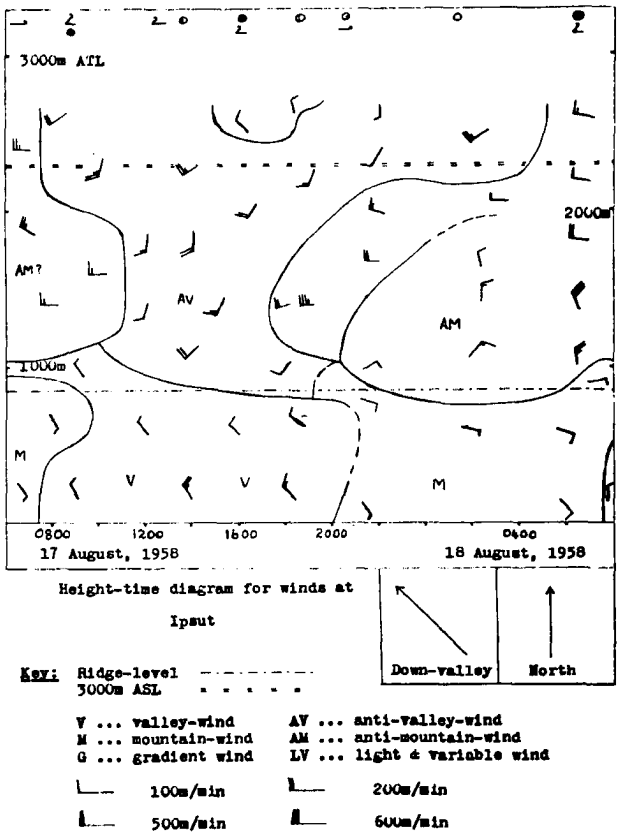

Fig. 18. Typical wind diagram for Ipsut Station, same data used in Fig. 2.

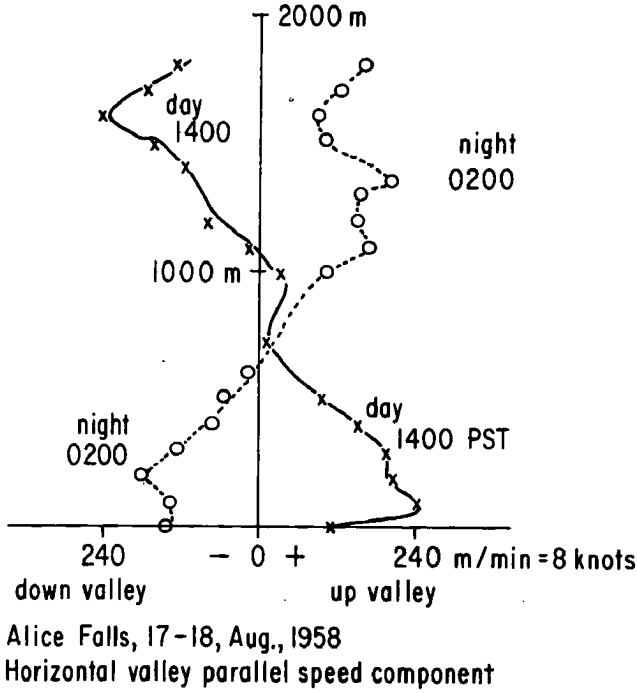

Fig. 19. Typical wind diagram for Ipsut Station, same data used in Fig. 2.

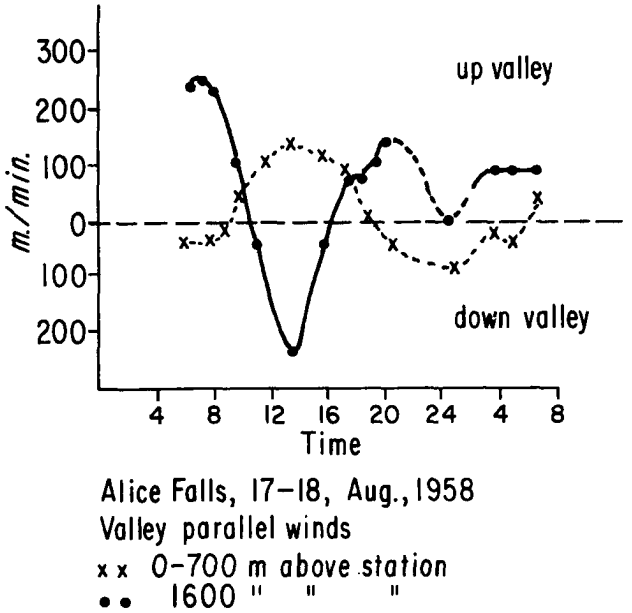

Fig. 20. Daily variation of valley and anti-valley system.

5. Some Ideas on Mass Fires

Mass fires of natural origin are, in peacetime, mainly those of forests and other vegetation or its dry remnants. Their role is probably underestimated in fields of air pollution, nuclei production of all kinds, heat balance, agriculture, climate, etc. The savannahs of inner Africa are regularly burned during the dry season. The smoke often fills all air up to 3000 m; it changes solar radiation drastically.

Start of a forest fire needs (a) dry fuel, (b) ignition. The number of fires reported ought to reflect the forests' vulnerability. Data (Baumgartner, personal communication) prove this: on fire days the pressure falls, wind speed is high, sun shines, maximum temperature is very high, relative humidity is extremely low and, of course, it does not rain.

What burns is mostly hydrocarbons and carbohydrates. Ideally $(CH_2)_n$ is to be converted in an ideal or stoichiometric process to $(CO_2)_n + (H_2O)_n$. In air, much more N_2 has to be heated to the stoichiometric point than the combined mass of C, H, and O. The ideal temperature is around 1600 C. Probing in an open wood fire with thermocouples or measuring the radiant heat output, one gets only 600 C (Buettner 1949, 1966).

Fires can be likened to three well-known examples:

(a) A Bunsen burner flame is blue, a poor radiator since only its hot gases emit; it has about 1600 C and the effluent is pure CO_2 and H_2O.

(b) The yellow core of a candle flame has about 600 C, contains much soot acting as radiation emitter. Around the yellow core is a very thin blue mantle of about 1600 C. In this mantle the CO still present in the yellow core seems to oxidize to CO_2, whereas, part of the soot passes through the flame, the time being too short for total combustion.

(c) In an open fire, there are not only "candle flames", but smoldering, distilling hot fuel parts. They create not only solid - liquid air pollution, but also large portions of CO. The ratio of CO/CO_2 coming out of a fire is a conservative element of that air and will be utilized in our fire tests.

The into-fire wind can be estimated as follows: Consider the fire as a large volume filled with air of 900 K surrounded by normal 300 K air. Density in the fire is then about 1/3 normal. Assume horizontal isobars above the fire of height h. It follows that there is a pressure gradient between the fire core; and this gradient increases with decreasing altitude within the fire. A fire of 10 m height should have, at NTP, a differential of .67 mb at its bottom.

Fresh air is accelerated into the flame. Assuming steady state conditions, equation (1) is simplified to:

$$\frac{\partial u}{\partial x} \cdot u = - \frac{1}{\rho} \frac{\partial p}{\partial x}$$

if u is the only wind component of interest, that is perpendicular to the fire wall. Assuming $u_o = 0$ we have $u^2 = - \frac{2\Delta p}{\rho}$ or for $\Delta p = 2/3$ mb $\Delta p = \frac{-2}{3} \cdot 1000 \frac{\text{dyne}}{\text{cm}^2}$ and $\rho \sim 10^{-3}$ gm cm^{-3} we find $v \sim 10^{\text{m/sec}}$. If as in big city fires, this surface wind is forced through adjacent narrow streets, it may be many times larger, as in this simple approach. Such into-fire winds of "hurricane force" are on record.

Physical tests and computer modeling of mass fires have barely been started. Some methods are suspect: a pile of dead vegetation under an inverted cone with good acess of air from the sides burns nearly ideally, with very little CO. Results are not comparable to a real fire.

Two spectacular and frightening forest fire effects await evaluation:

(a) The after explosion, sometimes seen high above the main fire. A possible explanation: The ascending flame is so "rich", i. e., its fuel/oxygen is too high for combustion, while ascending new air is admixed and the mixture becomes combustible again just waiting for a new spark.

(b) The fire devil: The enormous instability of a fire seems to promote these terrifying eddies, if there is no central upper flame air outlet. Violent eddies of more than one km length have been observed.

REFERENCES

Baumgartner, A., personal communication.

Buettner, K., 1949: Conflagration heat, German Aviation Medicine, World War II, U. S. Govt. Printing Off., Wash. D. C.

Buettner, K., 1966: Die gefaehrdung des menschen bei braenden, Katastrophenmedizin, 41.

Buettner, K., and N. Thyer, 1959: Valley and mountain winds I, AF Contract 19(604) - 2289, Dept. Atmos. Sci., U. of Washington.

Buettner, K., and N. Thyer, 1966: Valley winds in the Mt. Rainier area, Arch. Met. Geophys. Biokl., B 14, 125.

Defant, F., 1951: Compendium of meteorology, Am. Meteorol. Soc., Boston, 662.

Defant, F., 1948: Zur theorie der hangwinde, Arch. Met. Geophys. Bioklimat. A, 1, 421.

Estoque, M. A., 1961: A theoretical investigation of the sea breeze, Quart. Jour. Roy. Met. Soc., 87, 136-146.

Staley, D., 1966: The low level sea breeze of north-west Washington, J. Met., 14, 458.

Thyer, N., 1966: Theoretical explanation of mountain air valley winds by a numerical model, Arch. Met. Geophys. Biokl., B 15, 318.

Thyer, N., 1962: Valley wind theory, AF Contract 19(604) - 7201.

Thyer, N., and K. Buettner, 1961: Valley and mountain winds II, AF Contract 19(604) - 5578, Dept. Atmos. Sci., U. of Washington.

Van Bemmelen, W., 1922: Beitr. Phys. frei Atmos., 10, 169-177.

DISCUSSION

Question: Mr. Edward Hindman, USN Wx Res. Fac., Norfolk, Va.

Won't synoptic scale winds interfere with your "anti-valley" wind, which is above the ridge level?

Reply: Dr. Buettner:

Data used in this paper refer to gradients winds, small compared to anti-winds. A strong cross-valley gradient wind may, however, depress the anti-wind into the valley. We saw cases with valley-and anti-wind in the valley and, of course, in valley direction, topped above ridges by a cross-valley gradient wind.

MESOSCALE ASPECTS OF OROGRAPHIC INFLUENCES ON FLOW AND PRECIPITATION PATTERNS[1]

Tetsuya Fujita
Department of the Geophysical Sciences
The University of Chicago
Chicago, Illinois

ABSTRACT

Since horizontal dimensions of orography in relation to cloud formation and development are mostly in the mesoscale, we usually observe mesoscale nephsystems in areas with topographic influences. In addition to their barrier effects, mountains during the daytime act as effective high-level heat sources or as cloud generators. At night, however, they suppress the cloud formation and act as cloud dissipators. When these effects are combined with the height of the convective cloud base, which could be either higher or lower than that of the mountains, the patterns of orographic nephsystems and precipitation are quite complicated. By using actual cases of cloud and precipitation measurements, detailed climatological and mesosynoptic patterns of clouds and precipitation are discussed.

1. The research reported in this paper has been sponsored by the Meteorological Satellite Laboratory, ESSA, under Grant Cwb WBG-34 Research. The collection of precipitation data from the Flagstaff mesometeorological network in 1960 and 1961 was supported by the U. S. Air Force Office of Aerospace Research (GRD) under Contract AF 19(604)-7259.

MESOSCALE ASPECTS OF OROGRAPHIC INFLUENCES ON FLOW AND PRECIPITATION PATTERNS

Tetsuya Fujita
The University of Chicago

1. Orographic Clouds and Precipitation in Relation to the Base of Convective Clouds

It is well-known that the worldwide rainfall patterns are closely related to the large-scale flow patterns and the orography which blocks the flow in various ways. Even though the role of the mountains in natural stimulation of precipitation is not fully understood, the difference between the height of the convective cloud base and that of mountain tops results in significant variation in the rainfall patterns on and around the mountains.

When the condensation level or cloud base is considerably lower than the mountain tops, cloud growth and precipitation take place on the upwind side of the mountains. The effect of solar radiation becomes insignificant as soon as the upwind slopes are covered with thick convective clouds with high albedo.

The mechanical lifting of moist air is the most important mechanism for the release of latent heat of condensation when the stratification is conditionally unstable. Elliott and Schaffer (1962) showed that the ratio of amounts of mountain and flatground precipitation decreases appreciably with increasing air-mass stability, suggesting that the orographic stimulation of precipitation does not occur when the air mass is stable.

Even small mountains blocking a rapid flow of moisture in the tropics, such as that accompanying hurricanes and typhoons, result in a significant amount of precipitation on the upwind side of the mountains. Fig. 1 shows an example of orographic rainfall over Japan under the influence of Typhoon Bess in August, 1963. Winds plotted in the standard form in the lower figure represent velocities of the radar echoes computed by Fujita et. al. (1967). The height of the cumulus base on the upwind side varies between 1000 and 2000 ft. while the mountains are as high as 5000 ft. It is of interest to see in the upper chart that along the Pacific coast the one-hour rainfall ending at 0500Z is only several millimeters. Heavy rainfall, up to 18 mm, is seen only on the upwind slope of the mountains. No more than a trace of rainfall is reported from the downwind regions, thus showing the effective blocking of precipitation by such relatively low mountains.

When the condensation level is located near or above the mountain tops, convective clouds forming on the peak or over the leeward side of the mountain produce precipitation as they drift away from the ridge line. As seen in Fig. 2, such cloud formations are quite common over dry regions. Note that clouds over Baja, California, extend northeast from the ridge line of the Sierra de Juárez and that similar cloud formations in Nevada, Utah, and Arizona have the same relative location with respect to orography.

In such cases, the heating of the mountain slopes plays an important role upon the acquisition of buoyancy by orographic cumuli. Especially when the low-level wind is southerly, the orographic clouds forming and developing above the northern slopes of mountains do not effectively shield

the solar radiation reaching the southern slopes along which the heated air travels upward.

Braham and Draginis (1960), and Silverman (1960), using data obtained from an instrumented Air Force aircraft, made detailed analyses of the moisture and temperature patterns above the Santa Catalina Mountains north of Tucson, Arizona. They revealed that the heated moist air, because of the lifting effect of the barrier and the high-level heating effect of the mountain, reached 3000 to 5000 ft. above the mountain-top level after the slope was heated by the morning sun.

The growth of cumuli clouds after their formation above mountain-top level was investigated by Glass and Carlson (1963), who made detailed photogrammetric analyses of cumulus development over the San Francisco Mountains north of Flagstaff, Arizona. Their results indicate that initial

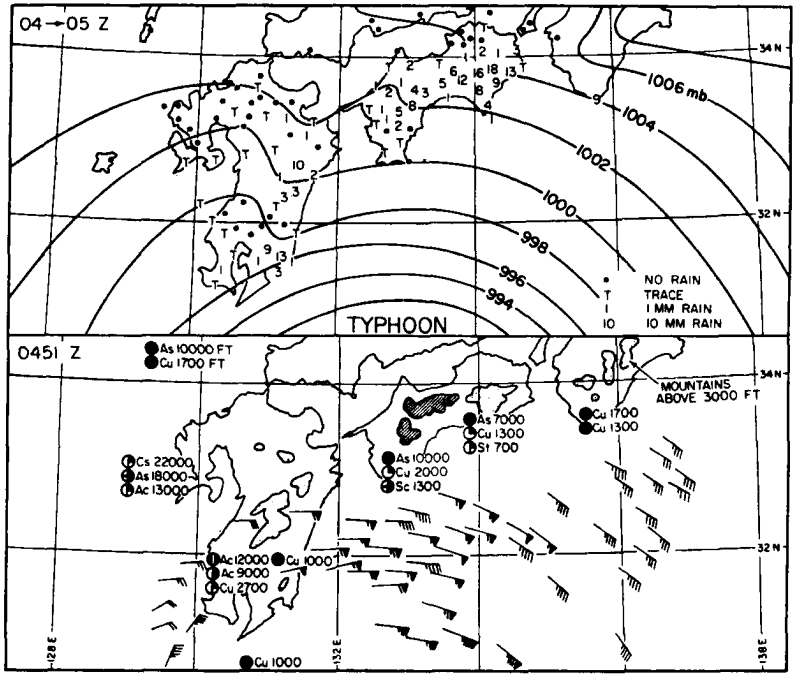

Fig. 1 An example of orographic precipitation with the convective cloud base much lower than that of the mountain barrier. Upper: Hourly precipitation in mm between 0400 and 0500 GMT 8 August, 1963. Lower: Cloud bases observed at 0500 GMT from ground stations in southern Japan and the velocities of radar echoes at 0451 GMT from Fujita et. al. (1967).

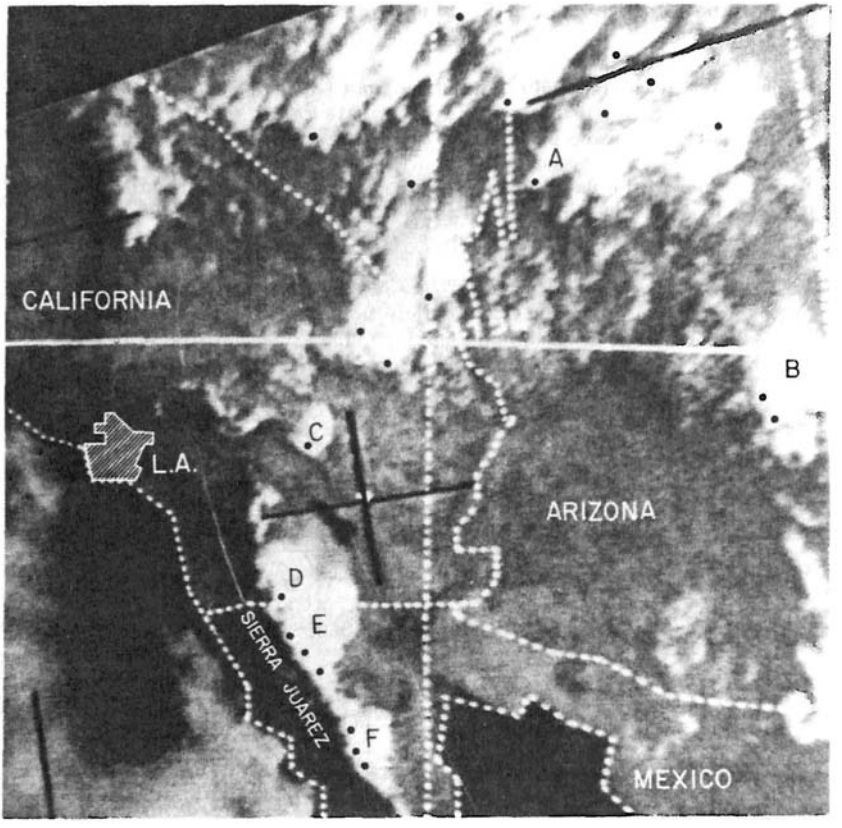

Fig. 2 An example of orographic clouds with their bases at or above the mountain-top level. Large cumulonimbi are identified by letters A through F. Black dots designate the positions of the moutain peaks, which are assumed to be the source regions. ESSA I picture taken at 1407 MST, 23 July, 1966.

clouds with their bases at 17,500 - 20,000 ft. formed a few tenths of a mile downwind from the 12,680 ft. peak. After the formation, each cloud drifted away from the source region while increasing its volume as much as 10 times. They studied mostly small cumuli which were eroded away after about 10 minutes. These clouds consisted mostly of up-slope thermals which were mixed with environmental air several thousand feet above the mountain tops. It is very unlikely that these small clouds would receive a continuous supply of moist air from the lower levels on the downwind side of the mountain. If one of these cumuli developed into a huge cumulonimbus, it would maintain its circulation practically independent of the orography which gave rise to the development of the initial cloud. Thus, a large storm could move away from the mountains for a great distance downwind.

2. Distribution of Rainfall Patterns around Isolated Mountains

In an attempt to investigate pressure disturbances associated with the orographic precipitation around the San Francisco Mountains of Arizona, a mesometeorological network of stations was established and operated by the University of Chicago and sponsored by the U. S. Air Force. Fig. 3 shows the area dominated by the San Francisco Mountains in northern Arizona.

Long before the attempt by the Air Force to study orographic convection in the Flagstaff area, Indians knew and told the participating scientists that their rainy season would start as soon as the traditional annual Rain Dance was performed at Flagstaff early in July. Both 1960 and 1961 networks began to operate shortly after the day of the Rain Dance, which actually signalled the beginning of the moist spell.

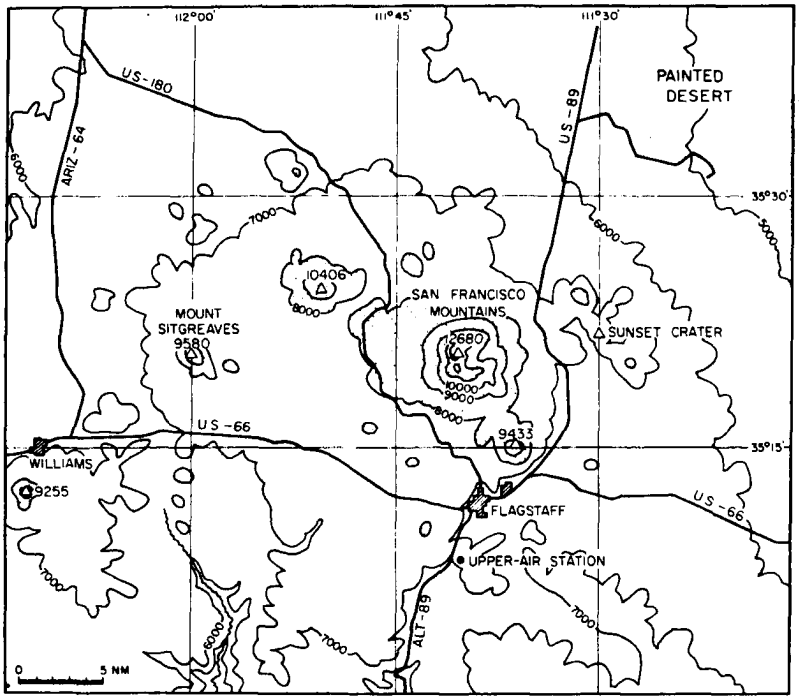

Fig. 3 Topography around the San Francisco Mountains in northern Arizona, where a rain-gauge network was operated during 1960 and 1961 seasons.

The total precipitation amounts for July 16-29, 1960, plotted and contoured in Fig. 4 clearly show a maximum directly over the mountains, and are surrounded by a ring-shaped zone of relatively low total amounts (see black dots circling the mountains). Outside this ring were scattered areas of high values up to 2.2 inches.

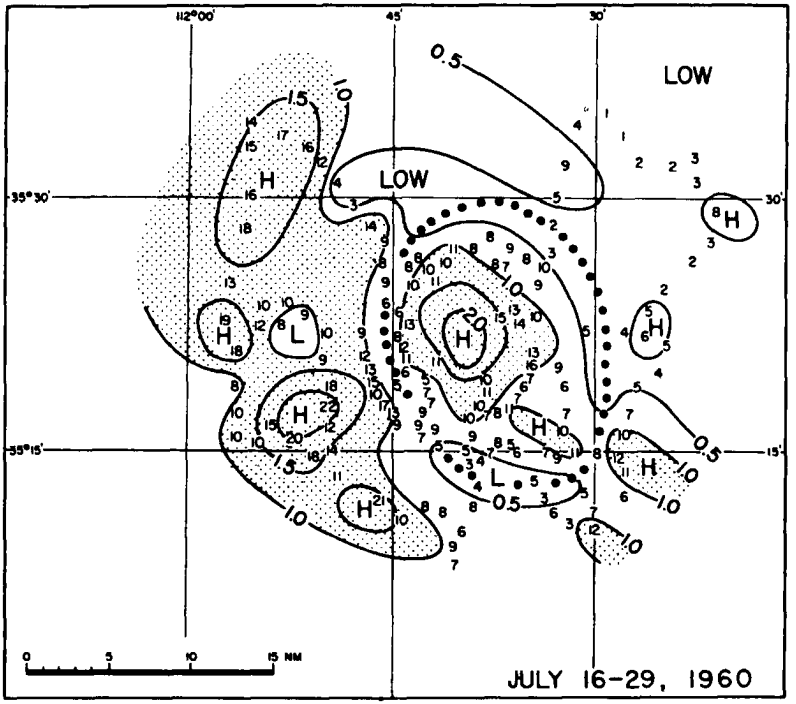

Fig. 4 Total precipitation during the period July 16-29, 1960, measured at about 150 stations around the San Francisco Mountains. Amounts were plotted in 0.1-inch units and contoured for every 0.5 inch. H and L designate high and low values, respectively. Black dots circling a high rainfall area over the mountains indicate a ring of low precipitation.

In order to learn whether the 1960 pattern of orographic rainfall represents a general distribution or not, a second and more extensive network was established in 1961. The number of rain gauges was increased from 150 to 220. The pattern of the total precipitation turned out to be very similar to that obtained in 1960. The total amount of rainfall in the 1961 period was about twice that of the previous year, due partially to more days of operation, which were increased from 14 to 19 days, and to the increased convective activity. Nevertheless, the low total-precipitation ring surrounding the mountains appeared practically the same as in 1960.

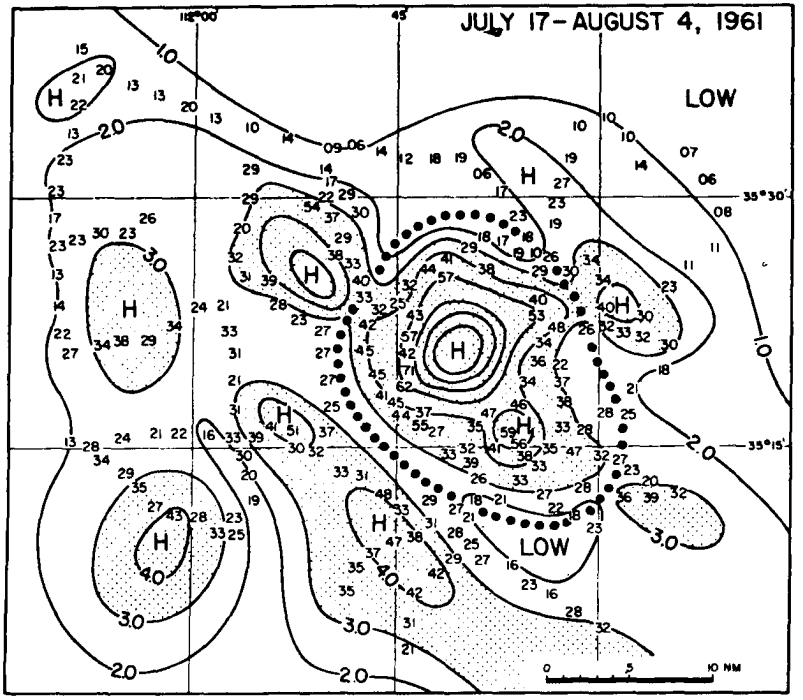

Fig. 5 Total precipitation during July 17 - August 4, 1961, measured at about 220 stations. Amounts are shown in increments of 0.1 inch, and isohyets were drawn at one-inch intervals. Note that a ring of low precipitation around the mountain existed again in 1961.

To represent variation in the rainfall as a function of the distance from the mountain, six pie-shaped areas were constructed by drawing six azimuths, 000°, 060°, 120°, 180°, 240°, and 300°, radiating from the center of the mountain. The scatter diagram (Fig. 6) obtained by plotting the precipitation within each pie-shaped area reveals the existence of a low-total-precipitation area at a distance of about 8 nm from the mountain. A ring of maximum rainfall is also seen along the radius of 10 to 12 nm. This evidence poses the question as to the cause of these rings of minimum and maximum precipitation.

Fujita, Styber, and Brown's (1962) study of daily precipitation during the 1960 season indicated that the over-mountain rainfall mostly occurred on the days with low wind speeds and that the distant rainfall, 10 to 12 nm from the mountain center, fell quite often at night. Braham (1958) concluded in his study of cumulus clouds in Arizona that every one of the cloud parameters showed marked day-by-day variations. His statement is very important since it implies difficulties in explaining the daily regime of orographic convection from the broad synoptic conditions.

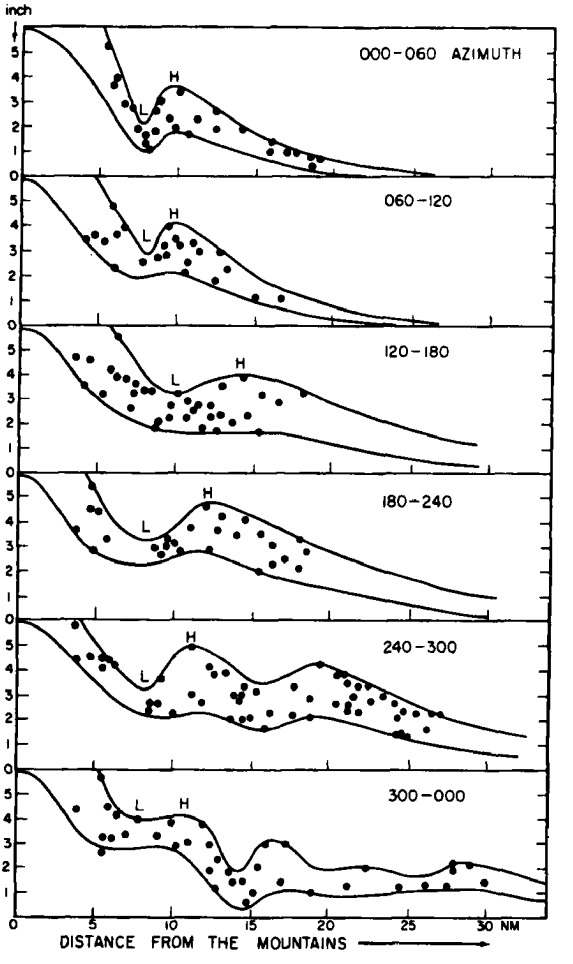

Fig. 6 Scatter diagrams showing the radial distribution of total rainfall around the San Francisco Mountains as measured during the 1961 season. The letter L indicates the position of the ring of low precipitation in each fan-shaped direction.

From this we may assume that over-mountain precipitation is predominant when straight convection takes place under the influence of relatively low wind speeds. A distant rainfall may occur at night when the mountains are cold, thus acting as cloud dissipators rather than cloud generators. If a very high cloud base and relatively high winds occur simultaneously, it is likely that convective clouds will drift away some distance from the mountains, producing precipitation far away from the mountains. Thus, somehow, a minimum amount of precipitation is received along a ring of about 15 mi. in diameter circling the mountains.

3. Influence of Airflow and Moisture

It is the common belief in northern Arizona that rainfall occurs when moist air, mostly from the southeast, blows against the plateaus and mountains. To obtain a quantitative relationship between the precipitation, the airflow, and the humidity, the winds aloft and relative humidities measured at Flagstaff are presented in Figs. 7 and 8, respectively. At the upper part of each figure is the variation of mean daily precipitation obtained by adding total daily amounts from all network stations and then dividing the total by the number of stations. The mean daily precipitation, therefore, gives approximately the mean precipitation which fell each day over the network area.

An overall inspection of these figures does not lead to a conclusion as to a cause and effect relationship. Therefore, the daily means of wind speed and relative humidity between the surface and the 10,000 ft. level were computed from upper-air data taken early each morning before the onset of daily orographic convection. These values are entered in Figs. 7 and 8 below the line representing the station elevation.

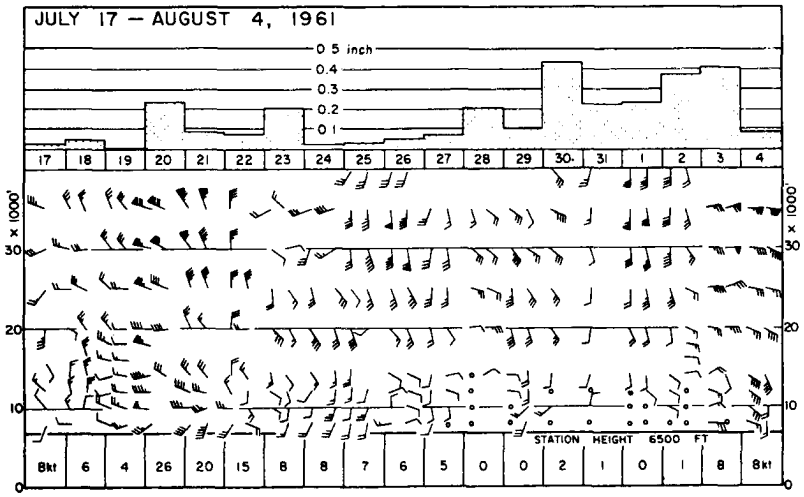

Fig. 7 Daily mean precipitation averaged over the network area compared with the winds aloft measured at the Flagstaff Airport by AFCRL. Winds were plotted in conventional symbols after doubling the wind speed; thus, one long barb = 5 kt and one flag = 25 kt. The daily wind speed entered below the station height line represents the mean wind below 10,000 ft. measured early in the morning.

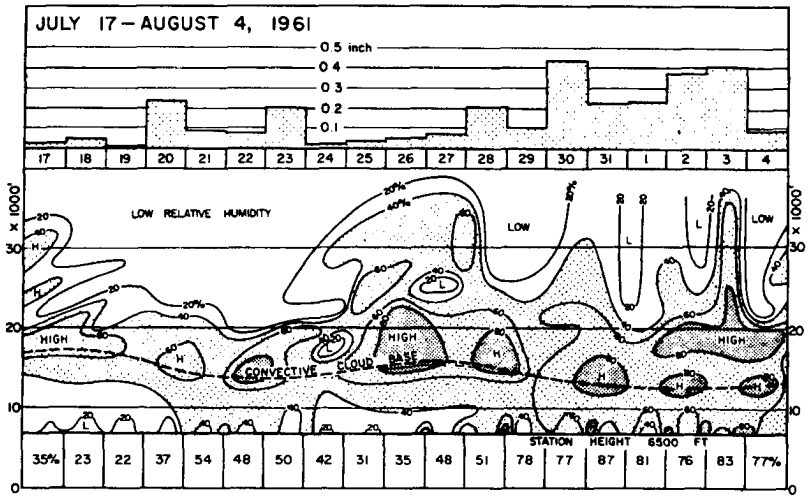

Fig. 8 Daily mean precipitation (upper) compared with the vertical distribution of relative humidity (lower) measured at the Flagstaff Airport by AFCRL. The relative humidity, measured by the GMD-1, was contoured for every 20%. Note that its diurnal variation extended to about 10,000 ft. Entered below the station elevation line (MSL) is the mean R.H. below 10,000 ft. measured early in the morning.

The standard presentation of 3-parameter correlation shown in Fig. 9 requires more observed values in order to find a conclusive relationship. Nonetheless, the scatter diagram of rainfall amounts vs. relative humidity permits us to draw a crude but reasonable straight line, indicating that there would be little rain when the mean relative humidity is less than 10 to 15%. In case the humidity exceeds 80% it is likely there will be more than 0.2 inches of rain no matter how weak the wind speed. Due to the fact that there were no cases of high wind speed when the humidity was 60% or more, it is not feasible to extrapolate the precipitation which would occur under high-wind and high-humidity conditions. For low-humidity cases, however, the precipitation tends to increase with increasing wind speed.

The most reasonable empirical formula for estimating mean precipitation, R, from V, the wind speed, and H, the relative humidity would be

$$R = 1/3\,(H-0.1)\,(1 + 0.01V)$$

and $R = 0$ when $H < 0.1$

where R is expressed in inches and V in knots. The line of a specific value of R in this formula is a rectangular hyperbola with V and H axes translated to V = -100 kt and H = 0.1, respectively.

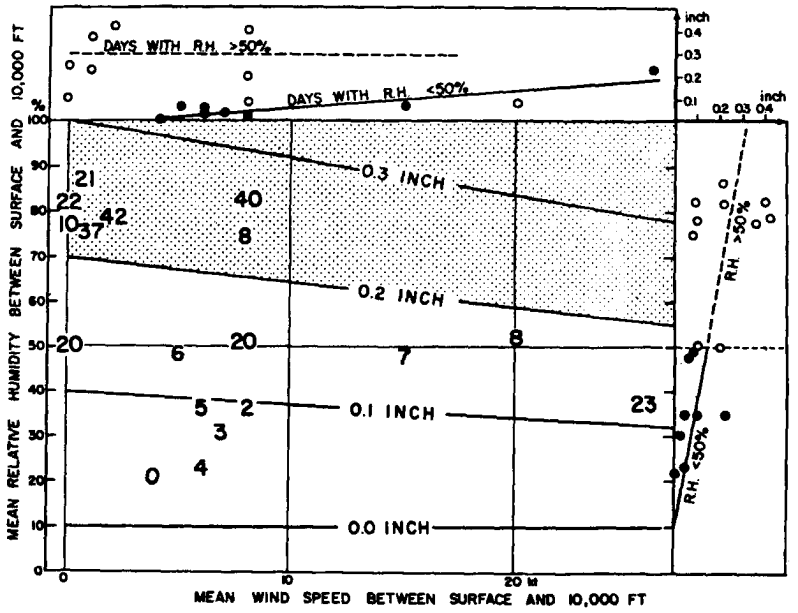

Fig. 9 Daily mean precipitation in 0.01-inch units plotted on relative humidity vs. wind speed coordinates. General trends of mean precipitation are contoured at 0.1-inch intervals from the empirical formula in the text. Solid and open circles in the R.H. vs. rainfall (right) and the wind speed vs. rainfall (upper) diagram represent the values with R.H. below and above 50%, respectively.

4. Split of a Thunderstorm in the Wake Flow of the San Francisco Mountains

Due to the barrier and heating effects of the isolated peaks, one would expect some unusual characteristics of thunderstorms in the wake region of the mountains. To monitor such thunderstorms, a time-lapse 16-mm camera was placed on the rim of Meteor Crater pointing toward the San Francisco Mountains, about 40 mi. away. Inspection of a large number of the movies thus obtained during 1961 operations revealed the fact that a precipitation area observed beneath a cumulonimbus cloud travelling downwind generally split into two separate precipitation areas.

A series of pictures enlarged from the film taken on July 19, 1961, is shown in Fig. 10. Although the exposures were made for every 15 sec, frames presented in the figure were selected at about 15-min. intervals. The first cumulus over the mountain appeared at 0845 MST. After repeating the processes as described by Glass and Carson (1963), a towering cumulus stage was reached around 1000 MST. A few minutes later, both anvil and virga extended from the cloud.

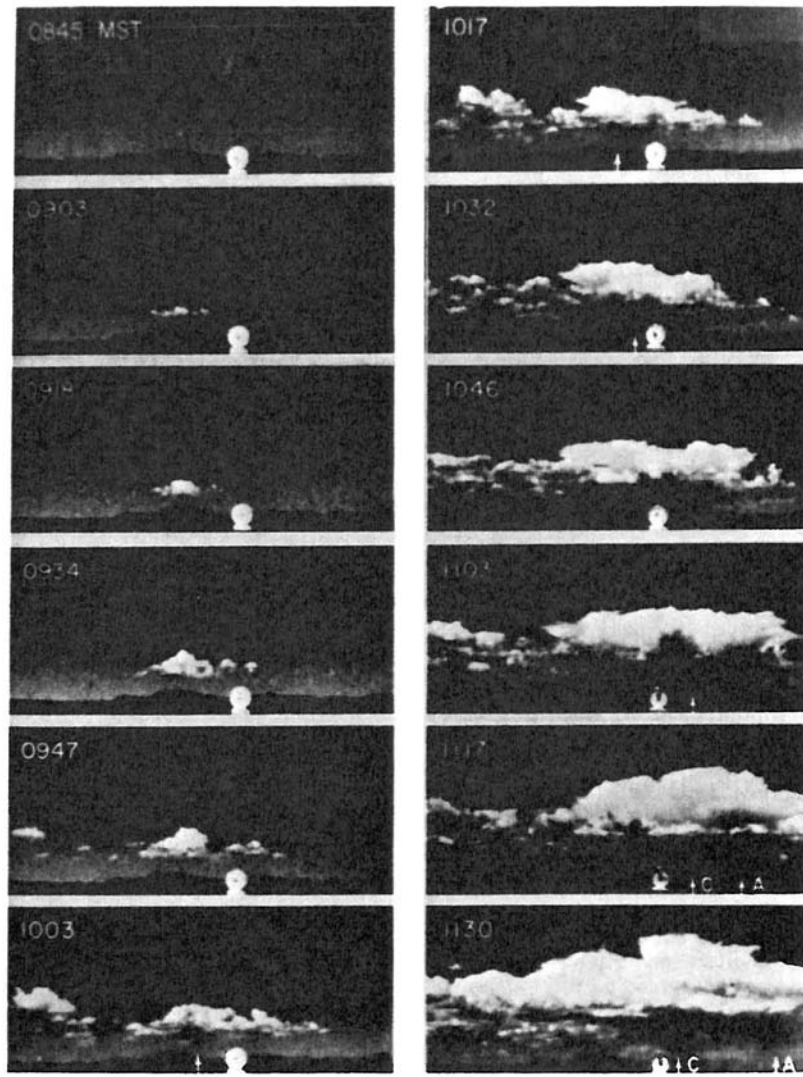

Fig. 10 Growth of orographic cumuli over the San Francisco Mountains on July 19, 1961. Note that a shower started at 1003 MST and gradually moved from left to right until 1103 MST when it split into A and C. Thereafter, C moved very slowly toward the left while A moved toward the right very fast. Such a motion of showers after the cloud split was computed by Fujita and Grandoso (1966) using their model of echo split.

Shortly after 1030 MST the rain area in the movie widened rapidly until it split into two parts. Then the one on the left moved almost toward the camera. A close inspection showed that the left part moved back slightly toward the direction of the peaks when viewed from the movie camera. The right part, on the other hand, moved to the right, very quickly moving out of sight shortly after 1130 MST.

A MRI SX6 radar with 3.2 cm wave length constructed and operated by Meteorological Research Incorporated, Altadena, California, was not turned on until 1127 MST, because the thunderstorm in question was previously hidden behind Elden Mountain when viewed from Flagstaff Airport, the site of the radar.

When the radar picture taken at 1130 MST and an enlarged cloud picture from Meteor Crater are combined precisely as shown in Fig. 11, it is found that the shape of the echoes from the split rain showers displayed rotational characteristics. This was especially true for the one on the right, viewed from the movie camera, which showed an anticyclonic rotation lasting for over 30 min after the radar was turned on. The other showed a slight cyclonic curvature. The estimated paths of the echo before and after the split revealed a remarkable resemblance with the echo-split phenomenon studies by Fujita and Grandoso (1966). They obtained a numerical model which included a pair of thunderstorms which rotated in opposite directions. If their concept of split-echo phenomenon is applied to this observational evidence, it may be concluded that an area of wake flow behind the San Francisco Mountains extends more than 30 mi. downwind.

A schematic-plan view of an estimated wake flow is shown in Fig. 12. Note that a zone of anticyclonic vorticity along the northern boundary of the wake and its counterpart zone of cyclonic vorticity along the southern boundary are produced as a result of the barrier effect. When a developing thunderstorm moves over this area sucking up the air from the wake region, the left-hand portion (facing the direction of motion) and the right-hand part will quickly accumulate negative and positive vorticities, respectively. Thus, the storm rapidly splits into one with cyclonic, and the other with anticyclonic rotation.

A Flagstaff sounding taken at 1235 MST, July 19, 1961, is shown in Fig. 12. It is seen that the layers up to 21,000 ft, slightly above the cloud base, were practically adiabatic with the moisture decreasing slightly with increasing height. This layer is topped by a thick layer of dry air moving from west to northwest at 12 to 15 kt. The temperature curve for the morning sounding, released at 0840, showed little difference from that of the noon sounding. Therefore, the flow probably remained unchanged during the morning hours, acting in favor of the establishment of a steady-state flow.

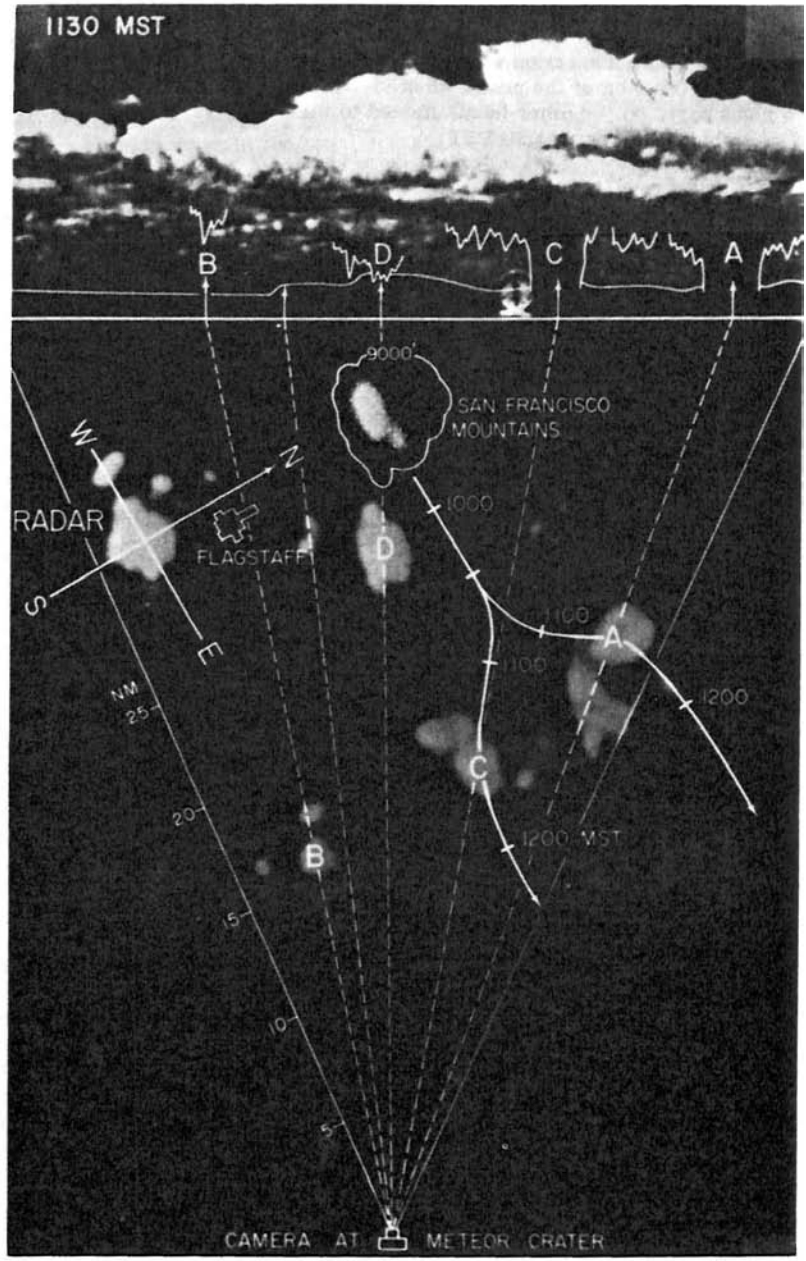

Fig. 11 A composite presentation of radar echoes and a cloud photograph taken from the rim of Meteor Crater, near Winslow, Arizona. The showers A and C in the cloud picture correspond to echoes A and C which were rotating in opposite directions. An anticyclonic rotation of echo A was very apparent for at least 30 min.

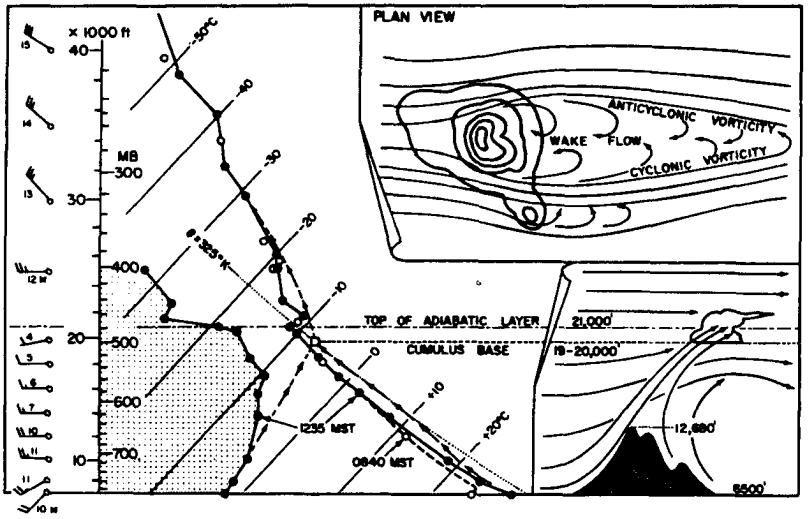

Fig. 12 Vertical distribution of wind, temperature, and dewpoint over Flagstaff measured by a GMD-1 sounding released at 1235 MST, July 19, 1961. 0840 MST temperatures are also entered for comparison. Short arrows in the adiabatic chart represent the schematic change in both T and T_d of an air parcel rising diabatically along the slope of the San Francisco Mountains.

5. Summary and Conclusions

The importance of the height of the convective cloud base in relation to that of the orography blocking the flow has been discussed, based on several examples. In interpreting satellite photographs it is always necessary to keep such regimes of convection in mind because the locations of clouds relative to the mountains vary according to the height of the cloud base.

The orographic precipitation around the San Francisco Mountains was studied in detail, and a related ring of light precipitation surrounding the mountains was found to exist during both the 1960 and 1961 operations. In order to explain such a distribution, the group of mountains is assumed to act as a cloud generator in daytime and as a cloud dissipator at night. Finally, the wake effect of the mountains, which gives rise to the echo split phenomenon as proposed by Fujita and Grandoso (1966), was discussed. A large number of satellite pictures over Arizona taken in July and August were examined in an attempt to find patterns of clouds associated with the wake flow behind mountains. However, no conclusive evidence of wake flow was found. The regions of wake flow in satellite pictures as described by Hubert and Lehr (1967) are considerably more extensive than the island which blocks the flow. These islands usually extend above the top of a shallow stable layer, but the mountains in Arizona block only the lower portion of an adiabatic layer over 10,000 ft. thick. When the nature of such wake flows is clarified in general, it will become feasible to use satellite pictures for the establishment of both barrier and heating effects of topography upon the mesoscale orographic convection.

REFERENCES

Braham, R. R., 1958: Cumulus cloud precipitation as revealed by radar--Arizona, 1955, J. Meteor., 15, 75-83.

Braham, R. R., and M. Draginis, 1960: Roots of orographic cumuli, J. Meteor., 17, 214-226.

Elliot, R. D., and R. W. Shaffer, 1962: The development of quantitative relationships between orographic precipitation and air-mass parameters for use in forecasting and cloud seeding evaluation. J. Appl. Meteor., 1, 218-228.

Fujita, T., K. A. Styber, and R. A. Brown, 1962: On the mesometeorological field studies near Flagstaff, Arizona, J. Appl. Meteor., 1, 26-42.

Fujita, T., and H. Grandoso, 1966: Split of a thunderstorm into anticyclonic and cyclonic storms as determined from numerical model experiments, SMRP Res. Paper No. 62, 43 pp. (Available from SMRP)

Fujita, T., T. Izawa, K. Watanabe, and I. Imai, 1967: A model of typhoons accompanied by inner and outer rainbands, J. Appl. Meteor., 6, 3-19.

Glass, M., and T. N. Carlson, 1963: The growth characteristics of small cumulus clouds, J. Atmos. Sci., 20, 397-406.

Hubert, L. F., and P. E. Lehr, 1967: Weather Satellites, Blaisdell Publishing Company, Waltham, Mass., 120 pp.

Silverman, B. A., 1960: The effect of a mountain on convection, Cumulus Dynamics, Pergamon Press, New York, 4-27.

ANALYSIS OF ISLAND EFFECTS FROM ATS DATA

L. F. Hubert

NESE - ESSA Washington, D. C.

ABSTRACT

Pictures taken at 23-minute intervals from an earth-synchronous satellite (ATS-1) over the central Pacific are examined to evaluate the cloud-producing efficiency of tropical islands. Can the numerous small islands induce deep convection as significant as, for example, the New Guinea-Borneo-Sumatra group?

Some island effects are easily seen by time-lapse presentation* but it appears that direct small-island effects are insignificant as a mechanism in producing moisture and heat flux to the high troposphere.

---

* Author's Note: Cloud motions and cirrus development are easily seen when viewed repetitively on a closed-loop time-lapse movie. Figures 2 and 3 are individual pictures from that sequence which are reproduced here to illustrate the general character of the region under discussion. The figures are, however, completely inadequate to illustrate the points made in this paper; the movie must be seen to appreciate the ATS-1 data.

ANALYSIS OF ISLAND EFFECTS FROM ATS DATA

L. F. Hubert

NESC - ESSA Washington, D. C.

1. Introduction

The primary purpose of this presentation is to display some ATS-1 data in order to illustrate the potential of the earth-synchronous meteorological satellite. A secondary purpose is to examine, in a very preliminary manner, effects of mountainous islands in the tropical South Pacific for their influence, if any, on convection, hence their influence on the flux of heat and moisture to the high troposphere.

ATS-1 has been transmitting pictures from the central Pacific, taken by the Suomi spin-scan camera, since the second week of December, 1966. Pictures taken at 23-minute intervals can be viewed in a sequence as time-lapse movies to reveal short-time cloud changes and motions. Movies produced by Dr. Fujita at the University of Chicago will be shown and comprise the main part of this presentation. The area that will be discussed here is bounded by about 5^{o}N and 20^{o}S, 120^{o}W and 170^{o}E, an area that encompasses part of the arid zone of the eastern Pacific.

Before examining the satellite data, let me review the general considerations that have suggested the question about island effects in this particular region. The basic mechanism under consideration is the flux of heat energy from low to high levels in the tropics.

In the simplest terms, the Hadley cells of the northern and southern hemispheres produce converging (trade winds) flow and ascent at their juncture in the equatorial trough. The heat energy carried to the high atmosphere is then transported poleward by the return branches of the Hadley cells. In the eastern half of the Pacific, the ITC and the maximum rainfall lie about 5^{o}N to 15^{o}N, indicating that the Hadley cells of both hemispheres are displaced northward. A very arid zone immediately south, but not north, of the ITC indicates significant differences between the cells, particularly in the amount of heat and moisture that is transferred from low to upper levels. Satellite data show that the dry zone, from about 5^{o}N to 15^{o} to 20^{o}S, is a region where synoptic systems and extra-disturbance convection are suppressed. There is thus a vast tropical area in which the vertical heat flux is very small compared to its counterpart in the northern hemisphere. In such a region, any mechanism that stimulates deep convection might relatively be important. For that reason, island effects might be relatively of greater importance than elsewhere.

Riehl and Malkus (1958) pointed out that undisturbed trade convection cannot produce the observed vertical profile of enthalpy (internal plus heat energy), and that the transfer of enthalpy from the low to the upper tropical atmosphere must occur in "hot towers" of convection. While the ITC must account for a large part of "hot tower" production, wave-like disturbances extending poleward from the equatorial trough must also make a significant contribution. Some such disturbances may produce deep convection on the southern boundary of the dry zone.

The possibility that islands might be important was suggested by the work of Saha (1966) who used TIROS infrared data to study the nighttime cloud cover in the equatorial southeast Asia region. He found that islands stimulated nearly a continuous source of convection when the general area was not under the influence of synoptic disturbances.

The suggested question is, "Do islands stimulate deep, extra-disturbance, convection that might contribute a significant percentage of the total heat flux to high levels in the tropical dry zone?"

In particular the island areas of Marquesas, Tahiti, Samoa and Fijis are considered here, Fig. 1. There are hundreds of other islands in this region but these four all have mountains above 3,000 ft. The effect on deep convection, if any, should be relatively easy to detect on satellite pictures and can indicate whether or not this preliminary inspection should be expanded.

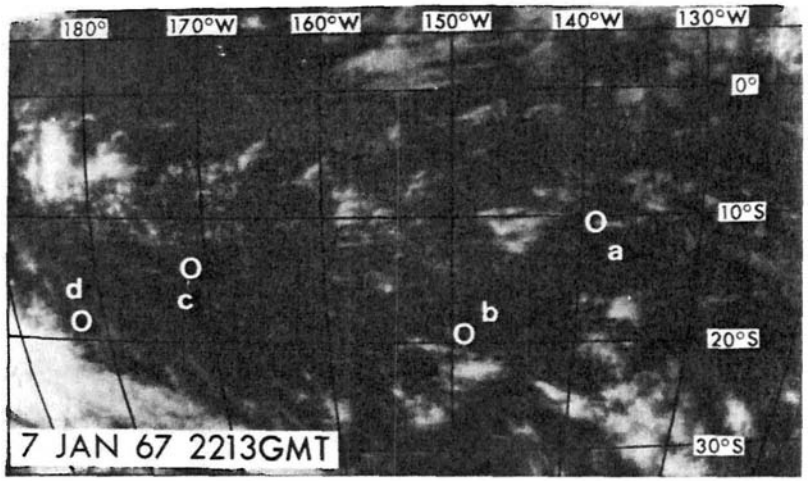

Fig. 1 A portion of the Pacific arid zone photographed from 37,000 km height by the earth-synchronous satellite ATS-1. Mountainous islands circled are: (a) Fatu Hiva, Marquesas Is. (b) Tahiti, Society Is. (c) Savai, Samoa Is. and (d) Suva, Fiji Is.

2. Interpretation of Satellite Pictures

Convection important to heat and moisture flux produces copious cirrus that can be recognized by experienced analysts. When the high level winds are much different from the lower winds (which they frequently are) cirrus anvils are sheared in one direction, the up-shear and cross-shear propagation of cirrus is quite small relative to the down-shear direction. Satellite image of a CB and its anvil is, therefore, an elongated streak, sharp on one edge and feathered off on the other. There is some justification, therefore, in judging the amount of significant convection by studying the cirrus canopy areas.

Deep convection that produces cirrus which is then carried down-stream is easily seen on time-lapse presentations, but is frequently difficult to interpret from a single snap-shot. Furthermore, some deep convection may exist for long periods while other cumulonimbus may produce hot towers for a short period during maximum heating of the island so a single photograph may be inadequate. This is illustrated by the afternoon development over Fiji and the all-day cirrus plume from Fatu Hiva of the Marquesas Island group.

The time-lapse movie of the cirrus development from the Fiji Island area covers the time span of Figure 2, from about 1300 to 1600 local time. Careful comparison of the cloud forms on the three pictures of Fig. 2 shows there is a development; but if one had, for example, only the middle picture, the interpretation might be ambiguous.

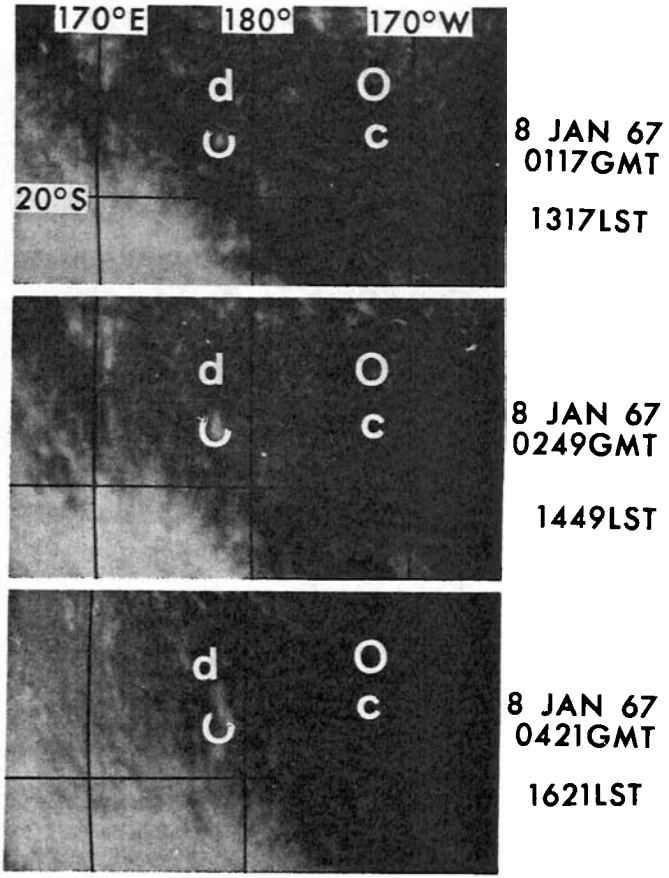

Fig. 2 Area of (c) Samoa and (d) Fiji Islands for three times illustrating cirrus plume development at the Fiji Island, but none at Samoa.

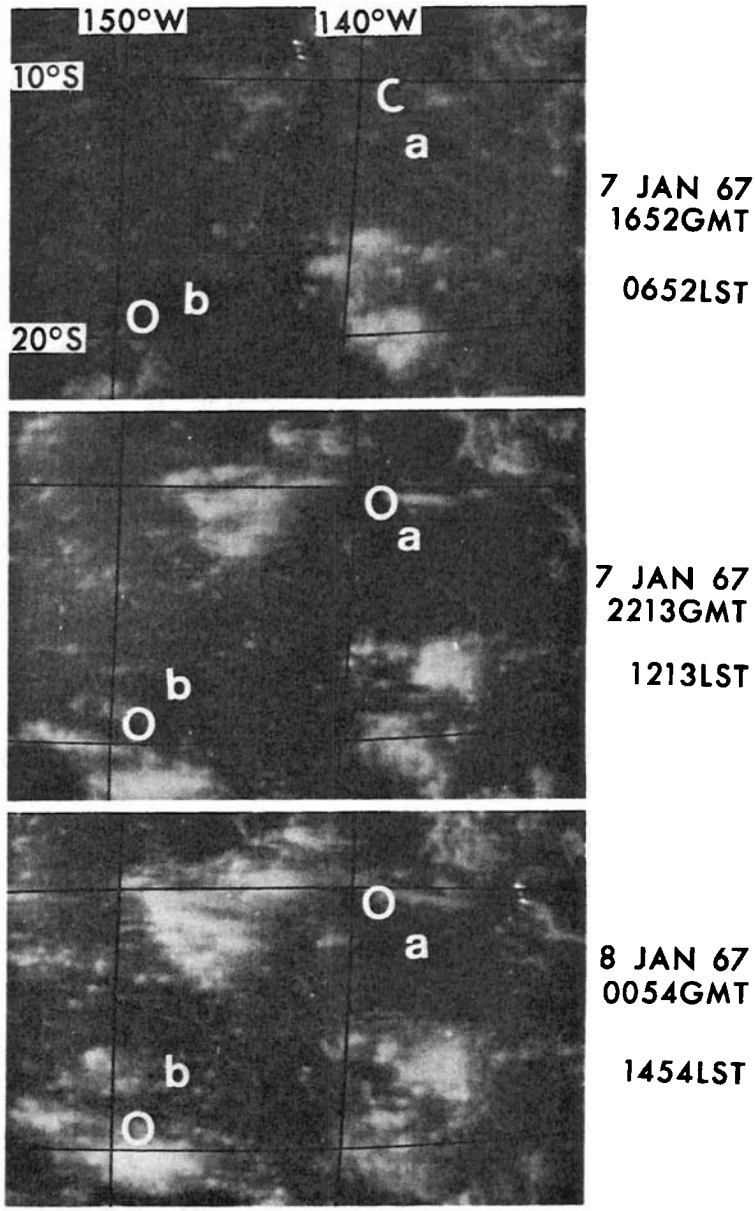

Fig. 3 Area of (a) Fatu Hiva and (b) Tahiti Islands for three times illustrating cirrus plume from Fatu Hiva, (but none from Tahiti) and changes of convection development in the non-island cloud areas.

The three-picture sequence of Figure 3 shows the cirrus plume downshear from Fatu Hiva, illustrating an anvil that was visible almost throughout the daylight hours. The time interval in the Marquesas sequence

extends from about 0700 to 1600 LST, and the movie will show that a line of cumuli existed shortly after dawn. The island group that includes Tahiti and Samoa (Fig. 1) does not show any such cirrus development.

On the other hand, there are several larger conglomerates of bright clouds that quite surely contain deep convection. The most prominent of these does not seem to be associated with islands. For example, there is the triangular shaped area at about 10°S, 145°W, the very bright patch at about 18°S 135°W and the larger area 5°S at the dateline. We will examine these particular conglomerates on the movie. It appears that there are one or two orders of magnitude more cirrus production (therefore, hot towers) for all the hours by the small scale systems unconnected with islands then there are from the islands. It is also of interest to notice the strong changes that take place in the brightness of the non-island cloud areas during the daylight period. This implies a change in the amount in middle and high clouds, therefore, in the total cloud (hot tower) production during the day; a diurnal cycle?

Dr. Fujita has computed the cloud motions from this movie sequence and these have been analyzed as streamlines and isotachs on Fig. 4. The cumuliform cloud motions are shown by shafts and arrowheads; and several ship observations in the area are shown with the standard feathered arrows. The analyses are drawn for the cloud motions, not the surface reports.

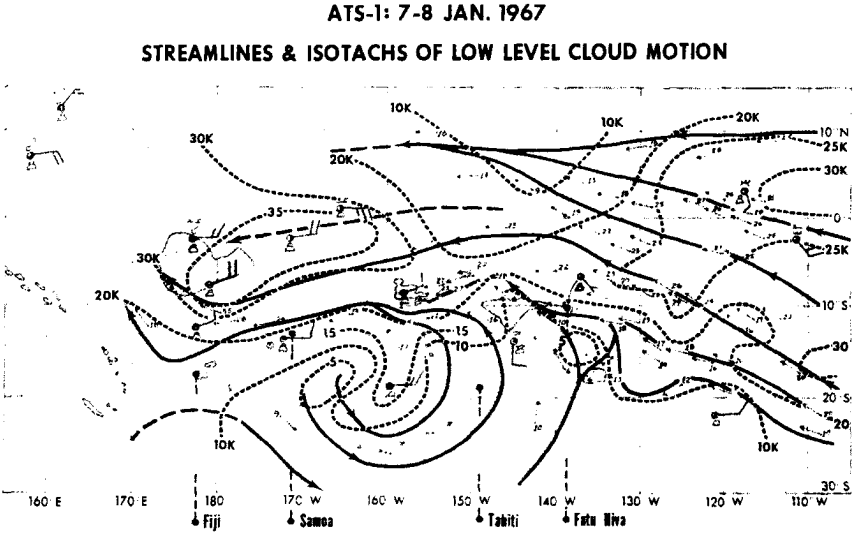

Fig. 4 Analysis of low-level cloud motion derived by Fujita (Univ. of Chicago) in area of Fig. 1.

There are some broad trough-ridge patterns, but no synoptic systems of any great amplitude. If the cloud displacement data are a good representation of the flow field in the moist layers, there appears to be only minor perturbation in the wind field associated with the small synoptic scale disturbances. With the ordinary ship data, it is unlikely that these would be analyzed as synoptic disturbances at all. Nevertheless, one can see some cloudiness in those areas.

The significant point, however, is that,poorly defined as these synoptic scale systems are, they still are much more important producers of convection than the four islands combined.

I have surveyed the ATS pictures for each day of January, 1967, (with the exception of 15, January) to see if the effects suggested by 7 January sequence were typical. The preliminary result is in the affirmative.

Many pictures showed the islands beneath bright cloud areas that extend upward in size from a degree (latitude) square. Judging from their distribution and movement, these appeared to be the small suppressed synoptic system similar to those of 7 January (movie and Fig. 1). An interesting tendency appeared in this cursory inspection. The islands seemed more likely to produce cirrus plumes if a synoptic system, however weak, were in the neighborhood. This suggests that the stabilizing effects of the large-scale circulation of the dry zone is sufficient to limit severely most deep convection. The combined effects of weak atmospheric disturbances and islands can, however, produce deep convection. This implies that islands only intensify the synoptic scale systems, but are inefficient deep convection producers by themselves.

3. Conclusions

The foremost conclusion (based especially on the time-lapse movie presented) is that data from earth-synchronous satellites are the greatest advance in meteorological satellite data since the launch of TIROS I. For research, the potential is exciting and enormous. It is essential that this new tool be exploited and time-lapse viewing of pictures appears to be a very promising approach*.

Although the examination of island effects was superficial, the analysis of 7-8 January, 1967, indicates that even in the zone of severely suppressed synoptic systems, very small scale disturbances are at least an order of magnitude more significant producers of hot towers. The islands appear to serve as focal points of deep convection when a weak disturbance is in the vicinity, but by themselves they are not significant producers of deep convection.

* NESC is exploring techniques to eliminate the movie-producing step by the electronic storage and replay of pictures on a closed-circuit TV system.

REFERENCES

Riehl, Herbert, and J. S. Malkus, 1958: On the heat balance in the equatorial trough zone, Geophysica, 6, 503-538.

Saha, K. R., 1966: A contribution to the study of convection patterns in the equatorial trough zone using TIROS IV radiation data, Tech. Report 74 - Dept. of Atmospheric Science, Colorado State University, Fort Collins, Colorado, March.

DISCUSSION

Question: W. E. Marlatt, CSU, Ft. Collins, Colorado

The ATS cloud photos show much detail on both the synoptic and mesoscale. What is the minimum resolution of the slides and movie shown here; i. e., what is the smallest cloud diameter identifiable?

Reply: L. F. Hubert:

The smallest individual element that can be seen on the film shown here is estimated to be 2-4 mi. providing that element contrasts well with its background, e. g., a dense white cloud over a "black" ocean. The original data received from the satellite and recorded in both analogue and digital tape, have somewhat better resolution--especially gray-scale (dynamic range).

Question: Dr. Edward J. Zipser, NCAR

1. The small synoptic scale cloud features noted near 10^{o}S are not simply curiosities; they are extremely common throughout the tropical oceans. Our experience during the Line Islands Experiment was that much of the sample, even within the equatorial trough, was produced by systems of this scale.
2. What confidence do you have that the apparent cloud motions are (a) free from the effects of cloud development or propagation and, (b) homogeneous with respect to altitude?

Reply: L. F. Hubert:

1. Amen
1. (a) Some ambiguities exist, but when a large field of clouds is measured, and the clouds are the type which are recognized to be the suppressed trade cumuli, we have considerable confidence that the main displacements are wind motions. The cross stream, and even some up- and down-stream propagation can be detected and some allowance made.
(b) The level(s) [layer] is probably homogeneous when a large field of clouds moves at a uniform speed, with horizontal speeds changing in a "logical" and smooth pattern. Middle and high clouds will probably give us the most trouble. These are much harder to resolve insofar as height is concerned.

Question: D. Fultz, University of Chicago

Noticed apparent wave propagation toward W in cloud patches along equator with cloud elements appearing to move Westward much more slowly. Is this type of motion frequent enough to be established and are there any ideas on the nature of the mechanisms and type of wave?

Reply: L. F. Hubert:

We have not examined for this feature, so cannot reply. We have seen several cases of apparent wave propagation at several different scales and these are subject for further research. One middle or high cloud propagation near the equator, on Fujita's "Hawaii Strip", looks very much like a gravity wave propagation nearly cross-stream, with wavelength the order of 100 to 200 km.

PRELIMINARY EXPERIMENTS ON BAROCLINIC WESTERLY FLOW OVER A NORTH-SOUTH RIDGE

D. Fultz and T. Spence
Hydrodynamics Laboratory
Department of the Geophysical Sciences

1. Introduction

There has been sustained meteorological interest over the last three or four decades in the phenomena associated with the flow of stratified currents over mountains and other barriers. Many theoretical, observational, and experimental advances have been made as a result of motivations ranging from the very striking cloud phenomena associated with orographic waves to the sporting aspects of glider pilotage on the wave updrafts, and to the important associations with the current aeronautical problems of clear air turbulence and its effects on high speed aircraft. All these and others are touched on in the present symposium so that it is unnecessary to expand at length on them.

The recent theoretical work began with Lyra (1943) and was pursued by a number of authors including Queney (1947) and especially Scorer (1949, 1953, 1954) in a series of papers after the War, where he examined the effects of more or less realistic vertical profiles of stratification intensity and horizontal wind. A particularly important series of combined theoretical and experimental investigations was carried out by Long (1953, 1954, 1955) and there have been a number of other related experimental investigations. All the above authors concentrated mainly on the lee wave problem where the wave length scales are sufficiently small to make the effects of the earth's rotation more or less unimportant. At the larger scales of motion that are strongly influenced by the earth's rotation, effects of mountain ranges are very important in influencing the wave states of the general mid-latitude westerlies. These effects were calculated in an equivalent barotropic approximation by Charney and Eliassen (1949) and have been an important element of the extensive development of numerical prediction models for the large-scale circulations since that time.

Over the same time period, the experimental investigation of general circulation problems by means of model thermal convection experiments in rotating cylinders has made rapid progress (Fultz, 1961) and it is an obvious extension to experiment with various barriers placed in the flow. About ten years ago, we attempted at Chicago to produce small-scale lee waves in such experiments because of the very attractive feature that typical convection experiments with rim heating develop spontaneous stratification and, simultaneously, vertical wind profiles comparable to those discussed by Scorer. Though there were some ink band observations in these trials of rather definite lee waves with wave lengths of a couple of mm downstream from narrow radial ridges, the intensities were not strong enough to encourage any extensive work. As will be seen from the discussion of the relevant parameters below, the vertical stability and the wind speed are the important quantities involved. Under the conditions we were working with, when we tried to increase the velocities by increasing the horizontal temperature differences, the vertical stabilities would

increase so as apparently to leave the system no nearer the parameter values for strong wave development.

As a result of these difficulties, we deferred any further work until recently when a difficulty in one of the annulus wave experiments stimulated a re-examination of topographic effects, this time on the large-scale motions. We had been working on an extensive series of experiments in the attempt to produce three-dimensional temperature measurements for a carefully chosen five-wave vacillation case so as to carry out the same type of dynamical analysis as was performed by Riehl and Fultz (1957, 1958) for a steady wave experiment. The analysis of this case is being carried out by Professor H. Riehl and Mr. R. Elsberry. Some preliminary results are mentioned by Fultz (1962). When high quality velocity field photographs of this experiment were finally obtained in 1965, it was discovered that there were slight but systematic irregularities in the cyclic behavior of the wave train that we eventually traced down, at least tentatively, to a very small deviation from flatness of the base. We then proceeded to make some tests with radial barriers to confirm the effect, since generally our experience had been that annulus waves are relatively insensitive to barrier effects when the barrier is of modest height. The results of these tests and related experiments on the small-scale lee waves constitute the present contribution.

2. Experimental Arrangements and Procedure

The cylindrical container used for all the experiments (DP-III-A) is the same as that used for the later experiments in Fultz, et al. (1959). It is a copper cylinder of nominal radius 19.5_2 cm with resistance heating wires wrapped around the outside (Fig. 1). The cold source is a concentric copper cylinder (CSS-15.64-10) of nominal radius 7.8_2 cm that is supplied with thermostated water from a source unit (WS X) that is capable of maintaining the cold source temperature steady to within 0.01°C. This temperature was 11.15°C for most of the runs and, with the exception of the five-wave vacillation case, there was a four-blade fan running at about 60-80 rpm in the cold source cylinder to sweep the boundary layer at the wall and maintain more nearly uniform wall temperatures. The working fluid, which was distilled water with 10^{-3} parts by volume of Triton X-100 solution, occupied the annular region between the two cylinders and had a nominal depth of 7.0 cm for all runs.

The whole cylinder assembly is supported rigidly on a centerless bearing apparatus (RB-I-C) which is rotated by a variable speed drive at the desired rate. Temperature measurements were made by means of copper-constantan thermocouples which were connected through mercury slip rings to an outside amplifier-recorder array.

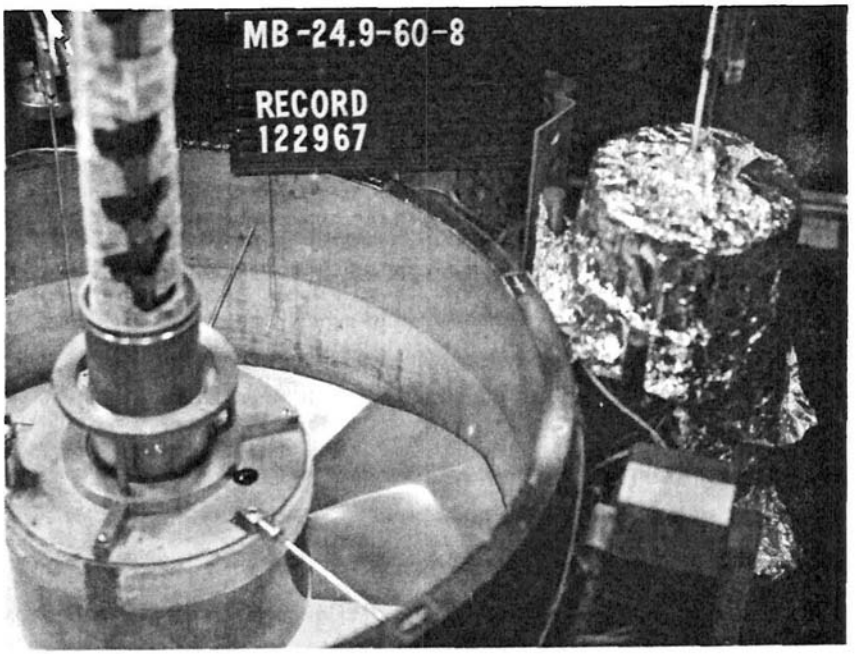

Fig. 1. Oblique photograph of the DP-III assembly with one of the synthane mountain ridges in place. The mountain is 60° in angular width and has a crest height of 24.9 mm. At the lower left is the cold source with supply and return hoses for the water supply extending upward along the axis of rotation. The cold source contains a brass fan assembly rotating about 60-80 rpm to maintain uniform inner wall temperatures. The outer wall is the heat source and is wound with an electrical heater, usually supplied with 80 w. The thermojunctions for temperature measurement were located at the bottom end of vertical hypodermic tubes carried on movable support bars. One of the tubes is seen at the left rear. The dimensions are: $r_o = 19.52_5$ cm, $r_i = 7.82_5$ cm, $r_i/r_o = 0.4008$, $\Delta r/r_o = 0.5992$, $d = 7.0$ cm. The source flux $Q = 32$ cc/sec. These values remained substantially unchanged throughout the experiments to be described.

The barriers used extended across the full width of the annulus and were of the two types shown in Fig. 2. The two examples in the center of Fig. 2 have radial ridge lines of constant height and slope linearly to zero height on radial lines that are 30° of longitude from the ridge line.

The total width is thus 60° of longitude and each side of the barrier is a screw surface of constant pitch. Ridge heights of 3.9, 7.6, and 25 mm were used for these triangular barriers. The remaining obstacles were narrow (6 mm) brass bars with a short triangle and rounded ridge line machined on the top side as seen to left and right in Fig. 2.

The prime difficulty, in principle, with any physical experiment where one hopes to discriminate the meteorological effect of presence, as against absence, of a given feature in the imposed conditions arises from the variety of instabilities and the great irregularity of the Rossby regime circulations that are the most appropriate for comparison with large-scale flows (Fultz, et al., 1959). In such flows, it is usually impracticable to obtain sufficiently dense fields of experimental measurements to resolve unambiguously the difference between mountain and no-mountain experiments or, at least, a very large measurement effort is necessary to obtain statistically significant discrimination. In the annulus geometry, on the other hand, one may have, even in the Rossby regime, a sufficiently predictable wave flow (Hide, 1958; Fultz, et al., 1959) so that even moderate effects may be easy to establish. The experiments were designed, depend-

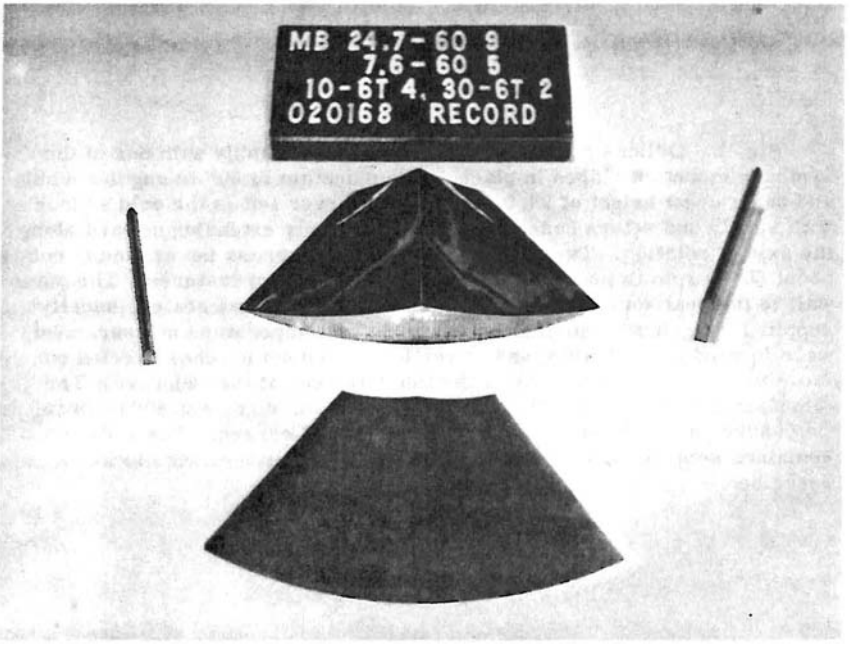

Fig. 2. A selection of the mountain ridge obstacles used in the experiments: The two center ones are 60° in angular width. The upper one of brass has a crest height of 24.7 mm while the lower one of synthane has a crest height of 7.6 mm. The left and right narrow ridges are brass, 6mm wide, and 10 and 30 mm tall, respectively. When placed in the cylinder assembly, they all extend from the outer to the inner wall.

ing on the immediate object, utilizing either symmetrical Hadley flows in the annulus or wave states, to search for evidence of strong and unambiguous effects of the presence of the barrier. Several types were in fact found in both regimes of flow.

The dimensionless parameters characterizing the experimental states can be taken in a number of ways (summaries of some convenient choices are given in Fultz, et al., 1959, and Hide, 1956) and we will confine the discussion to only a few. The thermal Rossby number, in some form, characterizes the thermal wind due to the horizontal temperature differences and will be $\mathcal{O}(0.1)$ for quasi-geostrophic Rossby regime experiments. We will use (see symbol list):

$$R_{oT}^* \equiv g \frac{E_r^* d}{(2\Omega\Delta r) r_o \Omega} \quad \text{and} \tag{1}$$

the gap Rossby number

$$R_{og}^* \equiv g \frac{E_r^* d}{(2\Omega \Delta r)\Delta r \Omega} \tag{2}$$

which is identical with Hide's π_4 aside from a numerical factor 1/2 (Hide, 1956, and Fowlis and Hide, 1965) and, in some respects, is the most appropriate form for annulus discussions. For atmospheric purposes, values of these parameters with the fractional expansion E_r^* taken across some interior radial interval are best, but we will also use a bath value R_{ob}^* defined by R_{oT}^* with a wall-to-wall E_r^*.

The vertical stability will be characterized by

$$S_z^* \equiv g \frac{E_z^* d}{(2\Omega)^2 (\Delta r)^2} \tag{3}$$

and by the internal Froude number

$$F_i^* \equiv U/(g E_z^* d)^{1/2} \tag{4}$$

although, compared with Long's situation (Long, 1955) of a nearly uniform flow in the vertical, the characteristic zonal speed U is a maximum in a profile that varies strongly, though usually nearly linearly, with height.

Heating was applied at the rim in amount, H_r, usually near 80-100 w and also, in a number of experiments, in amount H_b from a buried heater under a copper ring whose inner and outer radii are 11.7 cm and 15.6 cm, respectively. As will be seen, boundary layer effects are important both on the two vertical walls and at the bottom where both direct and indirect interactions with the barriers are undoubtedly present. Measurements indicate that the conventional Ekman layer depth is quite a good index of the depth of the bottom layer of frictional influence. This depth is

$$\pi \delta_v \equiv \pi/\sqrt{\nu/\Omega} \tag{5}$$

and we will use the Ekman number as the corresponding dimensionless parameter

$$E_k^* \equiv \nu/\Omega d^2 = \left(\frac{\delta_v}{d}\right)^2 \qquad (6)$$

A typical example of the temperature structure for a Hadley symmetrical experiment is shown in Fig. 3, which is a meridian-plane temperature profile obtained by thermocouple measurements over a considerable period of time while the state is steady. Five measuring junctions successively occupied the positions shown. Most of the general features of this profile are characteristic also of zonally averaged profiles for the wave states. The gently sloping isotherms in the interior give an internal $\Delta_r T$ of about 1.9_3° between radii of 8.5 and 18.0 cm which is quite small compared to the wall-to-wall ΔT_b of 9.4°. The corresponding Rossby numbers are $R_{oT}^* = 1.14$, $R_{og}^* = 1.91$, and $R_{ob}^* = 3.55$.

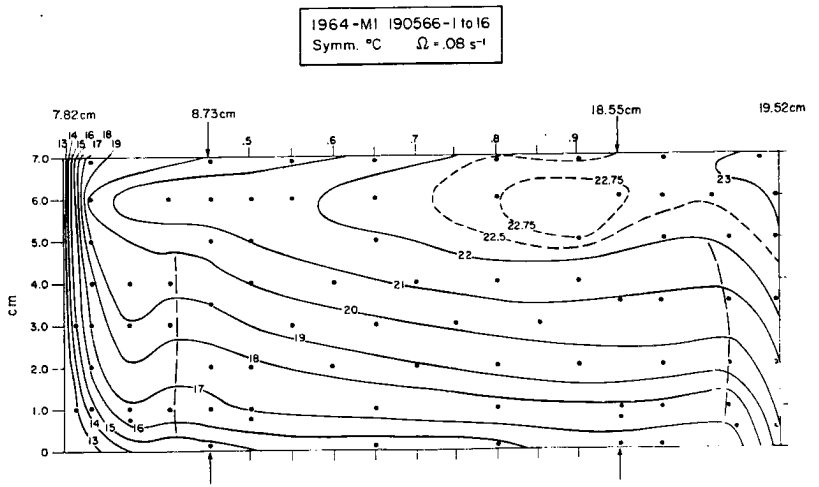

Fig. 3. A temperature cross-section (r, z) for a Hadley symmetric regime experiment (190566 - 1 to 16) without any barrier. The experimental conditions are characterized by the parameters defined in the text: $\Omega = 0.08\ s^{-1}$ counterclockwise, $R_{oT}^* = 1.14$, $R_{og}^* = 1.91$, $R_{ob}^* = 3.55$, $S_z^* = 2.95$, $F_i^* = 0.37$ using top maximum zonal velocity, $U_{max} = 1.2$ cm/sec, $\pi\delta_v = 1.12$ cm, $\overline{T} = 21.3^{\circ}C$, heating at the rim $H_r = 80$ w, $\Delta_r T = 1.9_5^{\circ}C$, $\Delta_z T = 7.7_1^{\circ}C$, heat flux to cold source $H_t = 97$ w.

The vertical stratification is stable except for the top centimeter, where there is an unstable gradient due to a slight evaporation (of the order of 5 watts) that cannot be fully controlled by glass lids above the surface. $\Delta_z T$ from 1/4 cm to 6.0 cm is 6.3_3° and the corresponding $S_z^* = 2.95$. These values give a mean interior isotherm slope of 0.4 in dimensionless units. This thermal field gives a very strong positive thermal wind so that the symmetrical zonal flow at the top reaches a maximum of 1.2 cm/s near $0.425\ r_o$ and about 0.6 cm/s near mid-radius. In $r_o\Omega$ units, these two values are 0.77 and 0.38. The corresponding value of F_i^* using the maximum speed is 0.37.

By far the strongest vertical motions occur in boundary layers on the inner and outer cylinder walls. The structure of these layers is strongly influenced by the stratification in the interior. In Fig. 3, the horizontal scale is increased by a factor of 4 between the arrows and the two walls and inside the space of 1 cm in each case; the thermal boundary layer is seen to exhibit a characteristic minimum at distances of about 7 mm and 3 mm from the respective inner and outer cylinder surfaces. A large fraction of the total temperature difference occurs across the inner cylinder layer. The oscillations of the temperature curves are associated in each case with flattened vortex rings (lying in the outer parts of the two velocity boundary layers). Very similar features also occur in the zonally averaged profiles in the annulus wave cases.

Over the interior region in Fig. 3, the strong, nearly linear, zonal wind profile goes to easterly at a height of about 1.2 cm reaching a maximum at about 0.6 cm. Approaching the bottom, the current backs rapidly as in an Ekman spiral to a northeasterly direction at the bottom. The ink bands in Fig. 4, which were initially vertical, show this clearly with the main radial components entirely in the friction layer, $\pi\delta_v$ being 11.2 mm. These velocity profiles, combined with the increase inward mentioned earlier, constitute the primary flow toward the barriers in the symmetrical experiments. While the barriers have considerable local effects, in the Hadley symmetric flows, the changes elsewhere are not very noticeable and the upstream flows appear very close to the comparison experiments without mountains. In the annulus wave experiments, the Ekman layers are much thinner, the general velocity fields in the interior considerably more variable, and usually very difficult to distinguish by simple direct observation from the comparison flows.

Northeasterly flow begins on the bottom, giving way to easterly and finally westerly at about 1.25 cm above the bottom. The maximum easterly component near 0.6 cm at the bend of the profile is about 0.063 cm/s. The significant radial components are mostly below this level. To the right of the photograph, the ink bands are tilting rapidly in the positive thermal wind shear toward the strong westerlies on the top surface.

As soon as a barrier is inserted in a particular experiment, it becomes a much larger measurement job to determine temperature fields, especially for Rossby regime waves. The field is both transient and variable from one region to another. A full three-dimensional array of sensing elements would be necessary to make an adequate determination of the temperatures. We did not carry out such determinations, but merely determined rough time-averaged profiles from measured traverses on three longitudes. All

were usually well removed from the mountain position. So far as the velocity field is concerned, we were able to determine a number of features with ink bands from dye crystals of malachite green or acid fuchsin as in Fig. 4. These were very effective especially at the very bottom, where plumes of dye from dissolving crystals showed most of the mountain effects in the Ekman layer that are discussed below. Finally, aluminum powder tracer on the top surface was observed directly or photographed through a rotoscope to give quantitative streak determinations of the velocity field there. In the cases of large-scale effects on wave trains, this was the only certain way of establishing that consistent differences existed between waves in the region near the mountain as against those elsewhere or those in experiments without mountains.

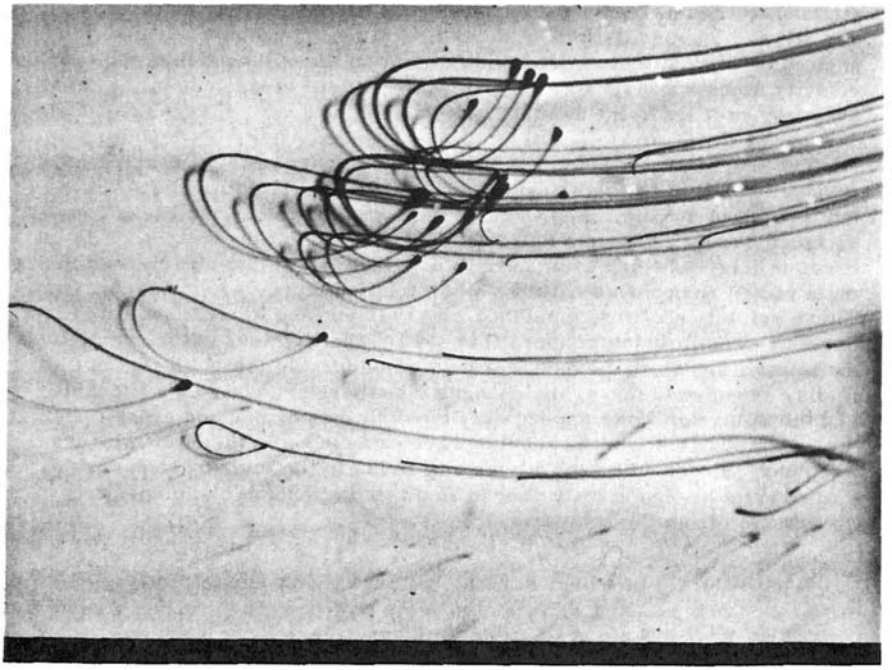

Fig. 4. Oblique ink band photograph (190565), of typical profiles near the lower boundary. Malachite green crystals were sprinkled on the top surface and left colored traces as they fell to the bottom. On dissolving there, the dye clearly shows the characteristic Ekman boundary layer profile associated with the symmetric flow regime. Conditions are substantially the same as in Fig. 3.

3. Experimental Results

The significant observations can conveniently be summarized in three groups: those concerned with large-scale wave effects, those observed in the boundary layer at the bottom mainly in symmetrical flows, and the small-scale waves observed with the narrow barriers also in Hadley flows.

3.1 Effects on Large-Scale Rossby Regime Motions

The experiment that forced us to reexamine some of the base topographic effects was the five-wave vacillation experiment mentioned above. A selection of streak photographs from one vacillation cycle is shown in Fig. 5. At revolution 59 there is a train of open radial wave troughs on a continuous

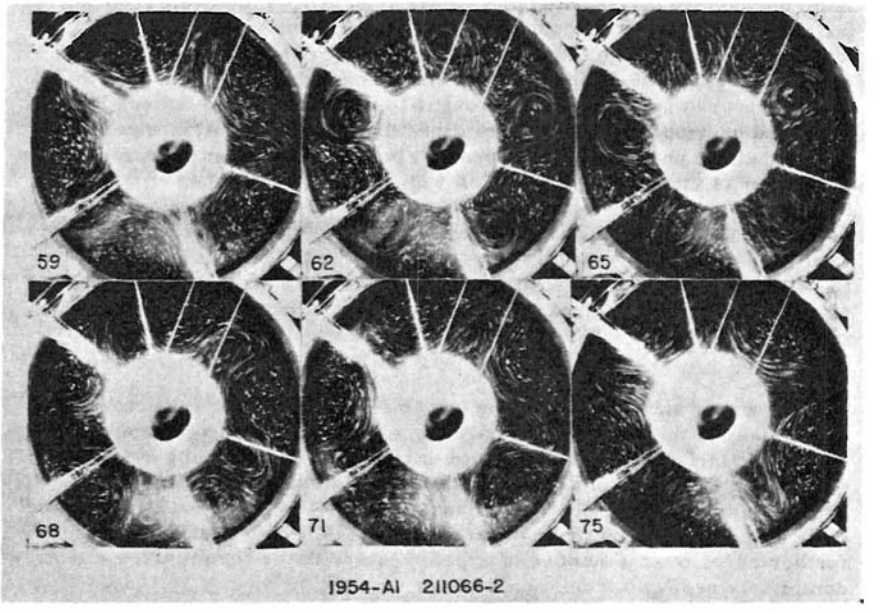

Fig. 5. Rotoscope streak photographs of a vacillating five-wave case (211066-2). Numbers at lower left indicate the rotation count (begun at photo 1). As described in the text, a phase lead occurs, consisting of one or two of the deepening cyclones at that particular stage in the vacillation cycle developing earlier than the others. The stronger vortex circulation in photo 62 near 10 o'clock is notable. The area of preferred development can be located relative to Fig. 6 by means of the support bars RP 1, 2, and 3, which are respectively at 5, 8, and 10 o'clock on the photos. Experimental conditions: $\Omega = 0.50\ s^{-1}$, $R_{oT}^* = 0.026$, $R_{og}^* = 0.044$, $R_{ob}^* = 0.12$, $S_z^* = 0.071$, $F_i^* = 0.24$, $U_{max} = 0.7$ cm/s, $\pi\delta_v = 0.44$ cm, $\overline{T} = 20.8^{\circ}C$, $H_r = 80$ w, heating at the base, $H_b = 15$ w, $\Delta_r T = 2.04^{\circ}C$, $\Delta_z T = 6.64^{\circ}C$, $H_t = 102$ w.

westerly jet at the top surface. The troughs tilt rapidly toward the southeast and cyclones form and deepen in each trough as shown at revolution 62. The cyclones reach maximum intensity, then decrease in intensity and begin to tilt back toward the southwest at revolution 65. The currents then gradually return to open waves until, at revolution 75, the state is almost identical with revolution 59. This fluctuation with a period of about 16 revolutions continues indefinitely as long as the imposed conditions are maintained constant. Many other properties of the waves fluctuate periodically in the cycle essentially as in the case discussed in Fultz et al (1959).

The conditions of this experiment were very carefully chosen so as to give as exact periodicity as possible both in space and time. This is essential for the analysis being carried out by Riehl and Elsberry. We noticed, however, in a large number of photographs taken in repeated experiments in 1965 and 1966 that there was always some slight deviation from periodicity. This was most easily seen around the cycle time corresponding to revolutions 59 and 62 in Fig. 5. One, or sometimes two, of the waves went through the cyclone formation process a little (1/2 to 1 revolution) ahead of the others. On close inspection, we found that this effect appeared successively at troughs to the west of those where it had occurred previously and finally realized that this propagation was at such a rate that the phase lead in deepening always occurred in the same sector of the pan as indicated by the arc in Fig. 6. After a number of trials in the attempt to find the reason for the asymmetry, which eliminated most of the possible thermal or cylinder wall effects that seemed likely, we made careful measurements of the base surface height. It turned out not to be flat as shown by the topographic contours in Fig. 6. The total variation over the annulus area was 0.3 mm or so with an elliptical distortion giving ranges of 0.1 - 0.2 mm at any one radius.

We were, and still are, reluctant to feel certain that such small deviations, of the order of two parts in 700 in the total depth, could cause such a distinct effect, but have been unable to find convincing evidence to the contrary. Thus, one might first suspect disturbance effects of the hypodermics carrying the thermojunctions; but the phase lead was distinct over experiments with many different positions of these junctions and, furthermore, over a number of experiments with the temperature elements completely removed from the fluid.

Our next step was to undertake an experiment designed to exaggerate the effect in order to test the conclusion that the base deformation was responsible. We taped a thin sheet of polyethylene in the shape of a sector of angular width about 52° longitude to the base with a radial wire underneath that was estimated to give a crest height of about 2 mm. In one sense the experiment failed because the effects were so strong that the wave train changed from 5 to 4 waves, and we did not obtain a strong enough vacillation to discriminate any phase lead effects. However, as shown in the streak photographs of Fig. 7, a very remarkable series of local events occurred in the wave train near the mountain at about 5 o'clock. As each wave trough approached the ridge, it sharpened and tilted more toward the southwest (revolution 65). The trailing shear line then developed a closed cyclone on the upwind slope of the ridge (revolution 67). This cyclone persisted as the next ridge in the jet approached and moved slowly east-

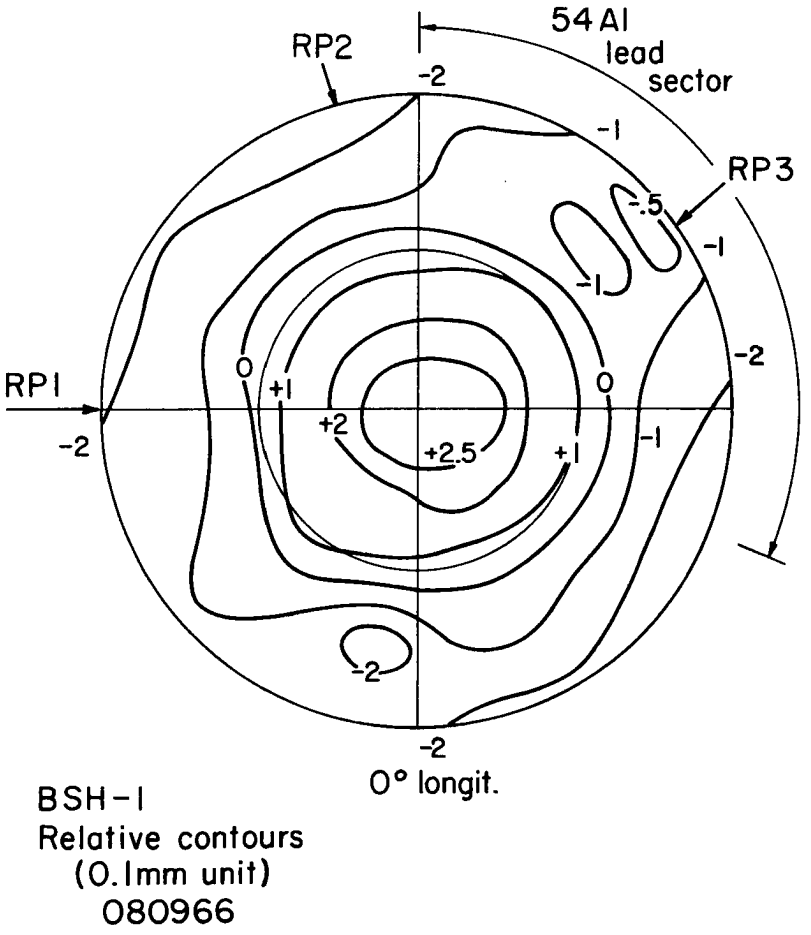

Fig. 6. Analysis of the base contours for the base (B-SH-1) used with the DP-III-A assembly. For comparison with Fig. 5, RP 3 is located near 10 o'clock, or a counterclockwise rotation of 90° for the contour analysis. (The relative maximum near the center is unimportant due to the size of the cold source.) Along zonal circles at intermediate radii, the total variation due to the elliptical deformation of the base is 0.1 - 0.2 mm compared to the total depth of 70 mm.

ward to cross the mountain ridge line (at revolution 73). It then weakened to a trough on the lee slope (revolution 76) and merged with the succeeding trough as the latter deepened to a cyclone downwind of the lee slope. This latter process was also part of a general vacillation of the wave train. The whole process was repeated six times in all essentials as successive troughs passed the ridge at intervals of about 14 revolutions. Such consistency is almost impossible to ascribe to anything but direct effects of the barrier on the wave in its vicinity.

It immediately struck us how many features of the above sequence are reminiscent of the behavior of some 500 mb troughs as they cross the Continental Divide and of the cold lows that so frequently form in the Southwest and near the California coast. One may compare, for example, the 500 mb charts over North America for 19-25 September, 1967, and 12-14 December, 1967, (these charts are not included in Figs. for this paper).

With such clear indications of interesting effects, we proceeded to construct several sizes of barriers of the type shown in Fig. 2 and to investigate a series of wave states. Briefly, the results were at first disappointing even though the barriers were all higher than the estimated 2 mm for the plastic sheet. The experiment in Fig. 7 had some special

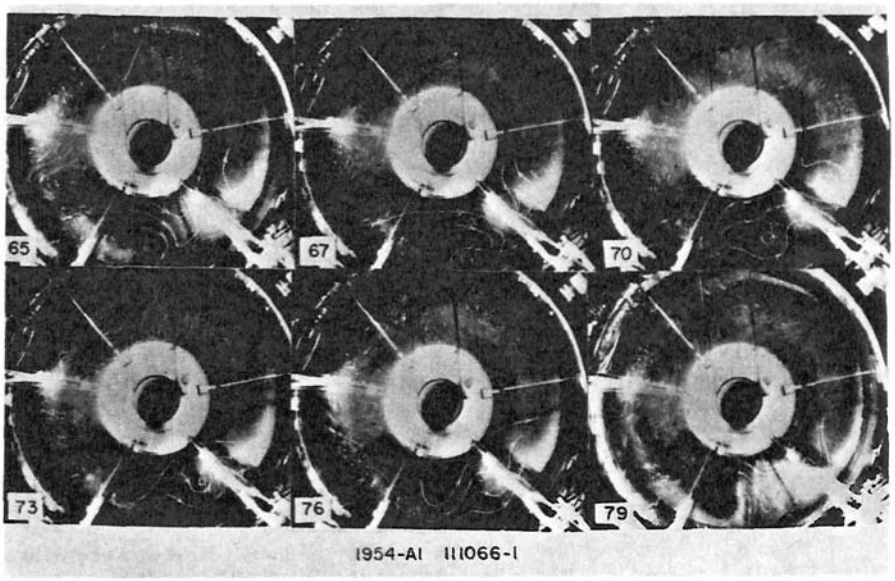

Fig. 7. Streak photographs of a four-wave case (111066-1) with a small plastic mountain, seen at 5 o'clock in the lower right. White lines outline the top surface streamlines since some of the streaks are too faint for reproduction. Experimental conditions are substantially those of Fig. 5, but the presence of the plastic obstacle has interfered with the more usual five-wave vacillation, producing four irregular waves and distinct differences in the wave near the ridge as compared with the other three. Numbers with each frame give the revolution count.

sensitivity that is still not clearly evident and many of the wave experiments showed only mild or almost unnoticeable effects as in our previous experience. Our current estimate is that for very low barriers the state of the fluid system must be sensitive in some way, near a wave transition curve (Fultz, et al., 1959) or vacillating, or near the Hadley symmetry transition curve. If the barrier is larger than some moderate critical value, the effects are very strong, easy to obtain, and reproducible. The examples below illustrate some of the principal types we found. All of those shown are completely reproducible.

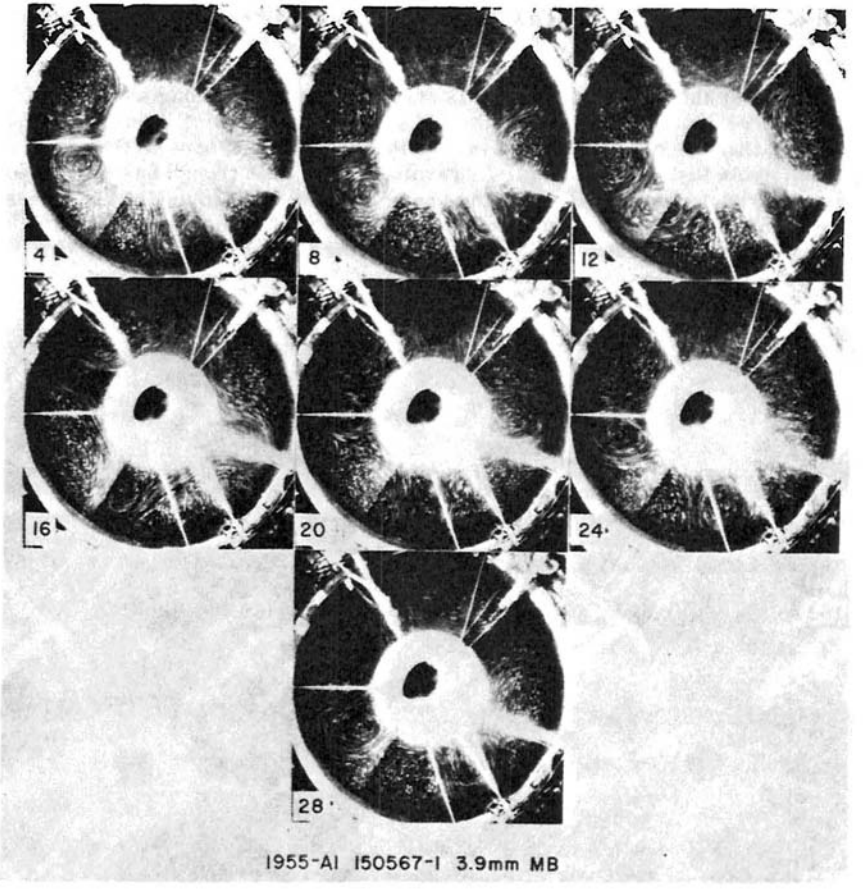

Fig. 8. Streak photographs (150567-1) of a four-wave case with a 3.9 mm obstacle centered near 6 o'clock. Relatively minor, if any, effects of the ridge are detectable in the top-surface flow. Experimental conditions are nearly those for a four-wave experiment with no obstacle: $\Omega = 0.50\ s^{-1}$, $R_{oT}^* = 0.03$, $R_{og}^* = 0.05$, $R_{ob}^* = 0.14$, $S_z^* = 0.06$, $F_i^* = 0.3$, $U_{max} = 0.97$ cm/s, $\pi\delta_v = 0.44$ cm, $\bar{T} = 21^oC$, $H_r = 80$ w, $H_b = 15$ w, $\Delta_r T = 2.5^oC$, $\Delta_z T = 6.7^oC$, $H_t = 106$ w.

Figs. 8 to 15 give data from a selection of these tests proceeding from low to high crest heights of the barriers, the heights being 3.9, 7.6, and 25 mm. Fig. 8, with a 3.9 mm ridge, is an example of a mildly vacillating four-wave experiment where it is very difficult to see any real differences between the wave behavior over the ridge at 6 o'clock and that elsewhere. There is, for example, only a slight impression that the cyclone on the lee slope in the frame for revolution 24 may be larger and more rounded than those in the other waves. There are almost certainly some differences, but very extensive measurements would be necessary to detect them.

In contrast, the photographs in Fig. 9, with a 7.6 mm ridge, show quite distinct dissimilarities between the waves near and away from the barrier that are evident to simple inspection and are consistent over the much longer series of photographs actually taken. At revolution 163, the trough over the ridge at 7 o'clock is sharper and has a strong southwest tilt. At revolution 166, it is on the lee slope, nearly radial, and much weaker than the others which have developed strong cyclones in the vacillation cycle that is occurring. At revolution 169, this trough has developed a strong cyclone downwind, but the shape is different than any of the others show and there is also a small cyclone in the ridge on the upwind slope of the ridge. This cyclone reaches the ridge line by revolution 172 and has

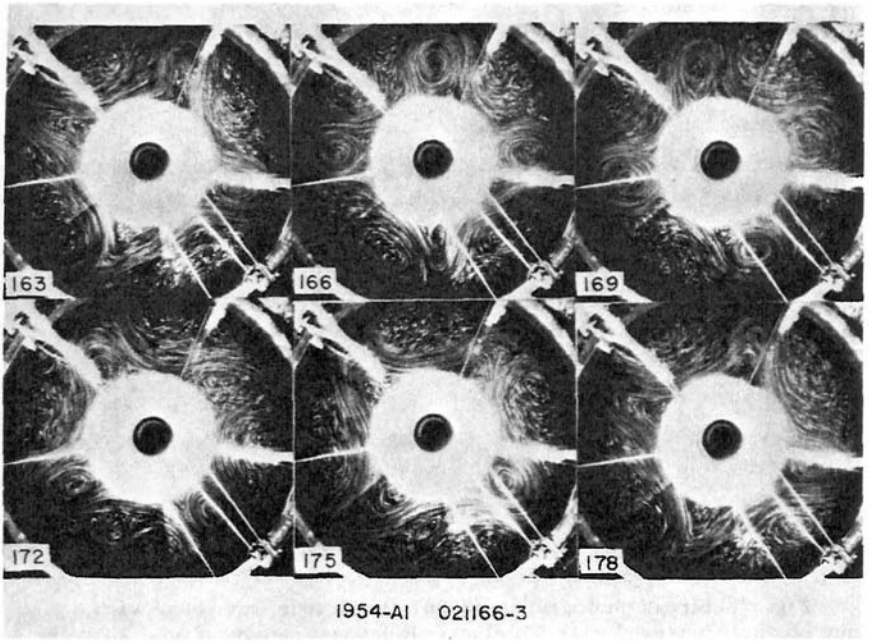

Fig. 9. Streak photographs (021166-3) of a four-wave case with a 7.6 mm obstacle centered near 7 o'clock. Here, in contrast to Fig. 8, definite differential effects are seen as each wave trough passes the ridge sector. Experimental conditions are nearly the same as those in Fig. 8.

decayed to a minor trough by revolution 175. None of the other ridges is so disturbed. This last sequence, though weaker, is the same sort of disturbance of the wave train as in Fig. 7.

Fig. 10, for a three-wave case, shows a time-averaged meridional temperature profile, the solid lines for an experiment with a flat base. Many of the general features are seen to be be very similar to the symmetrical profile of Fig. 3. The principal differences are in the middle of the annulus,where the isotherms are distinctly flattened by the wave convective effects. The dashed lines give the temperature deviation from the first profile of a profile where a 7.6 mm barrier was present. Because the data for the barrier experiment were not averaged over longitude, this deviation could be partly due to variations in longitude, but one can easily envisage overall mean thermal effects of the barrier of the type shown.

Streak photographs in Fig. 11 for the same order of magnitude of R_{oT}* as in Fig. 10, but with the highest 25 mm ridge, show that the barrier effects, though quite distinct are far from spectacular. The barrier is at 6 o'clock. As each upper trough approaches the barrier, it becomes narrower than the other two (revolution 42). It swings southeast on the downwind slope (revolution 44) and then becomes broader than the other two as it passes on eastward (revolution 46). The frames for revolutions 75 and 77 show the consistent repetition of these wave changes as against 42 and 44 respectively.

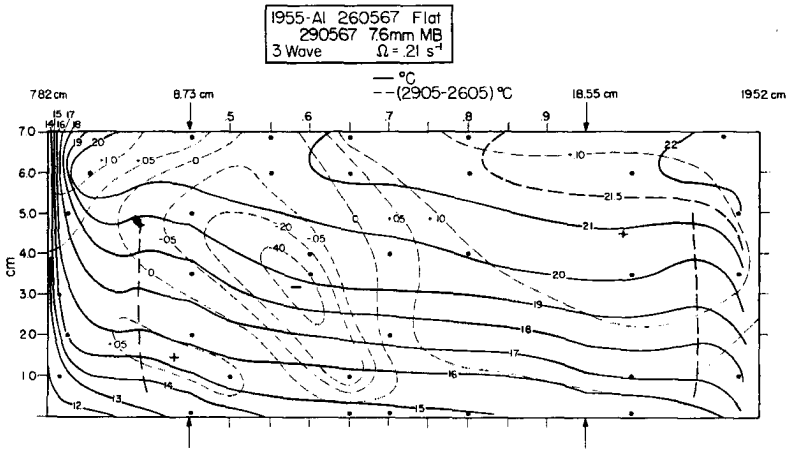

Fig. 10. Temperature cross-section for a three-wave regime. Solid line analysis for flat base (260567); dotted line analysis for the difference when an obstacle of 7.6 mm is inserted (270567). The obstacle was placed in the sector across from the three bars carrying the temperature elements at the three temperature measuring longitudes.

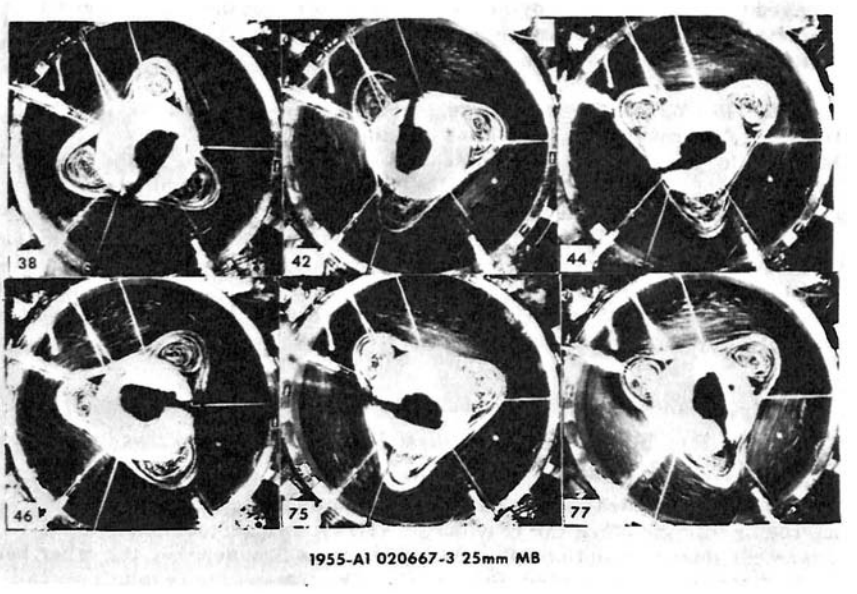

Fig. 11. Streak photographs of a three-wave case with the 24.9 mm obstacle centered near 6 o'clock in the photographs (020667-3). The effects on the upper flow, while definite, are quite slight, in view of the substantial ridge height. Experimental conditions: Ω = 0.19 s^{-1}, R_{oT}* = 0.25, R_{og}* = 0.43, S_z* = 0.52, F_i* = 0.22, estimated U_{max} = 0.7 cm/sec, $\pi\delta_v$ = 0.74 cm, $\overline{T}$ = 18.8°C, H_r = 80 w, $\Delta_r T$ = 3.19°C, $\Delta_z T$ = 7.49, H_t = 95.6w.

The above, very modest responses to the presence of a barrier whose height is as large as 0.36 d, contrast very strongly with the situations shown in Figs. 12 to 15. For this experiment, the Rossby number is much lower and the wave state is more sensitive to vacillation and other normal variations in this region of the annulus spectrum. The conditions are such as to give, for a flat base, the periodic vacillation of Fig. 5. Fig. 12 shows a selection of frames illustrating the complete disruption of the wave train produced by the 25 mm ridge at 6 o'clock. At various times, the wave train has 3 major waves, 4 major waves, 3 major waves at 90° from each other, and occasionally 5 major waves. There are varying degrees of minor wave and cyclone disturbance, these latter being usually in the sector over and downstream from the ridge. At 98 and 102 revolutions in Fig. 12, the main jet runs near the cold source wall over this sector with rows of two

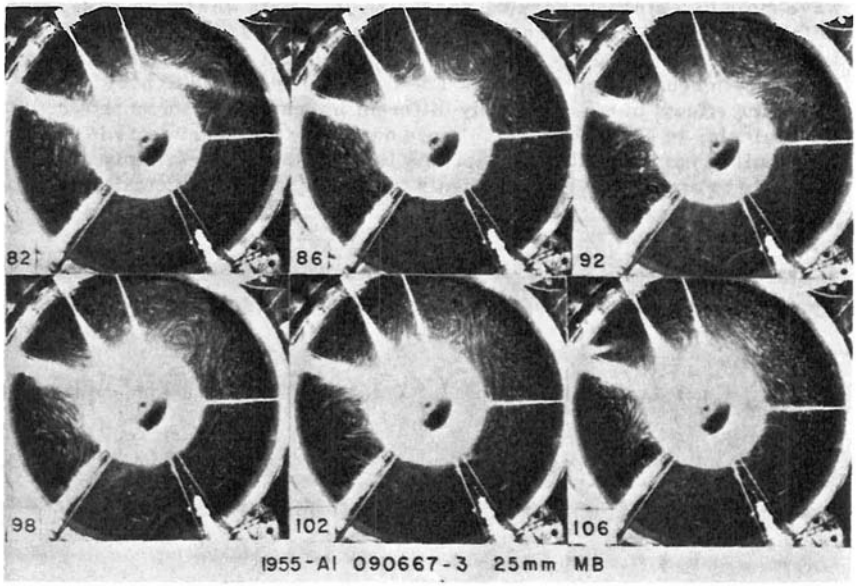

Fig. 12. Streak photographs of the top surface corresponding to the experiment noted in Figs. 14 and 15 (090667-3). Photo 82 corresponds to revolution 1673. The 24.9 mm mountain is barely visible at 6 o'clock in the photographs. The effects on the whole wave system are extreme and even local ones extend far from the ridge. Experimental conditions: $\Omega = 0.5\ s^{-1}$, $H_r = 80$ w, $H_b = 15$ w. Other parameters are probably close to Figs. 5 and 8.

or three cut-off cyclones extending downwind from the ridge. Figs. 13 and 14 illustrate the contrast between temperature observations for the two cases. Figure 13 corresponds to Fig. 5. There is a regular five-wave vacillation over the flat base and the upper three traces show the regular modulation produced by beating between the vacillation period and the wave passage period at each position. The last trace is ΔT_{cs} which is proportional to the heat flux to the cold source and varies periodically with the vacillation cycle. The irregularities in this last trace are mainly due to measurement noise of various sorts.

By contrast, in Fig. 14, which corresponds to Fig. 12 with the 25 mm ridge, the irregularities associated with the wave changes noted above are very pronounced. They are especially so at (r, z) = (13.67, 4.0) which is a point in the middle of the annulus of fluid. While there are definite heat flux variations like those associated with vacillation, they are quite irregular in amplitude and timing on the bottom ΔT_{cs} trace. The effects on the system of inserting the largest barrier are, thus, seen in these figures to be extremely drastic; one changes from a well-defined periodic vacillating

wave state to a strongly varying Rossby regime state where the wave number is far less well-defined than it usually is in annulus geometries and where local disturbances and cyclones near the barrier strongly affect the entire large-scale behavior of the fluid. The impression is hard to avoid that these are effects of a qualitatively different intensity than those shown, for example, in Figs. 9 and 11. While our range of experiments is much too small to establish directly that this is the case, it is certainly quite plausible to proceed on the hypothesis that there is some critical condition

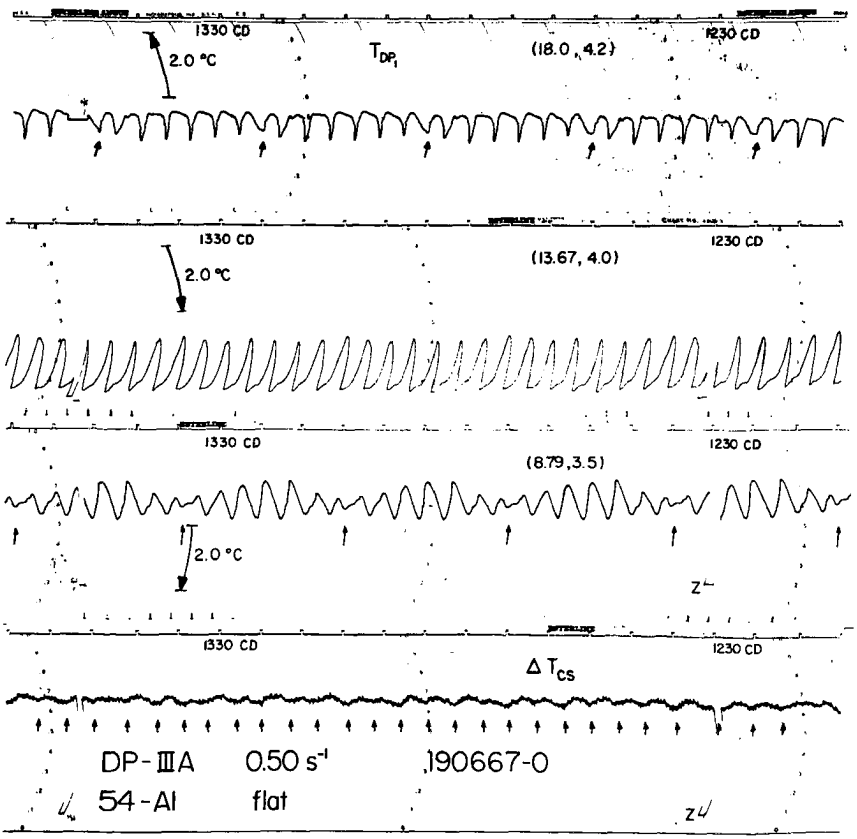

Fig. 13. Four representative temperature traces for the five-wave vacillation of Fig. 5 (190667-0). The top trace is from the permanently mounted thermocouple located at 18.0 cm from axis of rotation and 4.2 cm above the base. (This couple can be seen in Fig. 1, extending vertically down from the data board.) The small arrows indicate the modulation periodicity in this regular vacillation. The second and third traces are from r = 13.67, z = 4.0 and r = 8.79, z = 3.5, respectively. The bottom trace is from a difference junction ΔT_{cs} located inside the cold source itself, showing the periodic variation of the heat flux in the vacillation cycles.

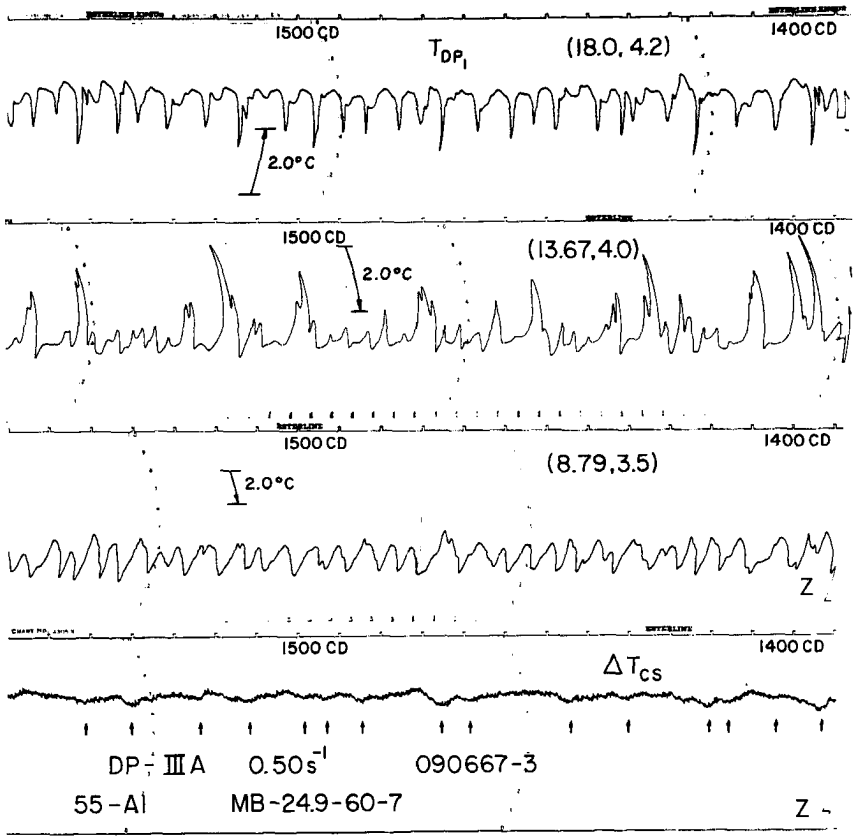

Fig. 14. Temperature traces from the same thermocouple locations as Fig. 13, but with the 24.9 mm obstacle in place (090667-3). The traces are now distinctly aperiodic as a result of the drastic time changes in the wave train (Fig. 12). The heat flux represented by ΔT_{cs} is highly irregular.

or parameter that has been crossed between the conditions of Figs. 5, 8, 9, 11, and 13, and those of Figs. 12, 14, and 15.

Fig. 15 finally shows a sequence of ink band photographs that exhibit, for the conditions of Figs. 12 and 14, the same type of cyclone behavior over the ridge as was seen in Fig. 7. In Fig. 15a, the bands show a cutoff cyclone just forming on the upwind slope of the ridge at the southwest end of a narrow upper trough. This cyclone persists, becomes nearly circular, and gradually drifts eastward until, in Fig. 15d, it is just crossing the ridge line as the next major trough approaches from the west. Thus, while we have not yet been able to repeat Fig. 7 consistently for very low ridges, Fig. 15, which is just one of a number of such sequences in the experiment of Fig. 12, shows that this life history can be a typical one.

Fig. 15. A sequence of near vertical views of the 24.9 mm by 60° synthane obstacle, several revolutions after the introduction of dye crystals (090667-3). A closed circulation is forming west of the mountain crest in Fig. 15a (revolution 589), is shown moving in an ENE direction in 15b (revolution 590), begins to cross the ridge line in 15c (revolution 593), and undergoes a deformation in 15d (revolution 596). The dark area on the eastern side of the obstacle is a shadow. Compare the trough behavior in Fig. 7. Experimental conditions are as in Fig. 12.

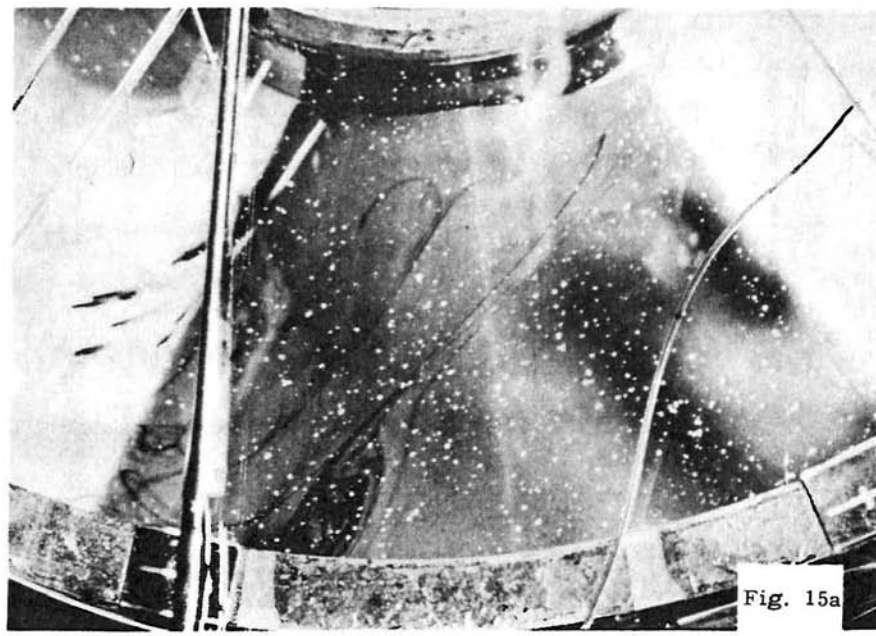

Fig. 15a

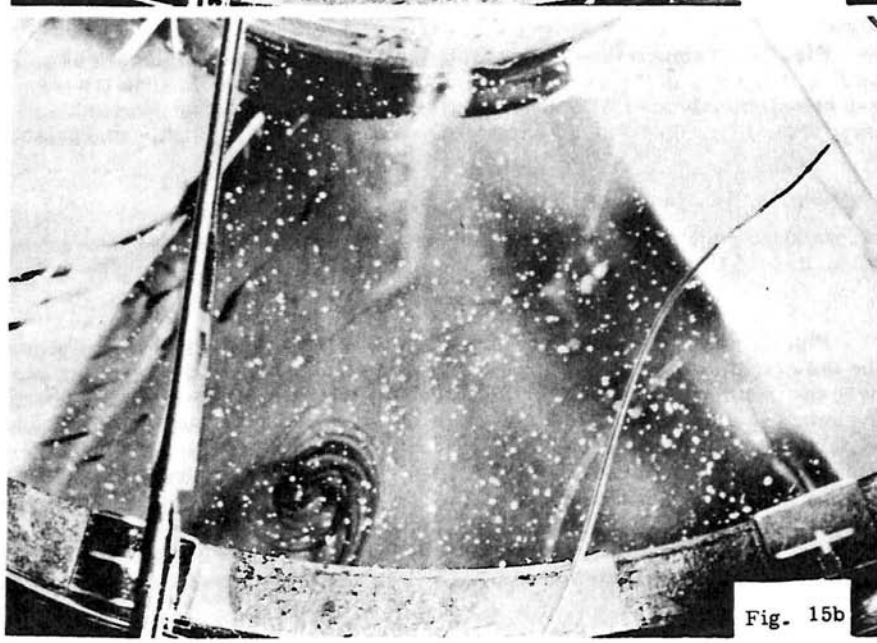

Fig. 15b

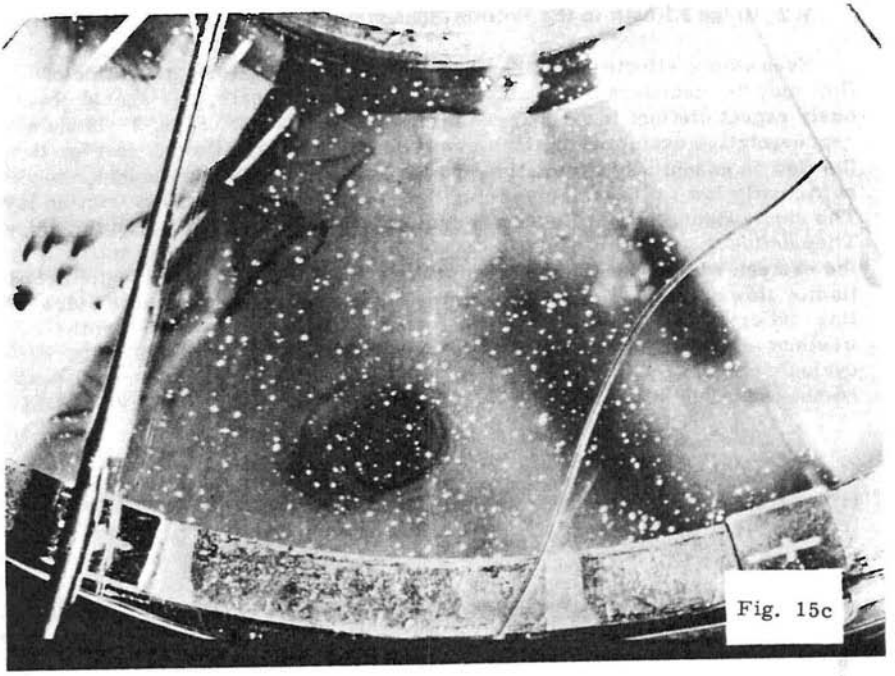

Fig. 15c

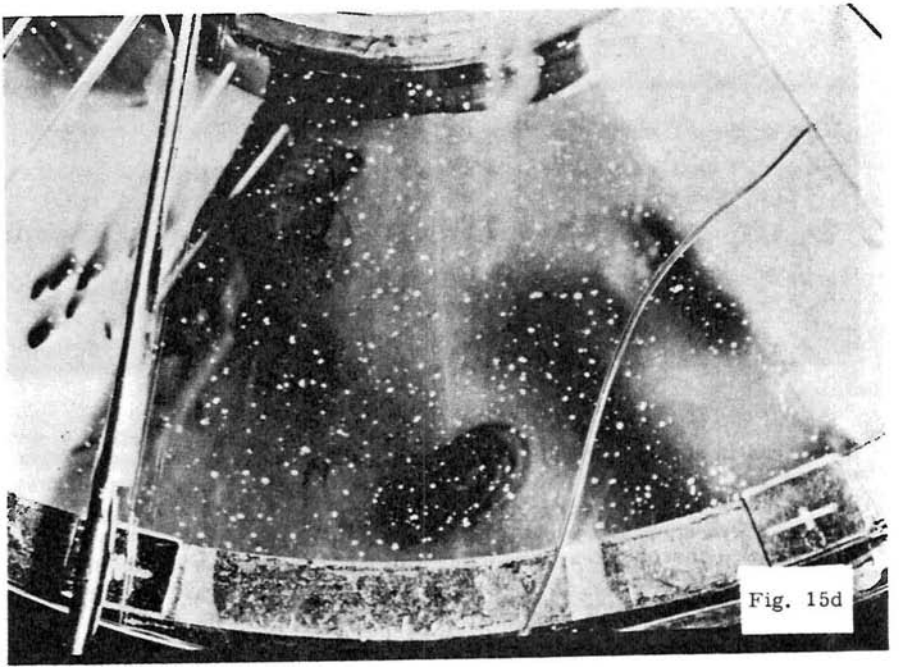

Fig. 15d

3.2 Ridge Effects in the Bottom Boundary Layer

Even where effects of the barriers on the large-scale organization of flow may be relatively small and difficult to discriminate, one should obviously expect distinct local changes in the Ekman layers. Figs. 16-18 show representative examples for both symmetrical and wave flows. In Fig. 16, the flow is essentially symmetric and the barrier, at 7.6 mm height, is sufficiently low to lie entirely within the easterlies of the bottom friction layer. The dark patches in this figure are plumes of dye from crystals on the ridge. They define the streamlines of a steady flow at the bottom which starts at the eastern edge of the barrier from the northeast just as in the undisturbed Hadley flow of Fig. 4. The flow curves anticyclonically toward the ridge line and crosses to the western side from slightly south of east. On the western slope, about one-third of the way down, it curves sharply in a cyclonic trough line west of which there is a flow from the north or north-northwest. The static stability shown in Fig. 3, of course, limits vertical

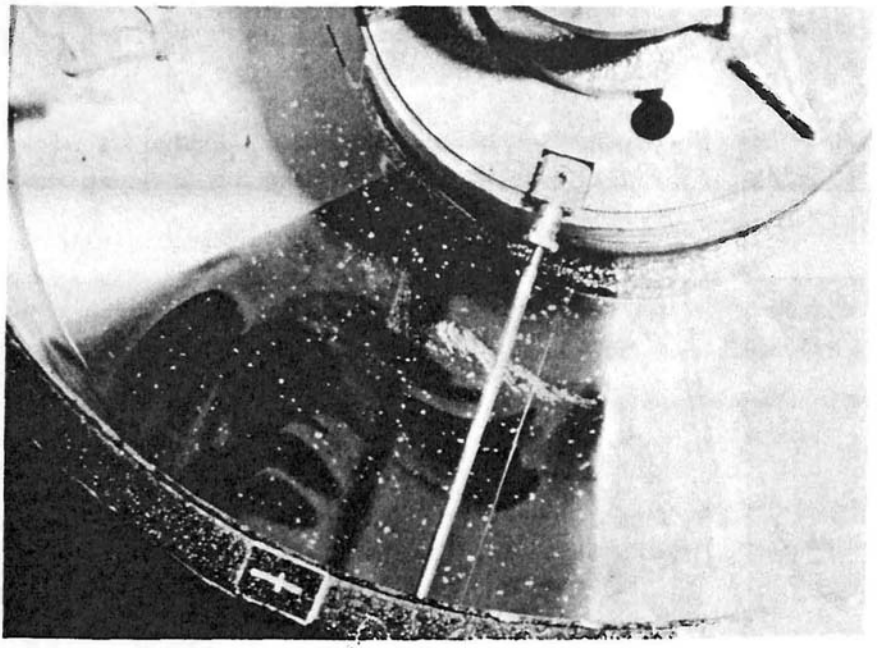

Fig. 16. Photograph of dye crystals dissolving on the obstacle of 7.6 mm height in a symmetric flow regime (230567). In the absence of the mountain, crystals would behave similarly to Fig. 4, and would have the Ekman boundary layer appearance. Here, however, plumes from the crystals on the eastern slope are swept up to the crest, cross at nearly a right angle, and then turn sharply toward the outer wall as they descend the western slope. Experimental conditions: $\Omega = 0.08\ s^{-1}$, $H_r = 80$ w. (Other values are similar to Fig. 3, where no obstacle is present, and Fig. 17, where a larger one is present.)

motion and the vorticities implied by this flow field are at least consistent with the elementary velocity divergence effects to be expected from the approach easterly flow in going over the ridge. The recovery to the normal boundary layer flow of Fig. 4 is quite rapid on the base away from the barrier on both sides.

Figure 17 shows a similar Hadley regime experiment with the 25 mm barrier which extends well up into the normal level of westerlies. The flow on the western slope is now northerly at the western edge and switches to a south-southwesterly current which then curves anticyclonically to cross the ridge line from slightly south of west. On the eastern slope the currents are west-southwest to southwest up to a separation surface, located about one-third of the way down the slope. Below this surface there are easterlies showing some definite anticyclonic curvature, as in Fig. 16. Ink from the plumes, and also some of the original ink bands, proceeds up the slope to the separation and then trails in streamers off to the right in the upper westerlies.

Fig. 17. Traces left by dissolving dye crystals in symmetric flow over the 24.9 mm obstacle (060667). Comparison with Fig. 16 shows that plumes from the crystals on the eastern slope are swept off with the westerly currents, and that a similar condition exists on the west, above a certain height. The 24.9 mm obstacle is clearly tall enough to be above the Ekman layer. Experimental conditions: $\Omega = 0.08\ s^{-1}$, $R_{oT}^* = 1.57$, $R_{og}^* = 2.62$ $R_{ob}^* = 3.99$, $S_z^* = 3.3_1$, $F_i^* = 0.23$, $U_{max} = 0.78$ cm/s, $\pi\delta_v = 1.1$ cm, $\overline{T} = 18.4$, $H_r = 80$ w, $\Delta_r T = 3.60^{\circ}C$, $\Delta_z T = 8.65^{\circ}C$, $H_t = 95$ w.

This latter feature of a separation surface on the eastern slope was the most clearly noted characteristic of the boundary layer flows when waves were present in the annulus. Fig. 18 shows an example as the upper trough approaches the ridge line of the barrier. There is a clear, almost radial, convergence line in the ink plumes on the eastern slope between southwesterlies and easterlies farther down the slope. Because of the increased geostrophic control at the higher rotation rate, there is almost certainly something approaching a frontal surface associated with the line which reminds one strongly of the behavior of Canadian polar air masses against the eastern slope of the Rocky Mountains.

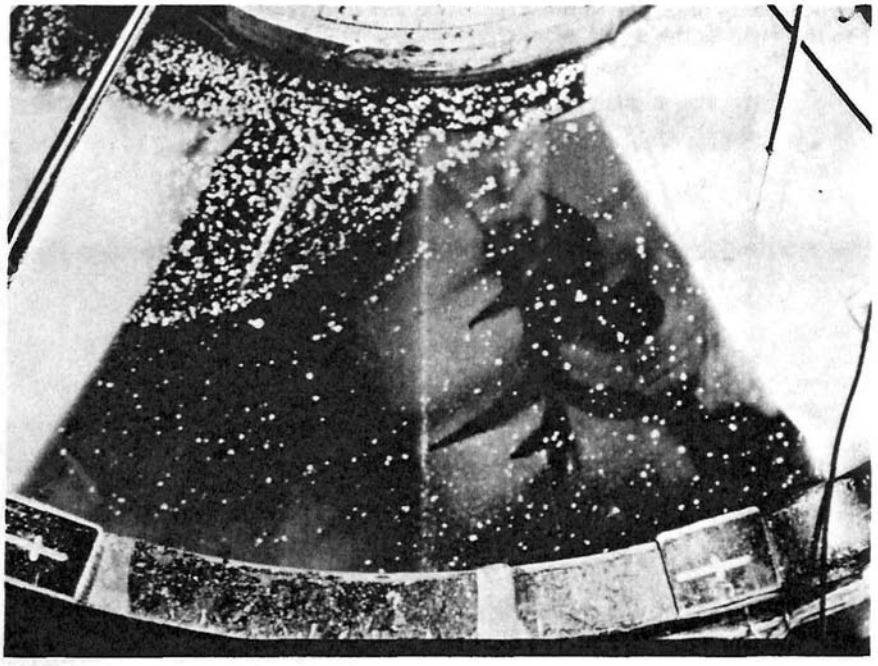

Fig. 18. Traces from dissolving dye crystals in a three-wave experiment with the 24.9 mm obstacle (050667). One of the waves can be seen in the upper left, where the aluminum particles have collected. In the eastern slope, a line of convergence is shown where westerly downslope flow meets easterly upslope flow. Experimental conditions are the same as in Fig. 11.

3.3 Small- and Medium-Scale Effects of a Narrow Ridge

With the 60° angle barriers of the previous experiments, there was no clear evidence of small lee-wave phenomena, though they might have been present and the detection methods merely inadequate. We, therefore, decided to try some narrow barriers, of the type shown in Fig. 2, with symmetrical flows as in the trials ten years ago. With a narrow ridge, whose crest height was 30 mm (which therefore extended well up into the westerlies), we were successful in obtaining lee wave responses of both medium and very short wave lengths, as shown in Figs. 19 to 24.

The tracer used for these photographs is density-balanced methylene blue dye that is slowly released from a hypodermic that is located just upwind of the barrier from positions that can be varied as desired in height and radius. Figs. 19 and 20 show the principal medium-length wave response in the lee of the 30 mm barrier. When released from heights

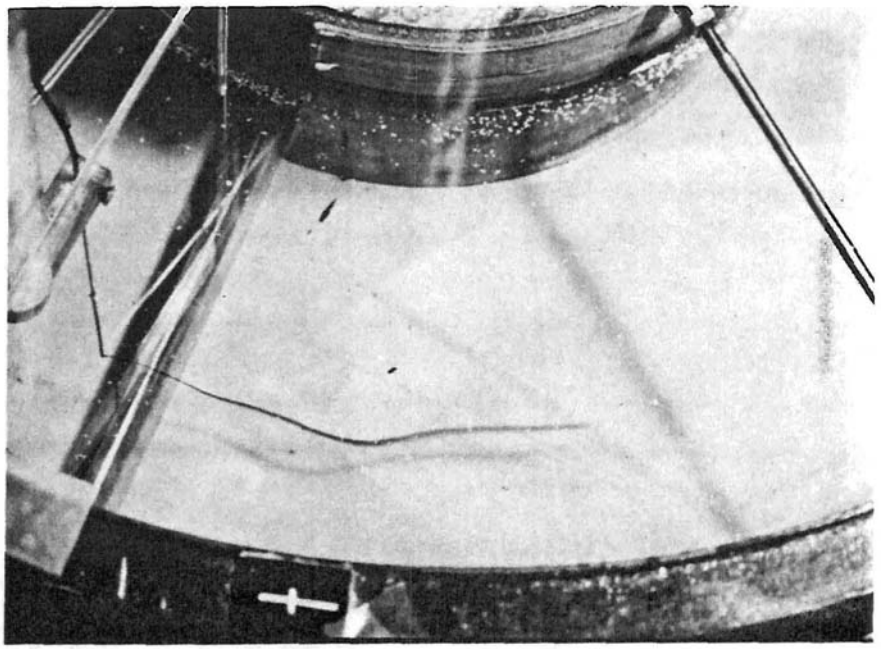

Fig. 19. Symmetric flow regime with 30 mm narrow obstacle in place (190667). The dark line is methylene blue dye introduced by means of vertical hypodermic tubing. This assembly is mounted on a rack and pinion which may be positioned wherever desired in the fluid. In this figure, the hypodermic is 14 cm from the axis of rotation, and 30 mm above the base, approximately 1 cm upstream from the ridge. One or two wave lengths of lee waves are present downstream from the ridge. Experimental conditions: $\Omega = 0.08\ s^{-1}$, $R_{oT}^* = 1.5$, $R_{og}^* = 2.5$, $R_{ob}^* = 4.3$, $S_z^* = 2.7$, $F_i^* = 0.11$, using velocity at crest, 3 cm, $U_{crest} = 0.36$ cm/sec, $\pi\delta_v = 1.1$ cm, $\overline{T} = 19.4$, $H_r = 80$ w, $H_b = 15$ w, $\Delta_r T = 3.2°C$, $\Delta_z T = 6.91°C$, $H_t = 102$ w.

near the crest level, the ink band rises in passing over, descends sharply to a lee trough, then rises and falls again in passing through about two wave lengths before the wave motion decays. The amplitude of vertical motion approaches 1 cm and the wave lengths are around 4-5 cm and vary somewhat both radially and downstream. In addition to the vertical oscillation, there is appreciable horizontal deflection of the dye band corresponding to a significant effect of the rotation on waves of this scale.

It is difficult to compare these obvious internal lee waves with any of the existing theoretical calculations because of the extreme form of the ridge profile and the lack of detailed information on the vertical profiles of zonal velocity and temperature. These are substantially different than any of Long's or Scorer's and other cases. From the rough data of Figs. 19 ff., however, it is clear that the orders of magnitude are about right.

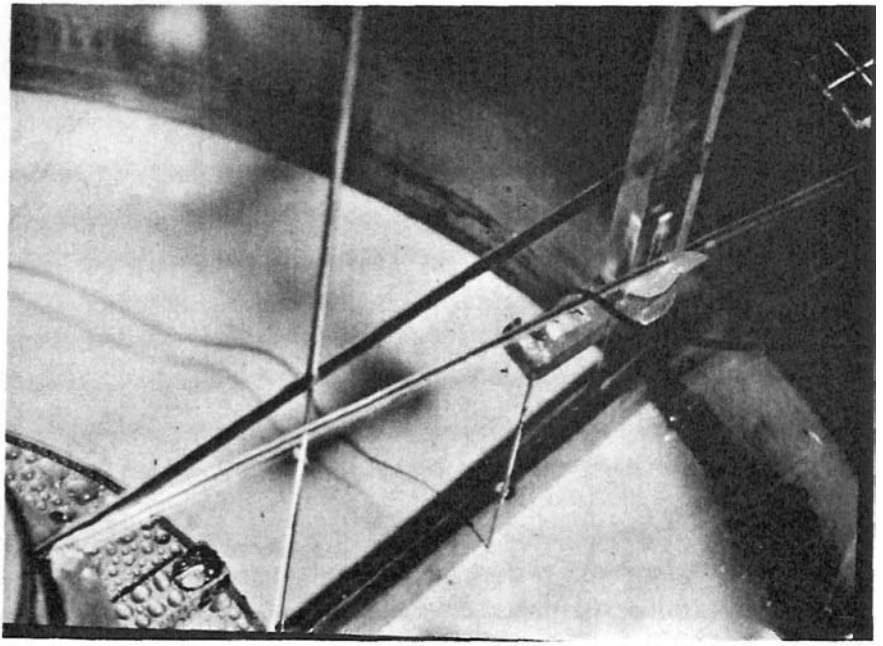

Fig. 20. Photograph taken about 2 min. after the dye was first released into symmetric flow at the same location as Fig. 19 (190667). The wave length most prominent is about 4 to 5 cm, as estimated from the annulus gap, 11.7 cm. Some horizontal curvature of the wave may be noted in wave lengths of this scale. Experimental conditions: $\Omega = 0.08\ s^{-1}$, $R_{oT}{}^{*} = 1.6$, $R_{og}{}^{*} = 2.7$, $R_{ob}{}^{*} = 4.8$, $S_z{}^{*} = 2.7$, $F_i{}^{*} = 0.11$, $U_{crest} = 0.36$ cm/sec, $\pi\delta_v = 1.1$ cm, $\overline{T} = 20.4^{o}C$, $H_r = 80$ w, $H_b = 30$ w, $\Delta_r T = 3.4^{o}C$, $\Delta_z T = 6.6^{o}C$, $H_t = 119$ w.

Thus, though Long's (1955) theoretical calculations are for much broader ridges and for velocity profiles that, applied to this case, deviate only slightly from a uniform flow, the internal Froude number

$$F_i^* \equiv U/(gE_z^* d)^{1/2} \tag{7}$$

for this experiment is around 0.20 to 0.12 depending on whether one uses a characteristic U from the top surface or one from near the crest height of the ridge that was observed to be about 0.3_6 cm/s. F_i^* is less than $1/\pi$ and greater than $1/2\ \pi$ or $1/3\ \pi$ depending on the choice, and thus Long's condition for existence of lee wave solutions is satisfied in spite of the different situations.

The simplest possible estimate of the expected wave length is also correct in order of magnitude. The Brunt-Väisälä frequency

$$\sigma_B \equiv (gE_z^*/d)^{1/2} \tag{8}$$

for the experiments in Figs. 19 to 25 is about $0.4_4\ s^{-1}$. Using the crest height velocity times the period of about 14 s gives a wavelength of about 5 cm. Obviously much closer estimates need to be made, but will depend on detailed observations of the experimental profile and probably a corresponding theoretical calculation. If one uses the observed wavelength of 4 or 5 cm, one obtains a value of the Scorer parameter

$$S_c^* \equiv \frac{gE_z^*}{dU^2K^2} \tag{9}$$

of about 0.6, where K is the wave number (Corby, 1954). This value is also a reasonable one and would not be substantially affected by the profile curvature term which should be very small in the experimental case.

While the waves in Figs. 19 and 20 thus appear to be normal lee waves, the most striking observations in this experiment were of some much smaller scale waves or fluctuations shown in Figs. 21 to 24. When the ink release point at mid-radius upwind of the ridge was traversed vertically, the ink bands at almost all heights were smooth and continuous as in Figs. 19 and 20 (except at such low heights that the ink remained in the trapped region upwind). However, between release heights of 27 and 32.5 mm, the band crossed the ridge smoothly, dipped strongly into the lee trough, and, just about at the minimum height in this trough, reached a region of very strong small-scale disturbance as in Fig. 21. The direct effect seemed to be due to rapid north-south horizontal current variations which diffused the ink

laterally at a rate of orders of magnitude larger than the normal trail diffusion. At the same time, there was a rough periodicity corresponding to wave lengths of 1 to 4 mm in the downstream direction. Figure 21 shows the onset of this fine scale motion for a position outside mid-radius, while Fig. 22 shows a later stage where the periodicity, changes of angle of what look like rolls of ink, and the simultaneous presence of the longer lee waves are all evident.

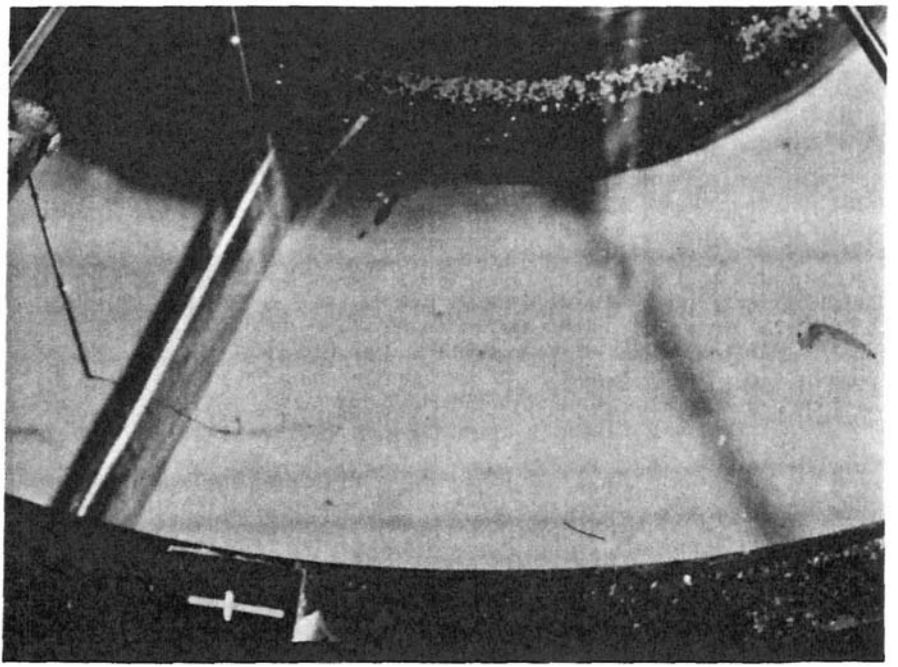

Fig. 21. Photograph illustrating a smaller scale of lee waves with wave length 1 to 4 mm (190667). The hypodermic tube is 27 mm above the base, but the smooth waves of Figs. 19 and 20 now show superimposed smaller wave lengths. Experimental conditions: $\Omega = 0.08\ s^{-1}$, $R_{oT}^* = 1.7$, $R_{og}^* = 2.9$, $R_{ob}^* = 4.7$, $S_z^* = 2.5$, $F_i^* = 0.11$, $U_{crest} = 0.36$ cm/s, $\pi\delta_v = 1.1$ cm, $\overline{T} = 21.3^{\circ}C$, $H_r = 80$ w, $H_b = 30$ w, $\Delta_r T = 3.4^{\circ}C$, $\Delta_z T = 5.9^{\circ}C$, $H_t = 132$ w.

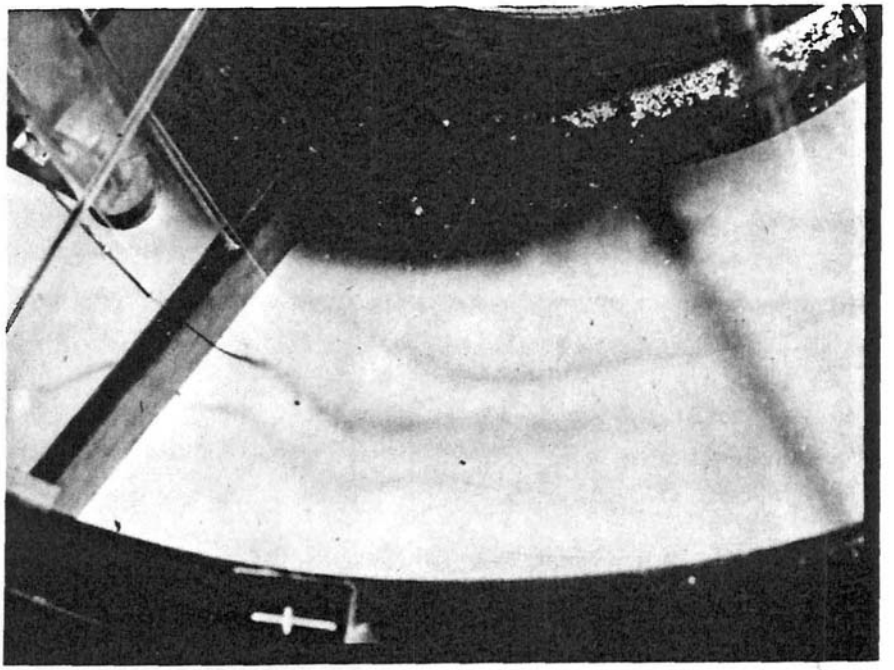

Fig. 22. Photograph of dye at a later time than Fig. 21, showing longer and shorter lee waves present (210667). The hypodermic was 31 mm above the base and dye had been flowing about 10 min. before the photo. Experimental conditions are the same as those in Fig. 21.

Figure 23, though faint because of the excessive dispersion of the ink trail, shows lateral displacements of 2 to 4 cm, which, at the speeds involved, occurred in a few seconds. These values correspond to lateral diffusivities of at least 10^{-2} cm^2/s, orders of magnitude larger than the molecular values, which for many solutes in water are around 10^{-5} cm^2/s. Finally, Fig. 24 shows a long persistent trail with somewhat longer wave lengths evident. Much of the far downstream part of this trail is probably convecting passively with the flow after having developed in the early portion.

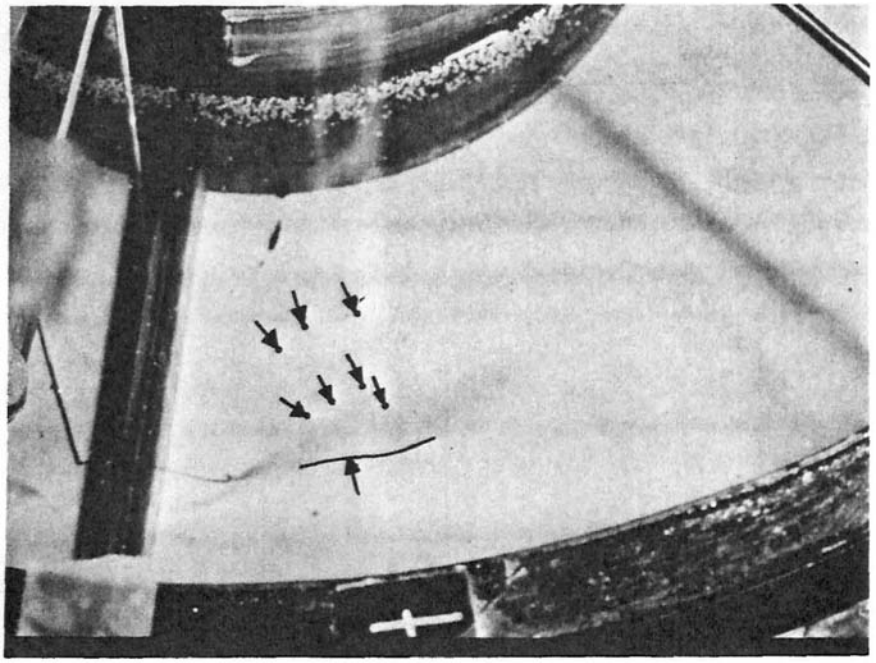

Fig. 23. Photograph of dye trace from hypodermic tube located at a radius beyond mid-gap (190667). Very strong oscillations may be noted downstream of the ridge, having amplitudes as large as 4 cm in a north-south orientation. These large amplitudes suggest a correspondingly large diffusion coefficient noted in the text. Experimental conditions are the same as in Fig. 21.

The identification of the nature of these small-scale disturbances is much more difficult than that of the other waves. They obviously involve some sort of flow instability that may be connected with strong vertical variations of the flow direction below the crest level in the lee of the ridge. The internal stratification is also certainly involved.

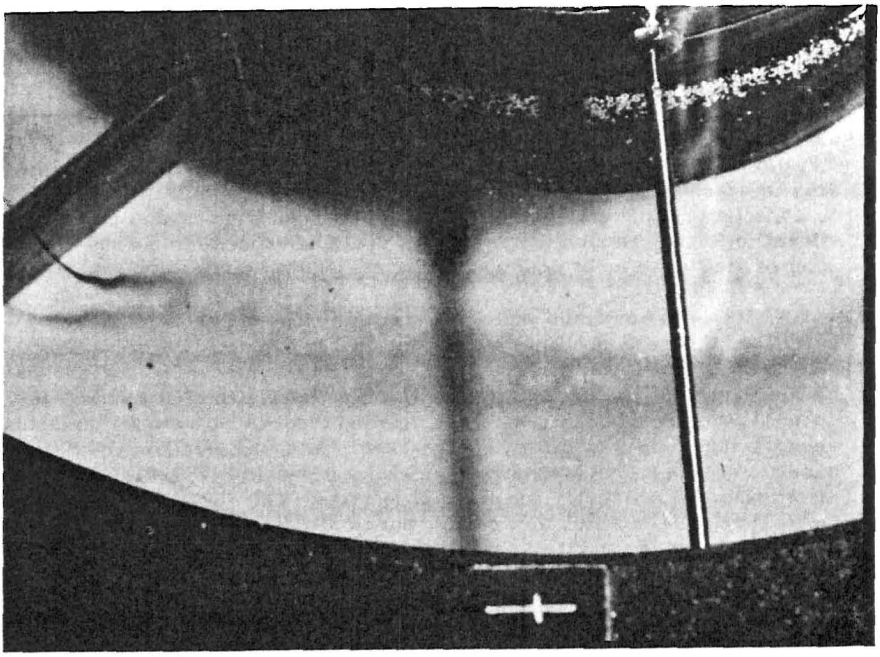

Fig. 24. Photograph of dye trace about 3 min after initial release (190667). A plume of dye illustrates the initial disturbance forming downstream of the crest, and the subsequent wave formation. The dye was released at 30 mm above the base. Experimental conditions are as in Fig. 21.

4. Conclusions and Acknowledgments

The work we have summarized is obviously quite exploratory and could be pursued vigorously in any of several directions implied by the three preceding subsections. In a number of cases, clearly, detailed measurements are needed for comparison with analytical or numerical solutions for the proper conditions. This should be particularly feasible for some of the boundary layer effects in Section 3.2.

Some of the cases may be quite difficult to do this for, and yet, clearly suggest important qualitative conclusions that could be pursued in a number of ways. In Section 3.1, the large-scale wave effects clearly have many important implications for general circulation questions. Thus, it would be extremely interesting, even in the absence of detailed three-dimensional measurements, to try to carry out numerical experiments to produce disturbance sequences like those in Figs. 7 and 15. Even more important are the suggestions, when one compares Figs. 11, 8, and 9, with Figure 12, of a drastic change in the magnitude and character of the system response to simple ridges of different heights. Simple potential vorticity arguments

of the same type as used by Hide (Hide and Ibbetson, 1966) to discuss the formation of Taylor columns in barotropic flows past obstacles, suggest that stronger disturbance effects on the flows should be expected the smaller the ratio of R_{oT}^* to h/d, where h is the crest height of the ridge. h/d is essentially an estimate of the nondimensional disturbance vorticities to be expected from barotropic effects. In the above figures, this ratio, $R_{oT}^* d/h$, is 0.7, 0.6, and 0.3 for Figs. 11, 8, and 9, respectively, while its value for the drastic case of Fig. 12 is about 0.1. A conjecture that a limiting value of this, or a similar ratio, of say, 0.2, divides pronounced from weak topographic effects in Rossby regime thermal flows would be valuable to pursue from the point of view of both physical and numerical general circulation experiments.

So far as the medium-scale lee wave questions of section 3.3 are concerned, there is probably not a great deal to be gained from rotating experiments that is not contained in Long's and other work though there would be some interest, for sharply enough defined experimental situations, in some quantitative verification of any detailed theory that matched the actual velocity and stability profiles. On the other hand, the small-scale disturbances would be worth a considerable exploratory effort to track down the mechanisms of instability and other properties. The very sharply limited vertical regions in which they occur, the close association with the longer regular lee waves, and the very strong lateral diffusivities, all suggest strong implications for orographic effects, clear air turbulence, and other related questions. We are not aware, for example, of any theoretical or observational suggestions that such strong lateral velocities relative to the downwind and vertical components might occur, though they may have been made in some discussions of clear air turbulence. Clearly, if some order, or merely suggestions as to what types of flow fields might be looked for, could be derived from a broad enough series of experiments, it would be well worth the effort.

We are much indebted to W. Moloznik for the careful machining of the obstacles, to A. Kordecki and G. Gray for assistance in the operation of the experiments, J. Weil for evaluation of much of the numerical data, and K. Taylor for typing of the manuscript.

The research reported herein has been supported by the Atmospheric Sciences Section, National Science Foundation, under grant GA-1023, by the U.S. Department of Commerce Environmental Science Services Administration under grant ESSA E22-107-67 G and by the National Center for Air Pollution Control, Bureau of Disease Prevention and Environmental Control, Public Health Service under grant no. USPHS BDPEC 1-R01-AP-00601-01.

SYMBOL LIST

r_o	outer radius of annulus
r_i	inner radius of annulus
Δr	either $(r_o - r_i)$ or an interior radial position difference
Δz	vertical position difference
d	depth
h	height of obstacle crest
g	magnitude of the gravity acceleration
Ω	angular velocity of the annulus with respect to laboratory coordinates
U or U max	characteristic zonal speed; usually an observed maximum value at the top surface
ν	kinematic viscosity; about 1.0×10^{-2} cm^2/s in all experiments
$\Delta_r T$	radial temperature difference averaged vertically
$\Delta_z T$	vertical temperature difference averaged radially
ΔT_b	wall-to-wall temperature difference averaged vertically
ΔT_{cs}	temperature difference between outflow and inflow water to the cold source
E_r^*	representative fractional expansion in the radial direction across distance Δr; may be an interior value or based on wall-to-wall temperature differences
E_z^*	representative fractional expansion in the vertical direction over Δz
H_r	rim heat applied to outer cylinder
H_b	heat applied to base ring
H_t	heat flux measured at cold source
R_{oT}^*	thermal Rossby number referred to $r_o\Omega$
R_{og}^*	gap thermal Rossby number referred to $\Delta r\Omega$
R_{ob}^*	bath thermal Rossby number based on estimated wall-to-wall ΔT_b
S_z^*	vertical stability parameter
F_i^*	internal Froude number
S_c^*	Scorer parameter
σ_B	Brunt-Väisälä frequency
$\pi\delta_v$	conventional Ekman layer depth

REFERENCES

Charney, J. and A. Eliassen, 1949: A numerical method for predicting the perturbations of the middle latitude westerlies, Tellus, 1, 38-54.

Corby, G., 1954: The airflow over mountains, Quart. J. Roy. Meteor. Soc., 80, 491-521.

Fowlis, W. W. and R. Hide, 1965: Thermal convection in a rotating annulus of liquid: effect of viscosity on the transition between axisymmetric and non-axisymmetric flow regimes, J. Atmos. Sci., 22, 541-558.

Fultz, D., R. R. Long, G. V. Owens, W. Bohan, R. Kaylor and J. Weil, 1959: Studies of thermal convection in a rotating cylinder with some implications for large-scale atmospheric motions, Meteor. Monogr., 4, No. 21, 104 pp.

Fultz, D., 1961: Developments in controlled experiments on large-scale geophysical problems, Advances in Geophysics, 7, 1-103.

Fultz, D., 1962: An experimental view of some atmospheric and oceanic behavioral problems, Trans. N.Y. Acad. Sci. (2), 24, 421-446.

Hide, R., 1956: Fluid motion in the earth's core and some experiments on thermal convection in a rotating liquid, Fluid Models in Geophysics, Proc. 1st Sympos. on the Use of Models in Geophys. Fluid Dynam., Baltimore, Sept. 1953, 101-116.

Hide, R., 1958: An experimental study of thermal convection in a rotating liquid, Phil. Trans. Roy. Soc. London (A), 250, 441-478.

Hide, R. and A. Ibbetson, 1966: An experimental study of "Taylor colums," ICARUS: Int. J. Solar System, 5, 279-290.

Long, R. R., 1953: Some aspects of the flow of stratified fluids: I - A theoretical investigation, Tellus, 5, 48-58.

Long, R. R., 1954: Some aspects of the flow of stratified fluids: II - Experiments with a two-fluid system, Tellus, 6, 97-115.

Long, R. R., 1955: Some aspects of the flow of stratified fluids: III - Continuous density gradients, Tellus, 7, 341-357.

Lyra, G., 1943: Theorie der stationaren Leewellenströmung im freien Atmosphäre, Z. angew. Math. Mech., 23, 1-28.

Queney, P., 1947: The problem of airflow over mountains; a summary of theoretical studies, Bull. Amer. Meteor. Soc., 29, 16-35.

Riehl, H. and D. Fultz, 1957: Jet stream and long waves in a steady rotating-dishpan experiment: structure of the circulation, Quart. J. Roy. Meteor. Soc., 83, 215-231.

Riehl, H. and D. Fultz, 1958: The general circulation in a steady rotating-dishpan experiment, Quart. J. Roy. Meteor. Soc., 84, 389-417.

Scorer, R. S., 1949: I - Theory of waves in the lee of mountains, Quart. J. Roy. Meteor. Soc., 75, 41-56.

Scorer, R. S., 1953: Theory of airflow over mountains: II - The flow over a ridge, Quart. J. Roy. Meteor. Soc., 79, 70-83.

Scorer, R. S., 1954: Theory of airflow over mountains: III - Airstream characteristics, Quart. J. Roy. Meteor. Soc., 80, 417-428.

THE INFLUENCE OF OROGRAPHY ON THE GLOBAL CIRCULATION PATTERNS OF THE ATMOSPHERE

Akira Kasahara
National Center for Atmospheric Research
Boulder, Colorado

ABSTRACT

The motions of the atmosphere are influenced by the conditions of the underlying surface of the earth. As far as the large-scale motions of the atmosphere are concerned, the following three factors are important: (1) the surface boundary layer effect, (2) large-scale heat sources and sinks due to the distribution of continents and oceans, and (3) the large-scale orography acting as barriers to atmospheric motions. In the first factor, the surface friction not only plays a role of energy dissipation, but also induces vertical motions which are proportional to the relative vorticity of flows at the top of the frictional layer. The second factor has a thermal effect caused by the temperature contrast between the air over the lands and the air over the seas. The third factor, on the other hand, is dynamical in nature. There are still controversies about the relative importance of these three effects upon the global circulation patterns of the atmosphere. The purpose of this paper is to discuss these three effects. In particular, based on the numerical calculations with a barotropic model and a general circulation model, inferences are made about the long-standing debate concerning the relative importance of thermal and orographic effects in determining the semi-permanent features of the atmospheric circulation.

THE INFLUENCE OF OROGRAPHY ON THE GLOBAL CIRCULATION PATTERNS OF THE ATMOSPHERE

Akira Kasahara
National Center for Atmospheric Research
Boulder, Colorado

1. Introduction

Large mountain barriers, such as the Rockies and Himalayas, influence atmospheric motions of all scales, from the scale of the long waves down through those of lee depressions to small turbulent eddies. When we speak of the effects of orography on the global circulation patterns of the atmosphere, the following three factors should be considered: (1) the boundary layer effect caused by the surface friction, (2) large-scale heat sources and sinks due to the distribution of continents and oceans, and (3) the large-scale orography acting as barriers for the atmospheric motions.

In a model of the general circulation of the atmosphere which we have been developing at the National Center for Atmospheric Research since 1964, these three effects are taken into account. In order to understand the relative importance of the above three effects, we are planning to make various controlled experiments with the general circulation model. As a guide to such experiments we will review in this paper the characteristics of the above three effects.

2. The Boundary Layer Effect

When a current of air moves over an uneven surface, the motion usually becomes irregular or turbulent. Because of the surface friction, the kinetic energy of the flow is dissipated by the eddy actions. If we consider large-scale motions under the effect of the earth's rotation, the surface friction not only acts to dissipate kinetic energy, but because of the presence of a cross-isobaric component of the flow in the boundary layer, it also acts to induce vertical motions at the top of the frictional layer. The importance of the latter effect was discussed by Charney and Eliassen (1949).

From the theory of the motion in the frictional layer (Ekman spiral), one can compute the vertical variation of the horizontal velocity in the frictional layer (see Brunt, 1939, or Haurwitz, 1941). Also one can compute the amount of divergence of the horizontal velocity integrated from the ground surface to the top of the frictional layer. Since there cannot be any significant accumulation of air in the frictional layer, we can evaluate the vertical velocity w_S at the top of the frictional layer from the total amount of divergence thus computed. The result is

$$w_S \doteq \zeta_g \frac{D}{2} \sin 2\alpha \tag{2.1}$$

and

$$D = \sqrt{\frac{2K}{f}}$$

where K denotes the eddy kinematic viscosity, ζ_g is the relative vorticity of the geostrophic wind at the top of the boundary layer, f is the Coriolis parameter, α is the angle between the geostrophic velocity and the surface velocity ($0 \leq \alpha \leq \pi/4$).

Thus the surface friction will cause ascending (descending) motion in regions of cyclonic (anticyclonic) vorticity. For instance, if we choose $K=10^5$ cm^2 sec^{-1}, $f = 10^{-4}$ sec^{-1} and $\zeta_g = f$ (for a rather intense cyclone), we obtain $D \doteq 447$ meters. By assuming that $\alpha = 25^\circ$, we find that $w_s = 1.7$ cm sec^{-1}. The boundary layer effect, therefore, is of some importance in influencing the vertical motion patterns of cyclones and anticyclones.

The magnitude of α in (2.1) depends on the surface condition of the earth. When (2.1) was derived from the theory of the Ekman spiral such as discussed by Haurwitz (1941), it was assumed that the shear of the wind at the anemometer level is parallel to the wind itself, namely

$$V_s = K \left(\frac{dV}{dZ}\right)_s \tag{2.2}$$

where V_s is the surface wind at the anemometer level and the proportionality factor K may be called the coefficient of surface friction. It can be shown that there exists the following relationship between α and K:

$$\cot \alpha = 1 + 2K \sqrt{\frac{f}{2K}} \,. \tag{2.3}$$

If we assume that the surface stress is proportional to the square of the wind speed, the coefficient of surface friction may be written as

$$K = \frac{K}{C_D V_s} \tag{2.4}$$

where C_D is the drag coefficient. It is easily seen that $\alpha \to 45^\circ$ as $C_D \to \infty$ and $\alpha \to 0$ as $C_D \to 0$.

Table 1 Values of α for various values of C_D

C_D (units 10^{-3})	α (degrees)	Comment
1	10.3	flat land
3	21.9	some low relief
6	29.8	moderately high mountains
10	34.5	very high mountains

The value of the drag coefficient depends upon the roughness of the surface. Apart from the difference between the drag over the land and that over the sea, it is necessary to take into account the greater frictional stress over mountainous areas compared with more nearly level areas. Cressman (1960) considers that the drag coefficient C_D is made up of two partial drag coefficients, C_1 and C_2, where C_2 is used to give the form drag of the orographic relief, and C_1 is relatively constant. Sawyer (1959) made an attempt to evaluate the drag due to a mountain ridge by considering the net downward transport of momentum by gravity waves generated in the flow over the ridge. By taking into account Sawyer's work and other literature on the magnitude of the drag coefficient, Cressman (1960) summarized as follows:

(a) land with trees or with some low relief

$$C_2 = 1 \sim 2 \times 10^{-3}$$

(b) moderately high mountains

$$C_2 = 2 \sim 5 \times 10^{-3}$$

(c) very high mountains

$$C_2 = 5 \sim 9 \times 10^{-3}$$

In considering the most appropriate value for C_1, Cressman gives $C_1 = 1.2 \times 10^{-3}$. The hemispherical map of C_D, reproduced as Fig. 1 in this paper, is the result of adding C_1 to the hemispherical distribution of C_2.

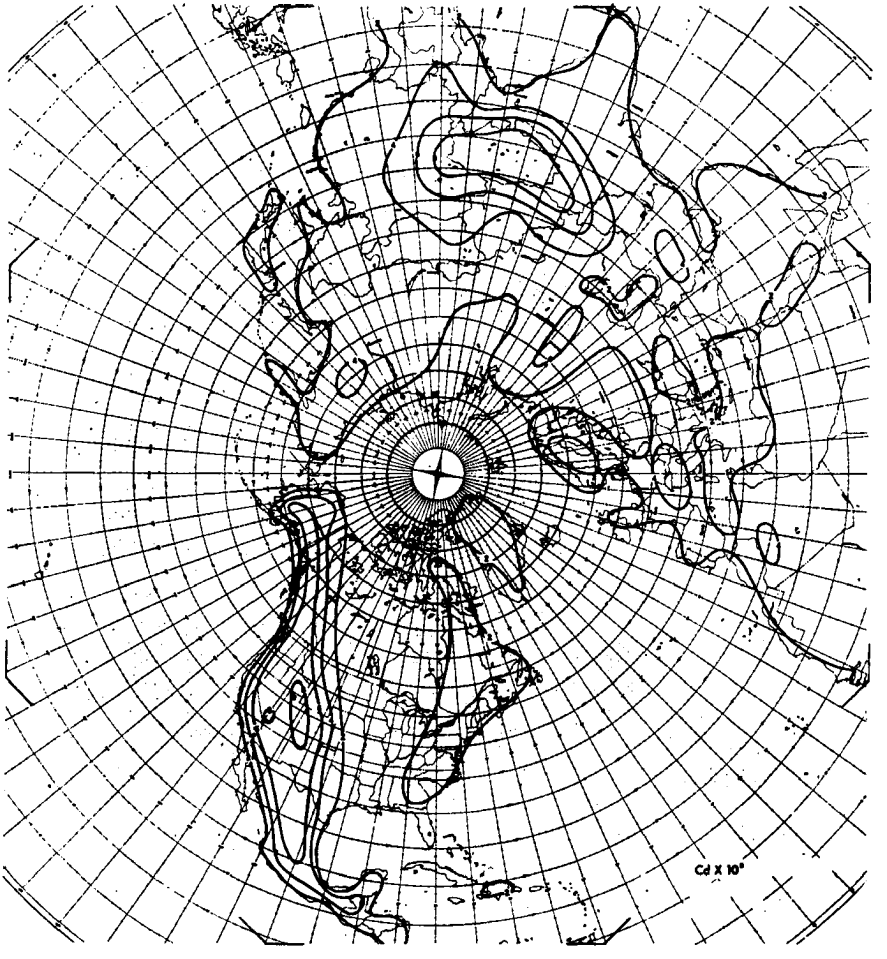

Fig. 1. Distribution of drag coefficient over the Northern Hemisphere (Cressman, 1960).

We can compute the value of α for a given value of C_D by using (2. 3) and (2. 4). By assuming that V_S = 10 m/sec and the numerical values of other parameters were chosen to be the same as before, we obtain the values of α for various values of C_D as shown in Table 1. Sawyer (1959) cited values of α over sea and land taken from the studies of Marshall, and these values are:

Over sea	$\alpha = 6^o$
Over land generally	$\alpha = 30^o$
Over mountainous country	$\alpha = 35^o$

By comparing the values of α listed in Table 1 with those obtained by Marshall, we conclude that the hemispherical distribution of C_D prepared by Cressman (1960) is in accord with the theory of the Ekman spiral with the present choice of numerical values for the physical parameters.

As we mentioned earlier, the boundary layer effect gives rise to a damping of the motions. However, the boundary layer effect can give rise to heating if we consider the release of latent heat of condensation in the moist ascending motion. For example, in a region with relative cyclonic vorticity, there will be a corresponding ascending motion, and if the air is saturated, there will be a release of the latent heat of condensation which in turn provides a heating of the air.

3. Orographic-Dynamic Effect

Charney and Eliassen (1949), Bolin (1951), and others demonstrated that large mountain barriers of the size of the Himalayas and Rockies play an important role in determining the position of the semi-permanent high-level flow patterns in the atmosphere. Their argument is based on the observation that certain basic characteristics of the flow pattern at upper levels in the Northern Hemisphere do not change essentially from summer to winter, in spite of the reversal in the thermal contrast between the continents and oceans.

Figs. 2 and 3 show the mean 500 mb height contours over the Northern Hemisphere for January and July published by the Free University of Berlin (Jacobs, 1958). Referring to Fig. 2 for January, we find two dominant troughs which lie along the east coasts of the North American and Asiatic continents. There is also a minor trough over western Europe. Looking at Fig. 3 for July, one finds that basic features of the flow remain unchanged from winter to summer, though the intensity of the westerlies becomes weaker during summer. This similarity between the January and July patterns is a cornerstone in the orographic-dynamical theory. Over the Southern Hemisphere, Boffi (1949) found that an upper trough in the mean is located to the east of the Andes Mountains and therefore the orographic effect is pronounced in the general circulation over South America.

Sutcliffe (1951) raised an objection to accepting the above orographic-dynamic hypothesis to explain semi-permanent tropospheric flow patterns. He argues qualitatively that a thermal-synoptic explanation, resting mainly on the direct thermal effects of land and sea modified by a baroclinic synoptic process, is regarded as satisfactory.

Smagorinsky (1953), Gilchrist (1954), Döös (1962), and others have investigated the influence of large-scale heat sources and sinks on the quasi-stationary mean motions of the atmosphere. While these results are not conclusive, they do indicate that the thermal effect may be as important as the orographic effect in producing the stationary motions.

In this section, we shall investigate the orographic-dynamical effect separately from other various modifying processes for the atmospheric motions. For this purpose, we consider the following system of barotropic

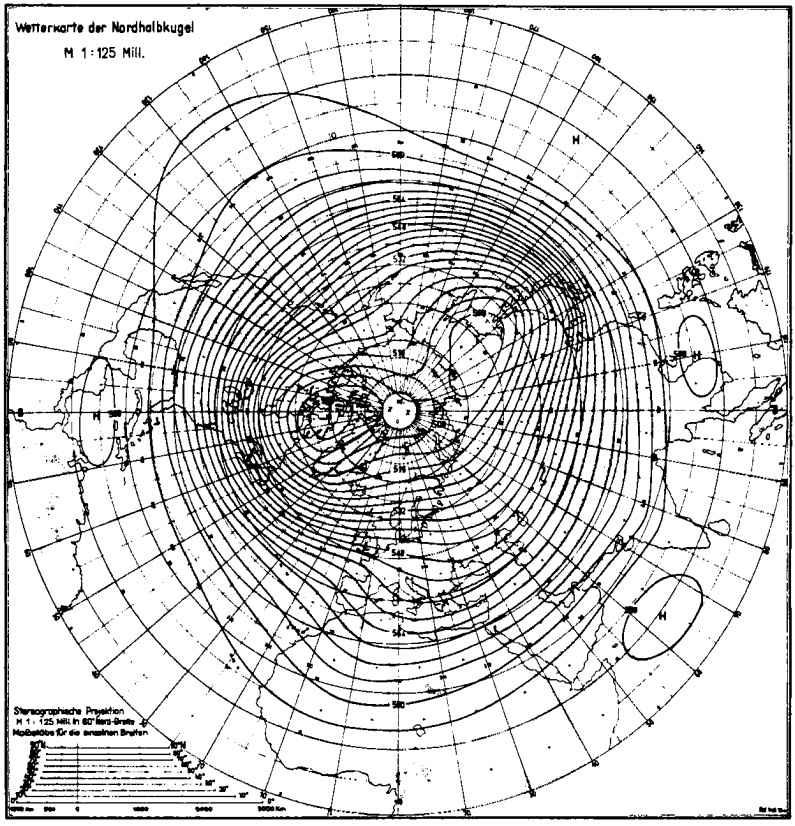

Fig. 2. Mean 500 mb height contours over the Northern Hemisphere for January (Jacobs, 1958).

equations which describes the motion of a homogeneous, incompressible, hydrostatic and inviscid atmosphere:

$$\frac{\partial u}{\partial t} = - \mathbb{V} \cdot \nabla u + \left(f + \frac{u \tan \phi}{a} \right) v - g \frac{\partial h}{a \cos \phi \, \partial \lambda} \tag{3.1}$$

$$\frac{\partial v}{\partial t} = - \mathbb{V} \cdot \nabla v - \left(f + \frac{u \tan \phi}{a} \right) u - g \frac{\partial h}{a \, \partial \phi} \tag{3.2}$$

$$\frac{\partial h}{\partial t} + \nabla \cdot [\mathbb{V} (h - H)] = 0 \tag{3.3}$$

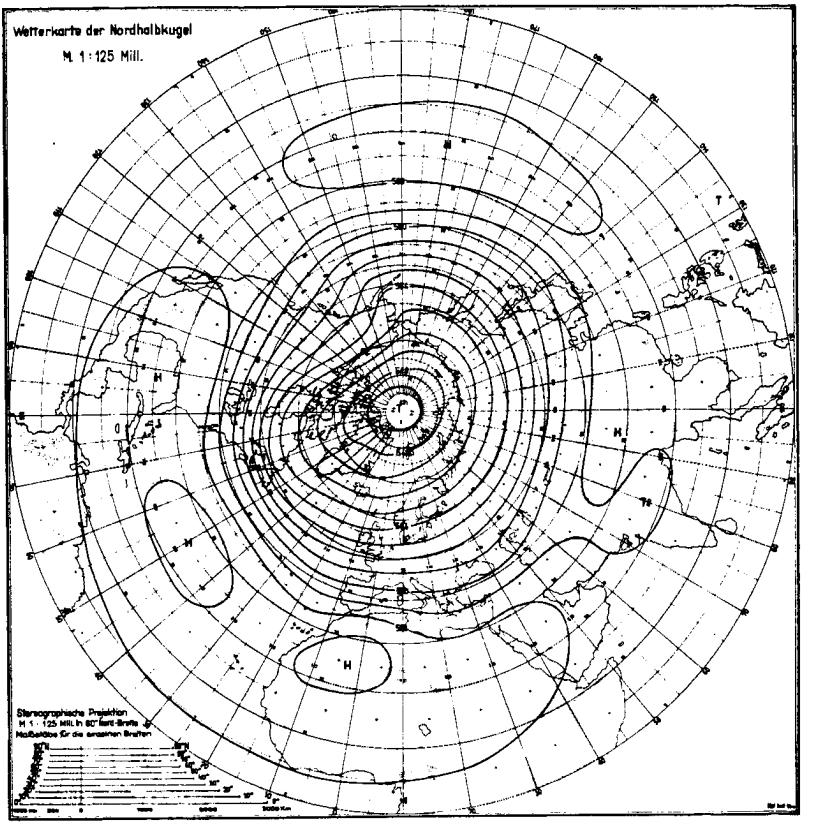

Fig. 3. Same as Fig. 2, but for July.

The notation is defined as follows:

λ = longitude (positive eastwards)
ϕ = latitude (positive northwards)
t = time
$\mathbb{V}$ = horizontal velocity
u, v = longitudinal and latitudinal components of $\mathbb{V}$
h = height of the free surface of the fluid
$f = 2\Omega \sin\phi$; Coriolis parameter
Ω = angular velocity of the earth
a = mean radius of the earth
g = acceleration due to gravity
H = height of the earth's orography

$$\mathbb{V}\cdot\nabla = \frac{u}{a\cos\phi}\frac{\partial}{\partial\lambda} + \frac{v}{a}\frac{\partial}{\partial\phi}$$

$$\nabla\cdot\mathbb{V} = \frac{1}{a\cos\phi}\left[\frac{\partial u}{\partial\lambda} + \frac{\partial}{\partial\phi}(v\cos\phi)\right]$$

Fig. 4 shows the height contour map of the earth's orography based on the 5° interval data published by Berkofsky and Bertoni (1955).* Fig. 5 shows the 500 mb mean zonal wind velocity for January and July, after van Loon (1964).

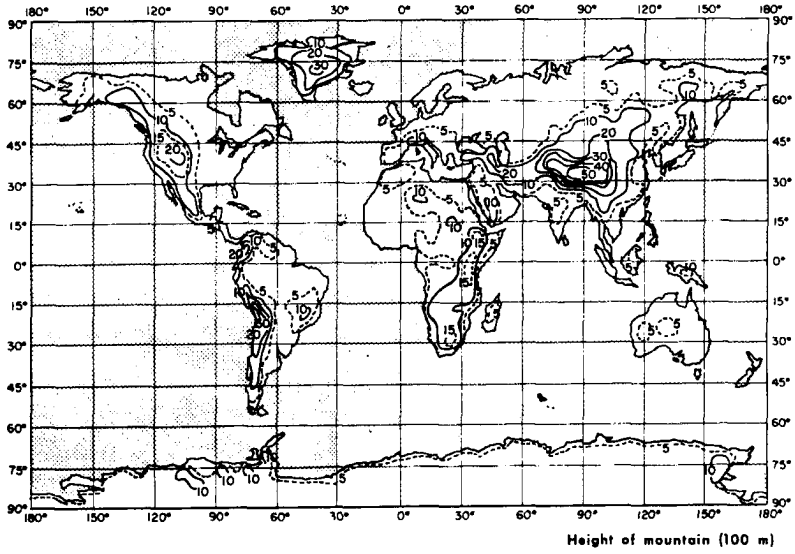

Fig. 4. Height distribution of the earth's orography (Berkofsky and Bertoni, 1955).

* It was pointed out by Mintz (private communication) that the elevation of Antarctica has been read off incorrectly by Berkofsky and Bertoni. We, therefore, have read off newly the elevation of Antarctica prepared by Bently, et al. (1964).

The problem is to obtain the time-dependent solutions of (3.1) - (3.3) by prescribing the height of the mountain $H(\lambda, \phi)$ as given in Fig. 4 and using the 500 mb mean zonal wind velocity, as shown in Fig. 5, as the initial condition.

We assume, then, at $t = 0$ that

$$u = \bar{u}(\phi)$$

$$v = 0$$

(3.4a)
$$\frac{\partial \bar{h}}{\partial \lambda} = 0$$

$$\frac{\partial \bar{h}}{a \partial \phi} = - \left(f + \frac{\bar{u} \tan \phi}{a} \right) \bar{u} .$$

These solutions satisfy the steady-state conditions in the case of no mountains. By integrating the last equation with respect to ϕ, we have

(3.4b)
$$\bar{h}(\phi) = \bar{h}_o - \int_o^{\phi} \left(f + \frac{\bar{u} \tan \phi'}{a} \right) \bar{u} a d\phi'$$

where $\bar{h}_o$ denotes the value of $\bar{h}$ at $\phi = 0$ and we assumed $\bar{h}_o = 12$ km.

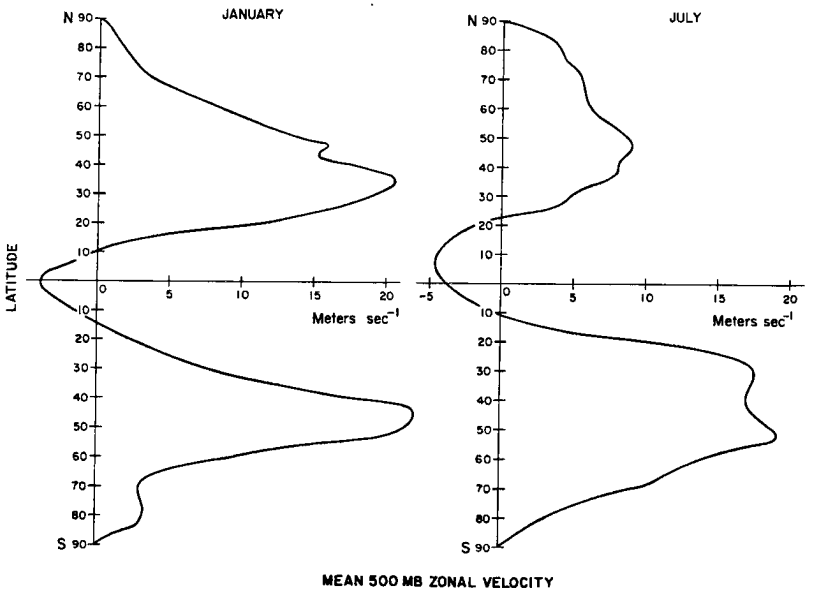

Fig. 5. Meridional distribution of the 500 mb mean zonal wind velocity for January and July (van Loon, 1964).

In the presence of mountains, (3.4) no longer describes the steady-state conditions. This means that the wind field and the pressure field are not balanced initially over the mountain regions. Therefore, one expects oscillations to be generated during $t > 0$.

The system of equations (3.1) - (3.3) with the initial conditions (3.4) was solved numerically using the method described by Kasahara (1966). The space grid points are placed at longitude and latitude intersections of 5° increments in both longitude and latitude. Near the poles equal increments of longitude result in the reduction of geographical distances in the longitude because of the convergence of the meridians. The reduction of geographical distances between grid points near the poles imposes a stringent restriction on the choice of a time increment for solving the equations. In order to avoid this difficulty, we put solid walls along the constant latitude circles at $\phi = 75^{\circ}$N and 75°S. It was assumed that the meridional component of velocity vanishes along the boundaries. This assumption automatically excludes the possibility of finding the orographic effect of Greenland in the Northern Hemisphere and of Antarctica in the Southern Hemisphere. *

The numerical integrations of (3.1) - (3.3) were made for the period of 20 days for both cases of January and July. The time step of 5 minutes was used. In the following six figures we show results of the calculations. These figures are constructed by taking the arithmetic mean of a dependent variable for the period of 15 days, namely from days 5 to 20. Moreover, these patterns are deviations from the corresponding initial conditions. Fig. 6 shows the mean deviation of the height of the free surface for January, and Fig. 7 shows the same variable for July. From Fig. 6 for January we see in North America that a ridge forms over the western slope of the Rockies and a trough develops on the eastern side. Similarly over the Asiatic continent, a ridge forms over the northwest slope of the Himalayas and a trough develops on the eastern side. The axis of the trough is tilted NE to SW. In the Southern Hemisphere, a trough forms over the eastern side of the Andes and a weak ridge forms on the western side. From Fig. 7 for July, we see features more or less similar to those on the map of January conditions. In the Northern Hemisphere, the intensities of ridges and troughs associated with the Rockies and Himalayas are generally weaker than those for the January condition because the intensity of the westerlies in July is weaker than that in January. In the Southern Hemisphere, the intensity of the ridge over the western side of the Andes is greater in July than in January. Some indication can be seen that the highlands of South Africa may influence the flow in a manner similar to that of the Andes in South America. The general tendency of mountain barriers to modify the flows around them is in agreement with the results of calculations by Bolin (1950) and Kasahara (1966) in which studies were made of the flow pattern generated by a circular mountain in a broad westerly current of constant intensity. Since two major ridges exist on the eastern sides of the Rockies and Himalayas for both seasons, and since these features agree more or less with those observed as shown in Figs. 2 and 3, one may be tempted to conclude that the orographic-dynamic effect of the Rockies and Himalayas determines the position of the semi-permanent high-level flow patterns.

* We are in the process of including the complete global orography in the NCAR general circulation model, and we shall investigate the orographic effect of Greenland and Antarctica in the near future.

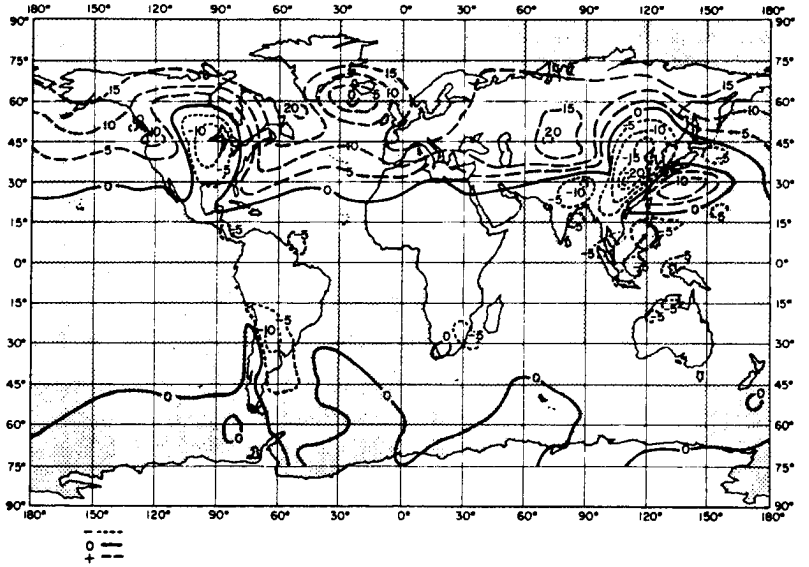

Fig. 6. Computed mean deviation of the height of free surface in decameters for January conditions.

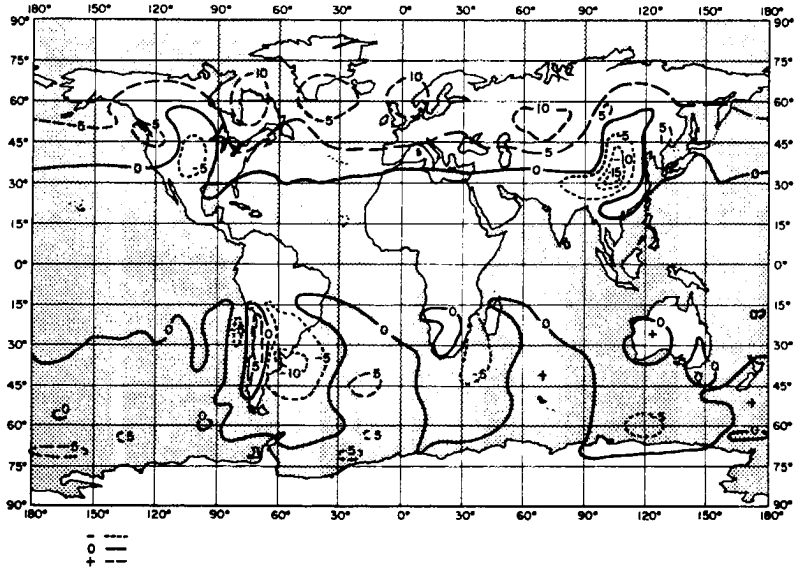

Fig. 7. Same as Fig. 6, but for July conditions.

The main point of this paper is to analyze this presumption a little bit more carefully to find out whether this is really the case. Before going into the analysis, a few points are worth mentioning. On Fig. 2, there is the third trough extending from northern Siberia southwest then south to the Mediterranean during the winter. In Fig. 6 for January, the numerical result does not show the existence of such a corresponding trough. There is in fact a weak trough over the North Atlantic, particularly on the east side of Greenland. The formation of this trough may be due to the orographic effect of Greenland. However, since we have the boundary along the 75°N latitude circle, the orographic effect of Greenland may be very much distorted. Another explanation may be that the weak trough over the North Atlantic is the second trough induced by the orographic effect of the Rockies. Perhaps both explanations may work together to explain the appearance of the weak third trough over the North Atlantic. In any case, it seems that the presence of the third trough over western Europe, as seen on Fig. 2, is not likely to be due to the orographic-dynamic effect.

Based on the results of laboratory experiments discussed by Fultz and Long (1951) and Long (1952) dealing with the flow of a liquid past an obstacle in a rotating spherical shell, Frenzen (1955) has suggested possible analogies between circulation in the experimental model and in the atmosphere. Frenzen suggested that the orographic-dynamic effect of the South American Andes during the Southern Hemisphere winter is strong enough to form a ridge over the South Atlantic which would reinforce the subtropical high cell in this position. Frenzen continues that "with the additional, though considerably smaller influence of the highlands of South Africa, the pattern may repeat and also strengthen the South Indian Ocean anticyclone." By looking at the calculated pattern in the Southern Hemisphere (Fig. 7) Frenzen's suggestion appears to be correct. According to van Loon (private communication), however, there is little evidence on the mean 500 mb height contour maps to support the appearance of such trough-ridge patterns downstream of the Andes and the South African Highlands.

A rapid cyclogenesis on the lee side of the Rockies is a well-known phenomenon in the field of synoptic meteorology. Newton (1956) made a detailed analysis of such a cyclogenesis and pointed out an important dynamical effect of orography.

Now let us look at Figs. 8 and 9 which show the distributions of the deviation of zonal wind speed for January and July. For the purpose of comparison with observed data, Figs. 10 and 11 show the distributions of mean zonal wind speed for the winter season and the summer season published by Crutcher (1959). On these figures, the minus sign indicates the wind component from the west, opposite to our convention. Also the units are knots, whereas we use units of meters per second (10 knots $\approx$ 5 m/s). Since Figs. 8 and 9 show the distributions of the deviation from the zonal wind profiles shown in Fig. 5, one must add the values of the zonal wind profiles to get the distributions of mean zonal wind speed in order to compare with those of Figs. 10 and 11. On Fig. 8, we see that the intensity of zonal wind deviation becomes larger over the Far East and over North America. Over the Far East, the maximum value is 20 m/s and adding to this value another 20 m/s which comes from the undisturbed zonal wind distribution for January, we find that the intensity of the total zonal wind speed becomes 40 m/s which is approximately 80 knots. Over North America, the maximum value of the deviation is 5 m/s, so adding to this value

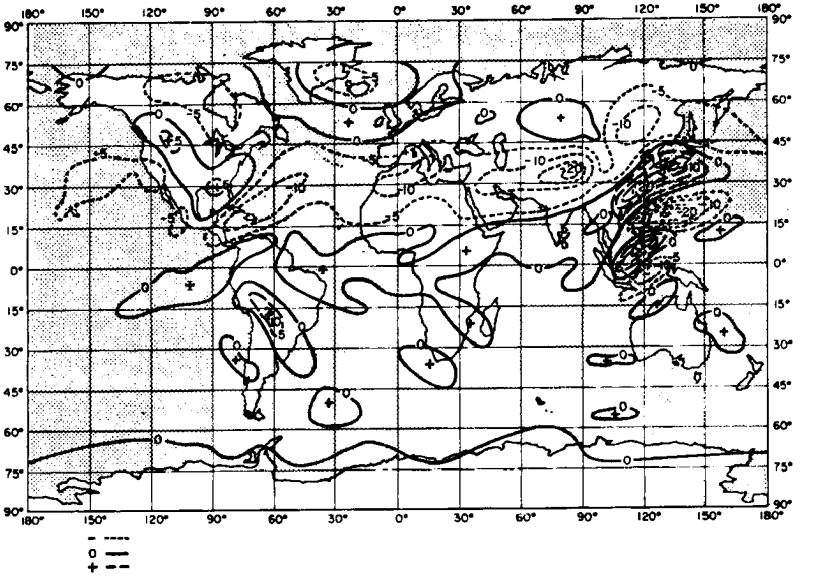

Fig. 8. Computed mean deviation of the zonal wind speed in meters per second for January conditions.

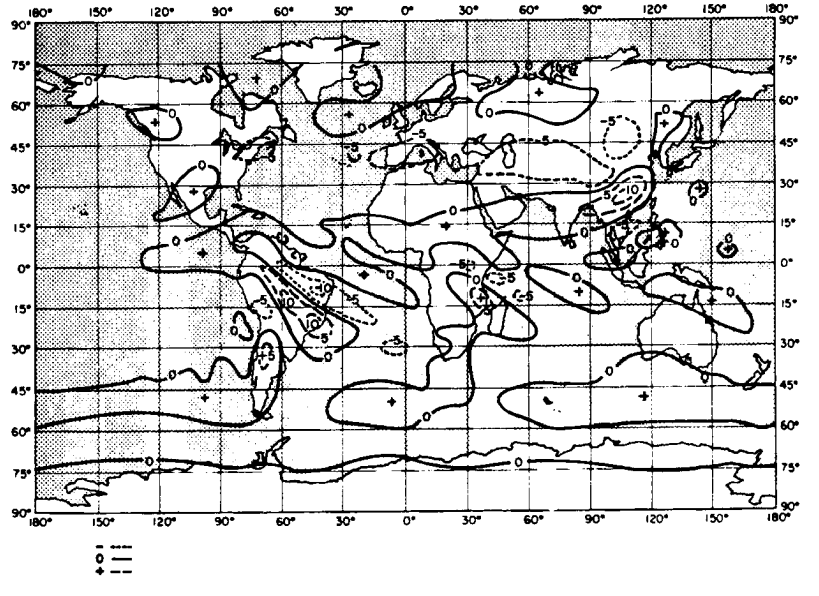

Fig. 9. Same as Fig. 8, but for July conditions.

another 20 m/s, we get a total of 25 m/s, which is approximately 50 knots. Except for the zonal wind maxima located over North Africa and over the Persian Gulf, the comparison between Figs. 8 and 10 is in reasonably good agreement. In particular, the presence of the narrow band of west winds over the Far East is reminiscent of the formation of a strong jet stream which was discovered during World War II (Namias and Clapp, 1949). The results of computations by Gambo (1956) also show the appearance of a strong westerly flow over the Far East due to the orographic dynamic effect of the Himalayas.

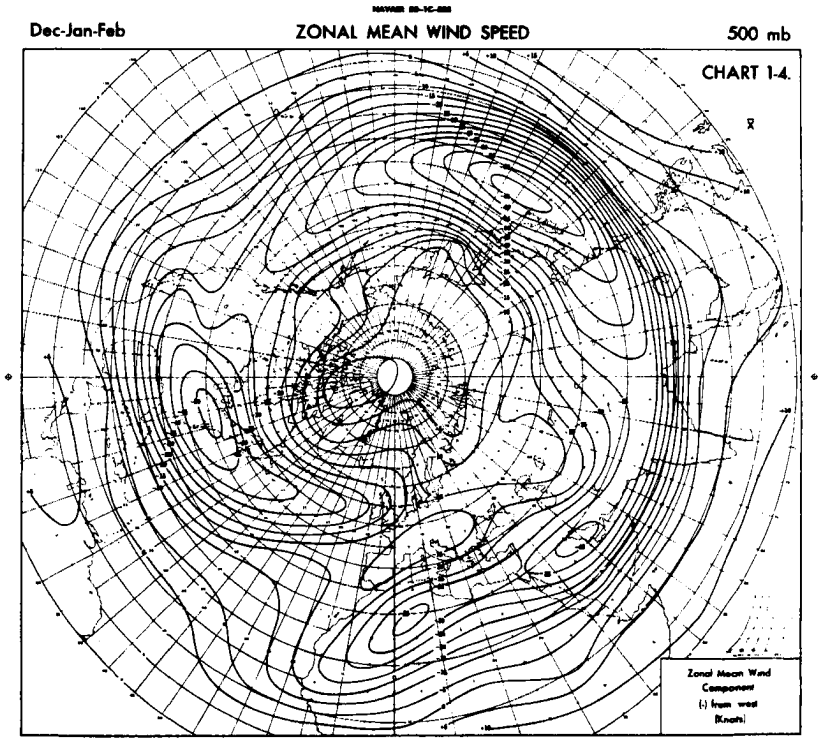

Fig. 10. Observed mean distribution of zonal wind velocity in knots at 500 mb for December-January-February (Crutcher, 1959).

When we turn our attention to the comparison between Figs. 9 and 11 for the July conditions, we find that the two patterns hardly resemble each other. On the observed patterns of Fig. 11, we see two major maxima located off the east coast of North America and over the North Pacific, and one minor maximum over the Mediterranean. Those features of the observed zonal wind distribution of summer are not seen at all in the calculated patterns of Fig. 9. We can draw almost the same conclusion by comparing the observed maps of Figs. 14 and 15 and the calculated maps of Figs. 12 and 13 concerning the distribution of meridional mean wind

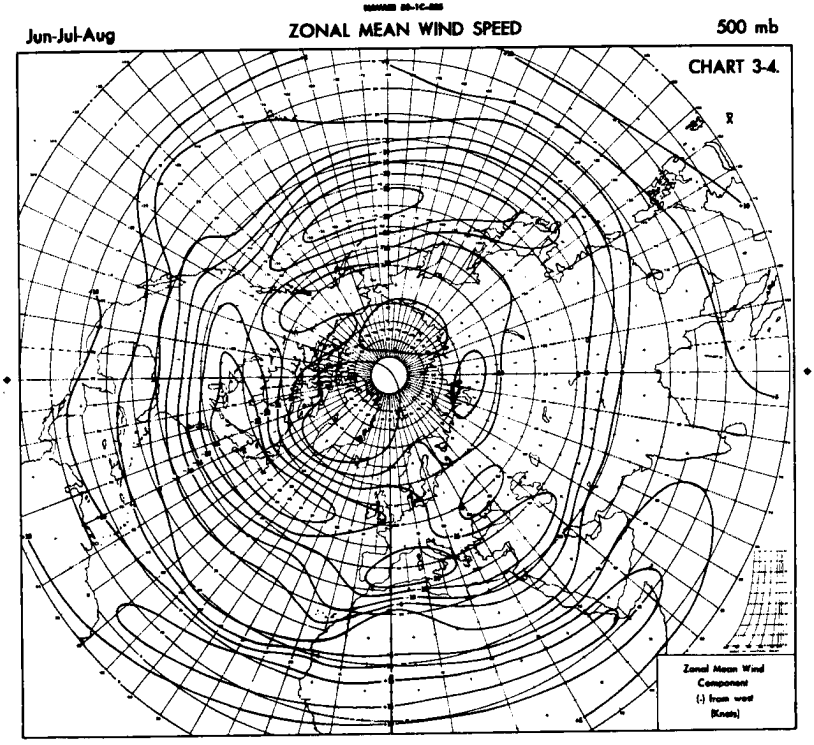

Fig. 11. Same as Fig. 10, but for June-July-August.

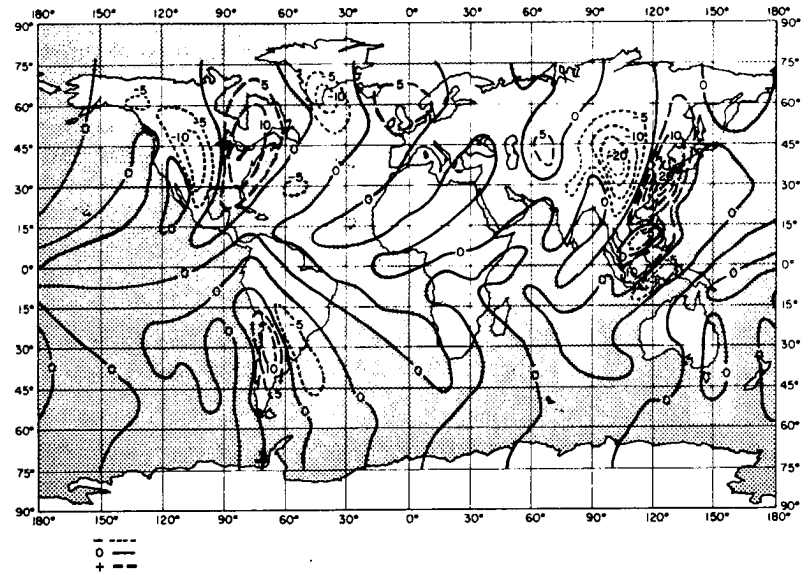

Fig. 12. Computed mean deviation of the meridional wind speed in meters per second for January conditions.

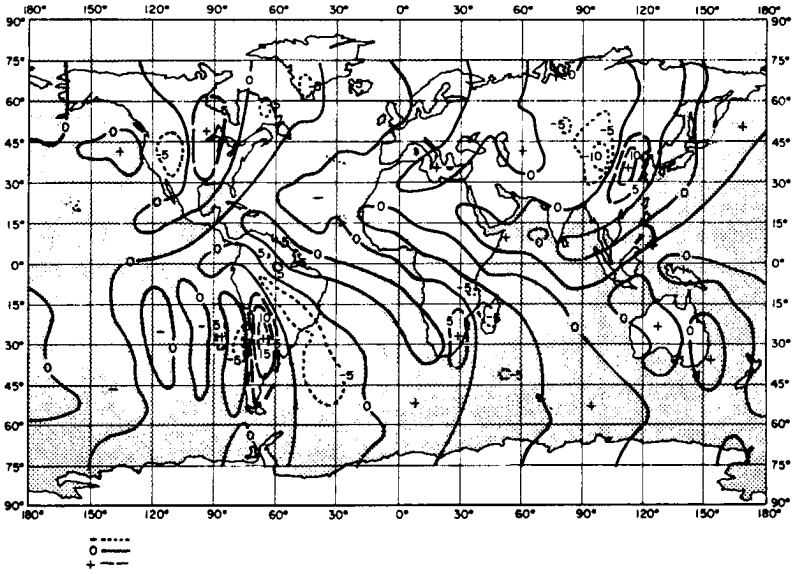

Fig. 13. Same as Fig. 12, but for July conditions.

speed. Again the calculated meridional wind distribution agrees fairly well qualitatively with that of observed distribution for January, but not for July conditions. The implication of this conclusion is that the orographic-dynamic effect cannot be a major factor in determining the mean circulation patterns in the mid-troposphere during the Northern Hemisphere summer season.

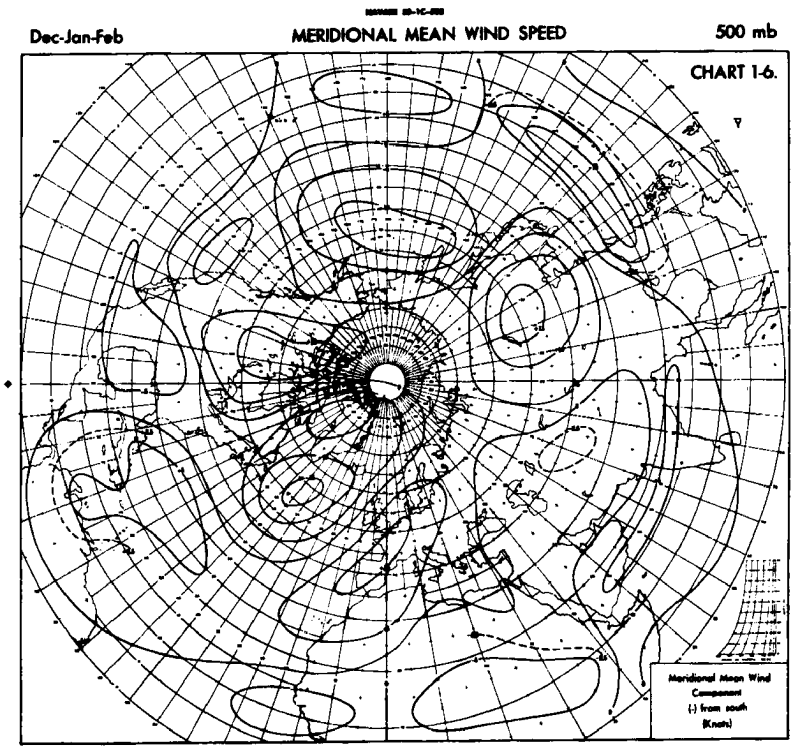

Fig. 14. Observed mean distribution of meridional wind velocity in knots at 500 mb for December-January-February (Crutcher, 1959).

In order to see the distributions of mean zonal wind at 500 mb in the Southern Hemisphere, Figs. 16 and 17 are reproduced from the work by van Loon (1964). Fig. 16 for January (summer) shows the well-defined zone of westerly maximum which lies along 45°S across the South Atlantic and Indian Oceans. As seen from Fig. 17, in July (winter) the maximum intensity of westerlies is somewhat reduced, but the width of the westerlies is increased. Although van Loon's analyses don't extend to the areas below 25°S, the features of the calculated zonal wind distribution (Fig. 9) over South America in July are not present in the observed distribution (Fig. 17). It appears to be reasonable at this stage to conclude that the orographic-dynamic effect is small on the mid-tropospheric large-scale flow in the Southern Hemisphere. This is a direct contradiction with the conclusions

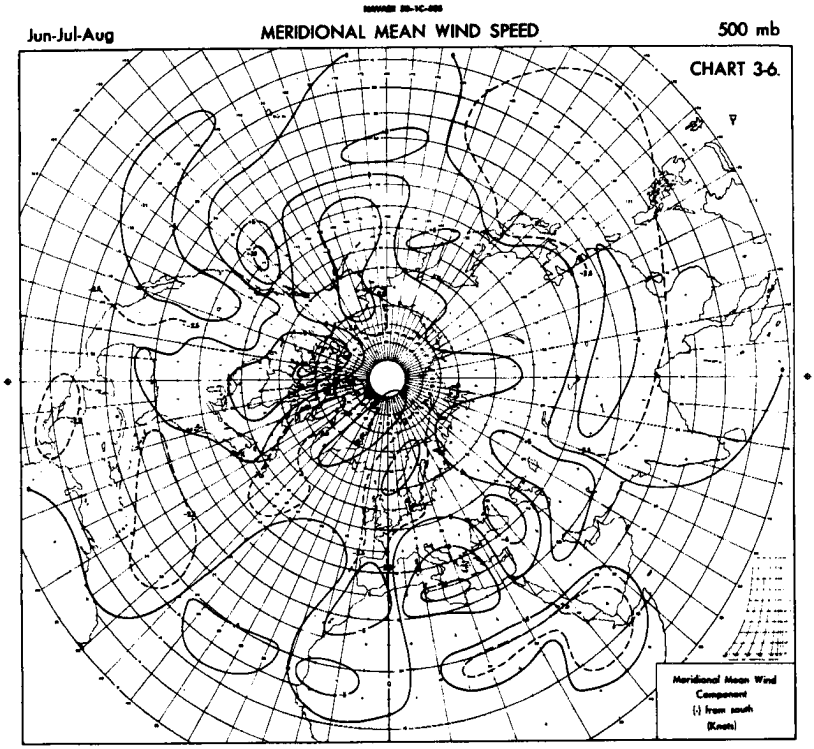

Fig. 15. Same as Fig. 14, but for June-July-August.

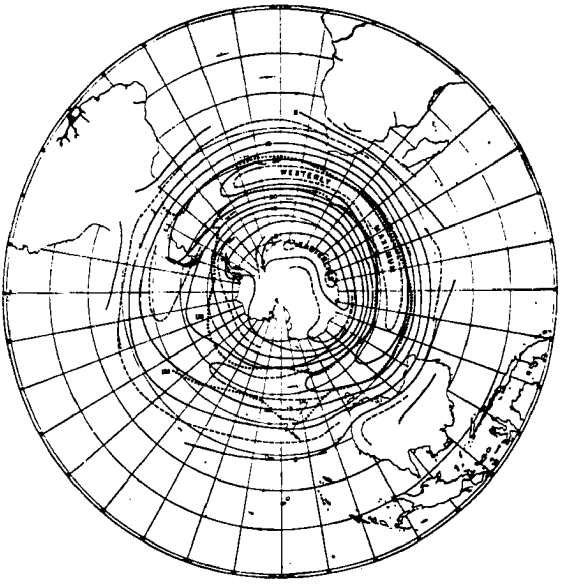

Fig. 16. Observed distribution of mean zonal wind in meters per second at 500 mb for January (van Loon, 1964).

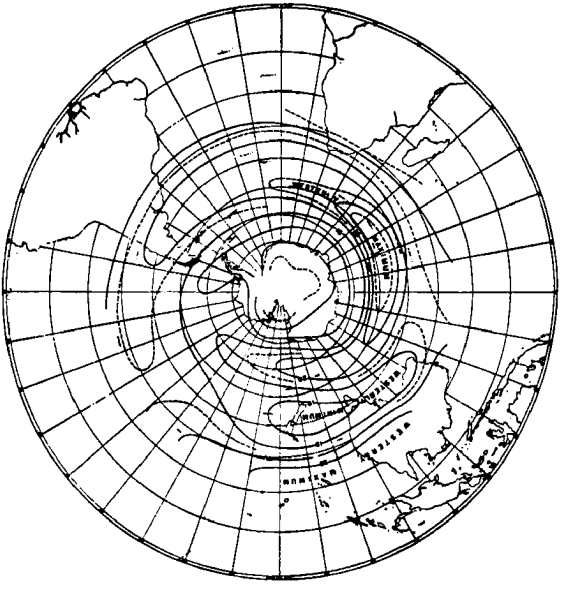

Fig. 17. Same as Fig. 16, but for July.

of Boffi (1949). However, Schwerdtfeger (1961) pointed out that the analyses of Boffi were biased by the scantiness of observed data. A more complete analysis shows that a trough does not exist on the eastern sides of the Andes on the mean 500 mb height contours as mentioned earlier.

4. Thermal-Synoptic Effect

We now turn our attention to the response of the large-scale heat sources and sinks due to the distribution of continents and oceans to the mean state of the atmospheric circulation. In the studies of Smagorinsky (1953) and Gilchrist (1954) on the influence of large-scale heat sources and sinks, the formulation of the mathematical models assumes that the motion is dependent on the height coordinate and the distance coordinate in the east-west direction, but independent of the distance coordinate in the north-south direction. Döös (1963), Staff Members of Academia Sinica (1958), Saltzman (1963, 1965), and Sankar-Rao (1965) considered the same problem by dealing with the three-dimensional large-scale motions. In their studies, however, only linearized models were considered. Linearized models are convenient to deal with an idealized case in which, for example, relevant differential equations of the problem have only constant coefficients. When the forcing term due to the distribution of heat sources is expressed as a complex function of space coordinates, an advantage of dealing with linearized equations is often lost for the purpose of obtaining the solution to the physical problems. Another major difficulty in the previous studies is that the distribution of heat sources must be prescribed as a forcing function of the model. Despite recent observational studies [e.g., Clapp (1961)] the distributions of heat sources are poorly known. A solution to this difficulty is to let the model evaluate various heating functions, such as those due to short and long wave radiation, the release of latent heat of condensation and the transport of sensible and latent heat from the earth's surface, etc. However, the complexity of this approach and the size of the computation involved are on the same order of magnitude as the general circulation experiments based on thermo-hydrodynamic principles such as those being carried out at ESSA, NCAR, UCLA and LRL (Smagorinsky, Manabe and Holloway, 1965; Manabe, Smagorinsky and Strickler, 1965; Kasahara and Washington, 1967; Mintz, 1965; Leith, 1965).

Here we shall describe the NCAR general circulation model very briefly. This model will be used to study the influence of the thermal effect due to the non-uniformity of the temperature of the earth's surface.

The prognostic equations for the NCAR model are the two horizontal equations of motion and the pressure tendency equation in spherical coordinates. We merely list the equations. For the derivation of the equations, the reader may refer to the paper by Kasahara and Washington (1967).

$$\frac{\partial(\rho u)}{\partial t} = -\nabla\cdot(\rho u\,\mathbb{V}) - \frac{\partial}{\partial z}(\rho uw) - \frac{1}{a\cos\phi}\frac{\partial p}{\partial \lambda} + \left(f + \frac{u}{a}\tan\phi\right)\rho v + F_\lambda \tag{4.1}$$

$$\frac{\partial(\rho v)}{\partial t} = -\nabla\cdot(\rho v\,\mathbb{V}) - \frac{\partial}{\partial z}(\rho vw) - \frac{1}{a}\frac{\partial p}{\partial \phi} - \left(f + \frac{u}{a}\tan\phi\right)\rho u + F_\phi \tag{4.2}$$

Besides the notation already mentioned in Section 3, we define the following: z is height above the earth's sea level, p is pressure, ρ is density, F_λ and F_ϕ are the longitudinal and meridional components of the frictional force per unit volume.

The pressure tendency equation is

$$\frac{\partial p}{\partial t} = B + g\rho w - g\int_z^{z_T} \nabla\cdot (\rho \mathbb{V})\, dz \tag{4.3}$$

where $B = \partial p/\partial t$ evaluated at $z = z_T$, the height of the upper boundary, where we have assumed in deriving (4.3) that

$$w = 0 \quad \text{at } z = z_T \ . \tag{4.4}$$

The diagnostic equations are as follows:

The equation of state:

$$p = \rho RT \tag{4.5}$$

where R is the gas constant for air and T is temperature.

The hydrostatic equation:

$$\frac{\partial p}{\partial z} = -\rho g \tag{4.6}$$

The vertical motion equation (Richardson's equation: see for example Thompson, 1961):

$$w = w_s - \int_H^z \nabla\cdot \mathbb{V} dz - \frac{1}{\gamma}\int_H^z \frac{1}{p}(B + J)\, dz + \frac{1}{C_p}\int_H^z \frac{Q}{T}\, dz \tag{4.7}$$

where H denotes the height of orography and

$$w_s = \mathbb{V}_s\cdot \nabla H \qquad \text{at} \quad z = H \tag{4.8}$$

and $\gamma = C_p/C_v$, C_p and C_v are the specific heats, Q the rate of heating per unit mass, and

$$J = \mathbb{V}\cdot \nabla p - g\int_z^{z_T} \nabla\cdot(\rho \mathbb{V})\, dz \ . \tag{4.9}$$

We can evaluate B by integrating (4.7) from the height of the mountain $z = H$ to the upper boundary $z = z_T$ where $w = 0$. This yields the following equation for B:

$$B = \frac{\frac{1}{\gamma}\int_H^{z_T} \frac{J}{p}\, dz - \frac{1}{C_p}\int_H^{z_T} \frac{Q}{T}\, dz + \int_H^{z_T} \nabla\cdot \mathbb{V} dz - w_s}{-\frac{1}{\gamma}\int_H^{z_T} \frac{dz}{p}} \tag{4.10}$$

The heating rate Q in (4.7) consists of the following three parts:

$$Q = Q_a + Q_c + Q_d \ . \tag{4.11}$$

The term Q_a denotes the rate of heating/cooling due to the radiational sources, which include the absorption of solar insolation by water vapor and the long wave cooling of the atmosphere. One of the important heat sources in the atmosphere is the latent heat released by condensation in

clouds. This heating rate is denoted by Q_c. The term Q_d is the rate of heating/cooling due to horizontal and vertical diffusion of heat and vertical transport of heat from the earth's surface.

The version of the model which is currently in operation uses a grid network of two height levels plus the surface level, with a vertical spacing of 6 km, and covers the entire globe with a horizontal spacing of 5° in both longitude and latitude.

We will describe the results of an experiment to simulate the circulation patterns of mean January conditions. In order to separate the thermal effect from the orographic effect, we ignore the dynamical effect of orography by setting the height of the mountains to vanish in these experiments. The experiment is started from an isothermal atmosphere of 250° K with no initial motion. As a mean January condition, the sun's declination angle is set for January 15 and the distribution of surface temperature (which in this experiment is that of sea level due to the lack of orography) is prescribed for a January mean, as shown in Fig. 18. Details of the results of this experiment will be described elsewhere. In this paper, we will discuss only the results of the global distribution of wind velocity. Fig. 19 and 20 show respectively the distributions of mean zonal and meridional wind speed at the level of 9 km in height, averaged for the period of 15 days between days 75 and 90. In the Northern Hemisphere, the westerly

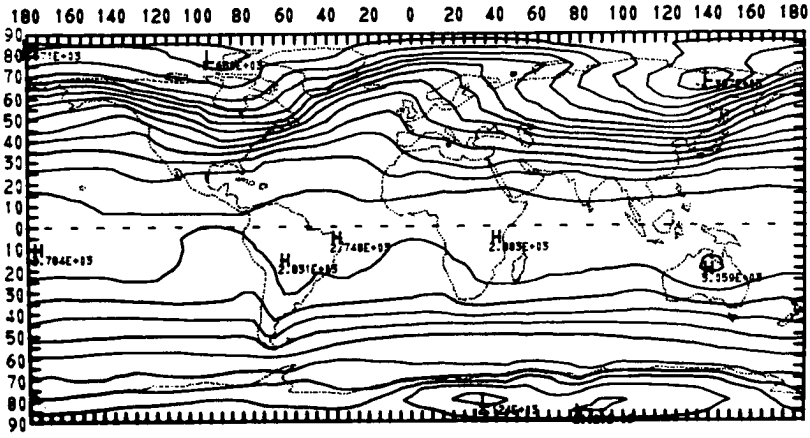

Fig. 18. Sea level temperature distribution for January.

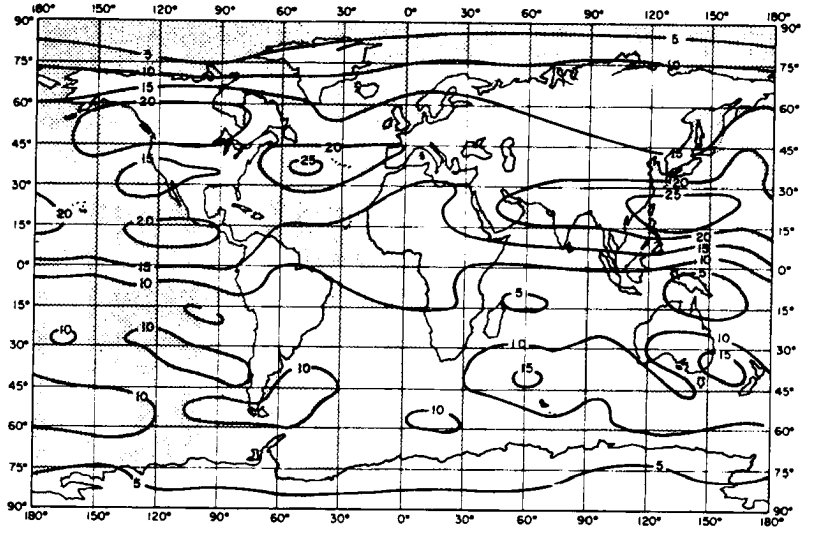

Fig. 19. Distribution of mean zonal wind in meters per second at the 9 km height for January.

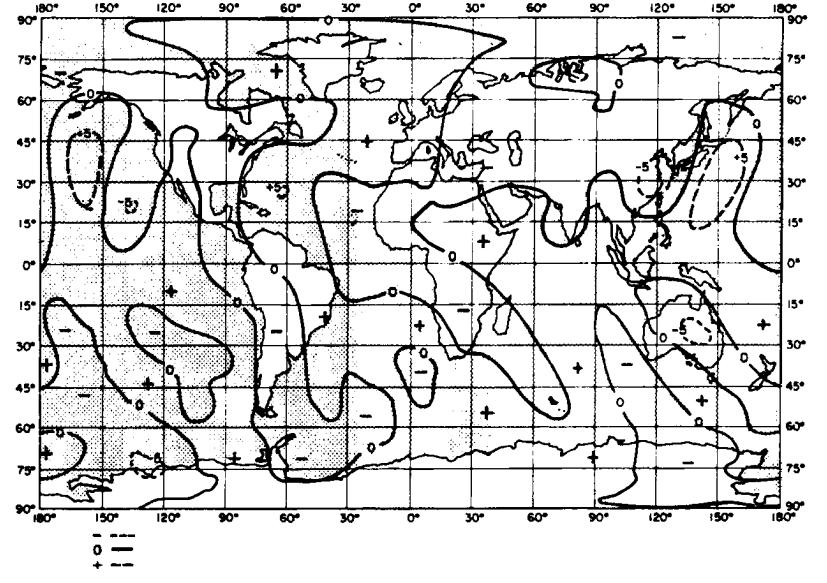

Fig. 20. Distribtuion of mean meridional wind in meters per second at the 9 km height for January.

flow maximum appears over the south of Japan around 20°N. Over North America, the westerly flow splits into two branches, one running around 50°N and the other around 10°N. These split westerly flows merge into one mainstream over the North Atlantic off the east coast of the United States. The locations of the westerly flow maxima agree reasonably well with those observed shown in Fig. 10. It is seen from Fig. 20 that the meridional circulation pattern also indicates a fair agreement with those observed as shown in Fig. 14.

In the Southern Hemisphere, the maximum westerly belt runs from 30°E to about 140°W at latitudes of about 40° to 50°. This geographical location of the maximum westerly flow in the Southern Hemisphere is in good agreement with that of observed maxima prepared by van Loon (1964). It is interesting to note that the orographically induced flow pattern as shown in Fig. 8 has no resemblance to that of observed patterns. Thus, it seems clear that the thermal effect plays an important role in determining a mean state of the global scale circulation.

It is worthwhile to mention that there is, in general, fair agreement in locations of westerly maxima shown in Fig. 19 and places where the surface isotherms are packed. In Fig. 18, the strong packing of isotherms is seen over the east coast of the U. S. to Greenland and also over the east coast of the Asiatic continent to Alaska. Indeed the westerly flow maxima exist roughly over these two areas. It is interesting to infer from this result the locations of the westerly flow maxima for a mean July condition. As seen from Fig. 11, two major westerly flow maxima appear over the North Pacific and over the Newfoundland area. Fig. 21 shows the distribution of sea-level temperature after Landsberg (Berry, Bollay and Beers, 1945). In the Northern Hemisphere, the locations of the westerly flow maxima agree well with the places where the temperature gradient is relatively strong. As seen from the results discussed in Section 3, the oro-

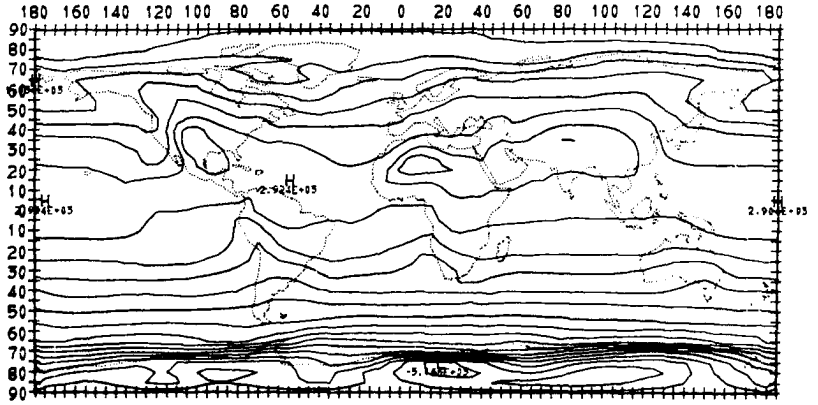

Fig. 21. Sea-level temperature distribution for July.

graphic-dynamic effect cannot be a major factor in determining the mean circulation patterns in the mid-troposphere during the Northern Hemisphere summer season. Therefore, it is reasonable to presume that the thermal effect is the determining factor. We have started a numerical computation to simulate the circulation patterns of mean July conditions. However, at the time of this writing, the numerical work has not been completed. Therefore, a close examination of this conjecture will be given at some other time.

5. Conclusions

Among the three factors influencing the large-scale motions of the atmoshpere which have been discussed in this paper, the surface boundary layer effect is probably minor except in the intense cyclones or anticyclones. Although the geographical variation in the value of the drag coefficient may have some importance, there is reason to believe that the effect of variation of the surface friction on the evaluation of surface wind stress may be rather small (Smagorinsky, 1953). If this is the case, the surface boundary effect does not play the role of anchor for the large-scale motions. A quantitative investigation of this effect can be done using our general circulation model, and we plan to do this in the future.

Concerning the relative importance of the thermal and orographic effects, the present results indicate that in the Northern Hemisphere the orographic and thermal effects both cooperate during the winter season, but the thermal effect dominates during the summer season. In the Southern Hemisphere, the orographic influence seems to be very small compared with the thermal effect for both seasons. However, the orographic effect of the Antarctic Continent may be important. The question was not investigated in this paper, and we hope to work on this problem very soon.

As pointed out in Section 4, the use of a general circulation model is a promising approach to investigate the thermal effect. If we include the release of latent heat of condensation as a heat source, then the inclusion of orography becomes an important problem because of the forced ascending motions associated with mountains. If the dynamical effect of orography is included, then the thermal interaction between the air and the ground must take place at the top of the mountains. Therefore, once the orography is introduced, we can no longer separate the two effects. The effect of orography has not been taken into account so far in the general circulation experiments, except by Mintz (1965). There is no question about the need for more research on the effect of orography in a more complete way. We are now working on the inclusion of orography together with surface temperature calculations in the NCAR general circulation model. The results of the experiments will be reported in a separate article.

ACKNOWLEDGMENTS

The author is indebted to Dr. Warren Washington for collaboration in the development of the NCAR general circulation model which was used in the present study. Thanks are also due to Bernard O'Lear and Joyce Takamine who assisted in programming part of the computations and running

the programs on the CDC 6600 computer. Consultations with Dr. Chester Newton and Harry van Loon concerning synoptic conditions of the atmosphere, especially in the Southern Hemisphere, were very useful. Placido Jordan prepared the map of global surface temperature distribution for mean January conditions used in the present computations. The author is grateful to Kathy Hatt for assistance in preparing the manuscript.

REFERENCES

Bentley, C. R., R. L. Cameron, C. Bull, K. Kojima, and A. J. Gow, 1964: Antarctic Map Folio Series, Folio 2, Physical Characteristics of the Antarctic Ice Sheet, American Geographical Society.

Berkofsky, L., and E. A. Bertoni, 1955: Mean topographic charts for the entire earth, Bulletin of the American Meteorological Society, 36, 350-354.

Berry, F. A., E. Bollay, and N. R. Beers, (Ed.), 1945: Handbook of Meteorology, McGraw-Hill Book Co., New York, 1068 pp.

Boffi, J. A., 1949: Effect of the Andes Mountains on the general circulation over the southern part of South America, Bulletin of the American Meteorological Society, 30, 242-247.

Bolin, B., 1950: On the influence of the earth's orography on the general character of the westerlies, Tellus, 2, 184-195.

Brunt, D., 1939: Physical and Dynamical Meteorology, 2nd edition, Cambridge University Press, 428 pp.

Charney, J. G., and A. Eliassen, 1949: A numerical method for predicting the perturbations of the middle latitude westerlies, Tellus, 1, 38-54.

Clapp, P. F., 1961: Normal heat sources and sinks in the lower troposphere in winter, Monthly Weather Review, 89, 147-162.

Cressman, G. P., 1960: Improved terrain effects in barotropic forecasts, Monthly Weather Review, 88, 327-342.

Crutcher, H. L., 1959: Upper Wind Statistics Charts of the Northern Hemisphere, issued by the Chief of Naval Operations.

Döös, B. R., 1962: The influence of exchange of sensible heat with the earth's surface on the planetary flow, Tellus, 14, 133-147.

Eady, E. T., 1949: Long waves and cyclone waves, Tellus, 1, 33-52.

Frenzen, P., 1955: Westerly flow past an obstacle in a rotating hemispherical shell, Bulletin of the American Meteorological Society, 36, 204-210.

Fultz, D., and R. R. Long, 1951: Two-dimensional flow around a circular barrier in a rotating spherical shell, Tellus, 3, 61-68.

Gambo, K., 1956: The topographical effect upon the jet stream in the Westerlies, Journal of Meteorological Society of Japan, 34, 24-28.

Gilchrist, B., 1954: The seasonal phase changes of thermally produced perturbations in the Westerlies, Proceedings of the Toronto Meteorological Conference, 1953, 129-131.

Haurwitz, B., 1941: Dynamic Meteorology, McGraw-Hill Book Company, New York, 365 pp.

Jacobs, I., 1958: 5-bzw. 40 jährige Monatsmittel der absoluten Topographien der 1000 mb, 850 mb, 500 mb und 300 mb Flächen sowie der relativen Topographien 500/1000 mb und 300/500 mb über der Nordhemisphäre und ihre monatlichen Änderungen, Meteorologische Abhandlungen, Band IV, Heft 2, Institut für Meteorologie und Geophysik der Freien Universität, Berlin.

Kasahara, A., 1966: The dynamical influence of orography on the large-scale motion of the atmosphere, Journal of Atmospheric Sciences, 23, 259-271.

Kasahara, A., and W. M. Washington, 1967: NCAR general circulation model of the atmosphere, Monthly Weather Review, 95, 389-402.

Leith, C. E., 1965: Numerical simulation of the earth's atmosphere, in Methods in Computational Physics, 4, Applications in Hydrodynamics, Academic Press, New York, 1-28.

Long, R. R., 1952: The flow of a liquid past a barrier in a rotating spherical shell, Journal of Meteorology, 9, 187-199.

Manabe, S., J. Smagorinsky, and R. F. Strickler, 1965: Simulated climatology of a general circulation model with a hydrologic cycle, Monthly Weather Review, 93, 769-798.

Mintz, Y., 1965: Very long-term global integration of the primitive equations of atmospheric motion, WMO Technical Note No. 66, WMO-IUGG Symposium on Research and Development Aspects of Long-Range Forecasting, Boulder, Colorado, 1964, WMO, Geneva.

Namias, J., and P. F. Clapp, 1949: Confluence theory of the high tropospheric jet stream, Journal of Meteorology, 6, 330-336.

Newton, C. W., 1956: Mechanisms of circulation change during a lee cyclogenesis, Journal of Meteorology, 13, 528-539.

Saltzman, B., 1963: A generalized solution for the large-scale, time-average, perturbations in the atmosphere, Journal of the Atmospheric Sciences, 20, 226-235.

Saltzman, B., 1965: On the theory of the winter-average perturbations in the troposphere and stratosphere, Monthly Weather Review, 93, 195-211.

Sankar-Rao, M., 1965: On the influence of the vertical distribution of stationary heat sources and sinks in the atmosphere, Monthly Weather Review, 93, 417-420.

Sawyer, J. S., 1959: The introduction of the effects of topography into methods of numerical forecasting, Quarterly Journal of the Royal Meteorological Society, 85, 31-43.

Schwerdtfeger, W., 1961: Strömungs- und Temperaturfeld der freien Atmosphäre über den Anden, Meteorologische Rundschau, 14, 1, 1-6.

Smagorinsky, J., 1953: The dynamical influence of large-scale heat sources and sinks on the quasi-stationary mean motions of the atmosphere, Quarterly Journal of the Royal Meteorological Society, 79, 342-366.

Smagorinsky, J., S. Manabe, and J. L. Holloway, 1965: Numerical results from a nine-layer general circulation model, Monthly Weather Review, 93, 727-768.

Staff Members of Academia Sinica, 1958: On the general circulation over eastern Asia (III), Tellus, 10, 299-312.

Sutcliffe, R., 1951: Mean upper contour patterns of the Northern Hemisphere -- the thermal-synoptic view-point, Quarterly Journal of the Royal Meteorological Society, 77, 435-440.

Thompson, P. D., 1961: Numerical Weather Analysis and Prediction, The Macmillan Company, New York, 170 pp.

van Loon, H., 1964: Mid-season average zonal winds at sea level and at 500 mb south of 25 degrees south, and a brief comparison with the Northern Hemisphere, Journal of Applied Meteorology, 3, 554-563.

Question: Dr. Richard J. Reed, University of Washington

What was your source of the surface temperatures for July over the oceans? My recollection is that temperature gradients in the western oceans, according to U. S. Navy Hydrographic maps, are much stronger than were shown on your slide.

Reply: Dr. Kasahara:

The distribution of sea-level temperature shown here for July was taken from the section on Climatology by H. Landsberg in Handbook of Meteorology (Ed. Berry, Bollay, and Beers, 1945). Temperature gradients in the North Atlantic given in the U. S. Navy Marine Climatic Atlas of the World appear to be a little bit stronger than those given by Landsberg, but they are not too different from each other.

Question: Dr. P. Koteswaram, NCAR

I agree that heating plays a predominant part in July. What about the heating of the elevated terrain?

Reply: Dr. Kasahara:

In the present work, I investigated the dynamic and thermal effects separately. The thermal forcing was given by prescribing the distribution of sea-level temperatures over the entire earth. In reality, as you questioned, the heating should be calculated at the surface of the earth including mountains. Presently I am working, in collaboration with Dr. Warren Washington, on the inclusion of the earth's orography and surface temperature calculations in the NCAR general circulation model to deal with the problems that you questioned.